EXPERIMENTAL AND NUMERICAL STUDY OF HEAT TRANSFER TO NANOFLUID FLOW IN SUDDEN ENLARGEMENT OF ANNULAR CONCENTRIC PIPE

HUSSEIN TOGUN ABDULLAH

FACULTY OF ENGINEERING
UNIVERSITY OF MALAYA
KUALA LUMPUR

2015

EXPERIMENTAL AND NUMERICAL STUDY OF HEAT TRANSFER TO NANOFLUID FLOW IN SUDDEN ENLARGEMENT OF ANNULAR CONCENTRIC PIPE

HUSSEIN TOGUN ABDULLAH

THESIS SUBMITTED IN FULFILMENT OF THE REQUIREMENTS FOR THE DEGREE OF DOCTOR OF PHILOSOPHY

FACULTY OF ENGINEERING
UNIVERSITY OF MALAYA
KUALA LUMPUR

2015

UNIVERSITI MALAYA

ORIGINAL LITERARY WORK DECLARATION

Name of Candidate: HUSSEIN TOGUN ABDULLAH

Registration/Matric No: KHA080070

Name of Degree: DOCTOR OF PHILOSOPHY

Title: EXPERIMENTAL AND NUMERICAL STUDY OF HEAT TRANSFER TO NANOFLUID FLOW IN SUDDEN ENLARGEMENT OF ANNULAR CONCENTRIC PIPE.

Field of Study: **HEAT TRANSFER**

I do solemnly and sincerely declare that:

1. I am the sole author/writer of this Work;
2. This Work is original;
3. Any use of any work in which copyright exists was done by way of fair dealing and for permitted purposes and any excerpt or extract from, or reference to or reproduction of any copyright work has been disclosed expressly and sufficiently and the title of the Work and its authorship have been acknowledged in this Work;
4. I do not have any actual knowledge nor do I ought reasonably to know that the making of this work constitutes an infringement of any copyright work;
5. I hereby assign all and every rights in the copyright to this Work to the University of Malaya ("UM"), who henceforth shall be owner of the copyright in this Work and that any reproduction or use in any form or by any means whatsoever is prohibited without the written consent of UM having been first had and obtained;
6. I am fully aware that if in the course of making this Work I have infringed any copyright whether intentionally or otherwise, I may be subject to legal action or any other action as may be determined by UM.

Candidate's Signature Date

Subscribed and solemnly declared before,

Witness's Signature Date

Name:

Designation:

ABSTRACT

Turbulent heat transfer to separation nanofluid flow in annular concentric pipe has been studied numerically and experimentally. In numerical study, finite volume method with standard k-ε turbulence model in three dimensional domains is used. Three different types of water based (Al_2O_3, CuO, TiO_2) nanofluids have been employed in this simulation. The adopted boundary conditions were expansion ratio (ER= 1.25, 1.67, and 2), Reynolds number ranging from 20000 to 50000, and Al_2O_3, CuO, TiO_2 water based nanofluids with volume fractions varied between 0 to 2% at heat flux varied from 4000 W/m^2 to 16000 W/m^2. For experimental study, Al_2O_3 water based nanofluid was used to validate numerical results. The outer cylinder of downstream section was heated by uniform heat flux whereas the outer cylinder of upstream section and the overall length of the inner cylinder were unheated. The results show that the volume fraction of nanofluid and Reynolds number significantly affect the surface heat transfer coefficient; an increase in surface heat transfer coefficient was noted when both volume fraction of nanofluids and Reynolds number were increased for all the cases. The peak of the heat transfer coefficient had occurred after the sudden expansion moved far from the step height with the increase of sudden expansion dimensions due to separation flow in case of both pure water and nanofluid. It has been noted from the counter of streamline the size of recirculation zone increased with the increases of Reynolds number and expansion ratio. Increase of volume fraction of nanofluid enhances the heat transfer coefficient due to augmented heat transport by nanoparticles in base fluid which raises the convection heat transfer. The lowest pressure drop and maximum thermal performance are observed at Reynolds number 50000, 2% Al_2O_3 water based nanofluid at expansion ratio 2 in comparison to others. The improvement of heat transfer was about 36.6 % for pure water at expansion ratio 2 compared to heat

transfer obtained in straight pipe. Augmentation of heat transfer could be achieved by using nanofluid at expansion ratio 2 where the total improvements were about 45.2% (TiO_2), 47.3 %(CuO), and 49 %(Al_2O_3). Also the increment in the pressure drop was about 42% for pure water at expansion ratio 2 compared with straight pipe whereas by using nanofluid they were 62.6% (TiO_2), 65.4% (CuO), and 57.6% (Al_2O_3). Good agreements were observed between numerical and experimental results all the way.

Extension studies on thermal performances and pressure drop for separation flow over single or double and Forward or Backward-Facing steps have also been performed. Studies were conducted numerically with different models for flowing water and different types of nanofluids. Here heat transfer and pressure drop enhancements were observed following the similar trend obtained for sudden expansion configuration.

ABSTRAK

Pemindahan haba secara gelora melalui pemisahan aliran bendalir nano di dalam paip anulus sepusat telah dikaji secara berangka dan ujikaji. Dalam kajian berangka, kaedah isipadu terhingga dengan menggunakan model standad k-ε gelora dalam ruang tiga dimensi telah digunakan. Tiga jenis bendalir nano berasaskan air (Al_2O_3, CuO, TiO_2) telah digunakan dalam simulasi ini. Keadaan Sempadan yang diguna pakai adalah nisbah pengembangan (ER = 1.25, 1.67, dan 2), nombor Reynolds antara 20000-50000, dan bendalir nano Al_2O_3, CuO, TiO_2 berasaskan air dengan pecahan isipadu di antara 0-2% dengan fluks haba berbeza diantara 4000 W / m^2 hingga 16000 W / m^2. Untuk kajian secara eksperimen, bendalir nano Al_2O_3 berasaskan air telah digunakan untuk mengesahkan keputusan berangka. Silinder luar bagi seksyen hiliran telah dipanaskan dengan fluks haba seragam manakala silinder luar di bahagian hulu dan panjang keseluruhan silinder dalaman tidak dipanaskan. Keputusan menunjukkan pecahan isipadu bendalir nano dan nombor Reynolds memberi kesan yang ketara kepada pekali pemindahan haba permukaan; peningkatan pekali pemindahan haba permukaan dialami apabila kedua-dua pecahan isipadu bendalir nano dan nombor Reynolds meningkat bagi semua kes. Kemuncak pekali pemindahan haba berlaku selepas pengembangan dimensi piap secara mengejut dan ianya bergerak jauh dari bahagian pengembangan dengan peningkatan dimensi pengembangan disebabkan oleh aliran pemisahan dalam kedua-dua kes air tulen dan bendalir nano. Ianya telah diperhatikan melalui garis arus dimana saiz zon edaran semula meningkat dengan peningkatan bilangan nombor Reynolds dan nisbah pengembangan. Peningkatan pecahan isipadu bendalir nano telah meningkatkan pekali pemindahan haba disebabkan kenaikan pengangkutan haba dengan penambahan nanopartikel di dalam cecair asas yang meningkatkan pemindahan haba perolakan. Penurunan tekanan terendah bersama

peningkatan maksimum prestasi terma telah direkodkan pada nombor Reynolds 50000, menggunakan 2% bendalir nano Al_2O_3 berasaskan air dan berdasarkan pada nisbah pengembangan 2 berbanding dengan bendalir nano yang lain. Peningkatan pemindahan haba adalah kira-kira 36.6 % dengan menggunakan air tulen pada nisbah pengembangan 2 berbanding dengan pemindahan haba yang diperolehi di dalam paip lurus. Peningkatan pemindahan haba boleh dicapai dengan menggunakan nanofluid pada nisbah pengembangan 2 di mana jumlah peningkatan adalah kira-kira 45.2% (TiO_2), 47.3% (CuO) dan 49% (Al_2O_3). Selaras dengan itu juga, kenaikan dalam kejatuhan tekanan adalah kira-kira 42% air tulen pada nisbah pengembangan 2 berbanding dengan paip lurus manakala dengan menggunakan nanofluid ianya adalah sebanyak 62% (TiO_2), 65.4% (CuO) dan 57.6% (Al_2O_3). Keputusan yang baik diperhatikan antara kaedah berangka dan eksperimen di keseluruhan kajian.

Kajian tambahan terhadap prestasi haba dan kejatuhan tekanan melalui aliran pemisahan pada pemisah individu atau berpasangan dan juga menghadap kehadapan dan kebelakang juga telah dilakukan. Kajian telah dilakukan secara berangka dengan model yang berbeza menggunakan air dan bendalir nano yang berbeza. Di sini peningkatan pemindahan haba dan kejatuhan tekanan diperhatikan mengikut trend yang sama untuk konfigurasi pengembangan secara mengejut.

ACKNOWLEDGEMENTS

First and above all, I express my gratitude to Allah (God) for providing me this opportunity and granting me the capability to completed my research successfully.

Also, I would like to express my sincere gratitude to my supervision committee, Dr. Kazi Md. Salim Newaz and Dr. Ahmad Badarudin Bin Mohamad Badry for guidance and supervision of this thesis. During the PhD candidature, I learn many things from their research experience in addition to get encouragements and supports.

Years ago my father used to say, "I wish my little son (Hussein) to be a doctor" I feel that my father who passed away recently is looking at this work from the Heaven.

My efforts would not be meaningful without the support of my mother, my wife and children (Ali and Malaak), and family members (Brothers and Sisters) for their encouragement all the time to do the best.

I also offer my warmest thanks to Dr. Hakim S Sultan Aljibori, all my research colleagues and others for their cooperation, encouragement, constructive suggestion and full support in completion of this research from the beginning till the end.

Lastly, I would also like to thanks to the University of Malaya and High Impact Research (MOHE-HIR) grant UM.C/625/1/HIR/MOHE/ENG/46-(D000045-16001), for support and providing the financial laboratory facilities during my academic study.

TABLE OF CONTENTS

LIST OF FIGURES

LIST OF TABLES

Nomenclature

a	Length of entrance section, m
b	Length of test section, m
Cp	Specific heat, kJ/kg.K
$C1\varepsilon, C2\varepsilon, C3\varepsilon, \sigma k, \sigma\varepsilon$	Model constants
De	Inner diameter of outer pipe at entrance section, m
di	Outer diameter of inner pipe, m
Dt	Inner diameter of outer pipe at test section, m
Dh	Hydraulic diameter of entrance section (Dh=Dt-De), m
ER	Expansion ratio Dt/De
K	Thermal conductivity, W/m.K
K_{eff}	Effective thermal conductivity, W/m.K
T	Temperature, K
Re	Reynolds number $Re= (\rho_{nf} UD_h)/\mu_{eff}$
U	Mean velocity (m/sec)
X, Y, Z	Cartesian coordinates

Greek symbols

μ	Dynamic viscosity
μ_{eff}	Effective viscosity
ε	Turbulent dissipation
μt	Turbulent viscosity
ϕ	Volume fraction (%)

CHAPTER 1: Introduction

1.1 Background

Heat transfer and fluid flow through the annular concentric pipe commonly used in power plant, heat exchangers, nuclear reactor, evaporator condenser, and industries, etc. therefore there are many experimental and numerical studies adopted analysis temperature distributions, pressure drop, and velocity profile in annular passages. For high performance of cooling system the researcher studied effect of reconfiguration geometry on efficiency of heat transfer devices such as put ribs or swirl generators in channel, expansion or contraction in passage, and forward and backward-facing step passages, …etc. The separation of fluid flow in annular channel occurred due to the change in pressure gradient that caused by increase or decrease of cross section area of annular channel. Thus the sudden expansion with one side or both sides of annular pipe are some the applications where the separation flow is seen.

The demand of energy is increasing day by day, but at the same time resources of nonreplenishable energy decreasing due to continuous extraction. In addition to that the growing environmental pollution is putting pressure on companies to become more energy efficient and reduce emissions. In thermal energy transportation, huge energy is lost due to lack of efficient heat exchanging equipment and use of inefficient materials. Many methods are applied to improve the situation, among them, use of efficient materials, adjusting process parameters, modifications of design etc.. Now researchers are more involved in exploration of better heat exchanging liquid where nanofluids are getting importance as heat exchanging liquid against conventional liquid.

1.2 The phenomena of separation flow

The separation of fluid flow is one of those viscous flow problems which are very important not only for science but also for practical applications. The classical concept of flow separation is due to viscosity; therefore its often expressed as "boundary layer separation" .In addition, a necessary condition for separation flow is flowing against an adverse pressure gradient . Flow is usually rotational, but never the less the flow net obtained for irrotational flow is very useful. If the fixed boundaries of the system are parallel or converge so that the stream line converge, the actual flow will be very nearly irrotational except immediately adjacent to the solid boundary. However, if the stream line of a flow net diverge rapidly (as in sudden enlargement passage) as they would for divergent boundaries the actual flow will be quite different from that indicated by the flow net .The flowing fluid tends to leaves the boundary whenever the stream lines are divergent. The fact that stream lines diverge in a flow net means that there is a tendency for separation to occur. Whether separation occurs or not depends on the velocity, density and viscosity of the fluid. For a given fluid, separations will not accurse until a certain velocity is reached. Generally there are two types of flow separation, separation at external and internal flow (Chang, 1976).

The turbulent flow separation has been studied to a greater extent compared to laminar range. This is because:

a) Turbulent flows are more frequently encountered than laminar flows.

b) Separation is more likely to occur when the flow is turbulent.

c) Due to inertial effects, separation has a much greater influence in turbulent flows.

There is a great change of the local heat transfer rate in the separated flow regions and considerable heat transfer augmentation may result up to the reattachment region (Hussein et al., 2011)

The turbulent flow field downstream of an axisymmetric sudden expansion is significant importance from both a fundamental and a practical standpoint. As a result such flows have been the focus of numerous analytical and experimental investigations (R.P. Durrett et al., 1988). The flow separation and the subsequent reattachment caused by sudden expansion in flow geometry, such as a backward-facing step, occur in many engineering application. The performance of fluid machinery in industrial flows is greatly influence by its presence. So, the control of flow separation is very interesting in the industrial field (Z. Mehrez et al., 2010).

For air flow in sudden expansion with heat transfer there are many experimental and numerical studies while very limited with water flow. Currently, the researcher have been challenged to improve heat transfer performance by using different variety of nanofluids which has higher thermal conductivity more than normal fluid therefore, nanofluid is used in the present investigation to obtain more augmentations of heat transfer in addition to the effect of separation flow due to sudden expansion and compared that result with water flow data.

Step flow in the form of backward facing play a vital role in the design of many equipment and engineering applications where heat transfer is concerned. The noted heat transfer applications are heat exchangers, environmental control systems, cooling systems for electronic devices, chemical process instrument and cooling channels in turbine blades. Mixing of low and high thermal fluid happened in the reattachment flow region of the

considered instrument which affects the heat transfer characteristic. Due to this phenomena, convection over forward and backward step geometries have been investigated by researches (Abu-Mulaweh, 2003). Figure 1.1 illustrates the backward facing step in a sudden expanded pipe where recirculation zone created after the step due to sudden expanded.

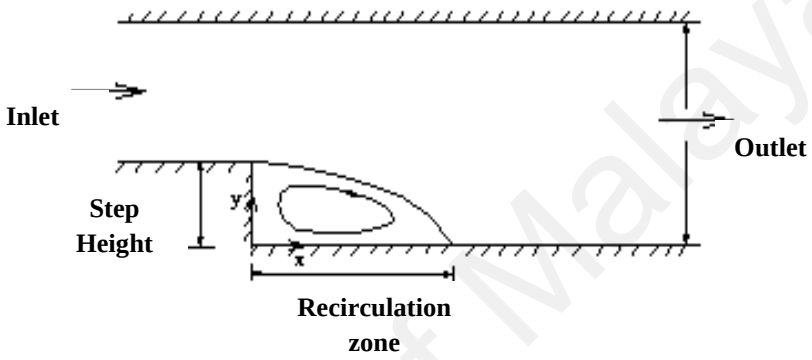

Figure 1.1: Backward facing step in sudden expansion pipe (Abu-Mulaweh, 2003).

1.3 Nanofluid

The nanofluid is a mix between fluid called base fluid and nanometer sized particles called nanoparticles. The base fluid commonly used is water, oil, and ethylene glycol while the nanoparticles having different types included metals, carbides, oxides, and carbon nanotubes. There are several parameter effects on the performance of nanofluid consisting of size and shape of nanoparticle, concentration, type of base fluid, type of nanoparticle metal or non-metal etc. The size of nanoparticles has significant impact on thermal conductivity where as small size of nanoparticle leads to increase in surface area therefore many of the researchers employed different types of nanofluid in different geometry to reach augmentation of heat transfer.

Nanofluid can be prepared by two methods: The first method summarizes by creating nanoparticle with chemical or physical processes (e.g., evaporation and inert-gas condensation processing), and then disperse them into a host fluid. The second method includes production and dispersion of the nanoparticles directly into a host fluid. In the present research, heat transfer and nanofluid flow in separated region are studied by experimental and 3D numerical analysis with turbulent range. As the feature of separation flow is complex and there are some features not appear with 2D then 3D numerical method has been adopted to make results more accurate and verified with experimental results.

The applications of presented study could be found in cooling systems and propulsion systems such as in heat exchangers, combustors, nuclear reactor cooling channels (Smyth, 1979), power plant (Pletcher, 1985) , in the wide angle diffusers, and the airfoils with large angle of attack and with sudden increases in area in channels (Moss, 1998).

.

1.4 Organization of the thesis

This thesis is divided into eight chapters. Chapter one contains the basic concepts, importance, actual objectives, and motivations for this study, as well a brief introduction to the separation flow in different configurations and effects on heat transfer to fluids and nanofluids. Chapter two is related to the experimental and numerical studies covering turbulent and laminar flow in sudden expansion over forward-backward facing steps, and in annular pipe. Chapter three is represented the simulation of numerical study. Chapter four is consisted of the experimental set up with details. Chapter five is presented the preparation and stability of nanofluids. Chapter six is concerned with the analysis of the

results. Chapter seven is consisted of conclusions and recommendations for further work linked to separation nanofluid flow through this configuration. Chapter eight is covered the extension studies on the effect of separation flow on thermal performance.

1.5 Motivation

The separation and reattachment phenomena take place in numerous industrial devices and important efforts have been done in the past decade to understand the hydrodynamics and thermal aspects of these coupled phenomena. However, in-depth studies of these problems are not completed and there are much work left to be done in this area. Furthermore, the turbulent separation nanofluid flow in sudden expansion has not been included in the thermal analysis through the years not only because of its complexity, but also for the high computational and experimental resources required for studying the problem. Basically, no enough information found for the effect of separation nanofluid flow through annular pipe with sudden expansion. The global incentive for this research is to provide new data that will be helping the designers of heat exchangers where nanofluids are used.

1.6 Objectives

The objectives of the present study are:

- To investigate the effect of flow separation due to a sudden enlargement of an annular concentric pipe on thermal and flow fields.
- To study the effects of nanofluids type and nanoparticle concentration on the heat transfer enhancement.

- To examine the effects of Reynolds numbers and heat flux on the heat transfer improvement.
- To explore the thermal performance obtained by sudden expansion and using nanofluids.

1.7 Thesis outlines

- The test pipe was heated to conduct the experiments at constant heat flux and the degree of separation varied by using different passage dimensions while the Reynolds number maintained in a range by regulating the flow.
- Different types and concentrations of Nanofluid were used in the numerical and experimental investigations.
- The flow separation induced with different heights of steps by reduction of dimension of the outer entrance pipe.
- The data simulated numerically by using software ANSYS FLUENT14.
- Experiment conducted in the laboratories of the University of Malaya in a newly built test rig.

1.8 The novelty of research

It is noted in the literature survey showed that the heat transfer and nanofluid flow for turbulent range in annular pipe sudden expansion has not been investigated as yet experimentally and numerically. In the recent years and according to the dramatic change in the energy field in general and in the heat transfer and heat exchangers specially in addition to the use of Nanotechnology and its important role in energy and heat exchangers may be able to create many new devices with a vast range of

applications. In another avenue same issues researchers have discovered a new way to add nanoparticles to cooling liquid to make heat transfer far more efficient, with important potential applications of conventional heating and cooling industry Therefore the novelty of this research is represented by

1. To evaluate high performance heat exchanger by using different geometrical configurations and imply that in real applications

2. Study the effect of separation flow in turbulence flow regime

3. Using different types of nanoparticles and use the most proper one

CHAPTER 2: Literature Review

2.1 Introduction

Enhancement of heat transfer has been widely researched in the last decades with different techniques. Most of researchers studied effect of change feature of geometry on heat transfer rate. The flow through an axisymmetric sudden expansion or contraction, over backward or forward facing steps, and ribbed channels create separation flow see Figure 2.1.

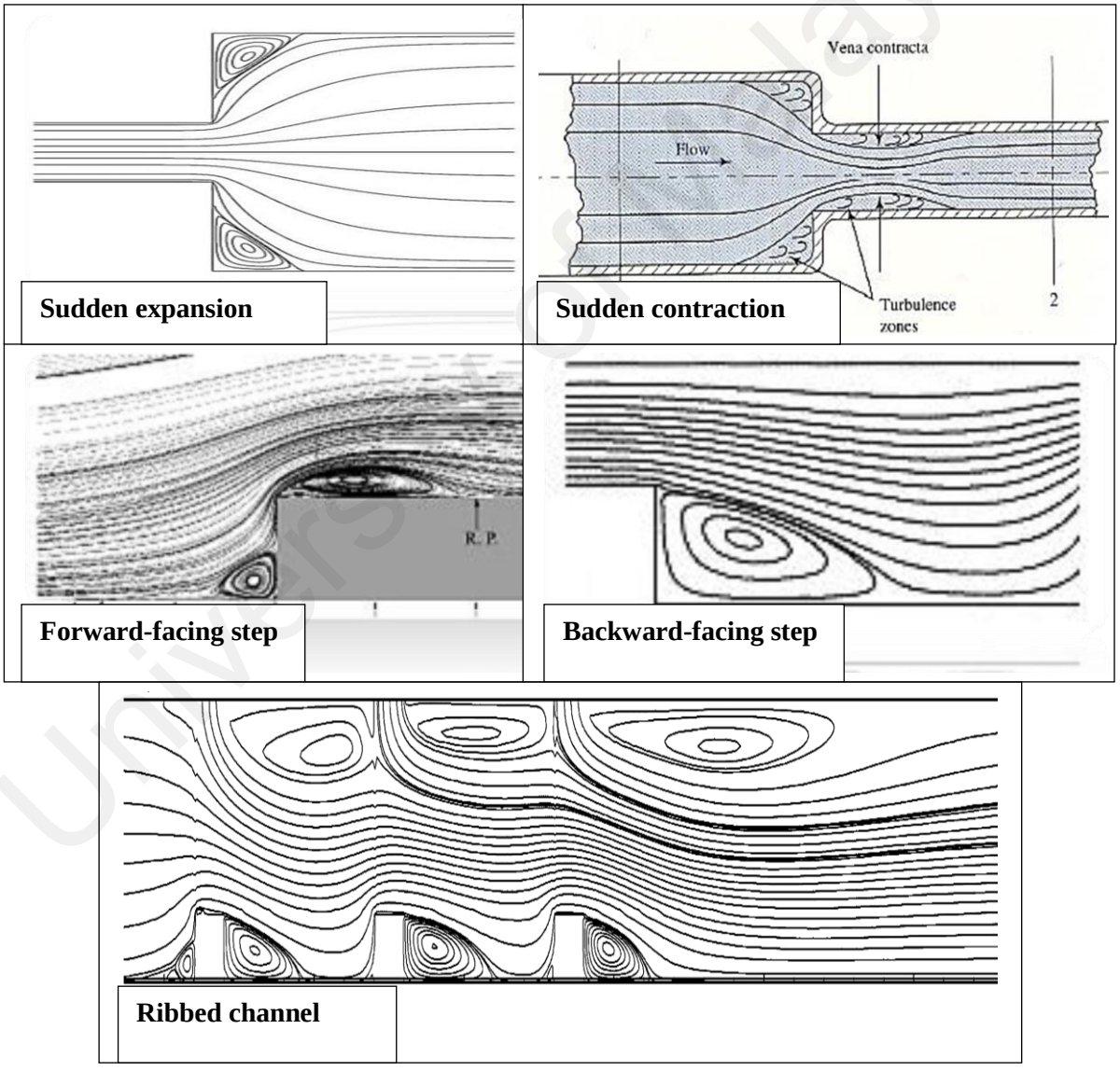

Figure 2.1: Pattern of separation flow.

There are many experimental and numerical studies adopted the effect of separation flow on performance heat transfer with different configurations and boundary conditions. Most of those investigations carried out for separation air flow and few of them for separation liquid flow in sudden expansion. In the last decade the researchers used nanofluid in their studies for increase augmentation of heat transfer. Study heat transfer to nanofluid flow in sudden expansion or over backward and forward-facing step is very limited for laminar range and most of those studies were numerical as well as turbulent range of nanofluid flow has not been investigated yet. The literature review presents that the main efforts for studying the separation flow were done in the late 1950's. All of these efforts were performed experimentally using many flow visualization techniques and deal exclusively with turbulent or laminar flows. This chapter covered most of investigations that studied heat transfer and pressure drop of separation flow with fluid and nanofluid in sudden expansion and backward facing step, also heat transfer and flow in annular pipe.

2.2 Heat transfer and flow through sudden expansion

Experimental and numerical studies which focused on heat transfer and pressure drop characteristics in sudden expansion consist of turbulent and laminar range with fluid and nanofluid. Those investigations have been divided to:

2.2.1 Laminar fluid flow

A. Experimental studies

The earliest investigations study of laminar flow in sudden expansion was carried out by Macango and Hung (Macagno, 1967). The obtained results presented the streamlines and vorticiy contour as functions of the Reynolds number. Also they analyzed the dynamic

interaction found between the main flow and captive eddy. Durst et al., (1974) have experimental study of flow visualtion and laser –anemometry measurements in the flow downstream of a plan 3:1 symmetric expansion in a duct with an aspect ratio of 9.2:1 downstream of the expansion. The flow was found to be markedly dependent on Reynolds number, and strongly three dimensional even well away from the channel corners expect at the lowest measurable velocities. The measurements at a Reynolds number of 56 indicated that the separations regions behind each step were equal length. Symmetric velocity profiles existed from the expansion to a fully developed parabolic profile for downstream although there were substantial three dimensional effects in the vicinity of the separation regions. Also the velocity profiles were in good agreement with those obtained by solving the two –dimensional momentum equation. At a Reynolds number 114, the two separations regions were different length, leading to asymmetric velocity profiles and at Reynolds number 252, third separation zone was found on one wall, downstream of the smaller of the two separation zones adjacent to the steps.

Afshin and Peter (2009) have experimentally studied laminar water flow through confined annular channel with sudden expansion. They used particle image velocimetry (PIV) and refractive index matching (RIM) to measure velocity and length of separation where they showed increase in separation regions with increase of Reynolds number and as shown Figures (2.2,2.3,2.4) also they obtained good agreement with numerical result reported by Nag and Datta (2007).

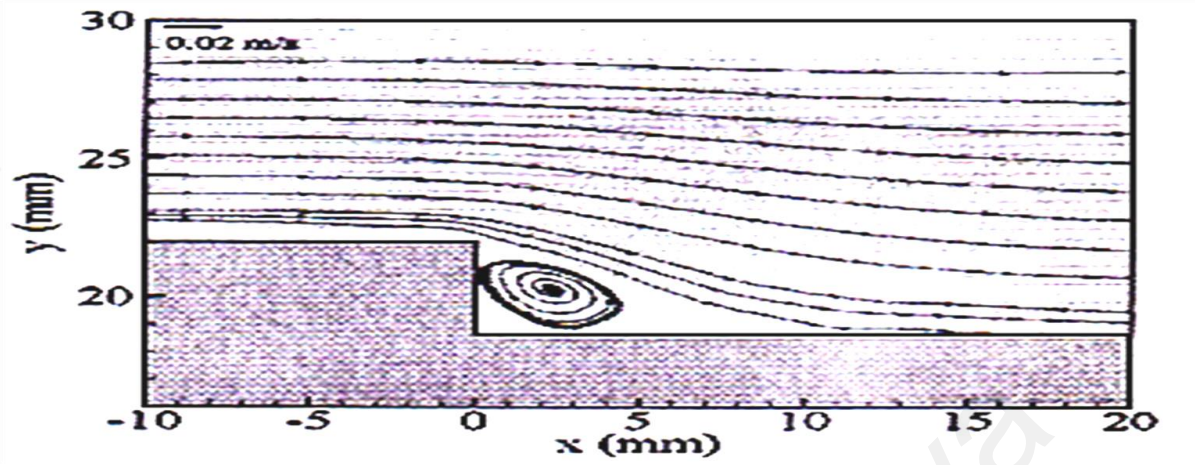

Figure 2.2: Measurements of velocity flow field at Re= 100, Afshin and Peter (2009).

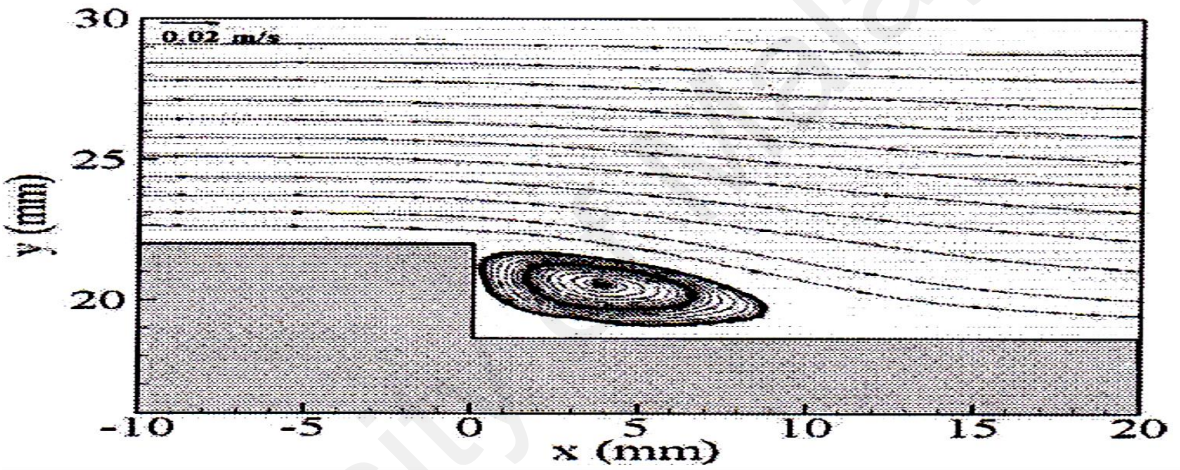

Figure 2.3: Measurements of velocity flow field at Re= 300, Afshin and Peter (2009).

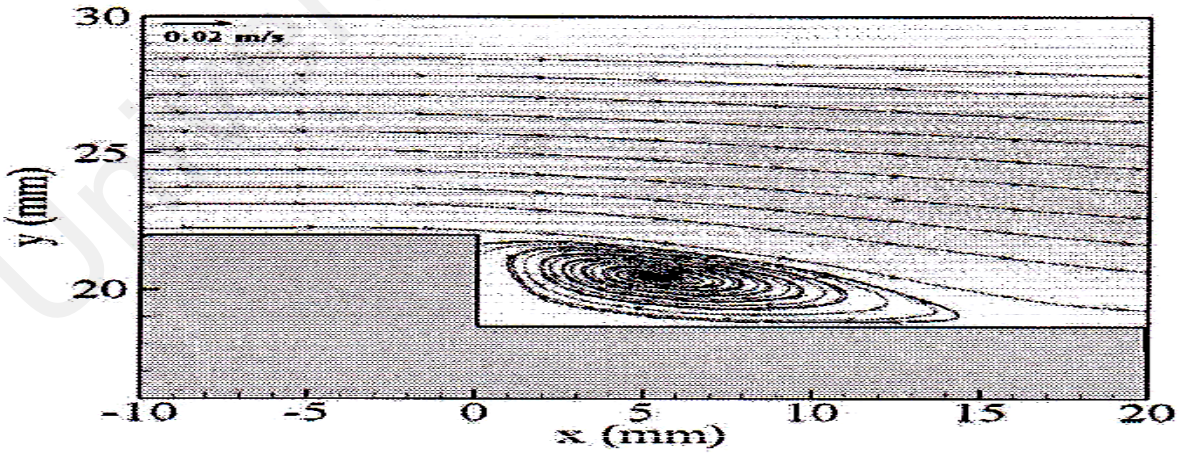

Figure 2.4: Measurements of velocity flow field at Re= 500, Afshin and Peter (2009).

B. Numerical studies

Guo et al., (1996) conducted numerical study of effect of heating on corner recirculation zone (CRZ) in sudden expansion with gas flow. They noticed decrease length of corner recirculation zone as increase heating gas flow in sudden expansion. Oliverira and Pinho, (1997) have numerical study of pressure drop coefficient of laminar Newtonian flow through sudden expansion by using finite volume method based second order differencing scheme. The numerical results indicate to decrease of local loss coefficient with increase Reynolds number between 1 to 225 also found correlation for local loss coefficient could be represented by equation 2.1.

$$C_I = \frac{19.2}{Re^{0.93}} - 2.55 + 2.87\, log\, Re - 0.542(log\, Re)^2 \qquad (2.1)$$

Chiang et al. (2000) have computational investigation of study of effect side wall on structure laminar incompressible fluid flow over a plane symmetric sudden expansion. In their analysis 14 aspect ratios used and were varied from 3 to 48, and Re=60 for three dimensional analysis and Re=60 and 140 for two dimensional analysis. The numerical results given a good agreement with experimental results conducted by (Fearn et al. 1990) where the previous experimental results indicated the symmetric flow occurred as Re= 26 while asymmetric flow happened as Re up to 36. Numerical simulations on viscoelastic liquids flow in symmetric sudden expansion reported by (Oliveira, 2003). The constitutive model follows FENE-MCR employed in this simulation as three meshes with different size cell and the range of Reynolds number from 0 to 100 and expansion ratio 1:3. Due to asymmetric vortex shapes a pitch-fork type bifurcation take place beyond the critical Reynolds number (Rec=64) while occurred as (Rec=54) with Newtonian fluid in the same

expansion ratio. Hammad et al. (2001) performed numerical study of laminar flow of non-Newtonian Herschel Bulkley fluid through axisymmetric sudden expansion. They used finite difference method for solve governing fully –elliptic momentum and continuity equations and get the regime of laminar flow for a range of yields numbers , Reynolds number, and power –law index values where the range of Re varied between 50 to 200, yield number varied between 0 to 2, and power- law index values between 0.6 to 1.2. They obtained significant dependence of the flow as the large values of yield number only while at lower yield number the power law index value become effect with yield number on flow field. They also found good agreement for reattachment length in comparison with (K.J, 1998) and available experimental results. While (Miranda et al. 2003) studied numerically of local loss coefficient for inelastic laminar fluids flow in axisymmetric sudden expansion by using finite volume method and the used sudden expansion varied the 1 to 2.6.They showed the local loss coefficient varied inverse with Reynolds number at low Re.

Boughamoura et al., (2003) presented numerical study of heat transfer and laminar flow of a piston driven in a cylinder with sudden expansion. The finite element method used with simpler algorithm of pressure –velocity coupling, and staggered and moved grid. The numerical results showed a good agreement with pervious experimental data where increase of expansion ratio lead to decrease recirculating zone of the step plane and they noticed there are three regions created by moved the piston with sudden expansion namely primary vortex, secondary positive vortex, and secondary negative vortex. Pinho et al. (2003) have numerical studied of pressure losses of laminar non Newtonian flow in sudden expansion having diameter ratio 1 to 2.6. They used power law model to found irreversible pressure losses coefficient by equation 2.2.

$$C_I = \frac{\Delta P_I}{\frac{1}{2}\rho U_1^2} = \frac{\Delta P - \Delta P_R - \Delta P_F}{\frac{1}{2}\rho U_1^2} \quad (2.2)$$

The numerical results revealed to decrease separation length with shear thinning and showed the variation of separation length linear at high Reynolds number and become asymptote to constant value as creeping flow condition.

Thiruvengadam et al. (2009) adopted investigations on study three dimensional mixed convections in vertical duct with sudden expansion. The effects of aspect ratio, heat flux, and buoyancy force on the laminar flow in separated regions were presented in their studies. The results obtained appear sharp increase in recirculation regions with increase Nusselt number and aspect ratio as shown in Figure 2.5 and linear increasing of streamwise distribution and independent aspect ratio after recirculation region as shown in Figure 2.6.

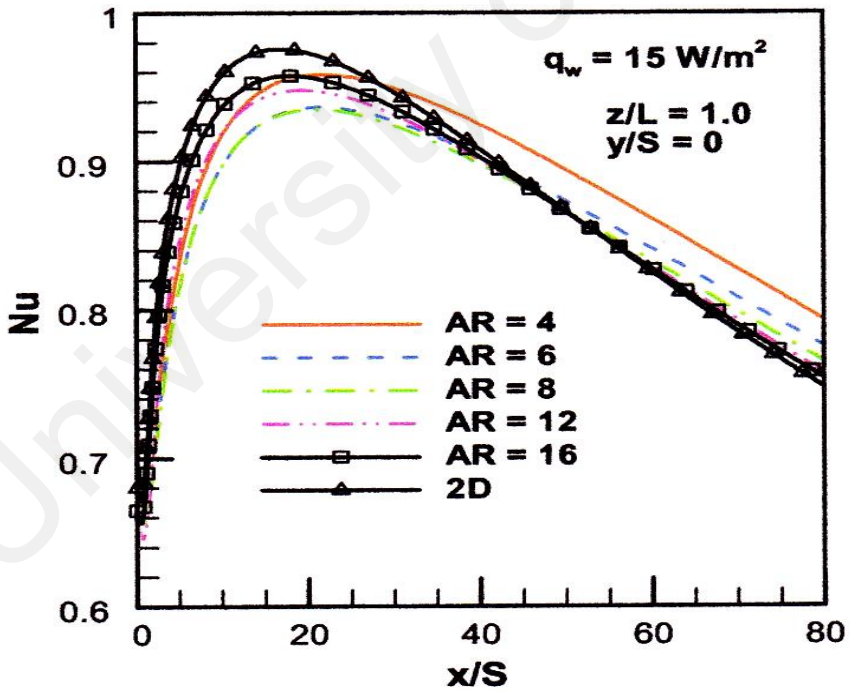

Figure 2.5: Distribution of local Nusselt number with aspect ratio, Thiruvengadam et al. (2009).

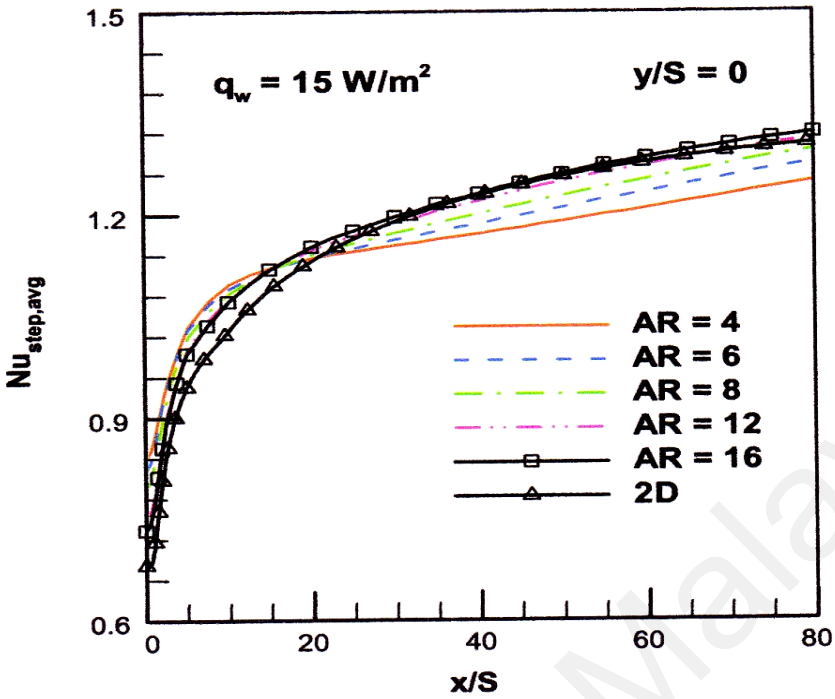

Figure 2.6: Distribution of streamwise of the average Nusselt number with aspect ratio, Thiruvengadam et al. (2009).

2.2.2 Turbulent fluid flow

A. Experimental studies

Boelter et al. (1948) presented results of investigations conducted to observe the distributions of the heat transfer rate of air flowing in a circular pipe in the separated and reattached regions downstream of an orifice. The investigation was performed in Re range of 17,000 to 26,400 and the test pipe having 2 inch outside and 1.78 inch inside diameters respectively. They used various entrance sections which makes variation of point of reattachment at entrance pipe. From the experimental data obtained, they found maximum heat transfer coefficient near the point of reattachment which is about four times away of the length of fully developed flow.

Ede et al. (1956b) have investigated the effect of an abrupt convergence of straight pipe on the local heat-transfer coefficient for flowing water. The experimental covered for Reynolds numbers from 800 to 100,000 corresponding to a smaller pipe of diameter 1 inch. The pipe was heated through the longitudinal passage with intense direct current during the wall. They have observed comparatively small disparity in local heat transfer coefficient. It does not differ significantly with the variation created in the entrance regions of pipes under more normal entry conditions. They also determined effect of an abrupt divergence at Reynolds numbers from 3,700 to 45,000 and they observed a considerable variation in local heat transfer coefficient.

Krall and Sparrow, (1996) conducted experiments to determine the effect of flow separation on the heat transfer characteristics of a turbulent pipe flow. The water flow separation was drive by an orifice situated at the inlet of an electrically heated circular tube. The degree of flow separation was varied by employing orifices of various bore diameters. The Reynolds and Prandtl numbers were varied from 1000 to 130000 and from 3 to 6 respectively and ratios of the orifice to the tube diameter ranged from 2/3 to 1/4. Results show that the augment of the heat transfer coefficient due to flow separation accentuated with the decrease of Reynolds number. They have also found the effect of expansion ratio on the distribution temperature. The point of flow reattachment, which corresponds to maximum value of the heat transfer coefficient, was found to occur from 1.25 to 2.5 pipe diameter from the onset of flow separation. Suzuki et al., (1982) performed experiment to study heat transfer and visulation of flow and surface temperature in the recirculating flow of an orifice in tube where they obtained results agree with (Krall and Sparrow, 1966).

Koram and Sparrow, (1978) had performed experimental study of turbulent heat transfer of water flowing in circular pipe with unsymmetrical blockage (segmental orifice plate) for range of Reynolds number from 10,000 to 60,000. They determined heat transfer coefficients around the circumferential and along of heated tube then show increase Nusselt number value to reach maximum and after that decrease toward the fully develop region.

Filetti and Kays, (1967) presented experimental study on separation flow and heat transfer through flat duct with double step. They showed the highest heat transfer occurs in both long and short stall on sides at the point of reattachment, followed by decay towards the achievement of fully developed duct flow also they observed at different distances on the two walls of the duct the boundary-layer reattachment occurred and these distances are independent of Reynolds numbers. Again the long and short stalls can be moved to the opposite walls by use of a vane well upstream of the separation point. Also Seki et al. (1976a, 1976b) performed experimental study on effect stall length and turbulent fluctuations on turbulent heat transfer for separation flow behind double step at entrance flat duct.

Zemanick and Dougall, (1970) carried out experimental study of heat transfer to fluid flow in abrupt expansion of circular channel. Three expansions maintained during the test ratios of upstream –to- downstream diameter of magnitudes 0.43, 0.54 and 0.82 were considered with air as the working fluid. They have presented data for Reynolds numbers from 4000 - 90000, corresponding to the geometry of the ducting. For the range of the Reynolds numbers and expansion ratios studied, the following conclusions could be drawn from the test data:

1-The flow beyond an abrupt expansion in a circular duct shows a significant augmentation (over the fully developed value) of the average convective heat transfer coefficient in the separated flow region.

2-The degree of heat transfer coefficient enhancement increase with the increase of diameter ratio.

3-The location of highest heat transfer moves downstream as the ratio of downstream to upstream diameter increases.

4-The peak Nusselt number observed an apparent dependence on upstream.

5-In the Nu-Re expression, the Reynolds number exponent raised to a magnitude of approximately 2/3. The equation (2.3) reasonably represents the maximum Nusselt number data of all three geometries tested:

$$\mathrm{Nu}_{\max} = 0.20\mathrm{Re}_{\mathrm{d}}{}^{0.667} \qquad (2.3)$$

Smyth (1974) conducted experiments to study of the physical effects of separation and the associated reattachment and redevelopment, on the heat transfer characteristics of turbulent flow in pipes and to compare the results of these flow conditions with the fully developed one-dimensional flow condition. He also compared results with a recently developed numerical technique for the solution of recirculation flows. Separation of the flow was induced in a 4 ft length of 2 in. internal diameter tube of wall thickness 0.001 in. by means of a sudden enlargement of diameter at the entry of the tube. The tube was electrically heated by the passage of a current along its length. The first 25 in. of the tube was monitored by thermocouples which gave the wall temperatures and from these the

local heat transfer rates were measured at Reynolds numbers up to 5 x 10^4 using air as the working fluid. He found modest agreement at points near the peak of Nusselt number but greatly poorer agreement in the developed region after reattachment of the flow. Baughn et al. (1984) presented experimental study of the local heat transfer coefficient to an air flow downstream of an axisymmetric abrupt expansion in a circular channel with constant heat flux. They used a range of expansion ratios (d/D), small diameter to large diameter of 0.266 to 0.800 over the Reynolds number range of 5,300 to 87,000. From the experimental data obtained for all expansion ratios, the value of Nu/NuDB falls monotonically for d/D= 0.266 with the increase of Reynolds number as shown in Figure 2.7. This behavior is qualitatively satisfying the water tests (24) but differs with the out come of air study (Zemanick, 1970) for downstream Reynolds numbers above 30,000, where the ratio of peak to fully developed Nusselt numbers became independent of Re. Further details, they have obtained the Reynolds number dependency on the maximum Nusselt number compared to the equation suggested by (Zemanick, 1970) using Red instead of ReD in order to find the effect of expansion ratios on the Nusselt number. Also (Runchal, 1976), Baughn et al.(Baughn, 1989, 1987a-a, 1987a-b, 1984), Iguchi and Sugiyama (Iguchi, 1988), and Habib et al. (1992) have investigated effects of Schmidt numbers, Reynolds number, expansion ratio, velocity, segmented baffles, baffle spacing, baffle material and heat flux on the local heat transfer coefficient where they obtained on the augmentations of heat transfer.

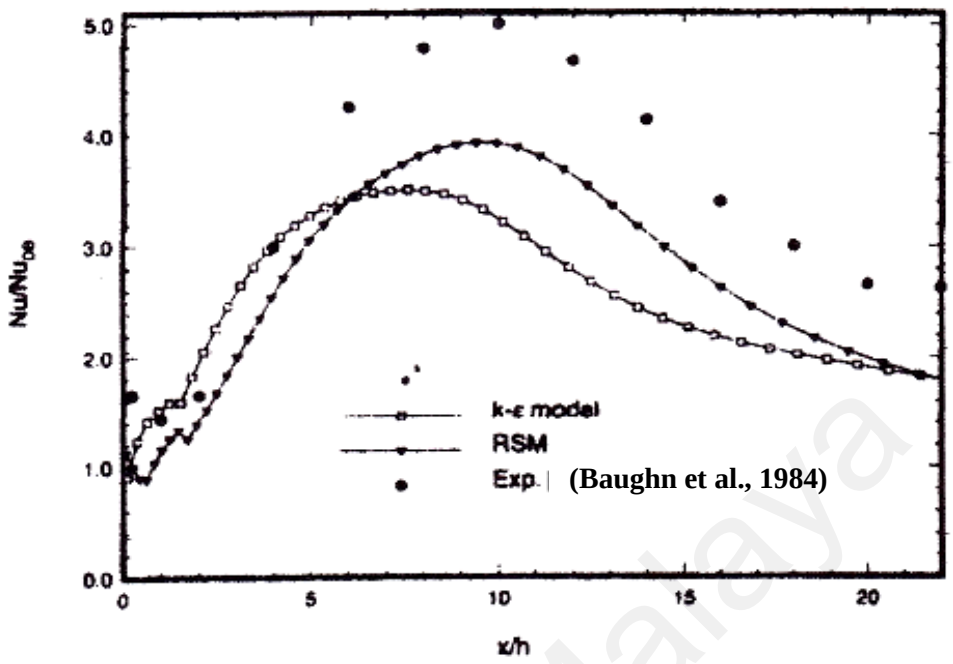

Figure 2.7: Nu distribution by predictions with Re stress model, k-ϵ model and experiment by (Baughn et al., 1984).

Khezzar et al. (1999) performed experiments to study the combustion of premixed fuel and air downstream of a plane sudden-expansion. They used an area expansion ratio of 2.86 and a Reynolds number of 20,000, and the combusting flows comprised of premixed methane and air over a range of equivalence ratios with emphasis on values of 0.72 and 0.92. The results showed that the degree of asymmetry of the isothermal flows was decreased by pairing the pressures between the two recirculation regions, and by striking oscillations at the half-wave or full-wave frequency of the duct, and by combustion. Periodic variations of velocities, acceleration, temperature and flame shape were showed in understanding with the main pressure fluctuation of rough combustion, and the length of the recirculation zones varied from less than 0.5 to 3 steps and those results confirmed the experimental data reported by (De Zilwa S.R., 1997).

Yang & Tsai, (1996) carried out experimental study of heat transfer from a hot stream flowing during a sudden expansion where cold air injected from its porous base. The combustor entrance used have 30 mm high and 200 mm wide and the aspect ratio (channel width to step height) for the step height (15mm) was 13.3. The results indicated, increase in the length of recirculation zone about 7.8 times of the step height when the Reynolds number go over 6300 so that the length of recirculation zone was in the same variety in comparison with Tsou et al. (1991), and Soong and Hsueh (1993). They have also reported that by decreasing the temperatures in the recirculation zone obtain from cooling effects of the injected fluid were more considerable in the recirculation zone than other regions due to the velocity in that region was much smaller than the measured velocity in the free stream and the redeveloped boundary layer. On the other hand they have found that the maximum and average Nusselt numbers were larger in a higher Reynolds number.

Park & Ota, (2010) presented experimental results on study of turbulent separation flow and heat transfer in a symmetric expansion plane channel. The step used was 20 mm high and 200mm wide and the Reynolds number maintained from 5,000 to 35,000. From the experimental measurements of the mean and turbulent fluctuation of temperatures and velocities, they obtained that local Nusselt number profile was significantly different at the lower and upper walls result the Coanda effect caused by instability between the lower and upper separated shear layers. These results show relevant agreement with Ohori-Yuki et al. (2004). In this study (Park & Ota, 2010) they used the empirical formulas (2.4, 2.5) and obtained the difference between heat transfer from the lower and upper walls which increased with an increase in Re and reached up to about 45%.

$$Nu_{max} = 0.079(U_{ref}\frac{H}{\upsilon})^{0.071}(\text{Upper wall}) \quad (2.4)$$

$$Nu_{max} = 0.053(U_{ref}\frac{H}{\upsilon})^{0.0712}(\text{lower wall}) \quad (2.5)$$

Lee et al., (2011) performed numerical and experimental study of heat transfer at axisymmetric sudden expansion followed by an sudden contraction called (cavity) in a circular channel with uniform wall temperature. The experimental results revealed that the maximum Nusselt numbers appeared between 9 and 12 step heights from expansion step. They also obtained a good agreement with numerical results evaluated by using equation (2.6) for local Nusselt numbers.

$$Nu(x) = \frac{h(x)D}{k_a} = \frac{V_s^2 D}{[A_s(T_s(x) - T_b(x))K_a R_s]} \quad (2.6)$$

Hussein et al., (2011) carried out experimental study of turbulent heat transfer and separated flow in annular passage. They found of effect separation flow on the average and local convective heat transfer and observed augmentation of local heat transfer coefficient occurred with increase heat flux and or Re while step height effect was clear at separation region and obtained increase in the local heat transfer coefficient with increase of step height.

B. Numerical studies

Numerous studies have adopted various models for analysis of heat transfer in separated flow with sudden expansion and compared the obtained results with experimental

data or with other numerical results. Chieng & Launder, (1980) performed numerical study of turbulent heat transfer and flow in separation region with an abrupt pipe expansion by using standard k-ε model thus they obtained a good agreement with experimental data performed by (Zemanick and Dougall, 1970).

Gooray et al. (1985) presented numerical calculations for heat transfer in recirculation flow over two dimensional, rearward- facing steps and sudden pipe expansions by using the standard k-ϵ model and low-Reynolds number k-ϵ model. In this study the Reynolds number range covered from 500-10,000. They applied turbulent modeling and computational procedures describing the two dimensional back-step and pipe expansion geometries, where the results obtained could be compared with the experimental data of (Zemanick and Dougall, 1970), (Aung and Goldstein, 1972), and (Sparrow and O'Brien, 1985), and with experimental fluid dynamic data of (Moss and Baker. 1980), and (Eaton and Johnston, 1980). The investigations considered have confirmed the improved k-ϵ procedure capable of providing an insight into complex phenomena having turbulent separated and reattachment flow with heat transfer.

Habib et al. (1988) performed numerical study on effect of Reynolds and Prandtl numbers, element spacing and length in channels with streamwise periodic flow on heat transfer and turbulent flow by using k-ε turbulence model and wall functions for high Reynolds number based on a finite-control-volume method to solve the time-averaged conservation equations of mass, momentum, and energy. They showed augmentation of heat transfer due to increase of Reyonlds number and element height and decrease of baffle spacing. They have also obtained a good agreement with experimental data as reported by (Habib et al., 1984) and (Berner et al., 1984). Kwang and Yong, (1994) carried out prediction study of turbulent flow and heat transfer characteristics at downstream of a

sudden circular pipe expansion by using the full Reynolds stress model. They adopted finite volume method with power-law scheme to discrete the governing differential equations. The full Reynolds stress model has considered the precise conditions taken from experimental data especially for dissipation rate of turbulence kinetic energy and remarkably improved the results, but the wall reflection model of pressure-scrambling term in turbulent thermal flux equations does not affect the results. The results with Reynolds stress model are much better than k-ϵ model in the predictions of velocity and temperature fields as well as the heat transfer coefficients

Chung and Jia (1995) studied numerically turbulent heat transfer from abrupt expansion by using new K-ϵ model then they showed augmentations in calculated turbulent kinetic energy and velocity and they also found good agreement with previous experimental data further (Hsieh and Chang, 1996) performed numerical study of calculation of wall heat transfer in pipe expansion turbulent flows by applying a new modified low-Reynolds number k-ϵ turbulence [Chang, Hsieh and Chen (CHC)] model. The objective of this study was to compare the performance of nine other conventional low-Reynolds number k-ϵ models developed earlier by of Launder and Sharma (B.E. Launder, 1974), (Lam and Bremhorst, 1981a), (Chien, 1982), (Nagano and Hishida, 1987), (Myong and Kasagi, 1990), (Nagano and Tagawa, 1990), (Yang and Shih, 1993), (Abe et al., 1994), and (KC Chang et al., 1995). They selected two experimental studies of ax-symmetrical, non-isothermal sudden expansion flows, one is the case with uniform wall temperature condition performed by (Baughn et al., 1989) and the second with uniform wall heat flux condition performed by (Zemanick and Dougall, 1970). From comparisons of the predicted distributions of the Nusselt number obtained through the low- Reynolds number k-ϵ models

with data of (Baughn et al., 1989) and (Zemanick and Dougall, 1970). only CHC model generates correct trend.

Said and Habib, (2003) carried out numerical investigation on the flow and heat transfer characteristics of pulsating turbulent flow in an abrupt pipe expansion. They classified flow patterns by four parameters; the Reynolds number, the Prandtl number, the abrupt expansion ratio and the pulsation frequency. In this study they obtain the influence of these parameters on the flow and heat transfer in separation region. Boughammoura and Nasrallah, (2003) presented numerical study on effect of piston drive on turbulent flow and heat transfer in a pipe with sudden expansion by using numerical method depending on control volume based finite element method with incompressible flow and a staggered and moving grid. In their numerical studies they used different values of the piston velocity, expansion ratio, and the initial clearance volume, where they have shown a good agreement between the numerical results and previous experimental data.

For the large eddy simulation (LES) method, Sugawara et al., (2004, 2005) applied LES to analyze numerically, three dimensional turbulent heat transfers and separated flow in a symmetric expansion plane channel. They used smagorinsky model and fundamental equations based the finite difference method, where the numerical results agree with previous experimental data. Several researches are concerned, to the numerical simulation for three dimensional heat transfer and separated flow in sudden expansion rectangular channel. For unsteady flow, represented by (Yoshikawa et al., 2002), and steady separated flow reported by (Yoshikawa et al., 2004), both of them employed Navier-Stokes equations and energy one based on finite difference method. They found due to increase of Reynolds

number the recirculation region and separated shear layer becomes unstable and they also showed the vortices created have significant by greater influence on the heat transfer rate. While (Ota et al., 2002) presented numerical study of two and three dimensional heat transfer and separated flow in enlarged channel by using Navier-Stokes equations and energy one based on finite difference method. They showed that the effect aspect ratio in both results of two and three dimensional on local heat transfer rate and the transitions from symmetric to asymmetric flow due to increase of the aspect ratio.

Terekhov and Bogatko, (2008) presented investigations of the effect of boundary layer thickness before the flow separation on aerodynamic characteristic and heat transfer behind an abrupt expansion in a round tube. They used menter turbulence model of shear stress transfer in fluent program for calculations and found decrease of maximum heat transfer coefficient due to increase of boundary layer thickness. While (Terekhov & Pakhomov, 2009) performed predictions of turbulent flow and heat transfer in gas droplets-laden turbulent flow at downstream of a sudden pipe expansion by using Euler/Euler two-fluid model for the gaseous and dispersed phases. They observed increase of heat transfer in separated flow by the addition of evaporating droplets which is more than two fold compared to one-phase flow at the mass concentration of droplets $ML1 \leq 0.05$ and also it experiences increase in reattachment length of dispersed phase in turbulent gas flow. An increase in the initial droplet diameter decreases the Nusselt number due to reduction of interphase contact area at a fixed mass concentration of droplets. Results obtained can be compared with previously reported experimental and numerical data for sudden expansion of two-phase flow through round pipes and plane flows passed through a backward-facing step.

2.2.3 Laminar nanofluid flow

A. Experimental studies

From the literature survey the laminar nanofluid flow though sudden expansion has not been investigated yet experimentally.

B. Numerical studies

The study of laminar of nanofluid flow in sudden expansion is very limited and appears only with (Santosh Christopher et al., 2012) where preformed numerical study on laminar Al_2O_3, Ag, Cu, SiO_2, and CuO nanofluid flow in sudden expansion. They used same method (Kanna & Das, 2006) for solve sudden expansion flow and backward facing flow with Reynolds number from 30 to 150 and volume fraction 0.1, 0.2, 0.5. The result obtained that decrease in reattachment length about1.3% as comparison with (Abu-Nada, 2008) as shown in Figure 2.8.

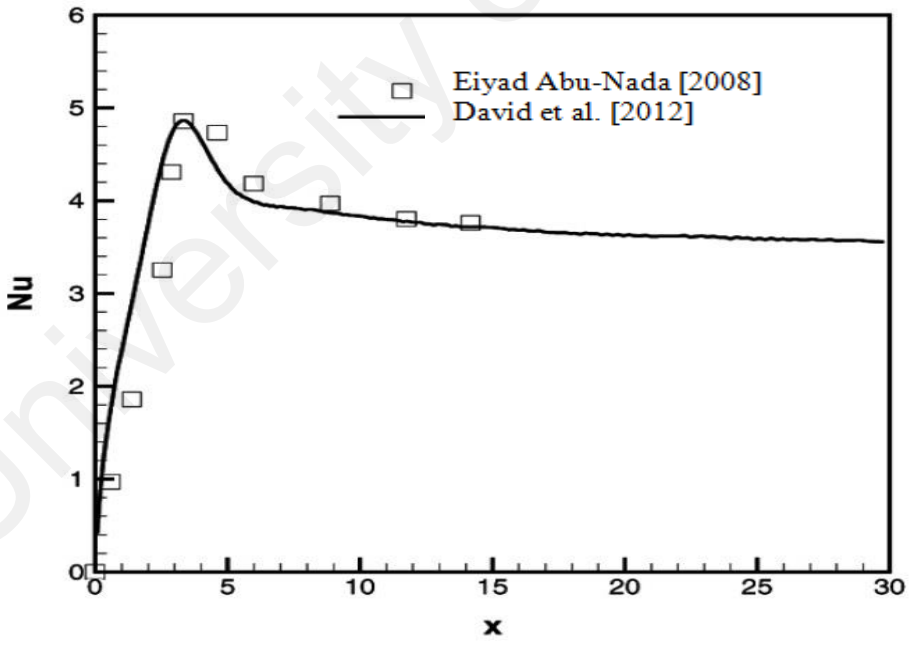

Figure 2.8: Comparison of Nusselt number for SiO2 at Re= 100, Christopher et al. (2012).

2.2.4 Turbulent nanofluid flow

A. Experimental studies

The study of turbulent of nanofluid flow in sudden expansion has not been investigated yet experimentally.

B. Numerical studies

Rahimi-Esbo et al., (2012) conducted numerical study of two dimensional force convection of turbulent nanofluid flow in converging duct. The simulations carried out with the range of Reynolds number from 4000 to 40,000 and the volume fractions from 1% to 5%, and aspect ratio from 1, 2,5,10 and 10. Governing equations solved by finite volume method and the Rhie and Chow interpolation for a collocated mesh. The results obtained leads to enhancement of Nusselt number at increase Reynolds number, aspect ratio, and volume friction.

2.3 Flow over a backward and forward-facing step

Backward and forward-facing step is one of configuration which separation flow found due to graduate pressure drop. This section also divided depends on experimental and numerical studies of turbulent and laminar heat transfer by using fluid and nanofluid.

2.3.1 Laminar fluid flow

A. Experimental studies

Armaly et al., (1983) conducted experimentally and theoretically two dimensional on effect Reynolds number on reattachment length flow downstream of a backward facing step in a rectangular channel by using laser Doppler measurement where the range of Reynolds varied between 70 to 8000 and aspect ratio 1:36. The experimental result obtained agrees

with data predicted that those results leads to increase reattachment length with increase Reynolds number.

Barton, (1997) used model particle phase with Eulerian-Lagrangian for study laminar flows over backward facing step with stream of hot particle. He focused in his investigation on effect heat transfer and thermal characteristic on recirculation regions and he noticed the streamlines in the separation region were 10 times smaller than the streamlines in the free flow. Lee & Mateescu, (1998) have experimental and numerical study two dimensional air flows over backward facing step. They measured lengths of separation and reattachment on lower and upper of duct by using hot wire probe with expansion ratio 1.17 and 2 and Re below 3000. The numerical and experimental results agree with previous experimental for separation and reattachment length and locations on the lower and upper wall of the duct.

Stüer et al., (1999) presented experimental study of laminar separation flow on forward facing step by using particle tracking velocimetry to get more information about separation phenomena. The experimental results obtained increase distance between the breakthroughs in span at decrease Reynolds number and they also noticed the transverse direction of separation was slowly in compared with short time scale over.

Armaly et al., (2003) adopted experimental measurements of velocity in three dimensional laminar separated flows on backward facing step by using two components laser Doppler velocimeter where expansion ratio 2.02 and the range of Reynolds number from 98.5 to 525. They showed increase size recirculation regions with increase Reynolds number and

the maximum locations of streamwise velocity line component (u) is zero at the stepped wall with constant Reynolds number happened as the sidewall.

B. Numerical studies

Neary & Sotiropoulos, (1996) carried out numerical study of incompressible laminar flow through 90 degree diversions rectangular cross section. In their investigations provide new data and compared those results with previous experimental data and analysis studies that adopted circular channel and rectangular channel where they showed at increase aspect ratio of duct the distance between top and bottom of symmetry plane effect on flow. Rouizi et al., (2009) investigated numerical study of two dimensional incompressible laminar flows over backward facing step. They employed model reduction and identification technique with finite element method where noticed as increase model order the accuracy increased also they showed validated the length of recirculation bubble with used identified reduced order model and obtained good agreement with previous studies.

Barbosa et al., (2005) have numerical study of three dimensional of mixed laminar air flow over horizontal backward step by using finite volume method. The bottom wall of channel heated with constant temperature and the other walls adiabatic, the aspect ratio equal 4 and range of Richardson number (Ri) varied between 0 to 3. The numerical results indicated the decrease of size primary recirculation region with increase Richardson number and also moved the maximum value of average Nusselt number. Li and Armaly, (2000) presented numerical study of laminar mixed convection in 3D backward facing step where solved the fill elliptic 3 coupled governing equation with using finite volume method. They found effect buoyancy force and temperature on reattachment length.

Lima et al., (2008) investigated numerically study of two dimension laminar air flows over backward facing step by using two CFD commercial codes the first one based on finite element method (COMSOL MULTIPHYSICS) and the other finite volume method (FLUENT) and the range of Reynolds number. The numerical results agree with previous experimental data and those result also appeared there are non-linear increase in reattachment length.

Velazquez et al., (2008) presented study of enhancements of heat transfer for laminar flow over a backward facing step by using pulsating flow. They showed at Re= 100 the maximum time average of Nusselt number was 55% higher in comparison with steady case and this increment represented augmentation of heat transfer.

2.3.2 Turbulent fluid flow

A. Experimental studies

R. A. Seban, (1959) studied experimentally heat transfer in the separated, reattached, and redeveloping flow regions around the downward facing step. They found that the heat transfer coefficient reached a highest value at the reattachment point, and after that decreases. To demonstrate the relative effect of the suction and injection, R. A. Seban, (1966) investigated experimentally the heat transfer and fluid flow in a separated region downstream of a backward facing step for fixed rates of suction and injection through a slot at the base of the step, with air velocities in the free stream varied in the range from 15 to 45 m/s. The apparatus was constructed providing a top wall of rectangular duct as test surface of the cross section 117.5 mm height by 300 mm width having a plate of 300 mm wide and 457.5 mm long at its forward edge a 5 mm slot providing a tangential inlet for

injected flow. The slot was surmounted by a 25 mm step making the total step height at this location 30 mm .With fixed suction , the length of the separated region decreases as the free–stream velocity is reduced and the maximum value of the group (h/k) (υ/Ua) 0.8 is also increased. With injection, there is no region of separated flow at the wall when the free–stream velocity is of the same order of the injection velocity and the local heat transfer is at first influenced primarily by the injection velocity.

Sogin, (1964) performed experiments on a bluff flat plate stripe in two dimensional flows. It was instrumented to measure local heat flux and temperature distribution under steady–state conditions. Different configurations were obtained by changing angle of incidence or modifying its cross–sectional profile. Air speed ranged from 12 m/s to 47.5 m/s and the Reynolds number based on 170 mm chord length ranged from 100000- 440000. The nominal blockage ratio was (0.21) when the angle of incidence was 90 degree. The local heat transfer by forced convection from the base surface of a bluff obstacle presented for a variety of configuration. The data were satisfactorily represented by equation of type (2.7).

$$\mathrm{Nu} = \mathrm{C}.\,\mathrm{Re}^{0.667} \qquad (2.7)$$

The coefficient (C) of equation (5) depends upon the configuration and the location. Its value was formally 0.2 on the rear of flat plate strip at 90 degrees angle of attack. It diminishes wherever any device can come close to the dead air space, or reduce its size. Results concluded that the device which increased the size of or open the dead air region had increased the heat transfer and those which reduced confinement had also reduced the

heat transfer. Habib et al., (1994) also presented experimental study of turbulent flow and heat transfer over baffles of different heights staggered in rectangular duct.

Mabuchi et al.,(1986) studied effect of free stream turbulence on heat transfer in the reattachment region on the bottom surface of a backward facing step (for different angles of separation) also Suzuki et al. (1991) have studies of effects of cylinder mounted near the top corner of the step, while Ota et al., (1995) performed investigation to observe the effect of inclined downstream step on turbulent separated and reattached flow, and (Oyakawa et al., 1996) made estimate of thermal performance on heat transfer improvement by passive and active methods at downstream region of backward-facing step. The effect of the step height on the turbulent mixed convection flows over a backward-facing step reported by (Abu-Mulaweh et al., 2002). (Abu-Mulaweh, 2002) studied effects of backward and forward facing steps on turbulent natural convection flow along a vertical flat plate where they showed that the highest local Nusselt number occurred at the reattachment region.

Vogel and Eaton, (1985) studied combined fluid dynamic and heat transfer measurements in separated and reattaching boundary layer, with emphasis on the near – wall region. A constant heat flux surface behind a single sided sudden expansion to flow was made to obtain Stanton number profiles as a function of Reynolds number and boundary layer thickness at the separation region at Reynolds number ranged from 13000 to 42000 with the expansion ratio 1.25. Investigation considering Reynolds analogy to determine heat transfer coefficient using the local skin friction, revealed that the reattachment causes a local augmentation of the heat transfer coefficient, so it recovers fairly and rapidly the flat plate behavior at the downstream of reattachment. Well

downstream of reattachment, the near wall layer behaves like that under an ordinary turbulent boundary layer. Results also showed that the peak in the Stanton number around reattachment varies as the (- 0.4) power of the Reynolds number ($Nud \times Re^{0.6}$), while for the flow over flat plate, Stanton number varies as the (- 0.2) power of Reynolds number ($Nud \times Re^{0.8}$).

For measuring details of the heat transfer near the reattached point of the separated flows, Mori et al., (1986) used the thermal tuft probe while (Kawamura et al. 1991) designed new heat flux probe to determine time and spatial characteristics of heat transfer at the reattachment region of a two dimensional backward facing step deign. Oyakawa et al.(1994, 1995) also used jet discharge at reattachment region downstream of backward facing step. While Tsou et al. (1991) carried out experimental study of the starting of heat transfer at downstream of a backward-facing step by using a Ludwieg tube wind tunnel to produce an incompressible flow.

Terekhov et al., (2003) reported experimental study of hydrodynamic characteristics of the gas flows past a rib and a downward step in feature separation flow regions, and distributions of temperatures, heat transfer coefficients and pressures behind the obstacles. They determined the effect of improved external turbulence on dynamic and thermal features of the separated flow and they also showed the results obtained agree with previous data for a downward step (Alemasov et al., 1989) where a 10-5% augmentation obtained at the maximum recirculation velocity. They have seen a decrease in the obstacle height results in a significant augmentation of the heat transfer and the maximum is located closer to the obstacle. For the flow with separation past a rib, the maximum heat transfer is

shifted also in the downstream direction from the flow separation point compared to the case of a downward step.

Abu-Mulaweh, (2005) studied experimentally the turbulent fluid flow and heat transfer of mixed convection boundary-layer of air flowing over an isothermal two-dimensional, vertical forward step. They studied the effect of forward–facing step heights on local Nusselt number distribution as shown in Figure 2.9, and obtained that the local Nusselt number increases with increasing step height and reaching a greatest value at the reattachment region. The present results indicated that the increase of step height leads to increase of intensity of temperature fluctuations, the reattachment length transverse velocity fluctuations and the turbulence intensity of the streamwise.

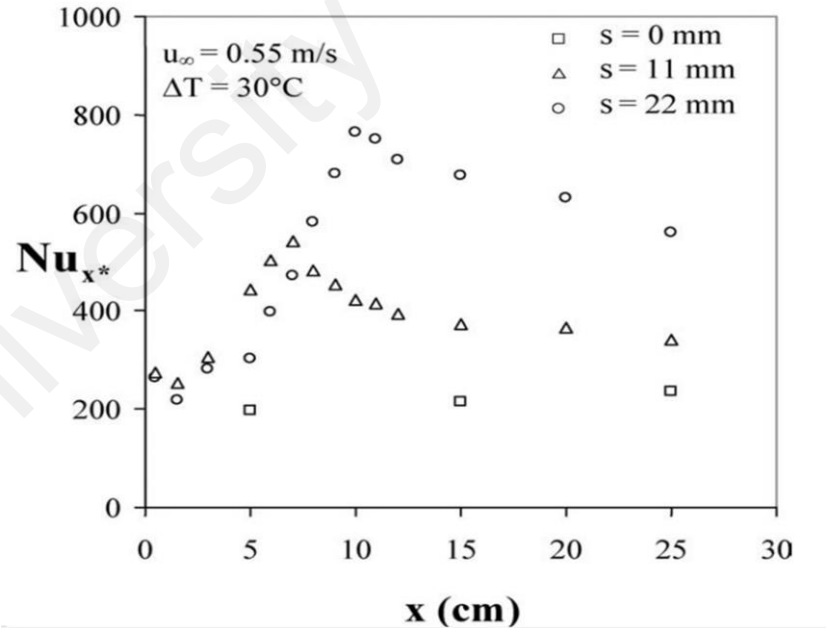

Figure 2.9: Local Nusselt number variation downstream of the step , Abu-Mulaweh (2005).

Sano Masatoshi et al., (2009) presented experimental results of the turbulent channel flow over a backward-facing step by using suction through a slit at the bottom corner of the step and the direction of the suction was perpendicular and horizontal to the main flow. They measured local heat transfer coefficient and wall static pressure behind the backward-facing step and the results indicated the enhancement of the heat transfer coefficient in the recirculating region by suction and reduction of the pressure drop. Also they observed improvement of the heat transfer coefficient occurred with the increase in turbulent energy.

B. Numerical studies

Abe et al., (1995) performed study on prediction of heat transfer and fluid flow in separation and reattachment over backward facing step by suggestion a new two equation of heat transfer model that obtained from developed model presented by Nagano et al. (1991). Thus they presented new model of latest low Reynolds number by using Kolmogorov velocity scale $u\varepsilon = (\nu\varepsilon)^{1/4}$ instead of the friction velocity uT.. After the modifications could predict heat transfer and fluid flow at downstream of backward facing step, while (Heyerichs & Pollard, 1996) used mathematical model with aid of the k-ϵ and k-w turbulence models to study heat transfer with both separated and impinging turbulent flow. They showed that the K-w model is more simple as numerical method to performed calculations of heat transfer in complex turbulent flows. All predication models were given reasonable results for the channel flow test case, wall functions have calculated Cf within ~ 2% accuracy and shown good agreement with the log law and temperature data of Kader (Kader, 1981). This result can be anticipated since they are derived on the basis of the log-

law and temperature log-law (Jayatilleke, 1969). All low Reynolds number models except LB predict Cf within 5%. When considered the low Reynolds number approach, there is a strong correlation between a models ability to predict the log-law, Cf and Nu. The models of LB (C.K.G. Lam, 1981b) and MK (H. K. Myong, 1990a) under predicted the log law, overestimate Cf and Nu. On the other hand, the models of CH (Hsieh & Chang, 1996), and LS (B.E. Launder, 1974) overestimate the log-law, under predict Cf and Nu. The WCP(W) Wolfshtein (Wolfshtein, 1969) and (CH) Chein et al. (KC Chang, 1995) model shows the best fit to the log-law and Nu as predicted within1% of the Dittus-Boelter correlation. When used the low Reynolds number approach, there is a strong correlation between a models ability to predict the log-law, Cf and Nu.

Finite volume methods to analyze turbulent heat transfer and separated flow such as has been reported elsewhere Zigh (Abdeleghani) presented computational study of simultaneous heat and mass transfer in turbulent separated flows. Finite volume numerical method used for the prediction and analysis of the flow over a cascade of turbine blades consists of three parts. The first part used finite volume algorithm in generalized body-fitted coordinates capable of handling turbulent separated flows with simultaneous heat and mass transfer. The second and main part involved the application of algorithm with the RNG based nonlinear K-ϵ model for the analysis of water based transpiration cooling for the turbine cascade. The third part was performed to analyze using a second-order accurate scheme. In this prediction the location of the maximum Nusselt number is better predicated by the RNG based nonlinear K-ϵ model and shows a good agreement with results of (Zemanick and Dougall, 1970).

Yin et al. (1992) performed numerical prediction of turbulent heat transfer in high Prandtl number fluids by using two equations turbulence model developed from model of

(Nagano and Kim, 1988) and comparison of numerical results with existing experimental data on water, aqueous ethylene glycol, and oil, where they obtained a good agreement with experimental data especially with data of water. Dutta and Archayra, (1993) performed comparative study on the standard K-t model, nonlinear k-ϵ turbulence model, and the modified k-ϵ turbulence model for analysis of heat transfer and flow past a back step, where they found the nonlinear k-ϵ and modified models agree batter with measurements than the standard K-t model. Furthermore Rhee & Sung, (1996) developed low Reynolds number kθ-εθ model that dealt with turbulent separated and heat transfer for flow field computations only presented by (Park & Sung, 1995) to predict the heat transfer in separated flows and they obtained satisfactory numerical results when compared with experimental data.

There are researchers applied a Large eddy simulation model for analysis turbulent heat transfer in separated flow over backward facing step where the pioneer researchers was represent by (Labbe et al., 2002), (Avancha & Pletcher, 2002), and (Mehrez et al., 2009; Zouhaier Mehrez et al., 2010). They showed significant improvement of heat transfer rate in the recirculation zone and obtained trends of heat transfer coefficients agreed to pervious experimental data.

For analysis heat transfer for flow over backward facing step and two dimensional jet entering across flow that presented by (Scherer and Wittig, 1991), where they compared experimental results with numerical results and obtained a good agreement between them. Yang and Huang, (1998) have numerically studied the heat transfer characteristics at downstream of a backward facing step by using jet discharge. They employed K-ε model and obtained predication reattachment point which is agree to experiment reattachment

point. While Tsay et al., (2005) performed numerical study on effect of baffle height, baffle thickness, and distance between backward facing step and baffle on temperature, Nusselt number, and flow structure. They found the maximum augmentation of Nusselt number about 190% for heating step and 150% for heating section of bottom plate.

There are several studies concerned three dimensional convective flow and heat transfer over backward facing step reported by (Nie & Armaly, 2002), (Carrington and Pepper, 2002), and (J.G. Barbosa Saldana et al., 2005). (Sakuraba et al., 2004), (Aya et al., 2007) and (Uruba et al., 2007). They focused on effect expansions ratio, Reynolds number, and suction or injection on augmentations heat transfer over backward facing step.

Chen et al., (2006) have conducted numerical simulations for two dimensional turbulent forced convection flows adjacent to backward facing step. The researchers focused to explore the effects of step height on turbulent separated flow and heat transfer. In this study the Reynolds number and duct's height at downstream from the constant step used are Re0 = 28,000 and H=0.19 m respectively, heat flux uniform and constant having value of qw = 270 W/m^2 at the stepped wall downstream from the step while other walls were treated as adiabatic. Both the velocity and the temperature fields were calculated using two equations at low Reynolds number turbulence models (Abe et al., 1994, 1995). Due to recirculation flow as created after the step the results showed that the peak values of the transverse velocity component have become smaller as the step height increases as shown in Figure 2.10 where the negative values of velocities represented the recirculation flow. The effects of recirculation flow on surface temperature are presented in Figure 2.11 where the maximum surface temperature becomes greater as the step height increases. They have also observed that the bulk temperature increases more rapidly as the step height increases.

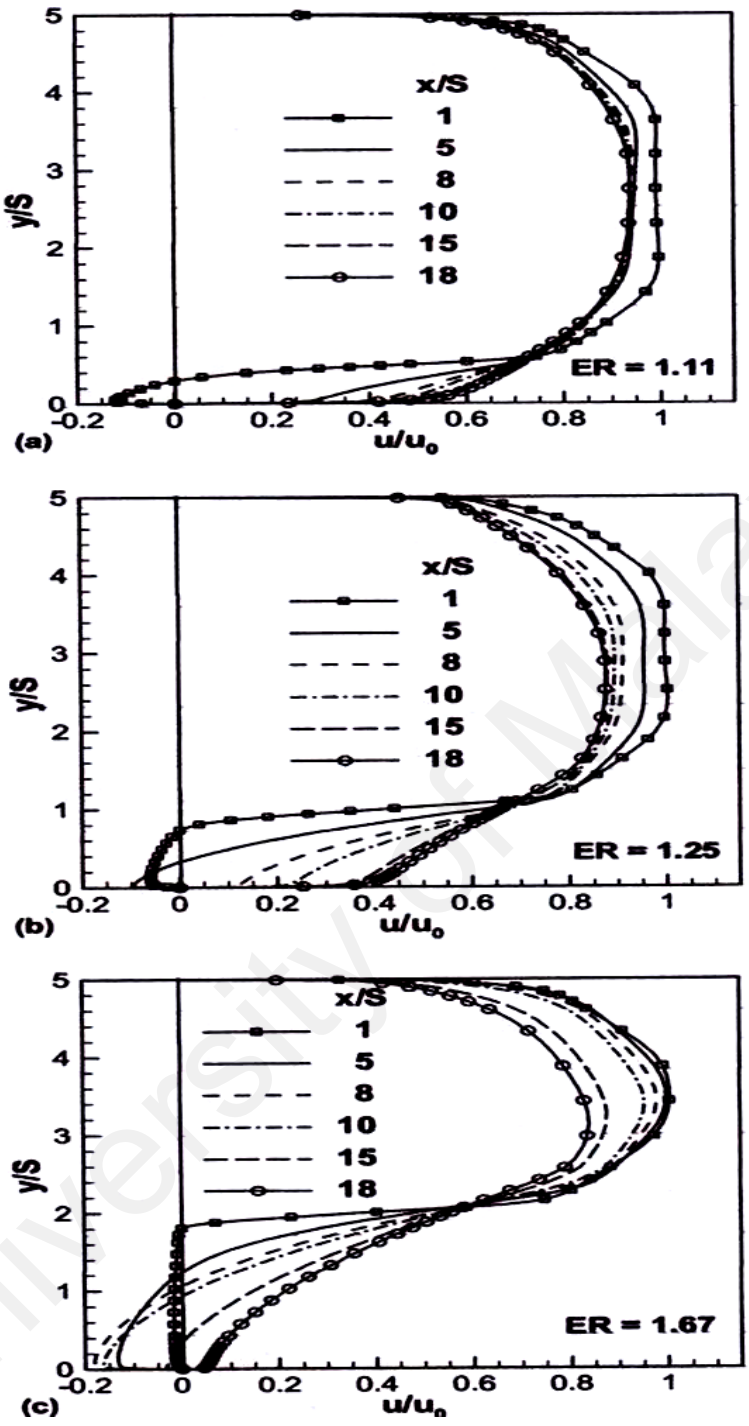

Figure 2.10: Distribution of the mean streamwise velocity component (u) at several x-planes, Abe et al., (1994).

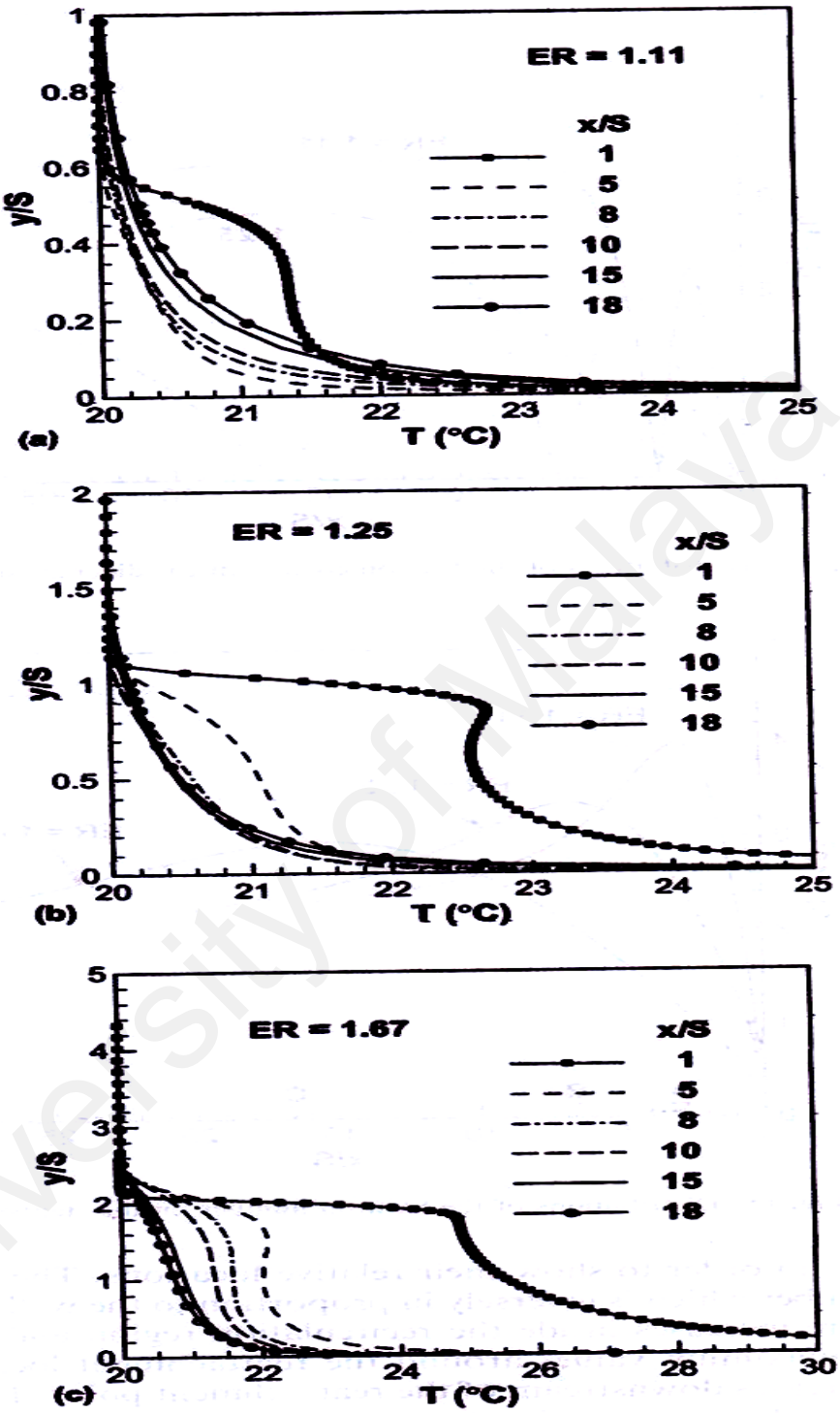

Figure 2.11: Distribution of the mean temperature at several x- planes, Abe et al. (1995).

Heat transfer and forced convection flow over double forward facing step was studied numerically by (Yılmaz & Öztop, 2006). The standard K-ε model used in simulations and the range of first step from 1 cm to 8 cm and second step from 2 to 8 cm also the length of step varied. The top of wall and steps were insulated whereas the bottom was heated, the results indicated the increase heat transfer rate with increase of Nusselt number and step height moreover the effect of length ratio of the steps on heat transfer rate and turbulent flow is very low. Subsequently (Oztop et al., 2012) conducted numerical study of turbulent flow and heat transfer over double forward facing step with obstacle and the bottom of wall is heated and the top of wall is insulated. The range of Reynolds number varied between 30,000 to 100,000 and the height of first step is 2, 4, and 6 cm and height of second step is 4, 6, and 8 cm, also aspect ratio of obstacle was ranged between 0.5 to 1. Finite volume method was used with K-ε model through FLUENT 6.2 software thus the results showed the enhancement of heat transfer as increase Reynolds number and step height also noticed the effect of obstacle aspect ratio on Nusselt number where the maximum of Nusselt number occurred at aspect ratio of obstacle Ar=1

2.3.3 Laminar Nanofluid flow

A. Experimental studies

The study of laminar nanofluid flow over backward or forward-facing step has not been investigated yet experimentally.

B. Numerical studies

Abu-Nada, (2008) can be considering as a pioneer in numerical study of heat transfer to nanofluid over backward facing step. The type of nanoparticles in this study represented by Cu, Ag, Al_2o_3,Cuo, and Tio_2 with volume friction between 0.05 to 0.2 and range of Reynolds number from 200 to 600. Momentum and energy equations were solved by using finite volume method where observed increase of Nusselt number at the top and bottom of the backward facing step. Also the investigations found high thermal conductivity of nanoparticles as outside of recirculation zones. Later, (Kherbeet et al., 2012) presented a numerical investigation of heat transfer and laminar nanofluid flow over a micro-scale backward-facing step. The Reynolds numbers ranged from 0.01 to 0.5, nanoparticle types comprised Al_2O_3, CuO, SiO_2, and ZnO, and the expansion ratio was 2. An increasing Reynolds number and volume fraction seemed to lead to an increasing Nusselt number; the highest Nusselt number value was obtained with SiO_2.

Additional last investigations concern nanofluid flow over a backward-facing step for the laminar range (Al-aswadi et al., 2010; Amirhossein Heshmati, 2013; Hussein A. Mohammed, 2013; Kherbeet et al., 2014; Mohammed et al., 2014; Mohammed, Al-aswadi, Abu-Mulaweh, et al., 2011; Mohammed, Al-aswadi, Shuaib, et al., 2011; Mohammed et al., 2012). Also the influences of magnetic field on nanofluid and nano boundary-layer flows over stretching surfaces are solved analytically by applying a newly developed method (Mehdi Rashidi et al. , 2011, 2014, 2014).

2.3.4 Turbulent Nanofluid flow

A. Experimental studies

Turbulent nanofluid flow over backward or forward-facing step has not been investigated yet experimentally.

B. Numerical studies

From the literature survey the study of nanofluid flow over backward or forward-facing step for turbulent range has not been investigated yet numerically.

2.4 Heat transfer and fluid flow in annular pipe

The study of heat transfer to fluid flow in an annular passage is one of the most important heat transfer studies due to its presence in many applications such as heat exchangers, reactors, packed bed, gas turbine, chemical industries etc. There are numerous published investigations which began about decades ago had included experimental and numerical investigations and dealt with different types of fluid and various boundary conditions.

Warren Rohsenow M., (1998) distinguished four fundamental thermal boundary conditions which could be applied in annular passage, such as:

First kind: Uniform temperature (different from the entering fluid temperature) at one wall; the other wall at the uniform entering fluid temperature.

Second kind: Uniform heat flux at one wall (i.e., adiabatic with zero heat flux) the other is wall insulated.

Third kind: Uniform temperature (different from the entering fluid temperature) at one wall; the other wall insulated.

Fourth kind: Uniform heat flux at one wall; the other wall maintained at the entering fluid temperature.

Also there are other kind of boundary conditions that represented by different and non-zero uniform heat flux at both walls of annular passage.

The geometry of annular passage in engineering applications is seen in various configurations such as circular, rectangular, elliptical, conical, polygonal, rhombic, triangular, square, and non-uniform annular passage, which found by concentric and eccentric configurations. There are some researchers who used in their studies concentric annular passage meaning the center line of inner pipe has the same coordinates as for the center line of outer pipe and others used eccentric annular passage meaning the center line of inner pipe has not the same coordinates for the center line of outer pipe.

2.4.1 Laminar fluid flow

A. Experimental studies

Schmidt (Worsøe-Schmidt, 1967) has reported a series of solutions in study of heat transfer with fully developed laminar flow in the thermal entrance region of circular pipes and annular passages where he used different boundary conditions involved in changing the temperature or the heat flux at the outer and inner wall. He obtained the calculated values of Nusselt number based on solutions of the second and third kind agreeing with (Lundberg et al., 1961), (Sellars et al., 1956) and (Munakata, 1962). Nada, (2008) adopted results of experimental study of natural heat transfer to horizontal and inclined annular fluid layers.

He observed of increase of heat transfer rate with increase of Rayleigh number and annular space and decrease inclination of annular passage. While (Yang et al., 2009) have experimentally studied natural convection heat transfer in horizontal annulus with square heating element at different positions in inner cylinder. Experimental results indicated the effect of placement of heated element in annular section on local heat transfer and it showed maximum value with heated element placed at 90 deg. from the bottom. Miaev et al., (1977) have experimentally studied the natural convection heat transfer and water flow in a horizontal eccentric annular duct. Grashof numbers, Reynolds numbers, eccentricity and radii ratios were presented against heat transfer data where they found increase of Nusselt number with enhanced free convection. Experimental and numerical study of two-phase flow in horizontal eccentric annuli was reported by (Sorgun et al., 2013). The experiment was conducted in air-water mixtures at different velocities and high speed camera was used for recording flow patterns while the numerical study employed Eulerian computational fluid dynamics model for gas –liquid flow in annuls. They obtained a good agreement between experimental and numerical data and noticed effect of eccentricity on flow patterns for all cases. Hosseini et al., (2009) have experimental study of natural convection heat transfer in vertical eccentric annular passage with heated outer cylinder and unheated inner cylinder. Their experimental were covered for single pipe, concentric annular, eccentric annular where the results bear a good agreement with results of (Al-Arabi et al., 1987) for single pipe.

B. Numerical studies

Avcı & Aydın, (2008) performed numerical study to thermally fully developed flows and hydrodynamically to flow laminar forced convection heat transfer in micro-

channel between two concentric cylinders. They applied two type of thermal boundary condition that included the first case uniform heat flux at inner pipe and the other case uniform heat flux at outer pipe. They showed increase Nusselt number at decrease Knudsen number and Brinkman number, and increase aspect ratio. Roschina et al., (2005) focused on two dimensional of natural convection in horizontal concentric annular cylinders with mathematical modeling approach and compared effects of the maximum temperature in horizontal annular cylinder to different geometry. Shi et al., (2006) applied finite difference method based on lattice Boltzmann model to simulate heat transfer of natural convection in horizontal concentric annular passage. They showed, the average Nusselt number values agree with obtained values from previous numerical and experimental studies reported by (Kuehn and Goldstein, 1978), and (Shahraki, 2002). Waheed, (2007) presented numerical study of simulation of natural heat transfer in between two horizontal concentric annular passages. He found increase of improvement of heat transfer in annular passage with decrease annular space width, also Prandtl and Rayleigh number, and different ratio of temperature having the effect on augmentation of heat transfer rate.

While Sambamurthy et al., (2008) have numerical study of two dimensional natural convection of horizontal annular cylinder with inner heated solid square cylinder and outer isothermal circular cylinder. Also they studied annular cylinder with inner solid circular cylinder for comparison with inner square cylinder. Generally, the numerical results revealed average Nusselt number depending on the average inner boundary temperature and also the results obtained in their studies are very useful in the design of thermal systems. Prakash & Renzoni, (1985) conducted numerical study of laminar fully developed flow in vertical concentric circular annular duct with radial internal fins. They showed effect of buoyancy increases both frictions and heat transfer. Mohanty & Dubey, (1996)

also conducted numerical and experimental investigations of buoyancy induced flow and heat transfer in a vertical annular passage. They obtained a good agreement between experimental and numerical data, especially for local Nusselt numbers.

Eraslan and Ozbelge, (2003) have numerical analyzed heat transfer to laminar water-slurry flow in vertical annular passage and compared previous experimental data reported by (Özbelge, 2001). They observed maximum heat transfer improvement ratio occurred with minimum Reynolds numbers of slurry. Laminar natural convection between vertical coaxial rectangular cylinders was numerically studied by (Gavara & Kanna, 2012). They observed that at the inner cylinder the local Nusselt number was increased towards the cylinder edges and increase of average Nusselt number was about 2.5 times at the bottom face compared to all faces.

2.4.2 Turbulent fluid flow

A. Experimental studies

Miller et al., (1995) studied turbulent heat transfer to water flowing in an annulus with heated inner pipe. They showed the effect of space ratio, Reynolds number and heat flux on enhancement of heat transfer and obtained the experimental results 20% higher than calculated value obtained by using Colburn's equation for internal flow in pipes for the equivalent diameter. Quarmby and Anand, (1967, 1970) conducted study of turbulent heat transfer and fluid flow in concentric annular passage for constant wall temperature and uniform heat flux. They observed that the values of Nusselt number for boundary conditions of uniform heat flux are higher in comparison to boundary conditions of constant wall temperature.

Donne & Meerwald, (1973) have studied heat transfer and friction loss of turbulent flow of air in smooth annuli at high temperature. They have measured subsonic turbulent flow of air in smooth annuli of diameter ratio 1.99 and 1.38, with heated inner pipe up to 1000°C. They have obtained their Nusselt numbers correlated with equation (2.8)

$$Nu_B = 0.018\,(\frac{D_2}{D_1})^{0.16}\,Re_B^{0.8}Pr_B^{0.4}(\frac{T_w}{T_E})^{-0.2} \qquad (2.8)$$

It was observed that (Petukhov and Roizen, 1965) correlated well with equation (1) at low temperature differences (T_W/T_E 1).

Also the average Nusselt numbers at inner pipe of the annulus given by correlation of equation (2.9).

$$Nu_B = 0.0217\,Re_B^{0.8}Pr_B^{0.4}(\frac{T_w}{T_E})^{-0.2} \qquad (2.9)$$

A good agreement for circular tubes was obtained by (Dalle Donne M., 1963) for experimental investigations. They have presented their experimental data by correlating factor, $A= (Nu_B/ Re_B^{0.8} Pr_B^{0.4})_{TW/TB=1}$ with ratio of diameter (D1/D2) and compared with previous theories and experimental findings reported by (Donne & Meerwald, 1966), (Petukhov and Roizen, 1965), (Wilson and Medwell, 1968) (S.O., 1968), (Kays & Leung, 1963), and (Sheriff and Gumley, 1966) (Sheriff & Gumley, 1966).

Heikal & Hatton, (1978) presented predictions and measurements of fully developed turbulent non-axismmetric flow and heat transfer in an annular channel by implementing the turbulence model. They showed a good agreement with experimental data especially for velocity profiles, friction factor and shear stress. They also showed the best agreement between the predicted and measured data when ratio of circumferential to radial mass diffusivity of heat was maintained 2 over the whole cross section. Robinson & Walker,

(1978) investigated to obtain the value of circumferential diffusion heat in symmetrical annular passage for turbulent flow and compared the obtained results with theoretical solutions.

B. Numerical studies

Stein & Begell, (1958) carried out investigation on turbulent water flow and heat transfer in internally heated annuli by implemented cosine and uniform lengthwise heat flux distributions where they computed 900 evaluates of local heat transfer coefficients of water flow with heated inner pipe. They observed no considerable effect of cosine heat flux distribution on the heat transfer coefficients. Chen & Yu, (1970) also studied turbulent heat transfer to flowing liquid metals in concentric annular channels. They focused on the effect of variable heat flux and entrance region dimensions on Nusselt number where they showed the predicted Nusselt number agrees to the experimental value. Lee et al., (1988) presented numerical results of heat transfer in fully developed flow by using K-ε equation model in annular pipe with rectangular roughness. They have obtained more improvement in Nusselt number by using curvature correlation model in comparison to that by the standard K-ε equation model. They also obtained maximum value for Nusselt number at near reattachment point of the separated flow. The computational results have shown a good agreement with previous investigations reported by (Kang, 1985) and (Hong et al., 1983). Ho & Lin, (1989) investigated numerically heat transfer to air-water flow in horizontal concentric and eccentric cylindrical annulus with constant heat flux at the outer wall, and isothermal condition at the inner one. They observed increase of heat exchange transfer to air-water interface occurred at mixed boundary conditions. Ahn & Kim, (1998) performed analytical and experimental study of heat transfer and fully developed fluid flow in rough

annuli by using artificial roughness elements on wall of inner pipe or outer pipe or both. They obtained enhancement in heat transfer coefficient due to the effect of roughness element on turbulence enhancement.

Chung et al., (2002) and Chung & Sung, (2003) used direct numerical simulation (DNS) of turbulent heat transfer and structure of flow in horizontal concentric annular pipe. They showed that the turbulent thermal structures near the outer wall were more active than those near the inner wall due to the vortex regeneration processes between the inner and outer wall. Yu et al., (2005) performed analysis of the computed characteristics of turbulent flow and convection in concentric annuli with uniform heated inner pipe and unheated outer pipe. Their investigation was dependent on the previous model, reported by (Churchill & Chan, 1995). Ould-Rouiss et al., (2009) developed turbulence models by using direct numerical simulation (DNS) to study fluid flow and heat transfer in annular pipe with random value of heat flux on the outer and inner walls. They showed as increase heat flux from 1 to 100 the Nusselt number increase on inner pipe and decrease on outer pipe.

2.4.3 Laminar nanofluid flow

A. Experimental studies

Yang et al., (2005) carried out experimental study of heat transfer properties of nanoparticle-in-fluid dispersions (nanofluids) in laminar flow with two liquids flowing in a horizontal tube heat exchanger. They obtained that the heat transfer coefficient increased with the Reynolds number and volume concentration of graphite. Moreover, different values of heat transfer coefficient observed with two graphite nanoparticle sources at the same particle loading. Performance evaluation on air cooled heat exchanger for laminar Al_2O_3 nanofluid flow has been experimentally studied by (Teng et al., 2011). Capacity of

heat exchange was higher for nanofluid in compared to pure water due to effect of nanoparticle suspension where the maximum enhancement was about 39%.

B. Numerical studies

Shahi et al., (2011) performed numerical study to natural convection heat transfer rate in vertical annular channels with nanofluid copper-water. By using finite volume method with Fortran software that the analysis equations and showed increase of Nusselt number with increase of solid concentration of nanofluid and maximum Nusselt number occurred as inclined angle of annular channel equal zero degree. They validated their result by comparison values of Nusselt number with (Guj & Stella, 1995) and (Davis and Thomas, 1969). Mehrizi et al., (2013) have numerically studied of natural convection heat transfer to Cu-Water nanofluid flow in horizontal cylinder annuli with inner triangular cylinder by using Lattice Boltzmann method. They showed increase enhancement of heat transfer and stream functions with increase of volume fraction of nanoparticles and at inner cylinder moving downward while decrease of improvement of heat transfer with the inner cylinder moving horizontally. In contrast, (Habibi Matin & Pop, 2013) presented numerical study of the natural heat transfer to Copper (Cu)-water nanofluid flow in horizontal eccentric annulus. They applied stream function vorticity formulation in polar coordinate in order to obtain high accuracy in the result on the effect of eccentric and volume friction of nanoparticles on Prandtl number and Nusselt number and obtained good agreement with previous investigations. Enhancement of heat transfer for two phase mixed convection of laminar Al_2O_3 nanofluid flow in annulus with constant heat flux was numerically studied by (Mokhtari Moghari et al., 2011). In their simulation three dimensional with Finite Volume Method were used as well as considered that the Brownian motions of

nanoparticles to calculate the effective of thermal conductivity and dynamic viscosity. The computational data found that the increase in Nusselt number with increased volume fraction of nanoparticles but the friction factor does not effected.

Izadi et al., (2009) have numerically study of laminar forced convection of a nanofluid of Al_2O_3/ water in an annulus. The results found that the profile of the temperature affected by the increase volume fraction of nanoparticle but axial velocity does not change with the nanoparticle volume fraction. Moreover, their results indicated that increasing ratio of heat fluxes for (outer to inner), the effect of one wall heat flux on the Nu of another wall increases which effects on the bulk temperature. Abu nada (Abu-Nada, 2009) have numerical study effects of variable viscosity and thermal conductivity of Al_2O_3–water nanofluid in horizontal annuli. They found that decrease of average Nusselt number with increased volume concentration of nanoparticles for Ra $\geq 10^4$ while its increases with increase increased volume concentration of nanoparticles for Ra= 10^3.on heat transfer enhancement in natural convection.

Kashani et al., (2013) presented numerical study of two phase mixture mode of heat transfer to Al2O3/water laminar flow in horizontal annulus with constant temperature. The numerical data showed that the increase heat transfer coefficient with increased volume concentration and found that effect length of annulus where decrease in the entrance and increased up to exit.

Lattice Boltzmann simulation of natural convection of nanofluid flow in a concentric annulus reported by (Ashornejad et al., 2013). Four type of nanoparticles were used in their

simulation included that the Cu, Al_2O_3, TiO_2, and Ag. They found a good agreement with previous experimental data and highest augmentation of heat transfer observed with silver in compered with other types of nanoparticles.

2.4.4 Turbulent nanofluid flow

A. Experimental studies

Duangthongsuk & Wongwises, (2010) performed experimental study of performance heat transfer and pressure drop for TiO_2 nanofluid flow in horizontal double pipe under turbulent flow. Their result showed that the heat transfer coefficient was about 26 % at vol. 1% while less than 14 % as vol. 2% due to their opinion that at increase of volume fraction of nanoparticle will leads combined tighter and then created bigger size which caused decrease the performance of heat transfer. While (Farajollahi et al., 2010) adopted experimental study on heat transfer to turbulent ɣ-Al_2O_3/water and TiO2/water flow through the shell and heat exchangers. They found that effect of volume concentration, Peclet number and particle type on heat transfer where the performance of heat transfer for two nanofluids shows that at a certain Peclet number, heat transfer characteristics of TiO_2/water nanofluid at its optimum nanoparticle concentration were bigger in compered to ɣ-Al_2O_3/water nanofluid. Zamzamian et al., (2011) have experimental study on heat transfer coefficient for turbulent nanofluid Al_2O_3/EG and CuO/EG through the double pipe and plate exchangers. The results showed that the significant augmentation in heat transfer coefficient for nanofluid flow in compared to base fluid where in double pipe the maximum augmentation was 26% and 37% for 1% of Al_2O_3 and CuO respectively but in plate heat exchangers was 38% Al_2O_3 and 49% CuO.

Heat transfer to Al_2O_3 nanofluid flow through heat exchangers experimentally studied by (Albadr et al., 2013). Increase in the heat transfer coefficient observed with increased either volume fraction of nanofluid or mass flow rate. Also the results showed that the increase of volume fraction of nanofluid leads to increase of friction factor due to increase viscosity of nanofluid

B. Numerical studies

Bozorgan et al., (2012) performed numerical study of performance turbulent nanofluid Al_2O_3 flow in heat exchanger where the results found that the decrease in flow rate of nanofluid coolant occurred with increase of volume fraction of nanoparticles in the exchanger. The flow rate of nanofluid was 24.5% at 2 Vol. 2 % of Al_2O_3 lower in compared to pure water but the pressure drop increase with increased volume fraction of nanoparticles. Forced convection heat transfer characteristics of nanofluids in a double-tube counter flow numerically studied by (Demir et al., 2011) where used TiO_2 for validation study and Al_2O_3 for simulation. They found that the effect of concentration of nanoparticles and Reynolds number on Nusselt number, heat transfer coefficient, wall shear stress, and pressure drop. Increase of volume fraction of nanofluid leads to increase both enhancement heat transfer and pressure drop in addition to increase of shear stress.

CHAPTER 3: METHODOLOGY

3.1 Introduction

This chapter concerns the methodology that has been adopted for present research. The computational fluid dynamics (CFD) used ANSYS FLUENT14 to do the simulation. Built geometry and meshing process is achieved by ANSYS ICEM and then export to FLUENT. Continuity, momentum and energy equations with the K-ε model are employed in these simulations based on finite volume method. For validation grid independent and code validations are applied. The last step compared numerical results with the obtained experimental results. Figure 3.1 showed that the flow chart of methodology for present research.

3.2 Background about CFD

With the aid of CFD it is possible to solve complex phenomena in nature at a faster pace in comparison to the results obtained from experiment investigations. Therefore, there are many researchers used CFD package to create simulation for saving the cost and time for building test rig. Furthermore, CFD can be used to notice the physical behavior and effect of configuration on flow at any position along the flow, study flow characteristics of single phase fluids (Ogugbue, 2011) and multiphase fluids (Pereira et al., 2007; Shah, 2004) using different geometries . The CFD process developed as a result of the recent increase in computer processing speed and existing memory. This division of fluid flow investigation complements experimental and theoretical work, providing economically interesting alternatives through the simulation of real flows and allowing an alternative form for theoretical advances under conditions unavailable experimentally. These have been used to

assess frictional pressure losses (Manzar, 2009; Pereira et al., 2007) without involving significant costs through experimentation.

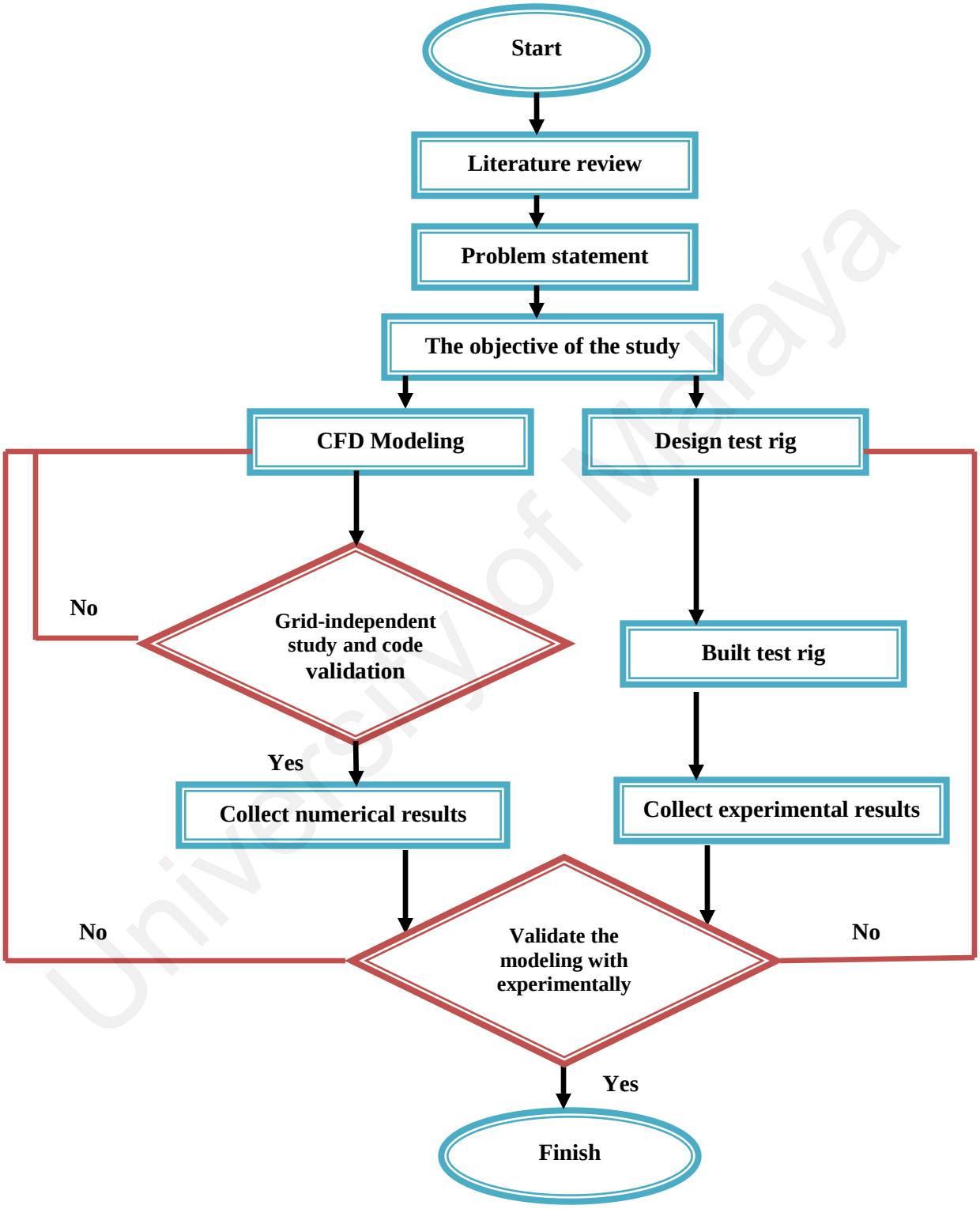

Figure 3. 1: Flow chart of methodology for present research.

3.3 Standard k- ε

The standard k- ε model is one of the most common turbulence models which represented by two-transport-equation model solving for kinetic energy k and turbulent dissipation ε. The standard k- ε model is used according to the presented studies by (Lee et al., 2011) and (Yılmaz & Öztop, 2006) for simulation of heat transfer and fluid flow in sudden expansion and over double forward facing step, respectively. This model can be used to calculate the eddy viscosity at single turbulence length scale where the turbulent diffusion determined with the specified scale. The hypothesis of gradients pressure has been employed in this model for correlating the Reynolds stresses to turbulent viscosity and velocity gradients. The disadvantage of this model is the absence of sensitivity to gradient of adverse pressure and numerical stiffness for the the integrated the equation at the viscous sublayer which is solved with the damping functions (Menter, 1993; Menter, 1994). Generally, Fluent offers five viscous models to be selected; Inviscid, Laminar, Spalart-Allmaras, k-epsilon (k–ε), k-omega (k–ω), and Reynolds stress (RSM) (FLUENT 2006. User's Guide).

3.4 Meshing process

The configuration is used in this numerical study is shown in Figure 3.2. ANSYS ICEM has been used for construction of the model configuration and meshing process then export to ANSYS FLUENT 14 as shown in Figure 3.3 and 3.4. The outer cylinder of entrance section is insulated and has variable inner diameters (De) of 80, 60, 50 mm and length (a) of 1500 mm) and the inner cylinder is insulated with a constant diameter (di) of 25 mm and length 2500 mm) while the outer cylinder of test section is heated with a constant diameter (Dt) of 100 mm and of length (b) of 1000 mm. Figure 3.3 and 3.4 represented create geometry with ANSYS ICEM based on dimensions then make meshing where non-uniform

refinement of hexahedron used near wall to calculate the high gradients by algebraic equations.

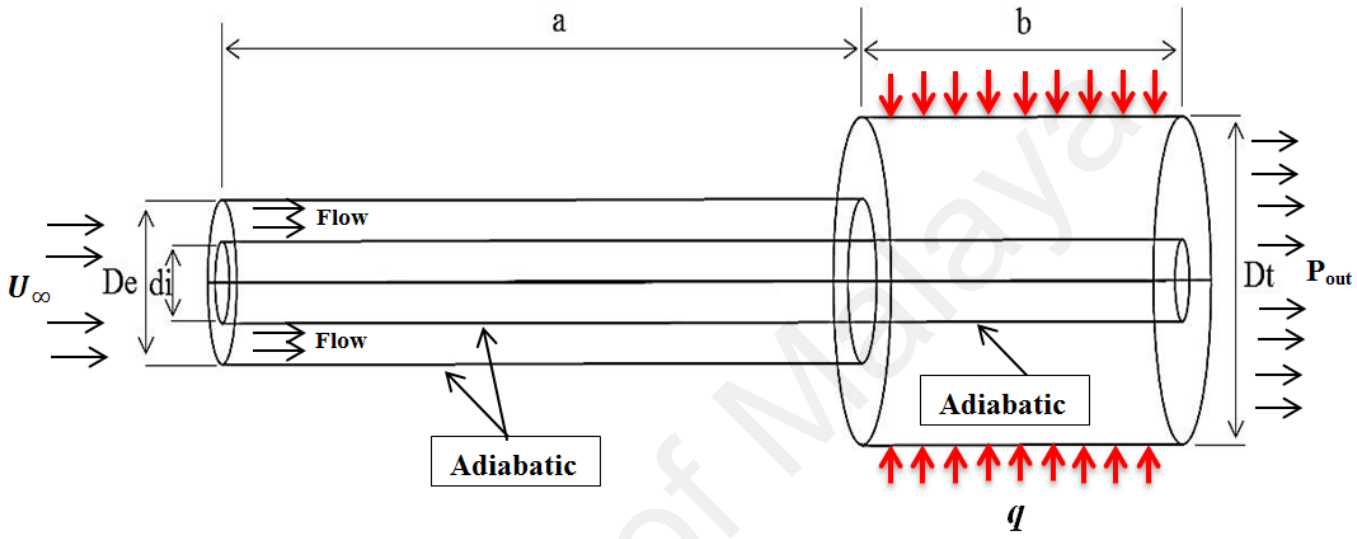

Figure 3.2: Schematic of the three-dimensional annular test section showing sudden expansion.

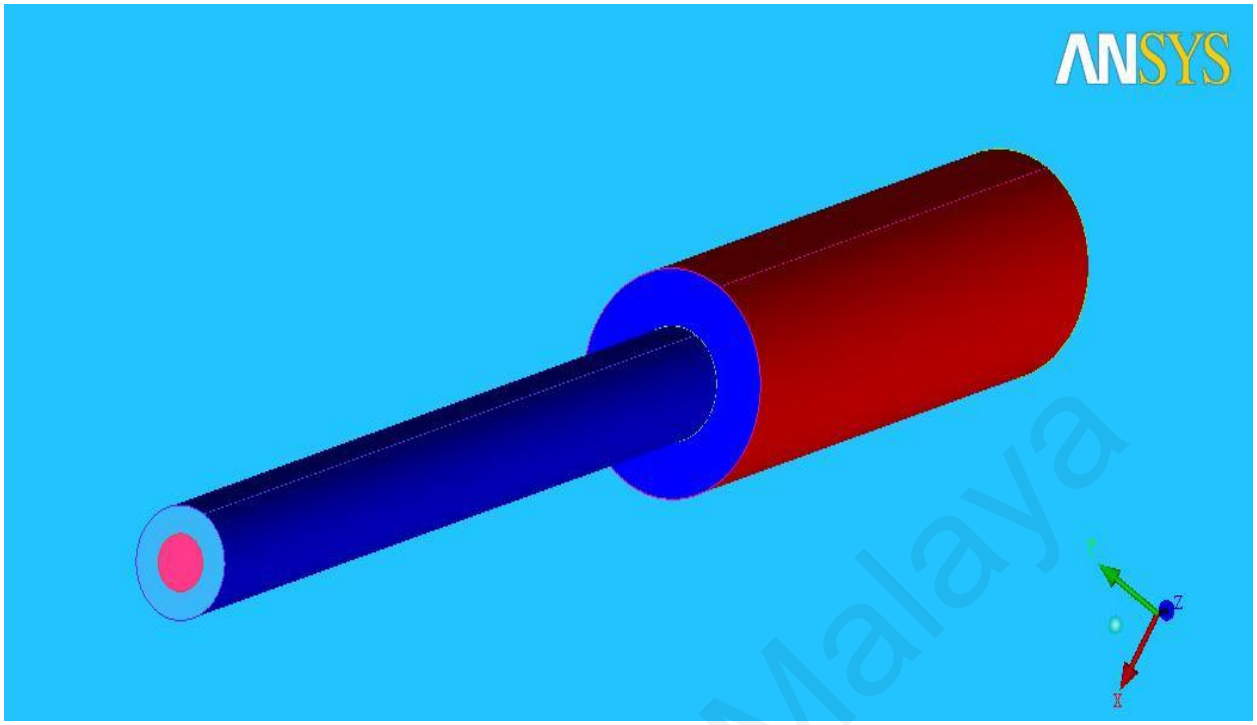

Figure 3.3: 3D –View of Mesh.

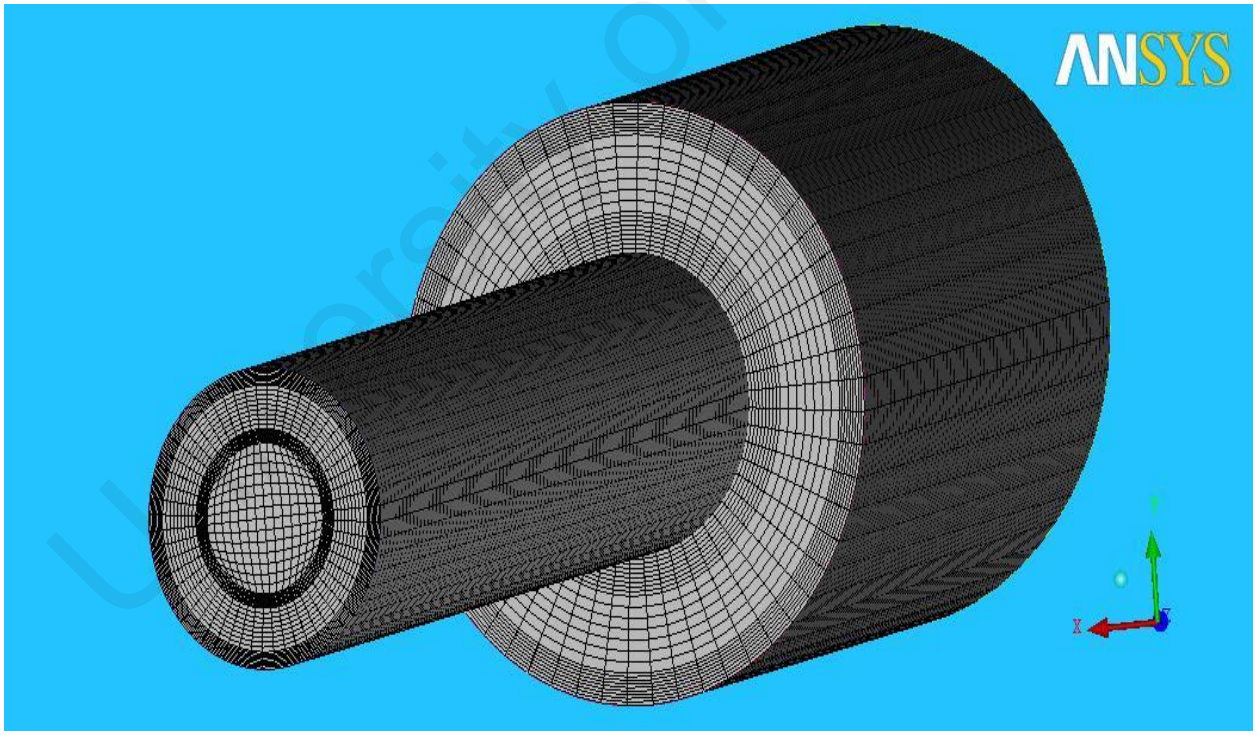

Figure 3.4: Geometry showing meshing.

3.5 Boundary conditions

The boundary conditions applied in this numerical simulation were range of Reynolds numbers varied from 20000 to 50000, expansion ratio varied from 1.25 to 2, and heat flux varied from 4000 to 16000 W/m^2 more details are presented in Table 3.1. The outer pipe of entrance section and whole inner pipe were adiabatic while the exit pipe is heated with uniform heat flux. The inlet fluid temperature was fixed at 300K while the streamwise gradients of all quantities at the outlet set to be zero. The working fluid was pure water or Al_2O_3, CuO, TiO_2 /water at different concentrations and assumes there is no slip conditions happen between them with thermal equilibrium. The velocity at entrance region of pipe was considered fully developed and thermally and hydrodynamically steady. Under the above of boundary conditions that numerical simulation proceeds.

Table 3.1: Boundary conditions

Reynolds number (Re)	20000, 25000, 30000,35000 40000, 45000, 50000
Expansion ratio (ER)	1, 1.25, 1.67, 2
Heat flux (q) W/m^2	4000, 8000, 12000, 16000
Volume fraction of Al_2O_3, CuO, TiO_2, %	0.5, 1, 1.5, 2

3.6 Governing equations

A three dimensional continuity, momentum and energy equations are used in numerical analysis for incompressible fluid. These equations could be solved by control volume method based on converting the governing equations to algebraic equations (Herrmann Schlichting, 2000).

$$\frac{\partial U_i}{\partial x_i} = 0 \tag{3.1}$$

$$\frac{\partial (U_i U_j)}{\partial x_j} = -\frac{\partial p}{\partial x_i} + \frac{\partial}{\partial x_j}\left(\mu \frac{\partial U_i}{\partial x_j} - \overline{\rho u_i u_j}\right) \tag{3.2}$$

$$\frac{\partial (U_i T_j)}{\partial x_j} = -\frac{\partial}{\partial x_i}\left(\frac{\mu}{Pr}\frac{\partial T_i}{\partial x_j} - \overline{\rho u_i t_j}\right) \tag{3.3}$$

The Reynolds stresses and heat fluxes are, respectively, given as:

$$\overline{\rho u_i u_j} = -\mu_t \left(\frac{\partial U_i}{\partial x_j} + \frac{\partial U_j}{\partial x_i}\right) + \frac{2}{3}\delta_{ij} k\Big] \tag{3.4}$$

$$\overline{\rho u_i t_j} = -\frac{\mu_t}{\sigma_\theta}\frac{\partial T_i}{\partial x_j} \tag{3.5}$$

The standard k-ε model has two transport equations for the turbulence kinetic energy and energy dissipation that are solved together with the equations of balance by the finite volume method (B.E. Launder, 1974). The corresponding transport equations are,

$$\frac{\partial \rho k U_i}{\partial x_j} = -\frac{\partial}{\partial x_j}\left[\left(\mu + \frac{\mu_t}{\sigma_k}\right)\frac{\partial k}{\partial x_j}\right] + \rho(G_b - \varepsilon) \tag{3.6}$$

$$\frac{\partial \rho \varepsilon U_i}{\partial x_j} = -\frac{\partial}{\partial x_j}\left[\left(\mu + \frac{\mu_t}{\sigma_k}\right)\frac{\partial \varepsilon}{\partial x_j}\right] + \rho\frac{\varepsilon}{k}(c_{1\varepsilon}G_b - c_{2\varepsilon}\varepsilon) \tag{3.7}$$

$$G_b = \mu_t \left(\frac{\partial u_i}{\partial x_j} + \frac{\partial u_j}{\partial x_i}\right)\frac{\partial u_i}{\partial x_j} \tag{3.8}$$

$$\mu_t = \rho c_\mu \frac{k^2}{\varepsilon} \tag{3.9}$$

The standard constants used in the k-ε model are

$$C_{1\varepsilon} = 1.44, C_{2\varepsilon} = 1.92, C_{3\varepsilon} = 0.09, \sigma_k = 1.0, \sigma_\varepsilon = 1.3, \text{and Pr} = 7.01.$$

The Reynolds number calculated based on hydraulic diameter by equation (3.10)

$$Re = \frac{\rho_{nf} U D_h}{\mu_{eff}} \quad (3.10)$$

In order to obtain good simulation results the standard k-ε turbulence model was selected, a second-order scheme with coupling between pressure and velocity is employed through the SIMPLE algorithm. Each iteration and the convergence criterion in the residual sum was computed and sorted where less than 10^{-6} for the continuity, and smaller than $10^{-7}$for the momentum and energy equations.

3.7 Thermo physical properties of the nanofluid

The Thermo physical properties of the nanofluid are evaluated by using well-known empirical correlations. The effective density of nanofluid (ρ_{nf}) is given by equation (3.11), (Vajjha & Das, 2009),

$$\rho_{nf} = (1 - \phi)\rho_f + \phi\rho_{np} \quad (3.11)$$

where ρ_f and ρ_{np} represent the density of the base fluid and the solid nanoparticles respectively.

The specific heat of the nanofluid is obtained from equation (12), (Vajjha & Das, 2009),

$$(\rho C_p)_{nf} = (1 - \phi)(\rho C_p)_f + \phi(\rho C_p)_{np} \quad (3.12)$$

where $(\rho C_p)_f$ and $(\rho C_p)_{np}$ represents the heat capacities of the base fluid and the nanoparticles respectively.

Effective thermal conductivity of solid–liquid mixtures calculated by using the Wasp model which given by (Xuan & Roetzel, 2000) and (B.-X. Wang, 2000) as:

$$k_{eff} = k_f \left(\frac{k_p + 2k_f - 2\emptyset(k_f - k_p)}{k_p + 2k_f + \emptyset(k_f - k_p)} \right) \quad (3.13)$$

(Brinkman, 1952) found viscosity correlation as it relates to concentrated particle suspension.

$$\mu_{eff} = \mu_f \times (1 + 2.5 \times \phi) \quad (3.14)$$

This correlation is used for low volume fraction ($\phi < 0.05$).

3.8 Computational domain and numerical details

A finite volume method based flow solver of computational fluid dynamics software ANSYS FLUENT 14 is selected in this simulation. The standard K-ε model is one of the most common turbulence models, although it just does not perform well in cases of large adverse pressure gradients. It is a two equation model, it includes two extra transport equations to represent the turbulent properties of the flow. This allows a two equation model to account for history effects like convection and diffusion of turbulent energy. The first transported variable is turbulent kinetic energy, K. The second transported variable in this case is the turbulent dissipation, ε. It is the variable that determines the scale of the turbulence, whereas the first variable, K, determines the energy in the turbulence. The K-epsilon model has been shown to be useful for free-shear layer flows with relatively small pressure gradients. Second order upwind is applied in solving the momentum, turbulent kinetic energy, turbulent dissipation rate, and energy discretizations.

3.9 Grid-independent test

A Grid independent study is achieved for water at Re=20000, expansion ratio of 2, and heat flux of 4000 W/m^2. In order to assess the grid independent results five sizes of grid were adopted with different dimensional units of x, y, z, as shown in Table 3.2 where the fourth grid is represented the grid independent due to the difference in average heat transfer coefficient between the fourth and fifth grid was less than 1%. . In contrast, non-uniformly grids distributed near wall were used to calculate the high gradients by algebraic equations.

Table 3.2: Grid independent for pure water at ER=2 and Re=20000.

Size of mesh	X=30, Y=30, Z=300	X=20, Y=20, Z=500	X=20, Y=20, Z=750	X=30, Y=30, Z=750	X=20, Y=20, Z=1000
Grid no.	1	2	3	4	5
h_{ave}	1233.43027	1246.70394	1247.764473	1248.151331	1248.237669

3.10 Code validation

The experimental and numerical data with the range of turbulent nanofluid flow through sudden expansion passages have not been published yet. However, the numerical simulations performed for laminar nanofluid flow over backward-facing step passage by (Al-aswadi et al., 2010) was used for model validation. The obtained results were shown in a good agreement as presented in Figure 3.5. For further validation of the present computational model, a numerical study of heat transfer and fluid flow over a vertical double forward-facing step as reported by (Tuqa Abdulrazzaq *et al.*, 2014) was referred. The numerical data are presented in Figure 3.6 and compared with the simulation data of (Tuqa Abdulrazzaq *et al.*, 2014) for case 1 at T=310 K, where good agreement was observed with our code.

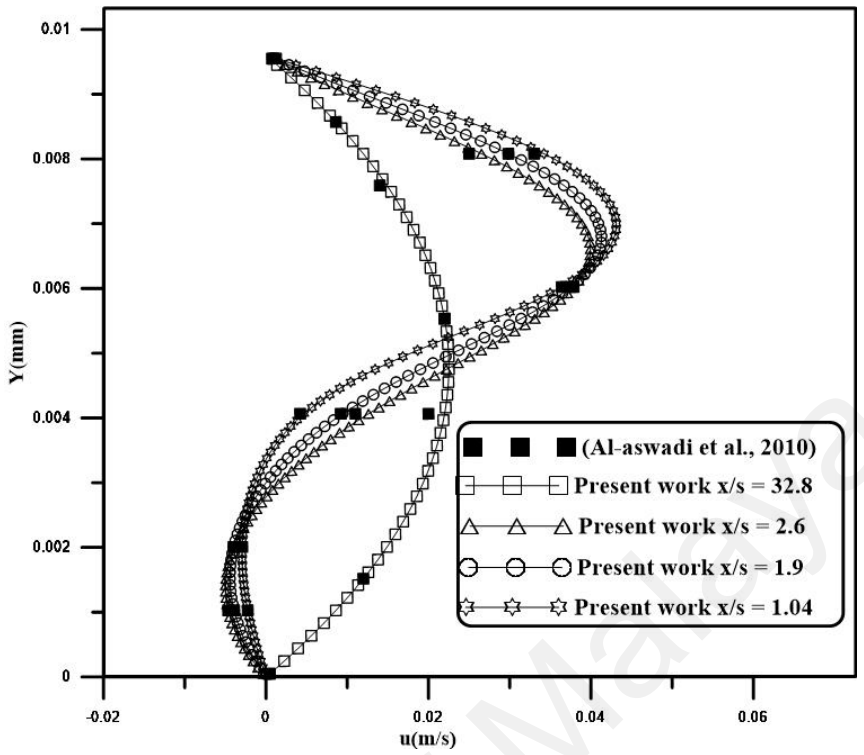

Figure 3. 5: Comparison velocity profile with Al-aswadi et al., 2010).

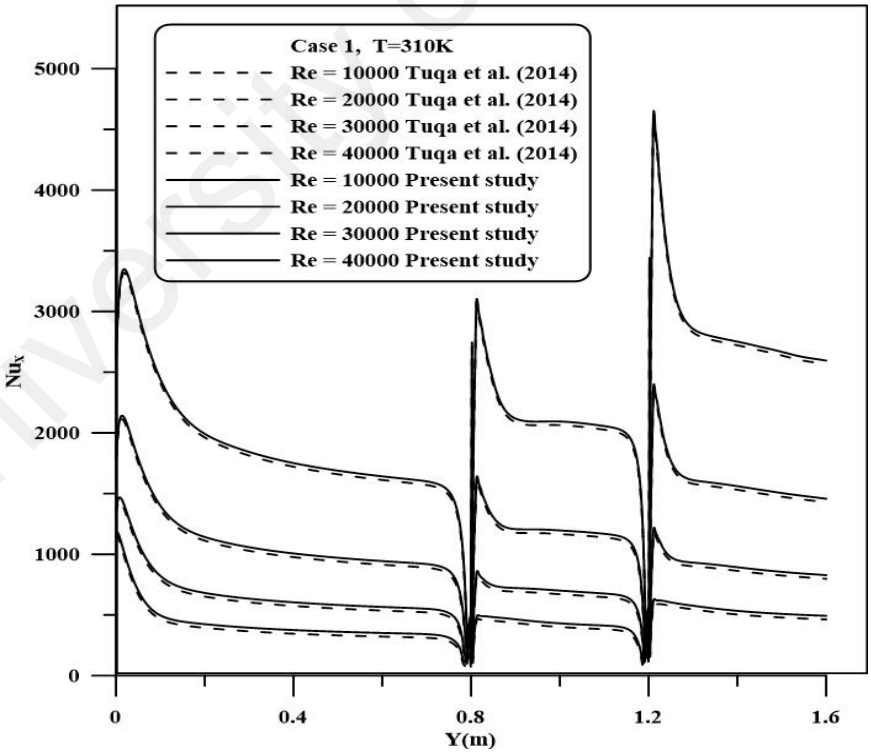

Figure 3. 6: Comparison Nusselt number with Tuqa et al. (2014)

CHAPTER 4: Experimental Setup

4.1 Introduction

The test rig is built and designed for nanofluid flow in annular pipe with close loop. The boundary conditions which is used in this setup creates sudden expansion in the passage by the reduced diameter of the entrance pipe, heat flux on the test tube by flexible ceramic pad heater was changed by power regulator, and variable velocity to the test section (variable Reynolds no) by a flow regulator. The suspension used in this experimental investigation was different concentration of Al_2O_3 nanoparticles with pure water as a base liquid. This chapter contents the design and construction of the test rig, the method of heating of the test section, the system of data acquisition, calibration measurements, test procedure, and finally the data reduction method have been described in this chapter.

4.2 Design and Construction

The experimental set up for nanofluid is shown in Figure 4.1 and Figure 4.2 schematic and photograph respectively. The facility mainly includes a jacketed liquid tank which has the capacity of 150 liters, stirrer motor (Branco Model BA 6324) with speed controller to make a homogenously dispersed solution, the chiller (Model-NWS-2AC) which is connected with the tank for adjusting the temperature of the liquid, a bypass pipe having diameter of 3cm and the length of 100cm is connected to the top part of the tank, stainless steel centrifugal liquid pump (Three Phase, 3000 RPM, 415V 3HP TO 20 HP, LIQUID Temperature 15C to +90 C) which has delivers the liquid to the test section, invertor to regulate the motor speed and run the centrifugal liquid pump and maintain different flow rate as used in this experiment, magnetic flow meter (Burkert S030) with

digital display (Burkert types 8202-8222) mounted at the entrance pipe to measure the fully developed liquid velocity at 15D from the inlet region, entrance pipe section has length of 150cm and has variable inner diameter (d= 10, 8, 6, 5 cm) to create the sudden expansion in the passage which is connected to the test pipe by Teflon flange to avoid the conduction losses, the test section has inner diameter 10 cm and length of 100 cm and the solid inner pipe has outer diameter of 25 mm and length of 270 cm which extent along the passage from the entrance section up to the end of test section mounted at the center of passage to make annular passage, a bend pipe of inner diameter 10cm and length 30cm is connected to the test section to channelize the discharge to the storage tank. Two thermocouples of PT100Tc located at the inlet and outlet of the passage to measure the inlet and outlet temperatures. 32 Groves on straight line are made on the surface of the test section for 32 thermowalls to hold 32 thermocouples type K on surface of the test pipe to measure surface temperature see Figure 4.3. Two thermocouples have been installed at the inlet and outlet of the test section to measure the inlet and outlet temperatures of the nanofluids. Flexible ceramic pad heater has been used to heat the pipe and obtain uniform heat flux. A differential pressure transmitter Model (Model EJA110E-DMS4J-912DB/D3) has been used to measure pressure drop of the flowing fluid. Two signal tubes from the inlet and outlet of the test section were connected to the pressure transducer which provides digital display and transmits signal to the data logger (Mounting Bracket:304 SST2-INCH PIPE). The specifications and the accuracy of the measuring equipment used in the present experimental setup are presented in Table 4.1:

Table 4.1: Specifications and errors for the measuring devices utilized in the present experiment.

Measured parameter	Type	Range	Error
Surface temperature	Type K thermocouple	0-300℃	±0.1℃
Bulk Temperature	RTD (PT-100) sensor	0-200℃	±0.1℃
Fluid flow rate	Burkert S030, Electromagnetic Flow Meter	0.1 m/s ~ 10 m/s	±0.5%
Fluid pressure drop	Model EJA110E-DMS4J-912DB/D3	0-25 kPa	±0.075%
Cooling unit	Dong Guan Naser- NWS-2AC	5 kW	±0.1℃

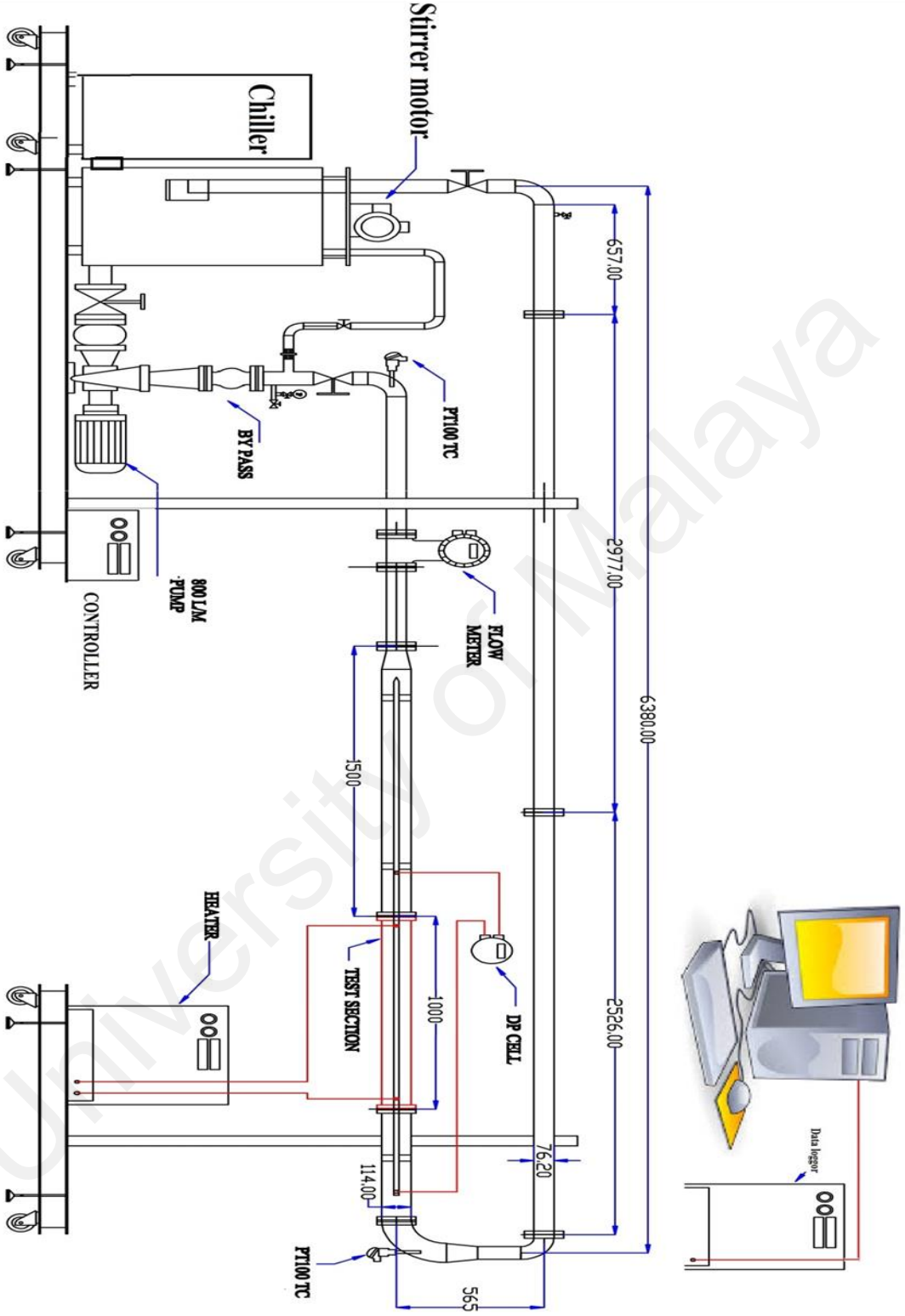

Figure 4.1: schematic of experimental set up.

Figure 4.2: photograph of experimental set up.

Figure 4. 3: The steps of make grooves and fixing thermowalls and installing thermocouples on the surface of the test section.

4.3 Heating and Cooling Method

The heating circuit represented by flexible ceramic pad heater c/w s/steel cover and insulation size A: 255MM SIZE B: 305MM 80V 3600W. Power regulator (SIPIN W5-SP4V060-24J 1 PHASE 60A) and temperature controller (SHIMADEN SRS11-8IN-90-N10000) have been used for adjust the electrical current and then get different heat fluxes. This type of heater used to obtain that uniform heat flux at the test pipe, also by measure current and voltage then calculate the heat flux. Cooling method contained of jacket around the tank and connected to the chiller which has ability to adjust the temperature. To reduce the heat loss to the surroundings, Rock ceramic insulation was used see Figure 4.4. This insulation's heat loss temperature was measured by three type K thermocouples that were located on the outer surface of the insulation.

The cooler with 5 kW of cooling capacity is used to keep constant temperature at the inlet of the test section where the technical parameters of water cooling chiller Naser (Model-NWS-2AC) presented in Table 4.2 and Figure 4.5. The flow rate is controlled with two adjusting valves, one at the main flow loop and the other at the bass line.

Table 4.2: Technical Parameters of Water Cooling Chiller Naser

Model	NWS-2AC	Type	Closed cycle scroll/Pistion	Standard freezing water flow
Measure	580*580*925	Flow regulator	Capillary tube/Thermostatic expension valve	Diameter of standard nipple
Machine Weight	102KG	Condenser style	High Effective Copper tube Covered Aluminum Fins	Buil-in pump
Power input	220v/1P/50HZ	Evaporator style &Volume	Water tank type/shell tube type/stainless steel plate heat exchanger (32L)	Refrigerant gas R 22/R407C

Figure 4. 4: Rock ceramic insulation

Figure 4. 5: Water cooling chiller.

4.4 Data Acquisition system

Figure 4.6 shows data logger (YOKOGAWA, MODEL MW100-E-1Q) as used in this experimental. To transfer and saving the experimental data all thermocouples and other devices connected to this instrument and then continuous monitoring and recording of the data by a personal computer. The RJC (Reference Junction Compensation) accuracy (Range Type T) is 0°C ± 0.5°C. The range of acquisition rates for these devices varied from 0.01 to 60 NPLC, where NPLC means “Number of Power Line Cycles” and 1 NPLC ' 16.7 ms. Quality inspection certificate for Data logger (No. 2000958301-00010-0001) get from YOKOQAW company for more details see Table 4.3.

Figure 4. 6: Data logger

Table 4.3: Inspection certificate for Data logger.

No.	Test Item	Result
1	Visual inspection and checking accessories and options	Good
2	Insulation resistance: between power supply terminal and earth;20MΩ or more at 500V DC	Good
3	Withstanding Voltage: between power supply terminal and earth:1500V AC(MW100-*-1*)/1000V AC (MW100-*-2*, AC (MW100-*-3*), 1 MIN.	Good
4	Continuity test for protective earth: between protective earth-functional earth . 60Hz 30A resistance 0.1 Ω or less	Good
5	Power frequency detection function test	Good
6	Battery frequency detection function test	Good
7	Communication function test with MX modules	Good
8	LED display function test	Good
9	Key switch function test	Good
10	Serial communication function test	Good

4.5 Calibration of measuring devices and sensors

In this section, calibration of measuring devices and sensors in experimental are presented. Thermocouples, Flow meters, and digital voltmeter are calibrated from vendor to obtain higher accuracy results.

4.5.1 Thermocouples

The K-type thermocouples, Omega TJC36-CPSS-032-U, come specified from the manufacturer to have an uncertainty of 0.5°C or 0.4% from 0 − 350°C. All thermocouples and RTDs were calibrated against an Ametek temperature calibrator (AMETEK Test & Calibration Instruments, Denmark).

4.5.2 Flow Meters

As stated above, the flow meters come calibrated from the manufacturer. Flow meters are used in the system Model (YOKOQAW-Burkert S030- model: AXF080G-D1AL1S-CA11-21A) with digital display (YOKOQAW-Burkert types 8202-8222) see Figure 4.7. Output signal: 4TO 20 MA DC with digital communication (BRAIN PROTOCOL) where Measurements span: 1 To 100 KPA (4 To 400 In H_2O) where the calibrated range is from 0 to 800 l/min.

4.5.3 Different Pressure Transmitter

The Different Pressure Transmitter Model: EJA110E-DMS4J-912DB/D3 is used in this experimental see Figure 4.8. The calibrated from the manufacturer represented by output signal: 4 TO 20 MA DC with digital communication (BRAIN PROTOCOL) where Measurements span: 0-20kPa, process connection for 1/2NPT FEMAL CONECTER with

BOLTS AND NUTSMATERIAK ASTM-B7 CARBON STEEL. The calibrated range is from 0 to 20kPa.

Figure 4. 7: Flow meter

Figure 4. 8: Different Pressure Transmitter.

4.6 Experimental procedure

The experimental procedure was as follows:-

1. A suitable entrance pipe diameter was selected to obtain the required expansion ratio.

2. All the instruments were calibrated to being used for data tuning.

3. The liquid pump -discharged liquid at different velocities was obtained by turning a regulator connected to the pump.

4. Power regulator and temperature controller were used to supply the required heating.

5. The steady state condition was achieved after 2 hours in each experimental observation. However, at every half an hour increment from the beginning, the readings were taken to observe the rate of increase of temperature. The subsequent runs for other Reynolds numbers and height ranges were conducted by following the same procedure.

6. During experiment two runs at the same condition were performed to provide data reproducibility. It was observed that the acquired data were correct within ± 2% accuracy and 95% confidence level.

7. For each test run, the following readings were recorded:-

The current in amperes, the voltage in volts, the readings of all thermocouples in (°C), and the step height in (mm).

4.7 Data reduction method

The heat transfer from the test section can be calculated from the input power

Power = V× I (4.1)

The total heat supplied (Q_t) = power

Convection heat transfer (Q_c) to flowing liquid is represented by the equation (4.2).

$$Q_t = Q_C - Q_{loss} \quad (4.2)$$

where Q_{loss} is the heat losses from the outer pipe and the insulation to the surroundings.

The total losses due to conduction from the outer pipe and the insulation can be calculated by equation (4.3).

$$Q_{loss} = Q_{loss}(\text{insulation}) + Q_{loss}(\text{outer pipe})$$

$$Q_{loss} = \left(\frac{\Delta T}{\frac{1}{2\pi KL}\mathrm{Ln}\left({}^{r_o}/_{r_i}\right)}\right)_{\text{Insulation}} + \left(\frac{\Delta T}{\frac{1}{2\pi KL}\mathrm{Ln}\left({}^{r_o}/_{r_i}\right)}\right)_{\text{pipe}} \quad (4.3)$$

where, $(r_o)_{pipe}$ is the outer radius of the outer pipe and $(r_o)_{fiber}$ is the outer radius of the insulation.

$(r_i)_{pipe}$ is the inner radius of the outer pipe, and outer (r_i) is fiber inner radius of the insulation

The convection heat flux is given by Holman (Holman, 2002)

$$q_c = {}^{Q_c}/_{A_s} \quad (4.4)$$

where, A_s is the surface area.

The local heat transfer coefficient is given by Holman (Holman, 2002)

$$hx = \frac{q_c}{(T_{sx} - T_b)} \quad (4.5)$$

Where, T_{sx} measures the local surface temperature.

$T_b$is the bulk temperature and is calculated by $T_b = \frac{T_i + T_o}{2}$ (Holman, 2002)

The local Nusselt number Nu_x based on the length of the test pipe is given by Holman (Holman, 2002).

$$Nu_x = \frac{h_x . L}{K_f} \quad (4.6)$$

The Reynolds number based on the hydraulic diameter is given by Holman (Holman, 2002).

The dimensionless pumping power is calculated by the nanofluid flow rate and the pressure drop across the passage.

$$P_{Pump} = \frac{Q.\Delta P}{\mu^3 \rho^{-2} D_h^{-1}} \quad (4.7)$$

Where μ and ρ are represent viscosity and density of nanofluid, respectively, Q is the flow rate and ΔP pressure drop across the passage, d_h hydraulic diameter

$$Re = \frac{UD_h}{\nu} \quad (4.8)$$

CHAPTER 5: Nanofluid Preparation and its Properties

5.1 Introduction

In the present work, a two-step method is used to produce Al_2O_3–water nanofluids with volume fractions from 0.5% to 2%. Preparing deionized water by using water distillation W4L FAVORIT (Model WCS4L / W4L favorit Distillate output: 4 L per hour single distillation Power Supply: 220 / 240 V, 1.5 Watt, single phase) before using it in the experiments see Figure 5.1. Al_2O_3 spherical nanoparticles with a mean diameter of 13 nm purchased from Sigma-Aldrich Co., Selangor, Malaysia was selected as the source material see Figure 5.2. The first step is to mix Al_2O_3 nanoparticles in the deionized water as a base fluid. PH is one of most important parameter as effect on colloidal stability of oxide nanoparticles by control electrostatic charge found on surfaces of the particles. To get good dispersed nanofluids with prevent the nanoparticles from agglomerating and settling the pH of deionized water adjusted about 4.5 by add HCl based on (Peyghambarzadeh et al., 2013; Saidur et al., 2011). Four different volume concentrations of Al_2O_3 nanoparticles selected as sample then dispersed in 100 ml of DI water which prepare by four straight sided clear glass jars. The second step is mixing Al_2O_3 nanoparticles in the DI water by an ultrasonic disrupter (120 W, 50 kHz) for 60 min. The sample preparation with different volume fractions is presented in Figure 5.3. To prevent the clustering of nanoparticles and obtain good thermal conductivity of nanofluids the time of ultrasonic vibration of 60 min. During the preparation process of nanofluids there is no surfactant added to avoid effects on the thermal conductivity and viscosity of nanofluids.

Figure 5. 1: Water distilling.

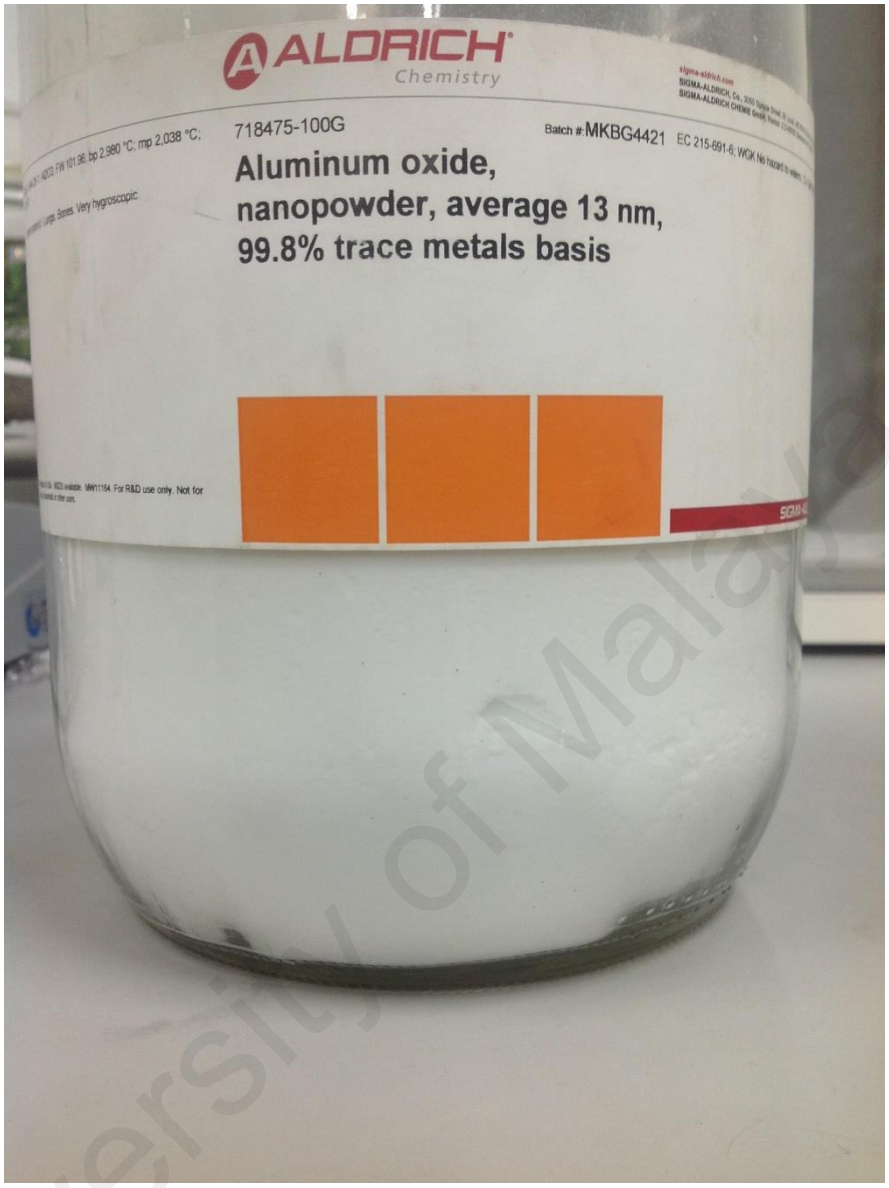

Figure 5. 2: Nano powder of Aluminum Oxide (13nm).

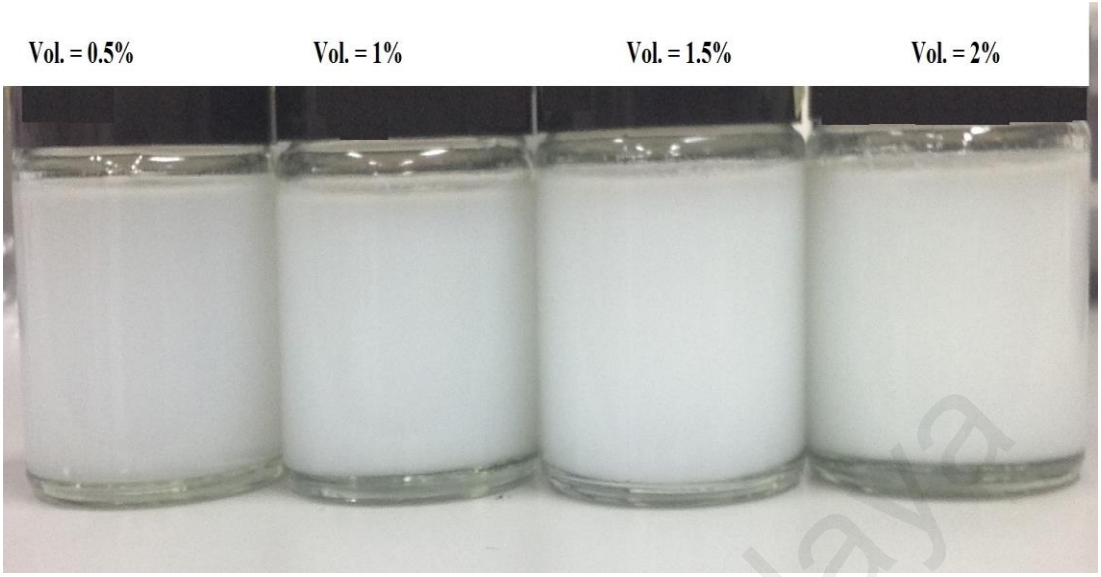

Figure 5. 3: The sample preparation with different volume fractions.

5.2 Thermal conductivity

KD2 Pro thermal analyzer (KD2 Pro, Decagon Devices, Inc., Pullman, WA, USA) has been used to measure thermal conductivity of nanofluids see Figure 5.4. The main principle works of KD2 Pro thermal analyzer based on a transient hot wire method with a 2-4% accuracy. A single needle sensor (1.3-mm diameter × 60-mm long) was used for measure thermal conductivity and was installed in a jacketed beaker connected to a water bath. In order to get high accurate measurements the experimental set-up ensures temperature stability. To keep the temperature at 20°C, 25°C, 30°C, 35°C, 40°C, 45°C when measuring the thermal conductivity of nanofluid samples water bath (WiseCircu, Witeg Labortechnik GmbH, Wertheim, Germany) with 0.1°C accuracy was used. Nanofluids were employed into the jacketed beaker, and the temperature was kept constant for each test. The water bath contain inlet and outlet tube for flowing and circulating water at a specific temperature for maintain temperature stability. Every 30 min the measurements for each sample were

recorded where the thermal conductivity of the sample is calculated as the mean of ten readings at the same temperature.

Figure 5.5 shows the effective thermal conductivity of the Al_2O_3 nanofluids as a function of the temperature at different volume fractions. The data showed that the thermal conductivity of nanofluids increases with increase of temperature for all concentrations where it is seen linear dependence of the thermal conductivity enhancement on the temperature. The enhancement of thermal conductivity after adding Al_2O_3 nanoparticles were between 5% to 20%.

5.3 The viscosity

The viscosity of the Al_2O_3 nanofluids at a different volume fraction was measured by using an Anton Paar rheometer (Physica MCR 301, Anton Paar GmbH, Graz, Austria) at different temperatures with a 1% error rate. The instrument contains of two parallel cylindrical surfaces with a gap of 0.500 mm; the mobile cylinder has a diameter of 50 mm. The viscosity of the nanofluids was measuring by varying temperatures and volume fraction of Al_2O_3 nanofluids. Figure 5.6 shows the viscosity with different temperatures and volume fraction of Al_2O_3 nanofluids at high shear rate of 100 S^{-1}. The results showed that the viscosity decrease with the increased of temperatures for all volume fraction of Al_2O_3nanofluids.

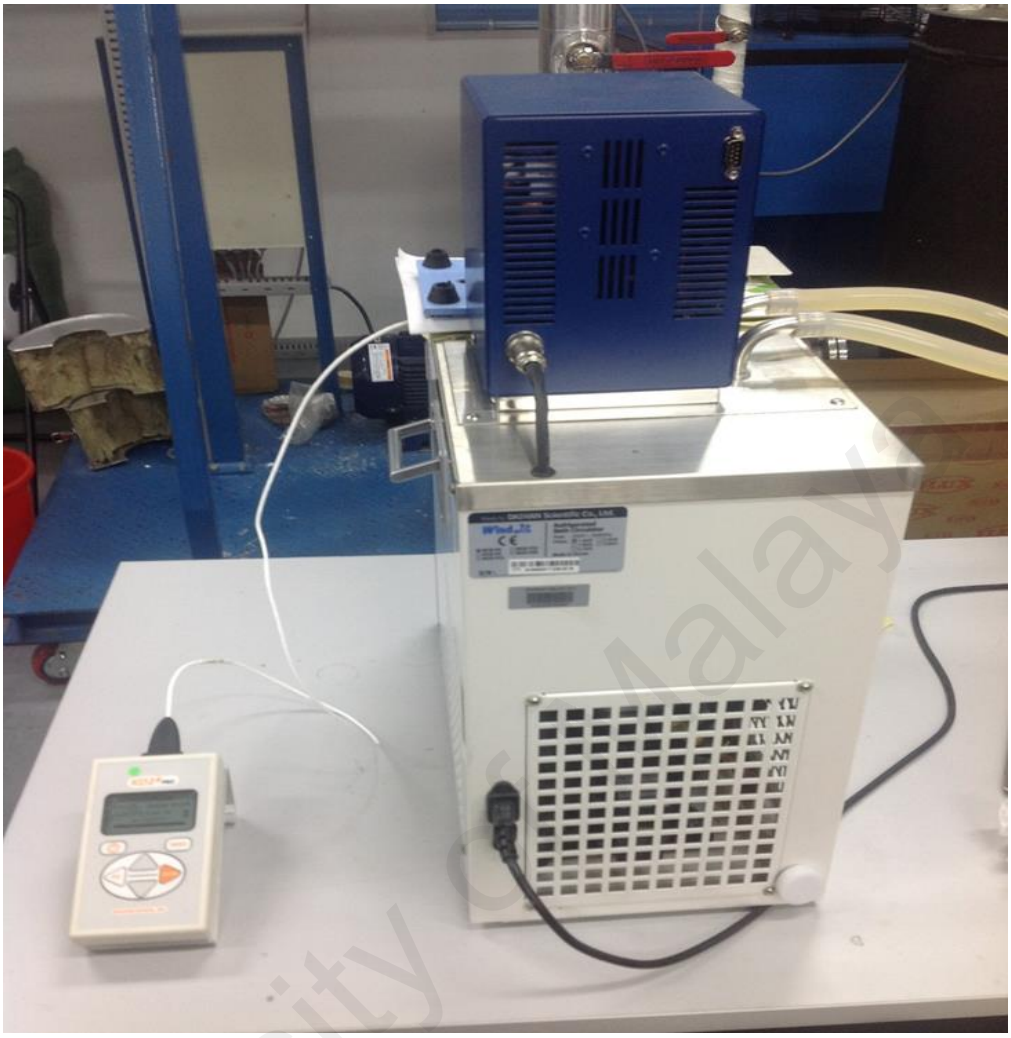

Figure 5. 4: KD2 Pro thermal analyzer and water bath

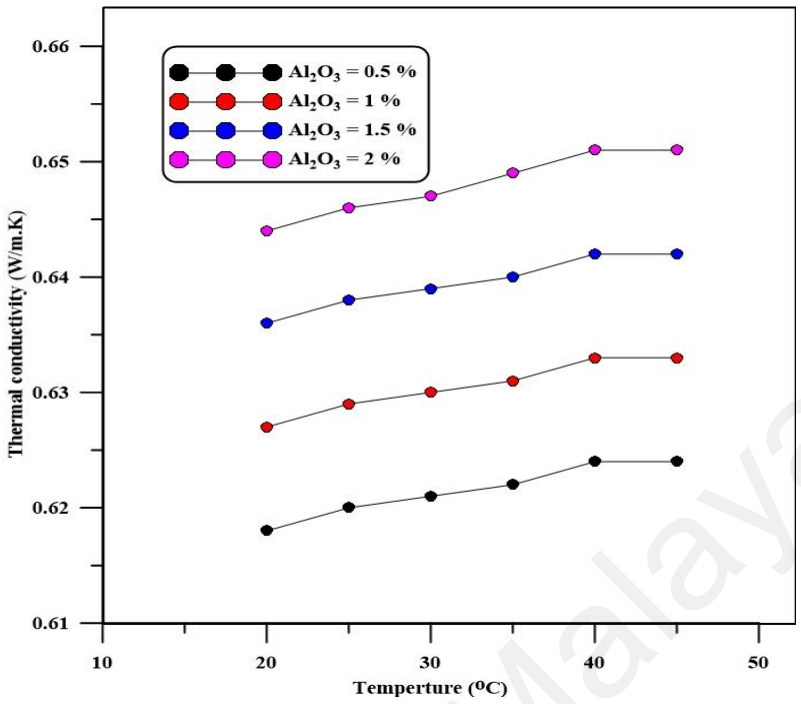

Figure 5. 5: Variations of thermal conductivity with different temperature and volume fraction of Al_2O_3 nanofluids.

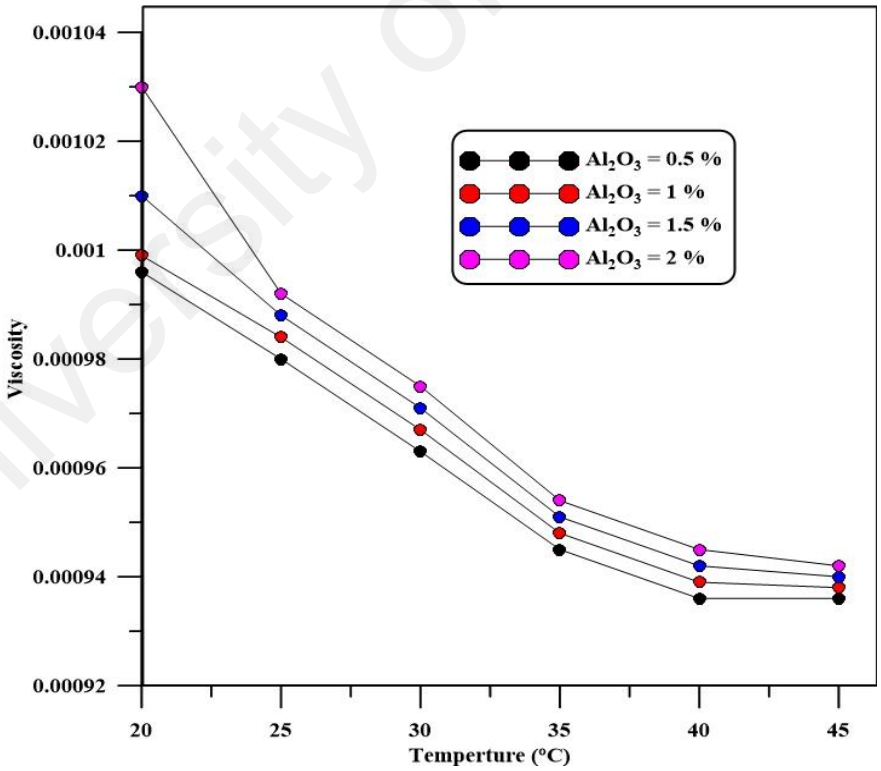

Figure 5. 6: Variations of viscosity with different temperature and volume fraction of Al_2O_3 nanofluids.

5.4 TEM Image

Transmission electron microscopy (TEM) is the main method to validate single particle sizes and to find agglomerations of particles. Figure 5.7 represents a transmission electron microscopy (TEM) image of the Al_2O_3 as received by using TEM LIBRA 120; Carl Zeiss, Oberkochen, Germany).Where the samples dried out of solution and located in the vacuum chamber of the TEM.

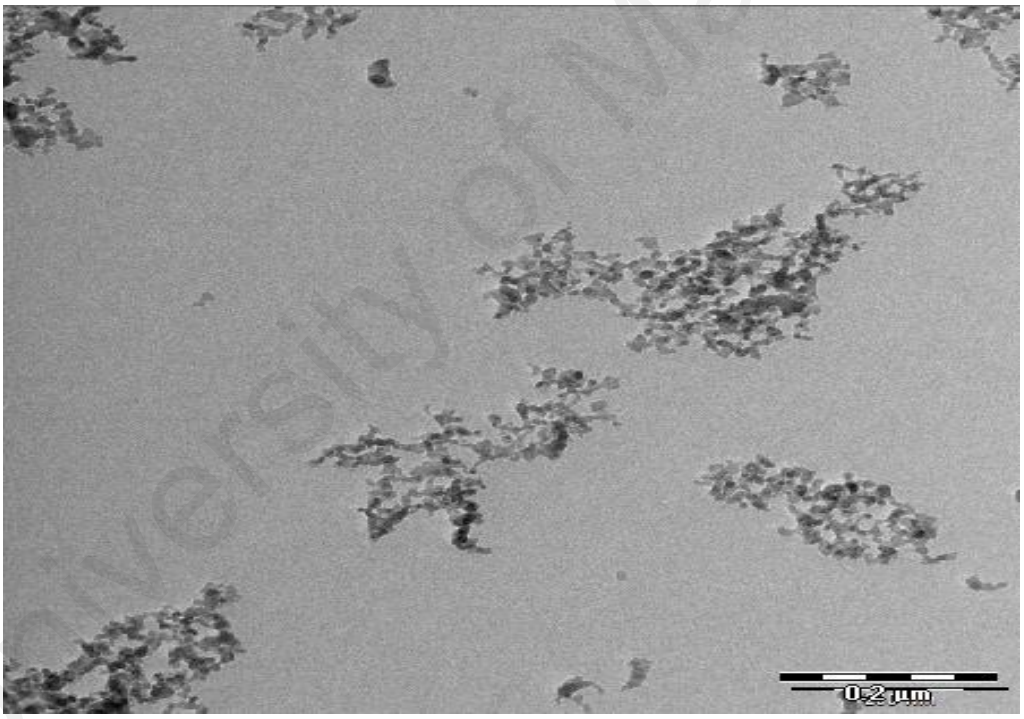

Figure 5. 7: TEM photograph of Al_2O_3 nanoparticle.

5.5 Stability

A. Stability investigation with UV–vis spectroscopy

UV–vis spectrophotometer analysis is a suitable approach to describe the stability of colloids quantitatively. Light absorbency ratio index can be computed using the Beer Lambert law as shown in Equation 5.1:

$$A = -\log\left(\frac{I}{I_i}\right) = \varepsilon bc \qquad (5.1)$$

where I is define transmitted light intensity, I_i is define incident light intensity, b is represent the optical path (cm), c is represent the molar concentration (mol/dm^3).

Figure 5.1 shows the UV–vis spectra of the Al_2O_3 dispersions at different volume fractions and wavelength with 60 min sonication. The results showed that the increase in absorbance with increased the volume fractions of the nanoparticle in the solution. The relative concentration of the Al_2O_3 dispersions during the specific time and different volume fractions are presented in Figure 5.2. It observed that decreases in concentration of Al_2O_3 nanofluids after long periods due to aggregation and sedimentation of the nanoparticles. Generally, after 12 days from dispersion by sonication the concentration of the Al_2O_3 nanofluids remains steady and no change.

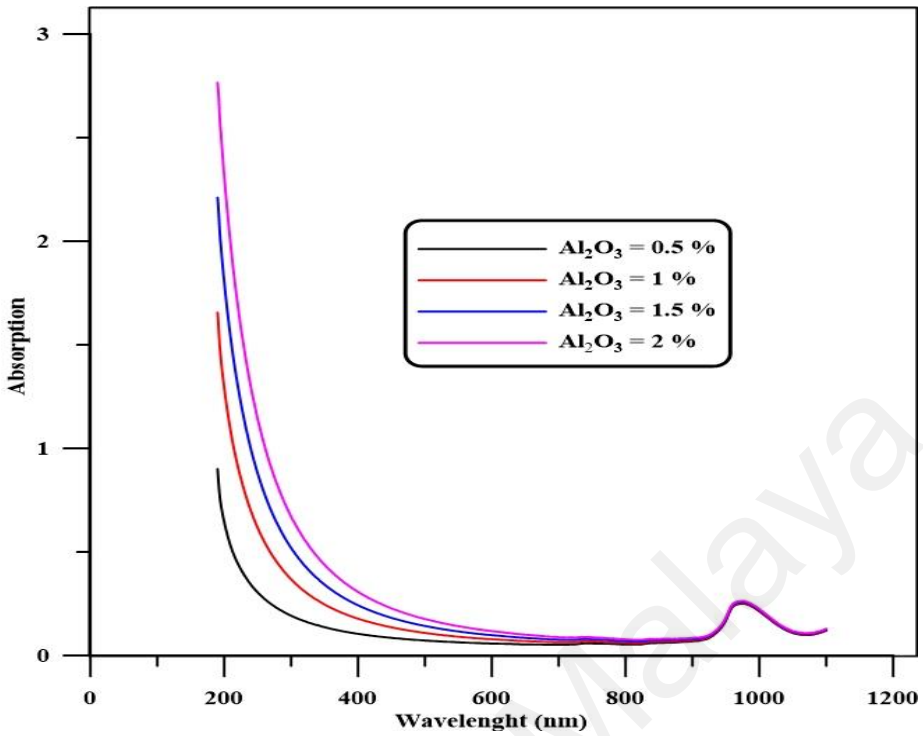

Figure 5. 8: UV–Vis spectrophotometer of Al_2O_3 nanofluids at different volume fractions and wavelength.

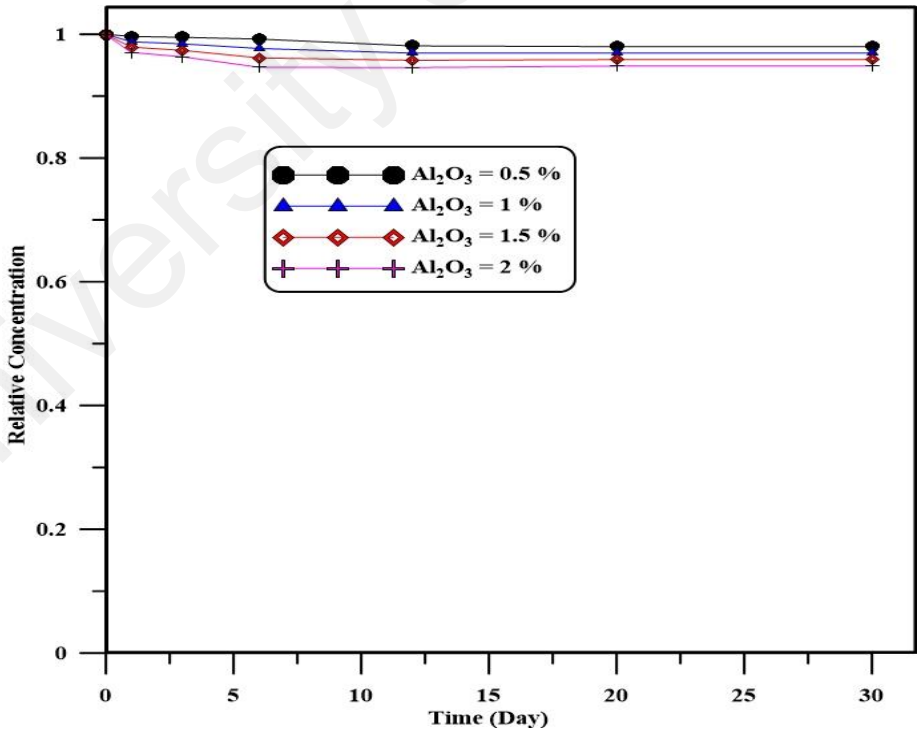

Figure 5. 9: Relative concentration of the Al_2O_3 of nanofluids with sediment time at different concentrations.

CHAPTER 6: Results and Discussions

6.1 Introduction

In this study, good agreements were achieved for comparisons of the behaviors of heat transfer between the results obtained from numerical simulations and experimental data with the maximum percentage difference between the two results of less than 9%.

Three dimensional numerical studies of heat transfer to separation Al_2O_3, CuO, TiO_2/ nanofluid flow in coaxial annular cylinders with sudden expansion are presented. The numerical simulation has been carried out by standard k-ε turbulence model with varied boundary conditions such as expansion ratio (ER= 1.25, 1.67, and 2), Reynolds number ranging from 20000 to 50000, and nanoparticle volume fractions of 0 to 2% at heat flux varied from 4000 to 16000 W/m^2.

6.2 Numerical results

6.2.1 The effect of Reynolds number

Effect of Reynolds number on heat transfer coefficient profile for pure water flow and Al_2O_3, CuO, TiO_2 nanofluid flow of 2% at expansion ratio 2 is presented in Figures 6.1, 6.2, 6.3, and 6.4, respectively. The computational results showed that increase in surface heat transfer coefficient with increase of Reynolds number where the regions of peak heat transfer coefficient observed closer to corner of sudden expansion due to the recirculation flow as generated in that region. Increase of nanoconvection as created between nanoparticles due to increase in flow rate which leads to increase of heat transfer coefficient. Moreover, the curves of surface heat transfer coefficient suffering decreases after the sudden expansion region where converge together up to exit.

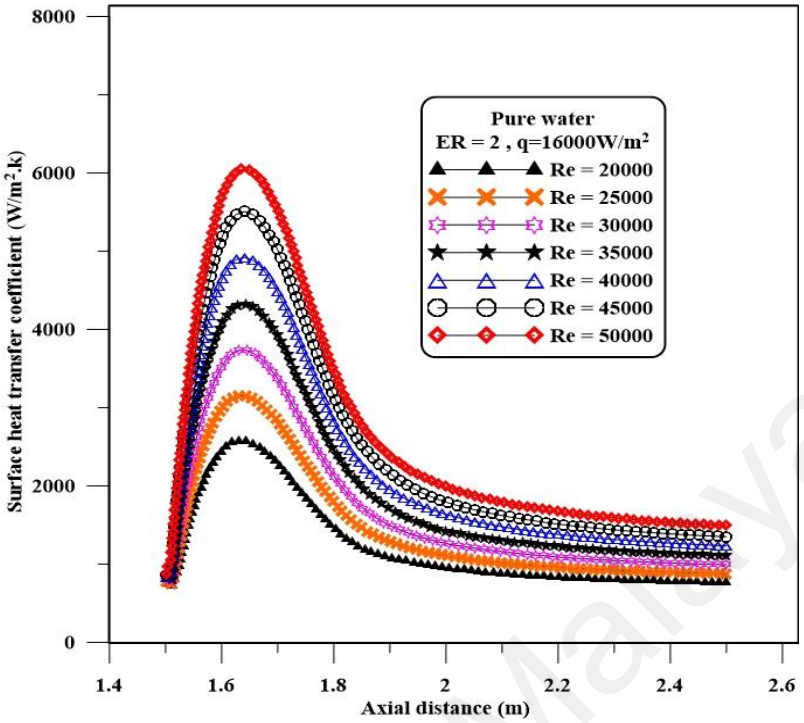

Figure 6. 1: Variations of surface heat transfer coefficient at different Reynolds number and ER=2 for pure water.

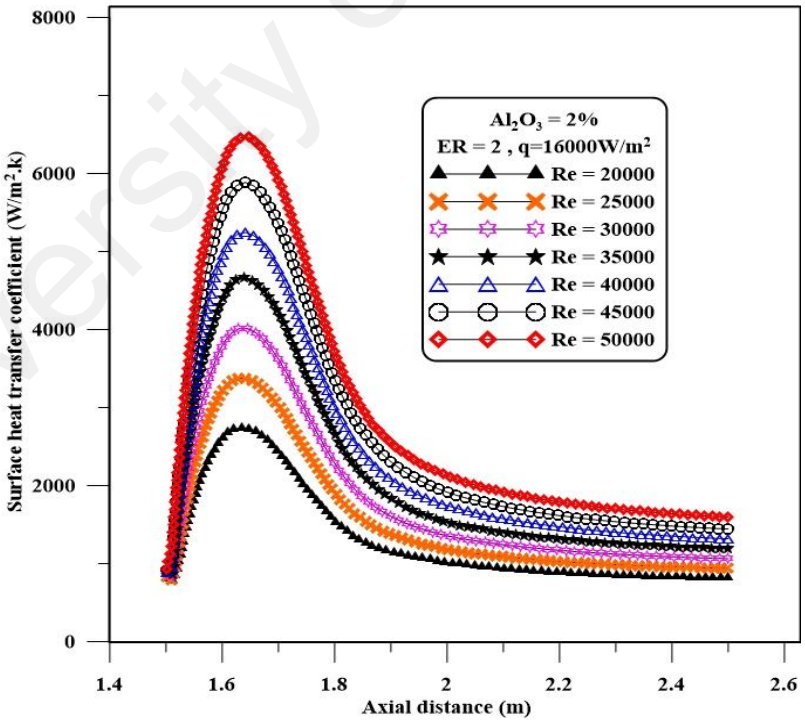

Figure 6. 2: Variations of surface heat transfer coefficient at different Reynolds number and ER=2 for 2%Al_2O_3.

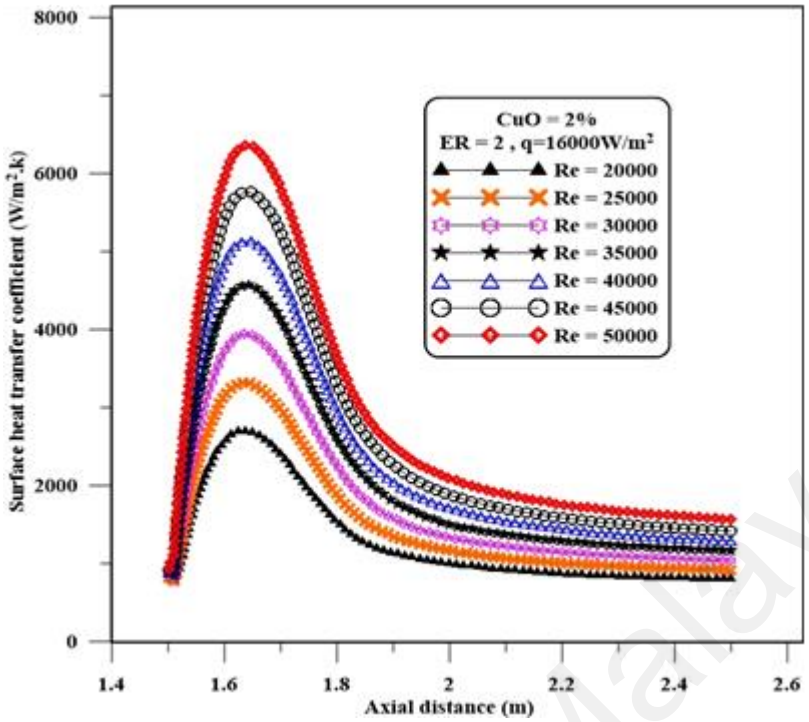

Figure 6. 3: Variations of surface heat transfer coefficient at different Reynolds number and ER=2 for 2%CuO.

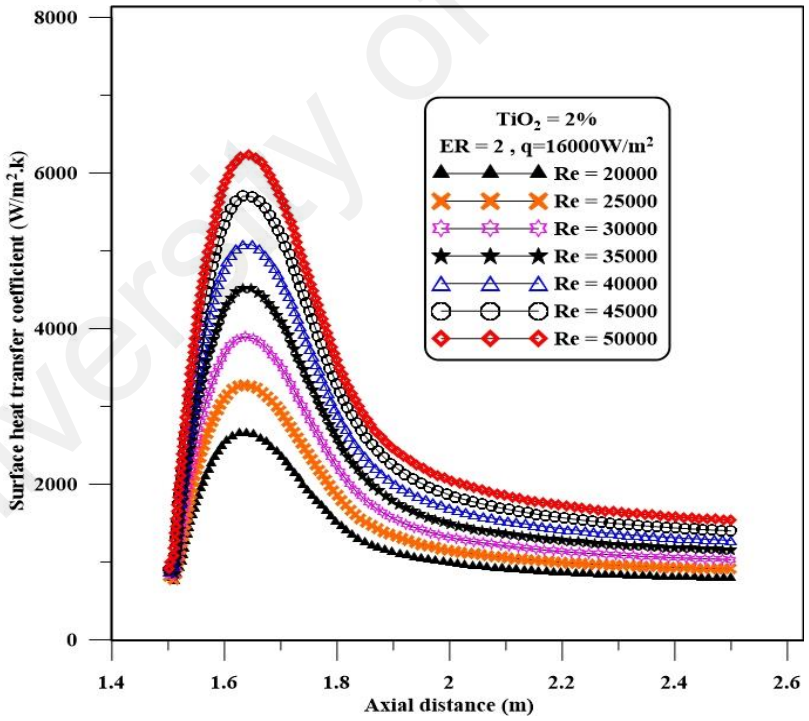

Figure 6. 4: Variations of surface heat transfer coefficient at different Reynolds number and ER=2 for 2%TiO_2.

6.2.2 The effect of expansion ratio

The effect of expansion ratio on surface heat transfer coefficient for water and Al_2O_3, CuO, TiO_2 nanofluid flow through the annular passage at Reynolds number of 50,000 is illustrated in Figures 6.5, 6.6, 6.7, and 6.8. Generally, the local heat transfer coefficient increase at the entrance region of sudden expansion where the peak of heat transfer coefficient point has been seen shifts far from the step heights and decreases gradually towards the exit of passage due to the separation flow which created at the expansion region. Results also showed that the increase in expansion ratio leads to increase of heat transfer coefficient. In the present investigation the highest value of heat transfer coefficient is noticed at the expansion ratio of 2 compared to other cases.

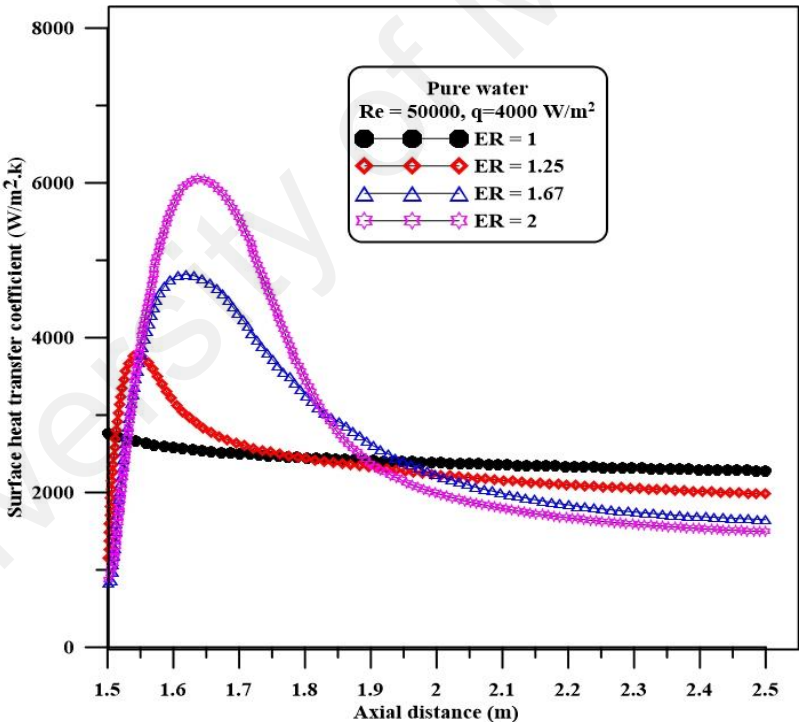

Figure 6. 5: Variations of surface heat transfer coefficient for at different expansion ratio and Re = 50,000 pure water.

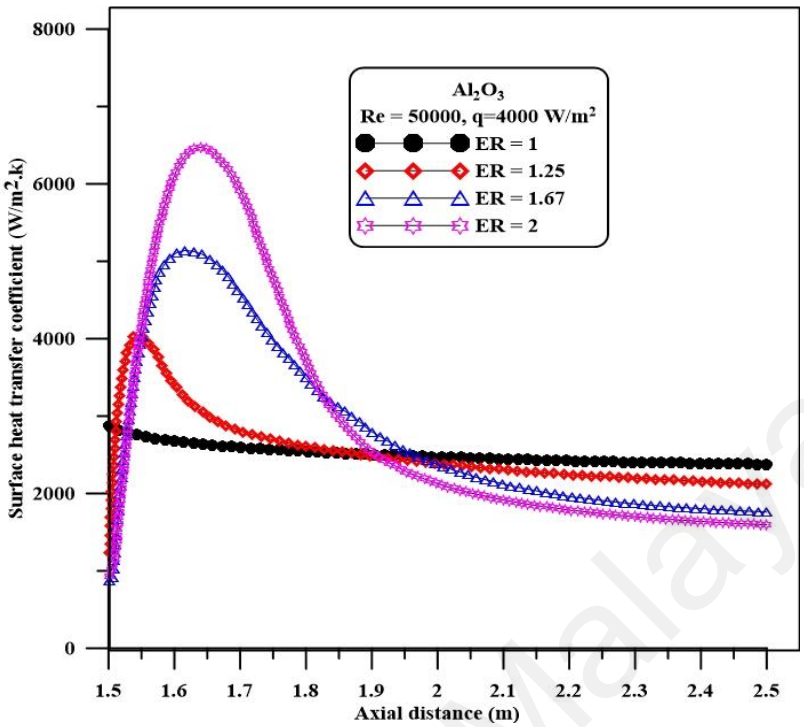

Figure 6. 6: Variations of surface heat transfer coefficient for at different expansion ratio and Re=50,000 for 2% Al_2O_3.

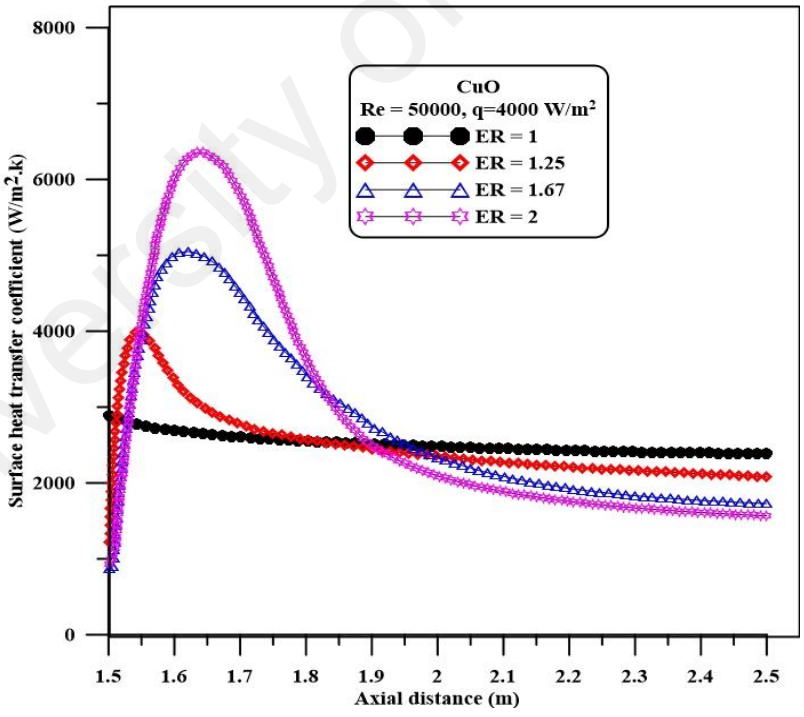

Figure 6. 7: Variations of surface heat transfer coefficient for at different expansion ratio and Re=50,000 for 2% CuO.

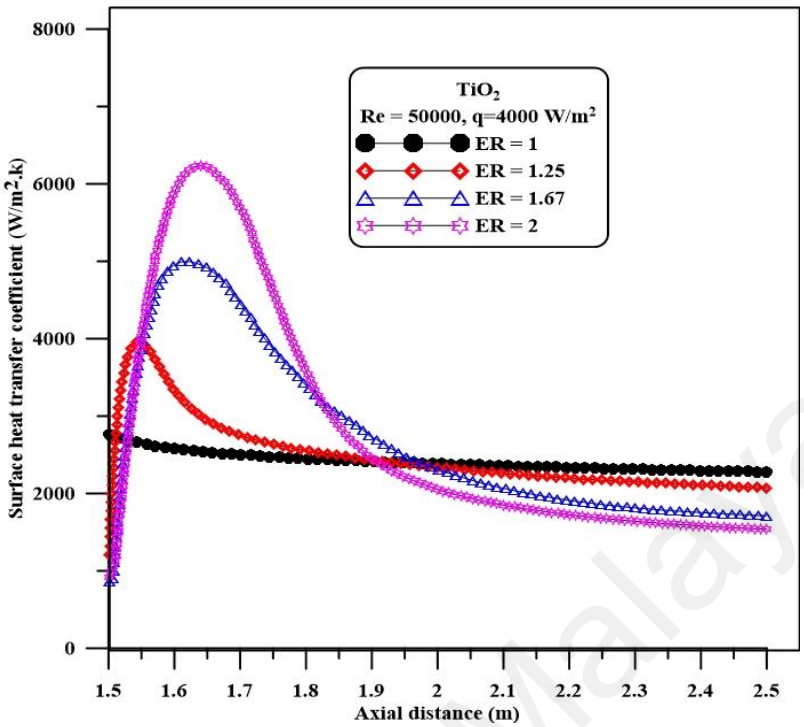

Figure 6. 8: Variations of surface heat transfer coefficient for at different expansion ratio and Re=50,000 for 2% TiO_2.

6.2.3 The effect of heat flux

Variation of the surface heat transfer coefficients of Al_2O_3, CuO, TiO_2 nanofluid at expansion ratio of 2 and Reynolds number of 50000 with different heat fluxes are presented in Figures 6.9, 6.10, and 6.11. The numerical results showed that the effect of heat flux variation is not very significant as the difference of hx between is not notable. In contrast, the surface heat transfer coefficients keep same the trend for all cases.

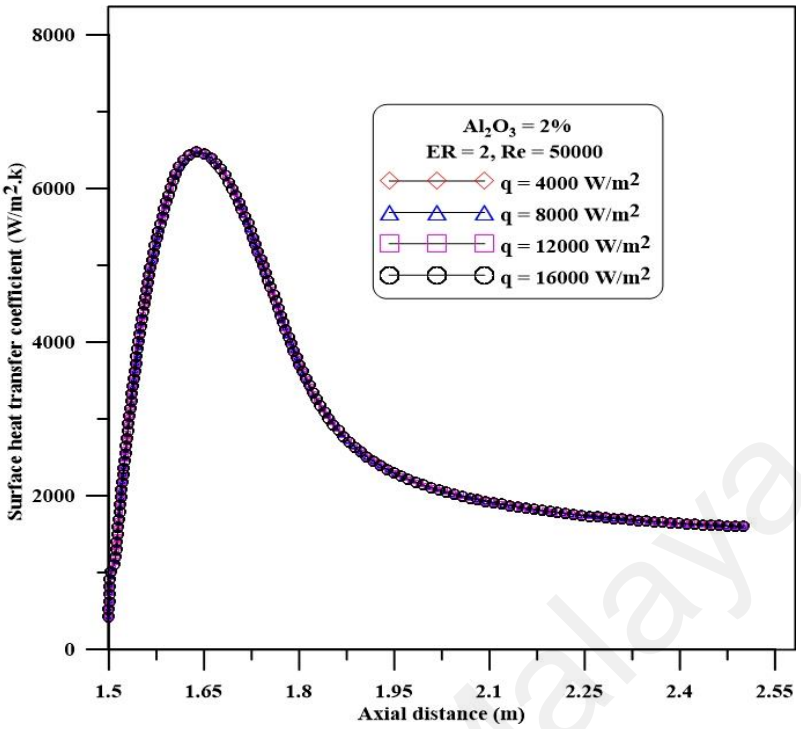

Figure 6. 9: Variations of surface heat transfer coefficient for at different heat fluxes and ER=2 with Re=50,000 for 2% Al_2O_3.

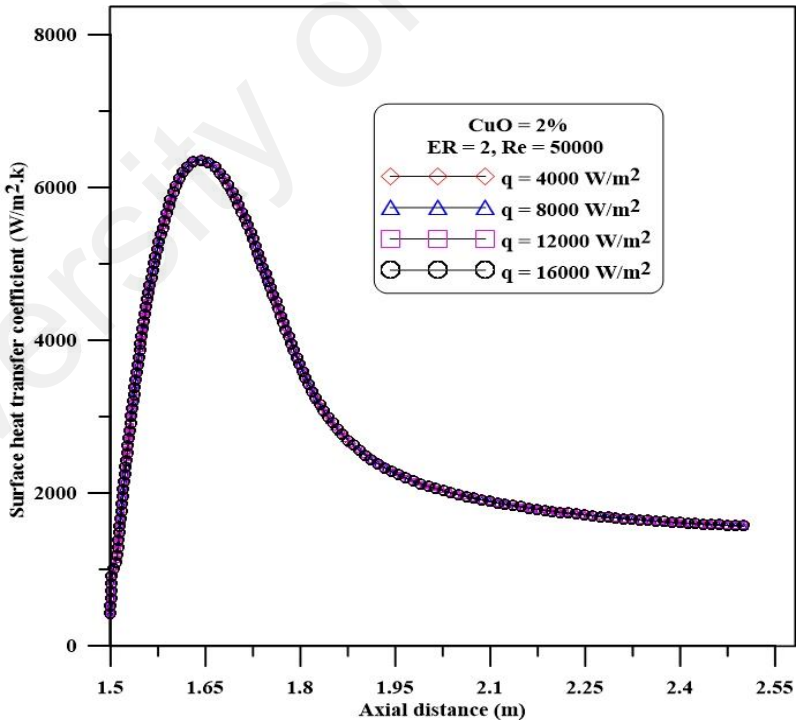

Figure 6. 10: Variations of surface heat transfer coefficient for at different heat fluxes and ER=2 with Re=50,000 for 2% CuO.

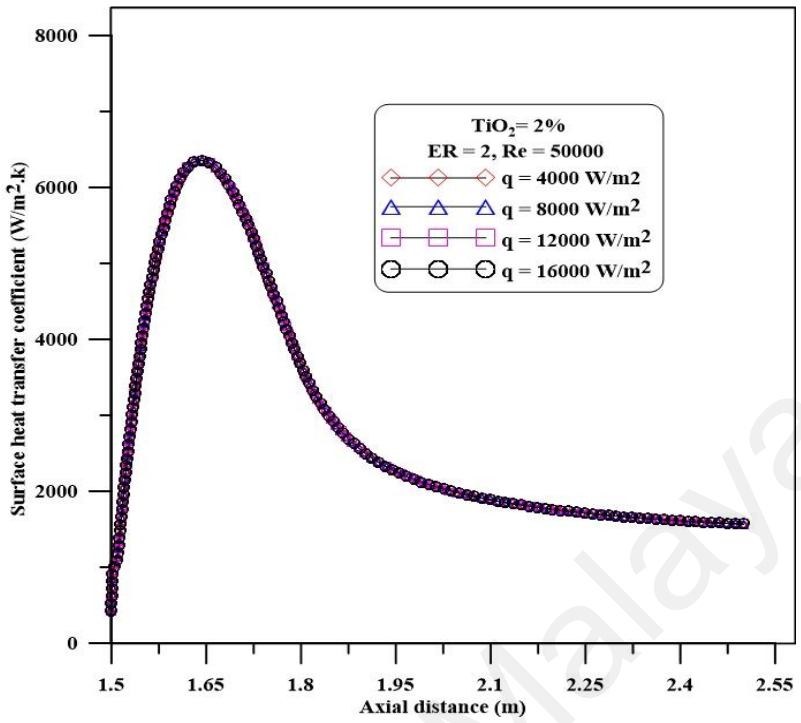

Figure 6. 11: Variations of surface heat transfer coefficient for at different heat fluxes and ER=2 with Re=50,000 for 2% TiO_2.

6.2.4 The effect of nanoparticles concentration

Figures 6.12, 6.13, 6.14 show that the variation of surface heat transfer coefficient at Reynolds number of 50000 and expansion ratio of 2 for pure water and different concentrations of Al_2O_3, CuO, TiO_2 nanofluid, respectively. It can be seen that increases in surface heat transfer coefficient with increase of volume concentration of Al_2O_3, CuO, TiO_2 nanofluid. The maximum heat transfer coefficient observed at volume concentration of Al_2O_3 nanofluid 2% and Reynolds number of 50000 compared to pure water and other concentrations of nanofluids.

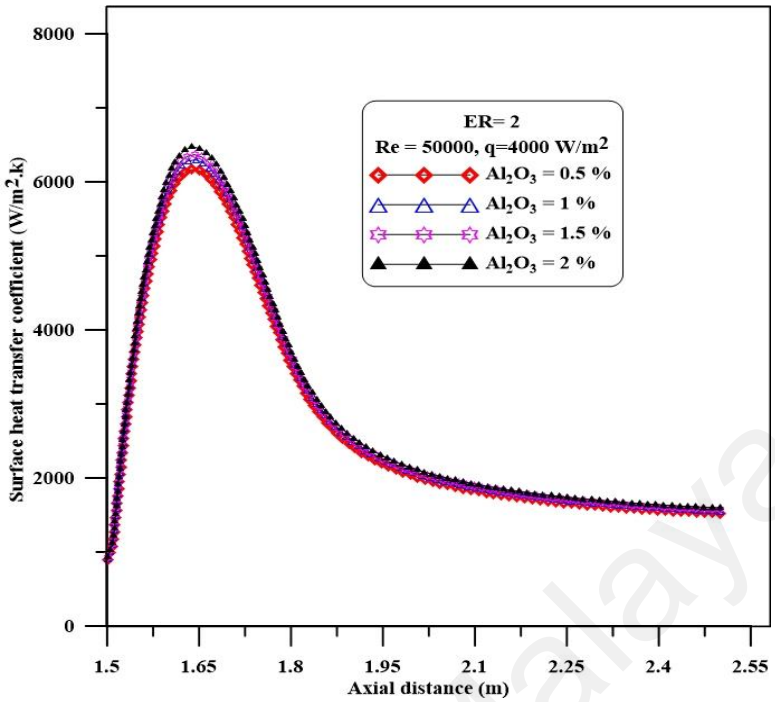

Figure 6. 12: Effect volume fractions of nanofluid on surface heat transfer coefficient at ER=2, q=4000W/m^2 with Re=50,000 for Al_2O_3.

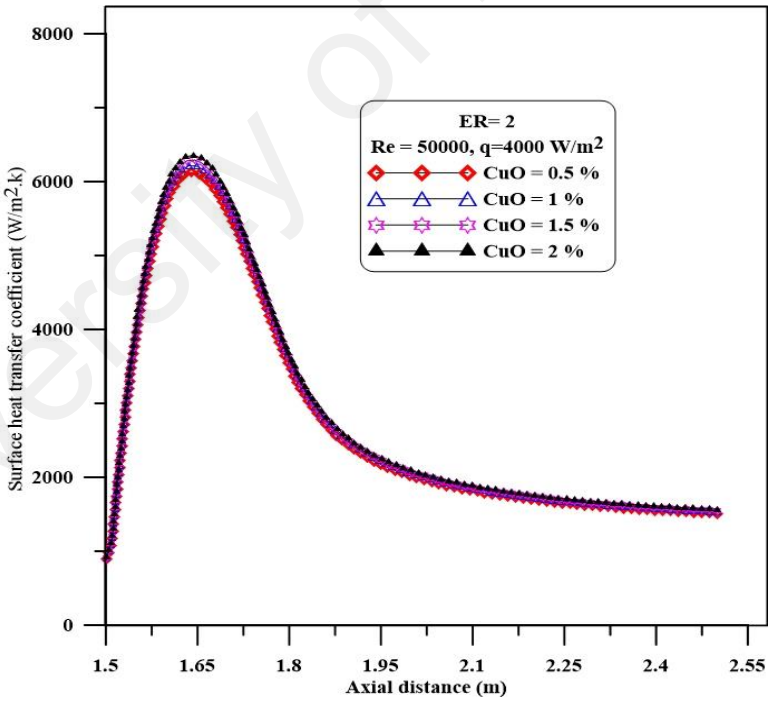

Figure 6. 13: Effect volume fractions of nanofluid on surface heat transfer coefficient at ER=2, q=4000W/m^2 with Re=50,000 for CuO.

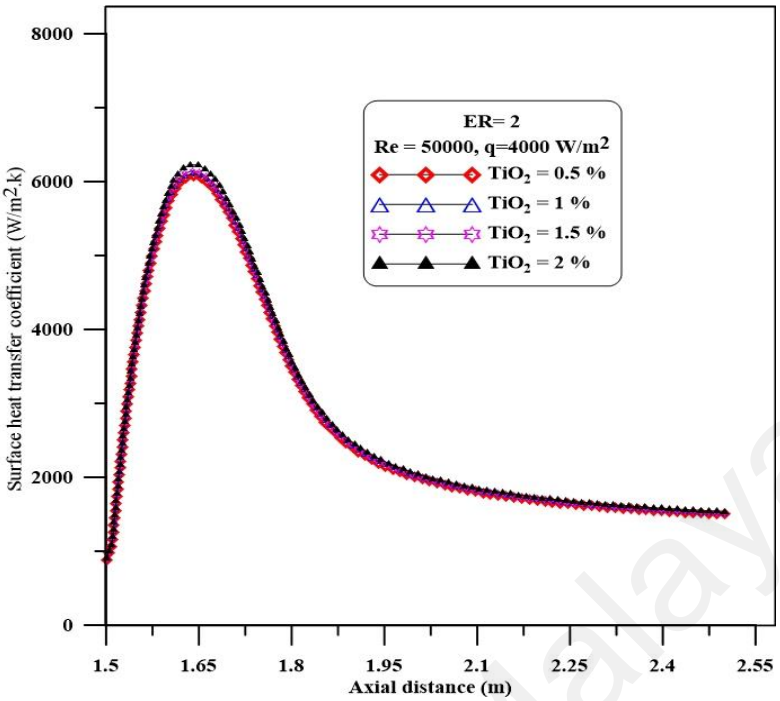

Figure 6. 14: Effect volume fractions of nanofluid on surface heat transfer coefficient at ER=2, q=4000W/m^2 with Re=50,000 for TiO_2.

6.2.5 The effect type of nanoparticles

The effect type of nanoparticles at Reynolds number 50000, expansion ratio of 2 and heat flux 4000 W/m^2 illustrated in Figure 6.15. It can be seen that the surface heat transfer coefficient was higher by using Al_2O_3 nanofluids compared with other type of nanofluids due to Al_2O_3 has higher thermal conductivity.

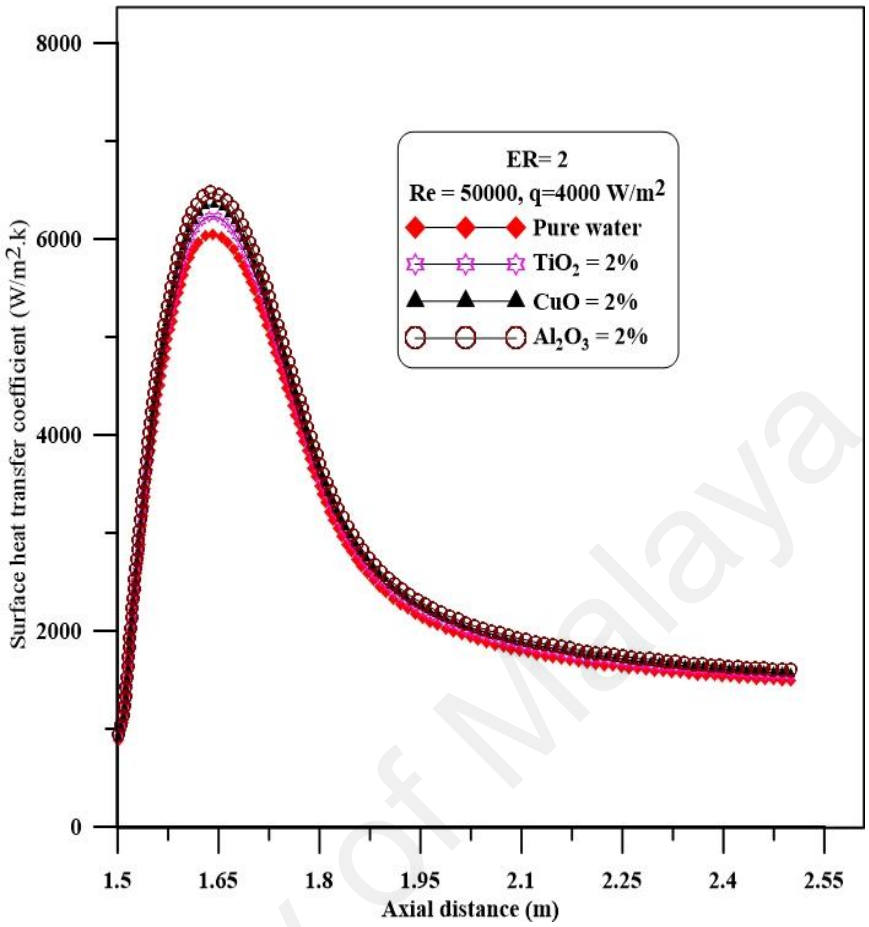

Figure 6. 15: Effect type of nanofluid on surface heat transfer coefficient at ER=2, q=4000W/m^2 with Re=50,000.

6.2.6 Streamline counter of velocity field

The streamlines at different Reynolds number with expansion ratio of 2 and 2% volume concentration of nanofluid are illustrated in Figures 6.16- 6.19. In general, the recirculation regions which created after the sudden expansion increase with the increase of the Reynolds number and the negative values of velocities represented the recirculation regions where the largest recirculation region found at the Reynolds number of 50000 in compared with others. Effect of expansion ratio on the variation of streamlines at 2% volume concentration of nanofluid and Reynolds number of 50000 is presented in Figure 6.20-6.22.

The numerical results reveal that the size of the recirculation region increases with the increase of expansion ratio due to increase of hydrodynamic pressure generated in recirculation regions. The larger recirculation region is seen at expansion ratio 2 as demonstrated where the higher enhancement of heat transfer is noticed.

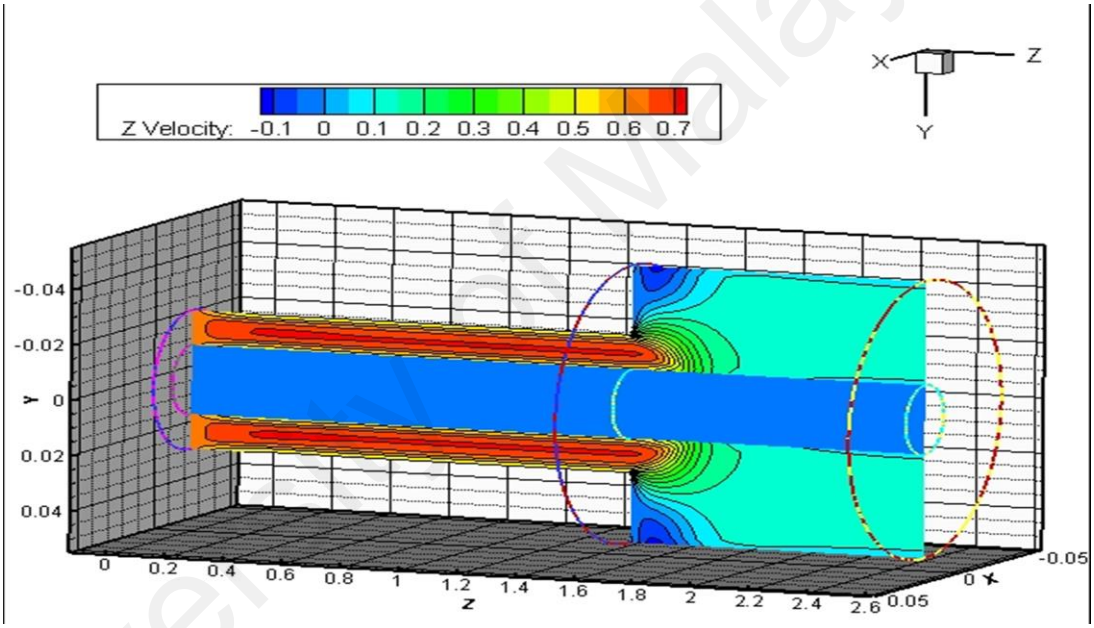

Figure 6. 16: The streamline of velocity at ER=2 and ϕ=2% for **Re=20,000.**

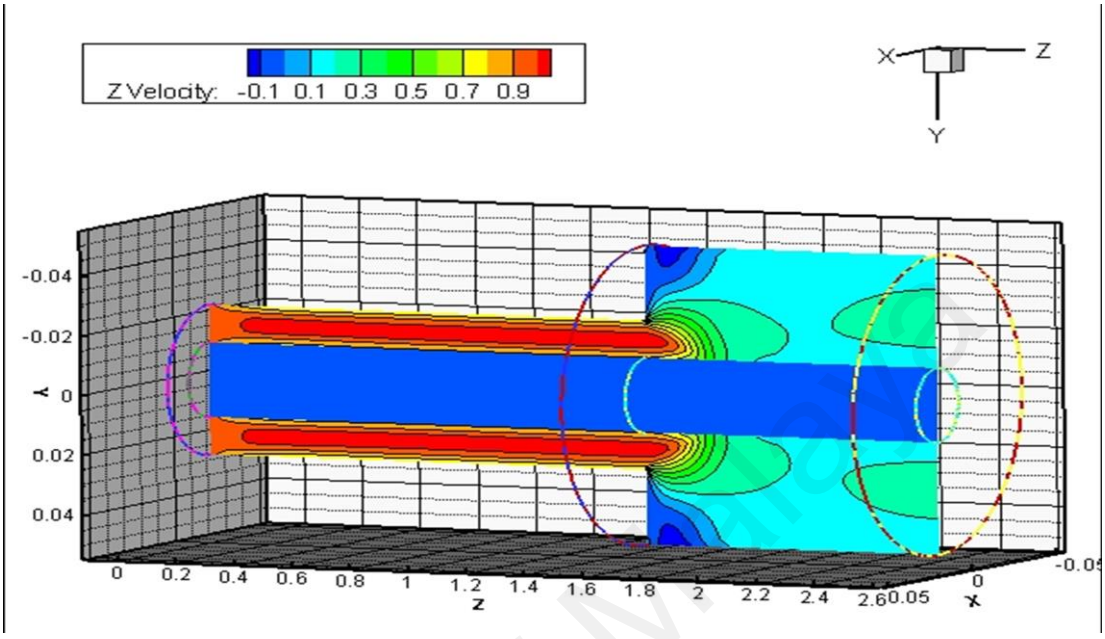

Figure 6. 17: The streamline of velocity at ER=2 and ϕ=2% for **Re=30,000**.

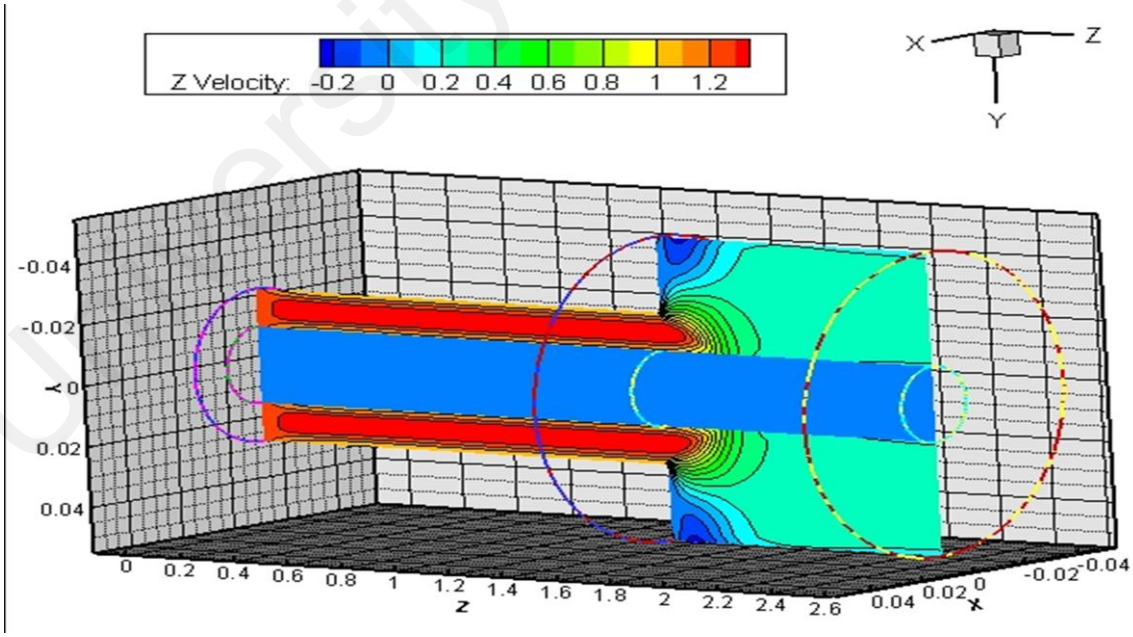

Figure 6. 18: The streamline of velocity at ER=2 and ϕ=2% for **Re=40,000**.

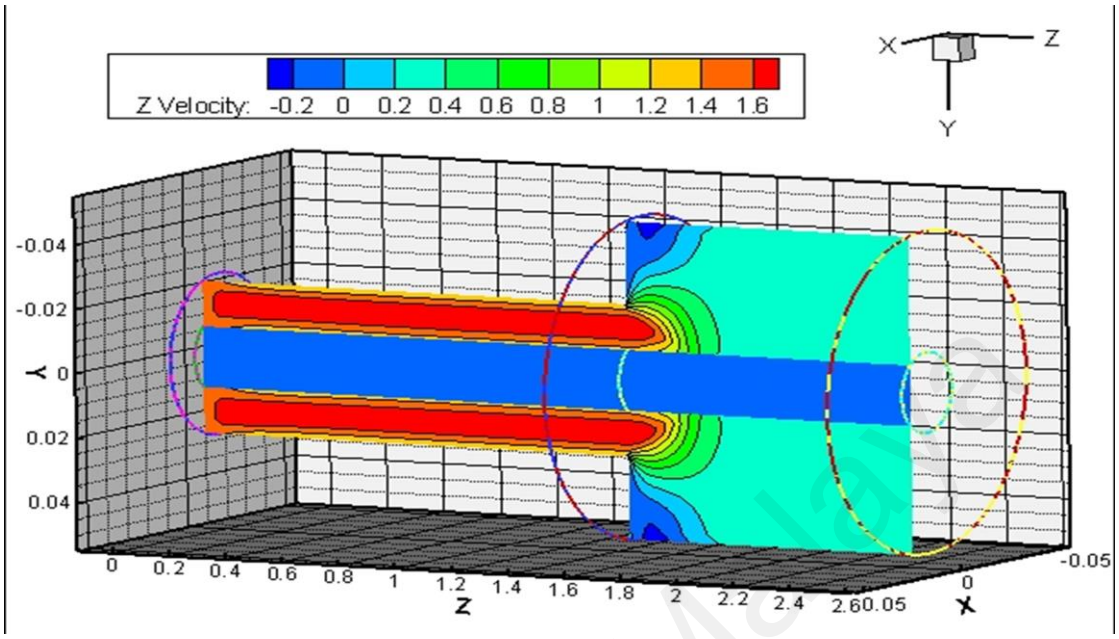

Figure 6. 19: The streamline of velocity at ER=2 and ϕ=2% for **Re=50,000.**

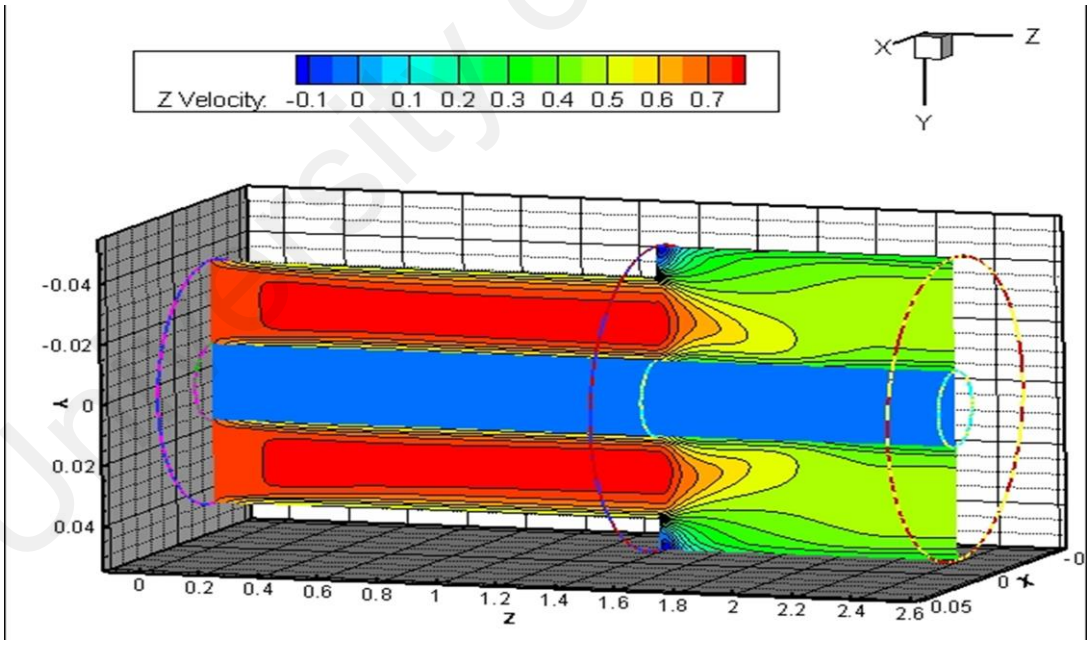

Figure 6. 20: The streamline of velocity at Re=50,000 and ϕ=2% for **ER= 1.25.**

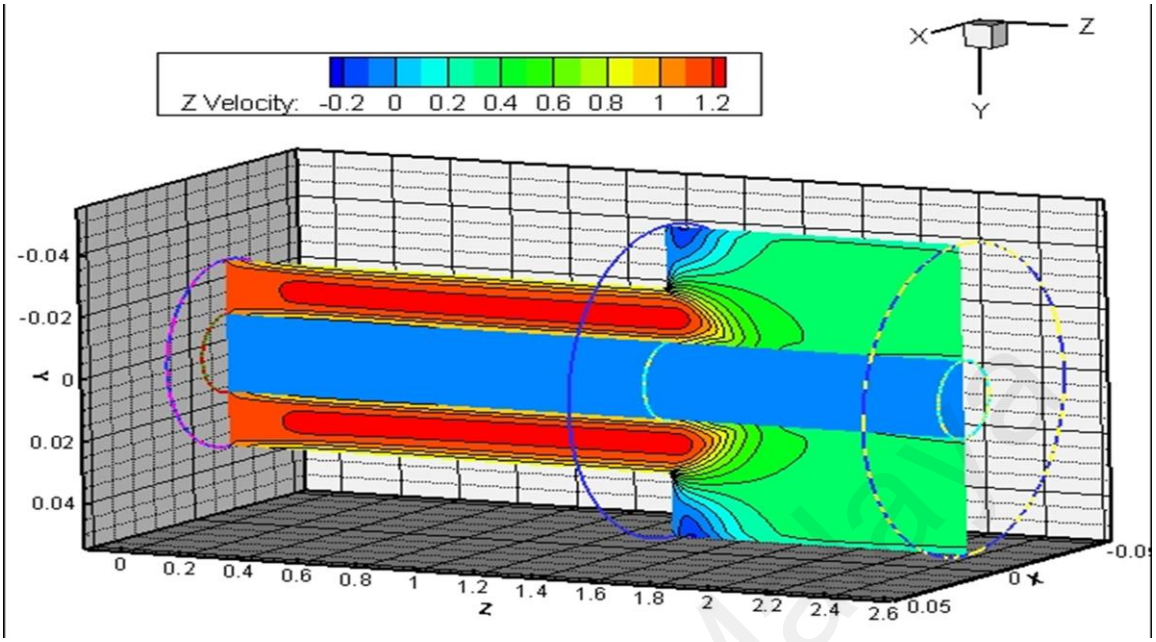

Figure 6. 21: The streamline of velocity at Re=50,000 and ϕ=2% for **ER= 1.67.**

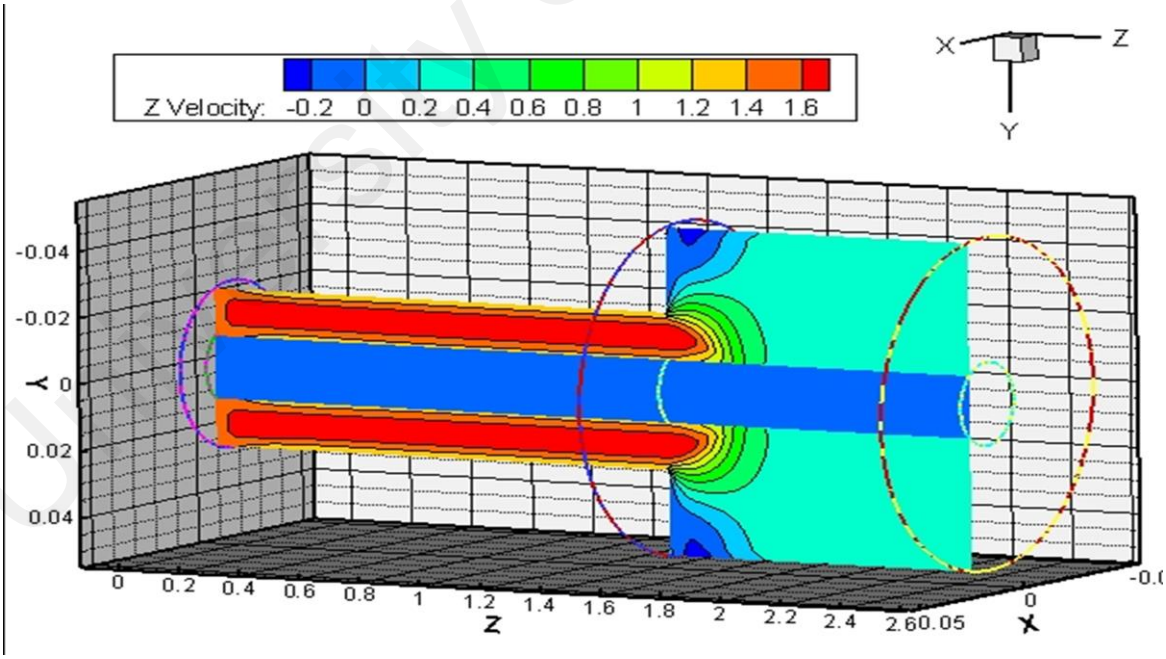

Figure 6. 22: The streamline of velocity at Re=50,000 and ϕ=2% for **ER= 2**.

6.2.7 The turbulent kinetic energy

The turbulent kinetic energy for 2% nanofluid at different expansion ratios and Reynolds number of 50000 is plotted in Figure 5.23-5.25. It can clearly be seen that increases in the turbulent kinetic energy with the increase of expansion ratio and the maximum of turbulent kinetic energy was at the expansion ratio of 2 in compared with others. The intensity of turbulent kinetic energy observed moves far from step with increase step height.

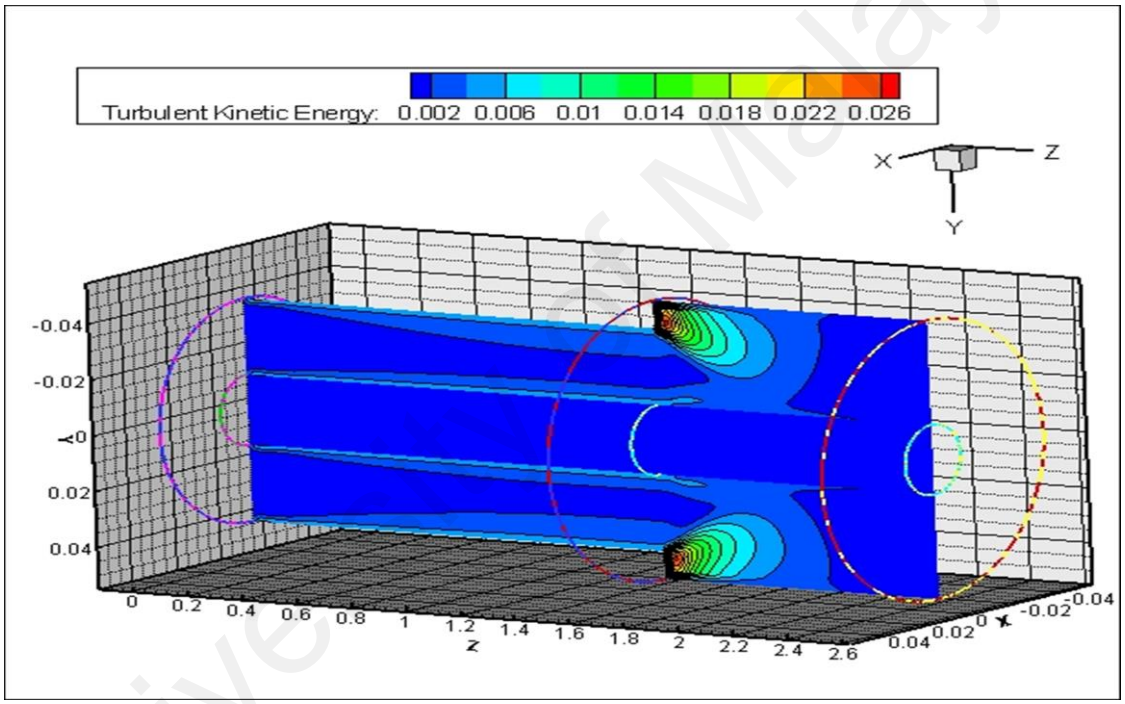

Figure 6. 23: The counter of turbulent kinetic energy for 2% nanofluid and Reynolds number of 50000 at **ER=1.25.**

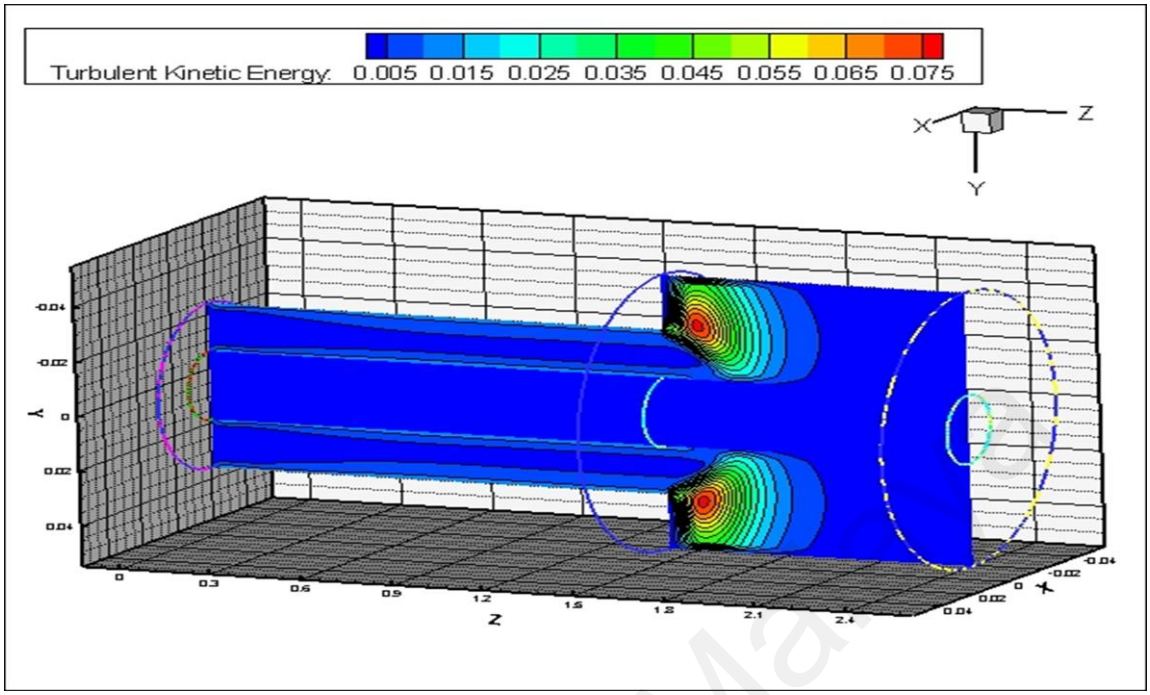

Figure 6. 24: The counter of turbulent kinetic energy for 2% nanofluid and Reynolds number of 50000 at **ER=1.67.**

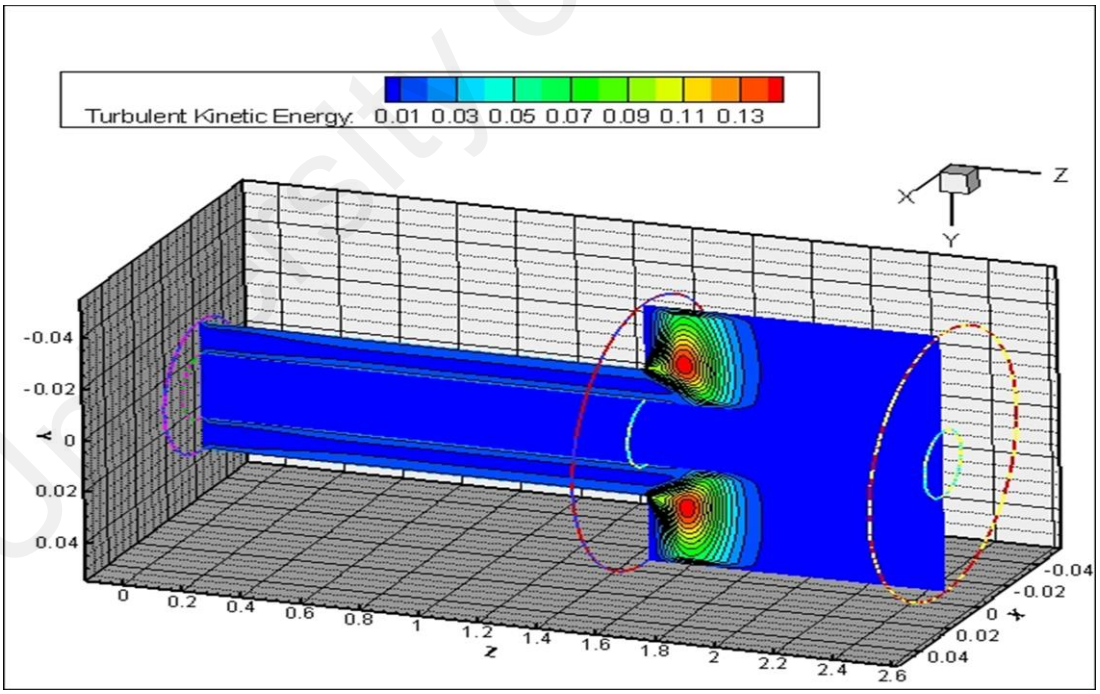

Figure 6. 25: The counter of turbulent kinetic energy for 2% nanofluid and Reynolds number of 50000 at **ER=2.**

6.3 Experimental results

The experimental measurements which used include the surface temperatures of section with a heat flux from 4000 to 16000 W/m^2, a Reynolds number from 20000 to 50000, the type of nanoparticles is represented by Al_2O_3, and expansion ratio from 1 to 2.

6.3.1 Distribution of surface temperatures

The distribution of the surface temperature on the test section at a heat flux of q= 16000 W/m^2 and Re= 50000 for different expansion ratios are shown in Figure 6.26. The trends of the surface temperature are same for both the numerical and experimental data. Generally, the surface temperature on the test section decreases at the inlet region and then increases towards the exit. The reduction of the surface temperature on the outer pipe represents the separation region, and the location of the separation point move far from the step with increase step height. The effect of the expansion ratio on the distribution of the surface temperature appears clearly at the inlet region of passage, where the minimum of the surface temperature represents the separation point. The separation regions, which causes an enhancement of the heat transfer due to turbulence enhancement. The increase of the separation region results from the increase of the expansion ratio, which leads to an increase of the augmentation of the heat transfer.

Figure 6.27 shows the effect of the Reynolds number on the surface temperature of the test section, where the decrease of the Reynolds number leads to an increase of the surface temperature at the heat flux q=16000 W/m^2 and the expansion ratio ER=2. All cases keep same trends where the surface temperature deceases at the inlet region of sudden expansion and then increase gradually up to exit.

Effect of volume fraction of Al_2O_3 nanofluids on distributions of surface temperature of the test section for Reynolds number of 50,000 and expansion ratio of 2 are presented in Figure 6.28. The results showed a decrease in the surface temperature with increase of volume fraction of Al_2O_3 nanofluids due to increase in heat transport by nanoparticles though the base liquid then obtained the good cooling on the surface of test section.

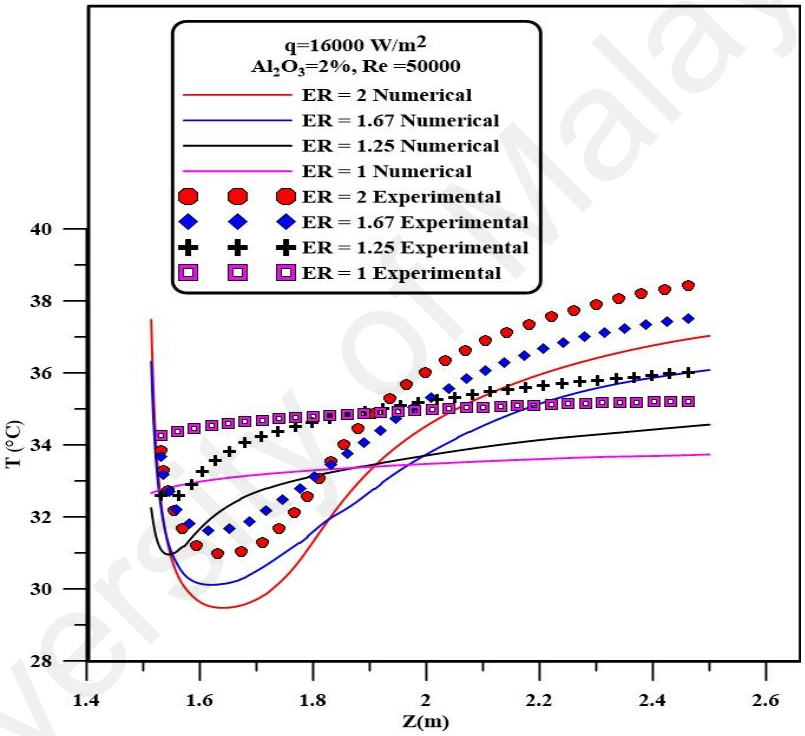

Figure 6. 26: Distribution of the surface temperature at heat flux of q= 16000 W/m^2 and Re= 50000 for different expansion ratios.

6.3.2 Average heat transfer coefficient (h_{ave})

The variations in the average convective heat transfer coefficient with different Reynolds numbers and expansion ratio of 2 at Al_2O_3, CuO, TiO_2 volume fractions of 2% and pure water are presented in Figure 6.29. Increases in average heat transfer coefficient with increases of Reynolds number observed for all type of nanofluids. The maximum average heat transfer coefficient showed with Al_2O_3volume fractions of 2% in compared with others and good agreement between numerical and experimental results noted for pure water and Al_2O_3 nanofluids.

Figure 6.30 illustrated the effect of expansion ratio on average heat transfer coefficient at Reynolds number of 50,000 for Al_2O_3, CuO, TiO_2 volume fractions of 2% and pure water. The numerical and experimental results showed that increase of average heat transfer coefficient with increased expansion ratio where the highest value of average heat transfer coefficient found at Al_2O_3 volume fractions of 2% and expansion ratio of 2 compared to others.

Effect of volume faction of nanofluids on average heat transfer coefficient at expansion ratio of 2 and Reynolds number of 50,000 are presented in Figure 6.31. It can be seen that the increase of volume faction of nanofluids leads to increase in average heat transfer coefficient due to increase thermal conductivity of base liquid. The maximum improvement of heat transfer observed at Al_2O_3 volume fractions of 2% compared with other type of nanofluids.

Generally, thermal performance for maximum expansion ratio (ER=2) is about 35% with using water while thermal performance for using different volume fractions of nanofluids with ER= 2 and Re= 50000 was presented Table 6.1

Table 6. 1: Thermal performance for using nanofluids with ER= 2 and Re= 50000

Vol. %	Thermal performance		
	TiO_2	CuO	Al_2O_3
0.5	5.3%	6.4%	7%
1	6.5%	7.8%	8.9%
1.5	7.7%	9.3%	10.5%
2	8.6%	10.7%	12.3%

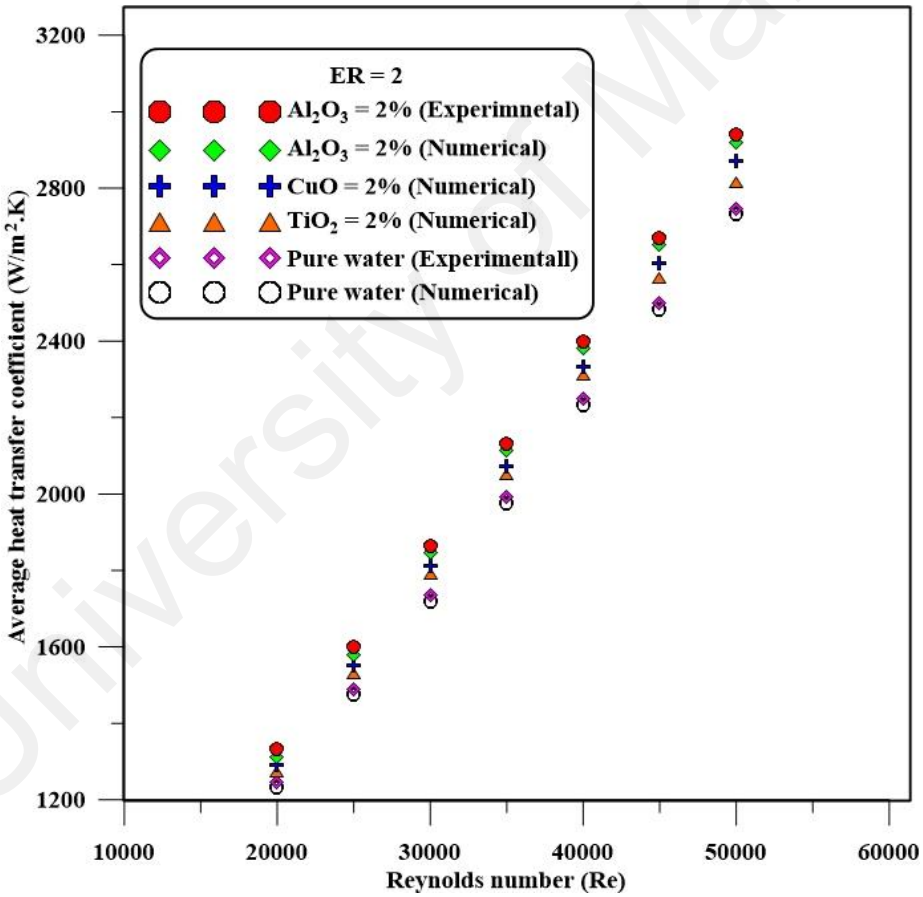

Figure 6. 29: Average heat transfer coefficient with different Reynolds numbers and expansion ratio of 2 at Al_2O_3, CuO, TiO_2 volume fractions of 2% and pure water.

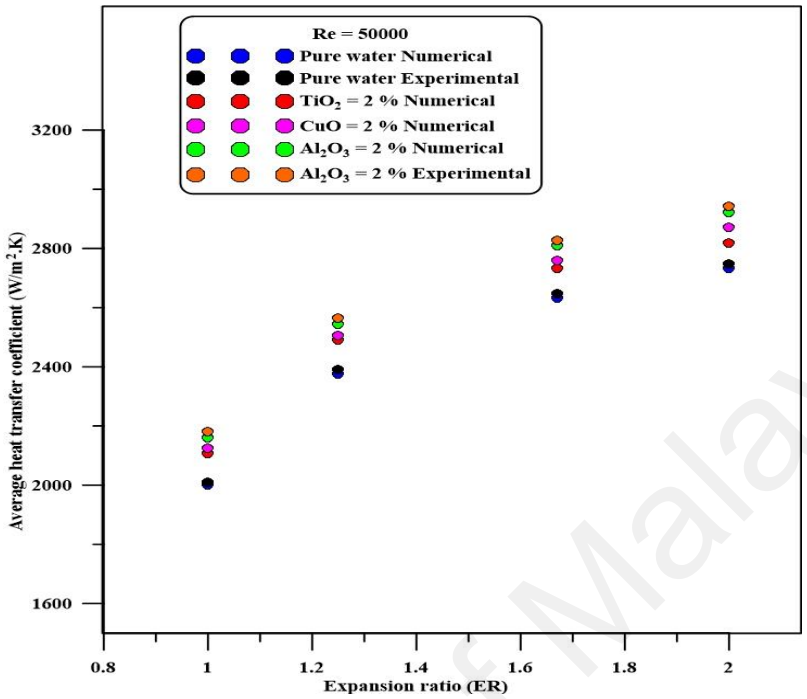

Figure 6. 30: Effect of expansion ratio on average heat transfer coefficient at Reynolds number of 50,000 for Al_2O_3, CuO, TiO_2 volume fractions of 2% and pure water.

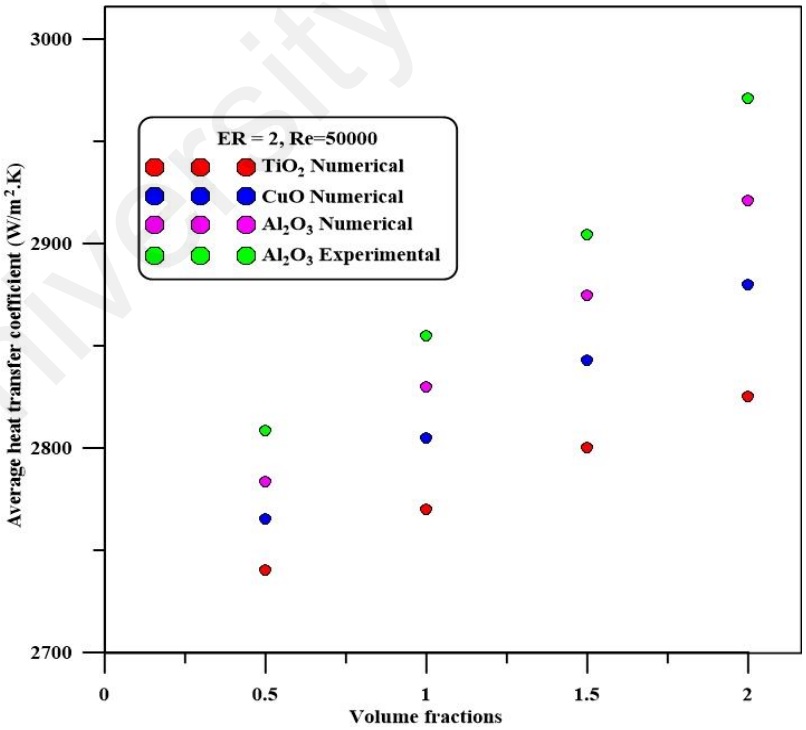

Figure 6. 31: Effect of volume faction of nanofluids on average heat transfer coefficient at expansion ratio of 2 and Reynolds number of 50,000.

6.3.3 Average pressure drop

Figure 6.32 and 6.33 showed that the effect of Reynolds number and volume fractions of nanofluids on average pressure drop at expansion ratio of 2, respectively. Generally, the average pressure drop increases linearly with increase both Reynolds number and volume fractions of nanofluids. The increment of pressure drop at expansion ratio of 2 and Reynolds number of 50,000 for different volume fractions of nanofluids presented in Table 6.2 where the highest increment of pressure drop obtained at CuO volume fractions of 2% compared with other type of nanofluids.

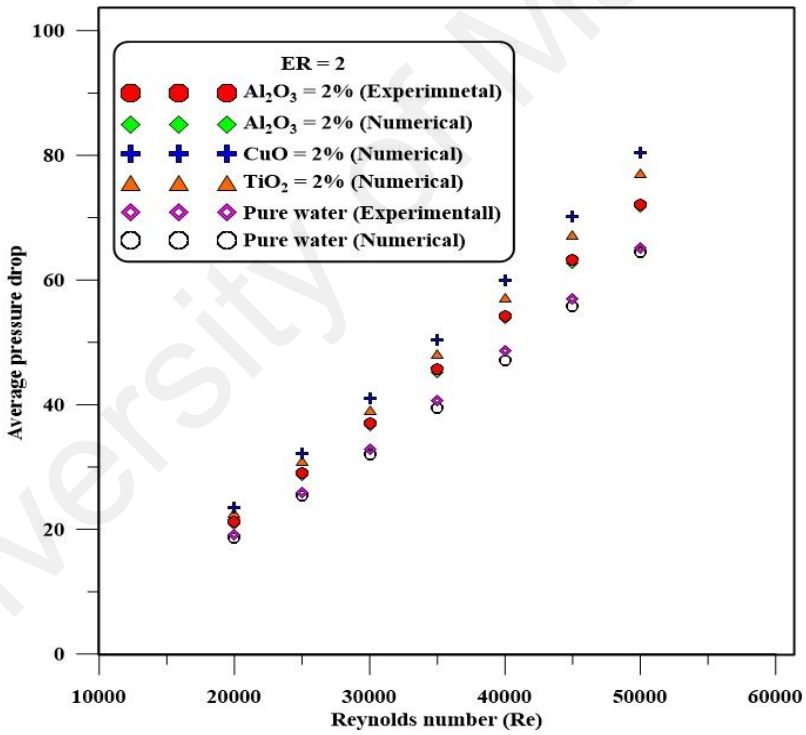

Figure 6. 32: Effect of Reynolds number on average pressure drop at expansion ratio of 2.

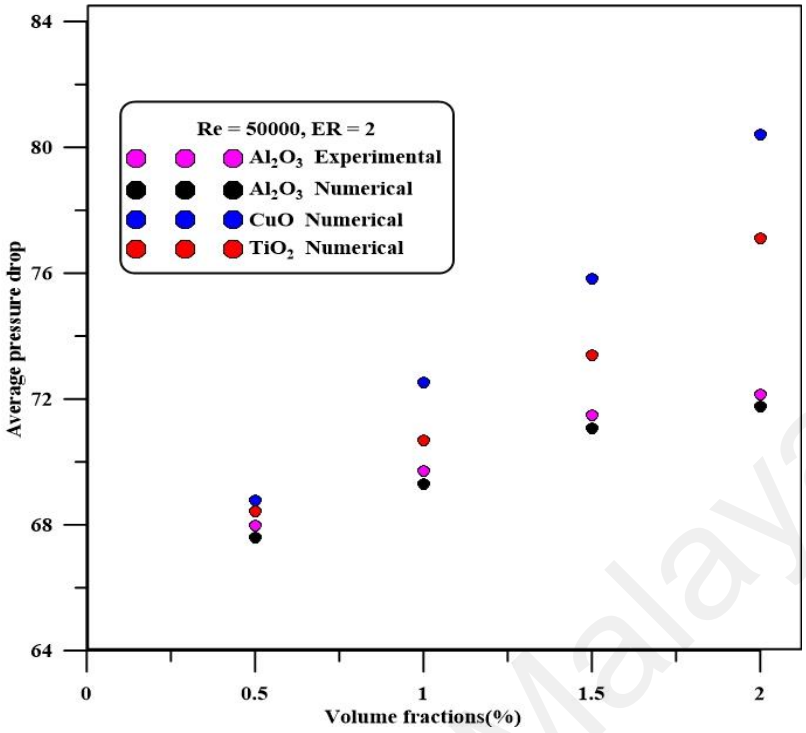

Figure 6. 33: Effect of volume fractions of nanofluids on average pressure drop at expansion ratio of 2.

Table 6. 2: Increment of Pressure drop at Reynolds number of 50,000 and expansion ratio. ER = 2.

Vol. %	Increment of pressure drop		
	TiO_2	CuO	Al_2O_3
0.5	3.5%	4%	3%
1	5.5%	7.5%	5%
1.5	8%	10.5%	6.5%
2	12%	15.5%	8%

CHAPTER 7: Conclusions and Recommendations

7.1 Conclusions

Experimental work and numerical simulations (using ANASYS FLUENT 14 software package) were done for the turbulent heat transfer and separation nanofluid flow through an annular pipe with sudden expansion. Three dimensional study based on finite volume method with standard k-ε turbulence model was performed. It is noted that the surface heat transfer coefficient increases when nanoparticle volume fraction or the Reynolds number increased. The results have shown that the separation regions formed after the sudden expansions considerably affect the surface heat transfer coefficient and pressure drop where the lowest of pressure drop and highest thermal performance are detected at Reynolds number 50000, 2% Al_2O_3 water based nanofluid at expansion ratio 2 in comparison to others. The enhancement of heat transfer was about 36.6 % for pure water at expansion ratio 2 compared to heat transfer obtained in straight pipe. Augmentation of heat transfer could be achieved by using nanofluid at expansion ratio 2 where the total improvements were about 45.2% (TiO2), 47.3 %(CuO), and 49 %(Al_2O_3). Moreover, the increase in the pressure drop was about 42% for pure water at expansion ratio 2 compared with straight pipe whereas by using nanofluid they were 65.4% (CuO), 62% (TiO_2), and 57.6 % (Al_2O_3). The counters of velocity and turbulent kinetic energy have demonstrated the feature of separation and reattachment region as generated after the sudden expansion. Good agreements obtained between numerical and experimental data all were obtained.

..

7.2 Recommendations

Thus depending on the specify purpose sudden expansion of different configurations could be used with the application of nanofluid instead of conventional fluids. Where consequently heat transfer is preferred over enhanced friction losses the present data could assist the designer to meet the requirement.

To keep investigation in the same line and to enhance investigation the separation problem in such geometry, following cases of investigation are supposed as a future work.

1. Continue investigation on the same rig, considering both the inner pipe and outer pipes are at constant heat flux at the test section.
2. Create double steps on both sides of the annular entrance passage and study the mutual effect of two separation zones on the heat transfer process.
3. Study the same geometry with non-Newtonian fluid.
4. Investigation of the effect of eccentricity on augmentation of heat transfer.
5. Study of the effect of angle of orientation on thermal performance.

CHAPTER 8: Extension studies on effect separation flow on thermal performance

8.1 Introduction

Three different studies based on configuration and boundary condition have been presented in this chapter. From the literature, the numerical simulation on study heat transfer and nanofluid flow through sudden expansion, over double forward facing step and single backward facing step for turbulent range has not been investigated yet.

8.2 CFD Simulation of heat transfer and turbulent fluid flow over a double forward-facing step

Abstract

Heat transfer and turbulent water flow over a double forward-facing step were investigated numerically. The finite volume method was used to solve the corresponding continuity, momentum, and energy equations using the k-ε model. Three cases, corresponding to three different step heights, were investigated for Reynolds numbers ranging from 30,000 to 100,000 and temperatures ranging from 313 to 343 K. The bottom of the wall was heated, whereas the top was insulated. The results show that the Nusselt number increased with the Reynolds number and step height. The maximum Nusselt number was observed for case 3, with a Reynolds number of 100,000 and temperature of 343 K, occurring at the second step. The behavior of the Nusselt number was similar for all cases at a given Reynolds number and temperature. A recirculation zone was observed before and after the first and second steps in the contour maps of the velocity field. In addition, the results indicate that the

coefficient pressure increased with increasing Reynolds number and step height. ANSYS FLUENT 14 (CFD) software was employed to run the simulations.

Nomenclature

a	Length of bottom wall before the first step
b	Length of bottom wall after the first step
c	Length of bottom wall after the second step
C1ε, C2ε, C3ε, σk, σε	Model constants
Cp	Specific heat
H	Width of channel before the steps
H1	Width of channel after first step
H2	Width of channel after second step
h1	Height of first step
h2	Height of second step
L	Total length of channel
K	Turbulent energy
Nu	Nusselt number
P	Pressure
Pr	Prandtl number
Re	Reynolds number
T	Temperature
U	Mean velocity
u, v	Axial velocity
X, Y	Cartesian coordinates
Greek symbols	
ρ	Water density
ε	Turbulent dissipation
μ	Dynamic viscosity
μ_t	Turbulent viscosity

8.2.1 Introduction

The goal of this study to investigate two-dimensional double forward-facing step flows, and the results of numerical computations for different step heights, temperatures, and Reynolds numbers are presented herein. Numerous studies have been performed on single forward- and backward-facing steps; however, the literature on double forward- and backward-facing steps is very limited, and the physical basis of flow separation and vortex creation remains unclear. Fluid flow over a backward- or forward-facing step generates recirculation zones and subsequent reattachment regions, due to sudden contraction or expansion in flow passages. Many practical engineering applications, such as the cooling of electronic devices, open channels, power-generating equipment, heat exchangers, combustion chambers, and building aerodynamics, involve separating flows. The first attempts to study heat transfer and fluid flow over forward- or backward-facing steps were made in the 1950's. Later, researchers were able to analyze complex flows in three dimensions due to the development of CFD software. Seban et al., (1959) and Seban, (1966) pioneered the study of fluid flow over backward- and forward-facing steps from a heat transfer perspective. The authors discovered that the maximum heat transfer coefficients occur at the reattachment point and decrease toward the outlet. The effect of stream turbulence on the heat transfer rate in the reattachment region on the bottom surface of a backward-facing step was demonstrated by (Mabuchi et al., 1986). Improvements in device capabilities have allowed researchers to measure reattachment points and heat transfer characteristics; Mori et al. (1986) used a thermal tuft probe, Kawanmura et al. (1991) obtained the temporal and spatial parameters of heat transfer in the reattachment region using a new heat flux probe, and Oyakawa et al. (1994, 1995) employed jet discharge. The hydrodynamic characteristics of gas flows past a rib and a downward step in feature separation flow regions were studied

by (Terekhov et al., 2003). The heat transfer coefficients, temperature distributions, and pressures behind the obstacles as well as the 5-10% enhancement of heat transfer at the maximum recirculation reported also agree with the results reported by (Alemasov et al., 1989). Aung, (1983), Vogel and Eaton (1985), Sparrow and Chuck, (1987), Chen et al., (2006), Masatoshi et al. (2009), and Khanafer et al., (2008) conducted numerical and experimental studies on the airflow over a horizontal backward-facing step with uniform heat flux or uniform temperature. The authors observed a decrease in the Nusselt number and recirculation zone with increasing buoyancy force and noted that the maximum Nusselt number was observed at the reattachment point. Abu-Mulaweh, (2005) experimentally studied the turbulent fluid flow and heat transfer of a mixed convection boundary-layer of air flowing over a vertical forward-facing step. The effect of the step height on the local Nusselt number distribution, namely, the increase in the local Nusselt number with increasing step height, reached a maximum value at the reattachment point. Both the inclination angle and step height affected heat transfer and flow behavior for the single forward-facing step studied numerically by (Nassab et al., 2009).

An early study on turbulent heat transfer and airflow over a double forward-facing step was reported by (Yilmaz and Hakan, 2006). The top of the wall and steps were insulated, and the bottom of the wall was heated. The authors used K-ϵ model and found that the step ratio affected the heat transfer and flow more strongly than the length ratio. Later, Hakan et al., (2012) presented a numerical study of heat transfer and turbulent airflow over a double forward-facing step with an obstacle. The bottom of the wall and steps were heated, and the top of the wall was insulated. The results showed that the obstacle aspect ratio (Ar) affected the heat transfer, with the maximum Nusselt number corresponding to Ar=1.

The objective of this paper is to contribute new data regarding water flow over double forward-facing steps to improve the design of heat exchangers.

To the best of the authors' knowledge, turbulent water flow and heat transfer over double forward-facing steps has not been reported in the literature; thus, this work is the first such study.

8.2.2 Numerical model

A. *Physical model*

A schematic diagram of the double forward-facing step and the flow shape employed in this study is presented in Figure 8.1. The bottoms of the wall and the steps were heated to a given temperature (T_h), while the top of the wall was adiabatic. The first step height (h1) was varied from 2 to 6 cm whereas the second step height (h2) was fixed at 2 cm. The entrance width (H) was 10 cm while the exit width (H2) was 6, 4, and 2 cm according to the first step height. Three cases corresponding to three step heights were investigated, as shown Table 8.1. In addition, the Reynolds number was varied from 30,000 to 100,000, and calculated based on entrance width (H), and four different temperatures from 313 to 343 K were adopted.

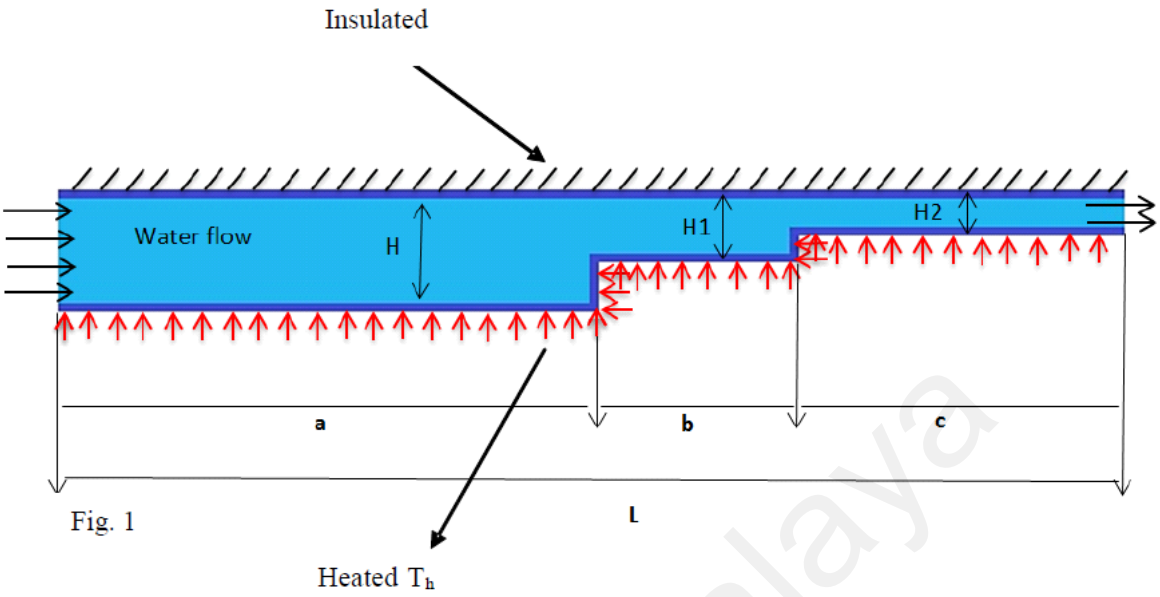

Fig. 1

Figure 8. 1: Physical model.

Table 8. 1: Cases and dimension of geometries.

Cases	H(cm)	h1=H-H1	h2=H1-H2	a(cm)	b(cm)	c(cm)
1	10	2	2	100	20	40
2	10	4	2	100	20	40
3	10	6	2	100	20	40

B. *Governing equations*

The SIMPLE algorithm couples velocity and pressure (Mahmoudi et al., 2012; Rahgoshay et al., 2012) and links the momentum and mass conservation equations using pressure corrections (Patankar & Spalding, 1972). Therefore, in this study, the SIMPLE algorithm was combined with the finite volume method to discretize continuity; X, Y momentum; and energy equations in the computational domain. The conservation equations (8.1, 8.2, 8.3, 8.4) assuming two dimensions, steady flow, and a Newtonian fluid, can be written as follows (Yılmaz & Öztop, 2006).

$$\frac{\partial u}{\partial x}+\frac{\partial v}{\partial y}=0 \tag{8.1}$$

$$\rho\left(u\frac{\partial u}{\partial x}+v\frac{\partial u}{\partial y}\right)=-\frac{\partial p}{\partial x}+\mu\left(\frac{\partial^2 u}{\partial x^2}+\frac{\partial^2 u}{\partial y^2}\right) \tag{8.2}$$

$$\rho\left(u\frac{\partial v}{\partial x}+v\frac{\partial v}{\partial y}\right)=-\frac{\partial p}{\partial y}+\mu\left(\frac{\partial^2 v}{\partial x^2}+\frac{\partial^2 v}{\partial y^2}\right) \tag{8.3}$$

$$\rho\left(u\frac{\partial T}{\partial x}+v\frac{\partial T}{\partial y}\right)=\propto\left(\frac{\partial^2 T}{\partial x^2}+\frac{\partial^2 T}{\partial y^2}\right) \tag{8.4}$$

The standard k−ε turbulence model was employed for turbulence flow modeling (Launder & Spalding, 1974). In FLUENT, Near-wall treatment based on standard wall functions was selected for high accuracy results where it was suggested by Chung and Jia (Chung & Jia, 1995) for predication separation flow and heat transfer in sudden expansion. The transport equations were applied to determine the turbulence kinetic energy k (5) and dissipation rate ε (8.6):

$$\frac{\partial}{\partial x}(\rho k u)=\frac{\partial}{\partial y}\left(\left[\left(\mu+\frac{\mu_t}{\sigma_k}\right)\frac{\partial k}{\partial y}\right]\right)+G_k-\rho\varepsilon \tag{8.5}$$

$$\frac{\partial}{\partial x}(\rho \varepsilon u) = \frac{\partial}{\partial y}\left(\left[\left(\mu + \frac{\mu_t}{\sigma_\varepsilon}\right)\frac{\partial \varepsilon}{\partial y}\right]\right) + C_{1\varepsilon}\frac{\varepsilon}{k}(G_k + C_{3\varepsilon}G_b) - C_{2\varepsilon}\rho\frac{\varepsilon^2}{k} \quad (8.6)$$

where G_k describes the generation of turbulence kinetic energy by the turbulent viscosity and velocity gradients-and is computed using equation 7:

$$G_k = -\rho\overline{v'u}\frac{\partial v}{\partial x} \quad (8.7)$$

μ_t is calculated using equation (8.8):

$$\mu_t = \rho C_p \frac{k^2}{\varepsilon} \quad (8.8)$$

The values of the constants employed in the simulations are shown in Table 8.2.

To enhance the accuracy of the simulations, the second-order upwind scheme was used. Additionally, after each iteration, the residual sum was computed and stored for every conserved variable. The required scaled residual for the convergence criterion was less than 10^{-8} for the continuity, and smaller than 10^{-7} for the energy and momentum equations.

Table 8. 2: Value of the constants in Transport equations

Value of constants	
$C_{1\varepsilon}$	1.44
$C_{2\varepsilon}$	1.92
$C_{3\varepsilon}$	0.09
σ_k	1.0
σ_ε	1.3
Pr	7.01

8.2.3 Numerical procedure and code validation

Simulations were carried out using ANSYS FLUENT 14 (CFD). The ICEM was used for meshing, and the k-ε standard model in Fluent was used to analyze the water flow and heat transfer over the double forward-facing step in the turbulent region. The computational conditions used in the numerical simulation are shown in Table 8.3. Grid independence was verified by increasing the grid size step-wise, which yielded similar results. Independent verification was performed for Re=30,000, case1, and initial grid sizes of 9099, 37397, and 67117. The difference in the Nusselt number relative to that-of the selected grid was less than 1% as shown Figure 8.2. The geometric dimensions were based those reported by (Yılmaz & Öztop, 2006).

Table 8. 3: Computational conditions

Computational conditions	
Fluid	Water
Pressure-Velocity Coupling (Scheme)	SIMPLE
Density	998.2 kg/m3
Viscosity	0.001 kg/m-s
Pressure	101,325 Pa
Viscous model	*K* and ε
Reynolds number ($Re = \frac{\rho UH}{\mu}$)	30,000, 50,000, 80,000, 100,000
Temperature	313, 323 , 333, 343 K

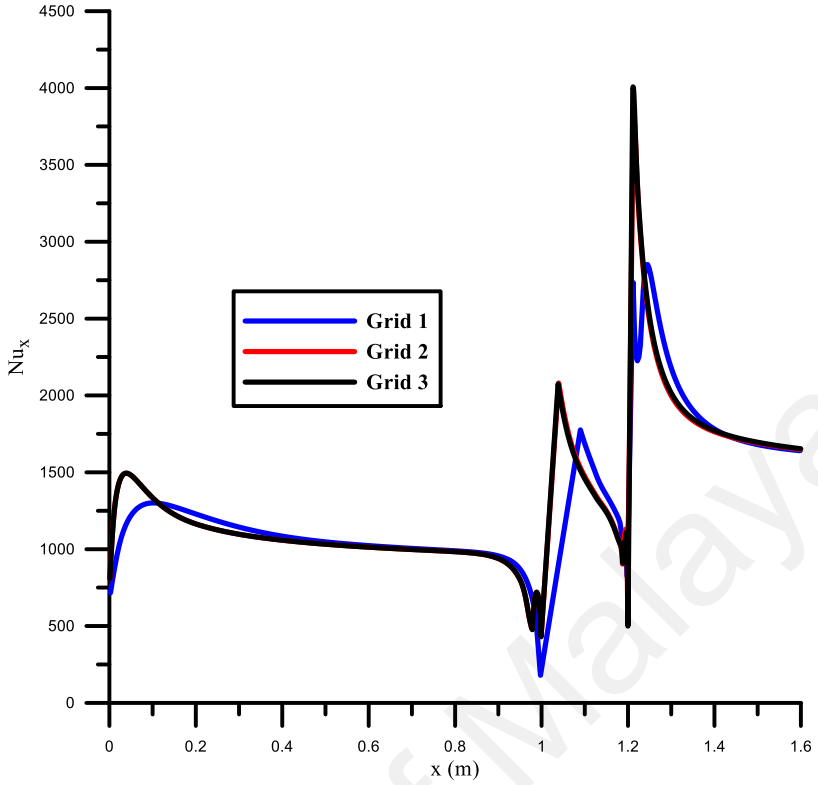

Figure 8.2: Comparison Nusselt number case 1, with Re=30,000 and T=313 K for grid independent.

8.2.4 Results and discussion

Numerical simulations were performed for heat transfer and turbulent water flow over a double forward-facing step. Three cases with different step heights at Reynolds numbers of 30,000, 50,000, 80,000, and 100,000, and temperatures of 313, 323, 333, and 343 K were studied.

A. *Nusselt number*

Figures 8.3-8.5 show the variation in the local Nusselt number for cases 1, 2, and 3 at T=343 K and different Reynolds numbers. In all cases, the Nusselt number increased with the Reynolds number, and a sudden increase in the Nusselt number was observed at

the first and second steps due to recirculation vortices. A higher Nusselt number occurred at the second step for case 3 compared the Nusselt numbers observed in other cases. The effect of temperature on the local Nusselt number for cases 1, 2, and 3 is illustrated in Figures 8.6-8.8. As shown, the trends of the Nusselt number are similar before the first and second steps, and the Nusselt number decreases sharply at the same Reynolds number for all cases. A decrease in temperature leads to a decrease in the Nusselt number. For all temperatures, the maximum value of the Nusselt number was observed at the first and second steps for all cases; in case 3, however, a higher Nusselt number occurred at the second step compared with the numbers observed in the other cases, as shown in Figure 8.9.

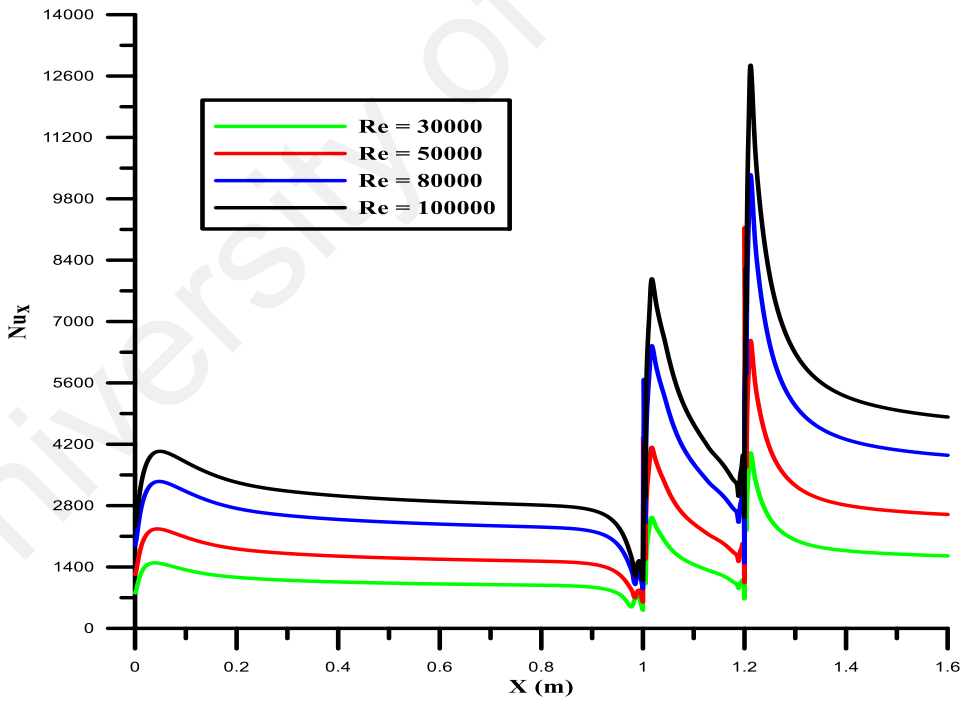

Figure 8.3: Distribution of local Nusselt number for case 1, with T=313 K and different Reynolds number.

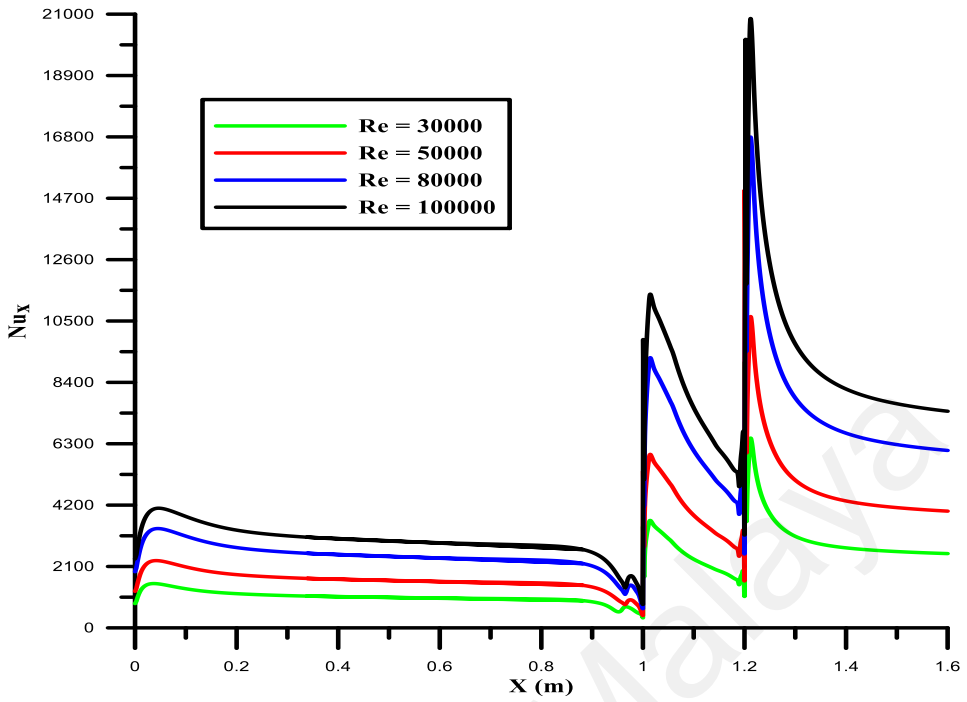

Figure 8.4: Distribution of local Nusselt number for case 2, with T=313 K and different Reynolds number.

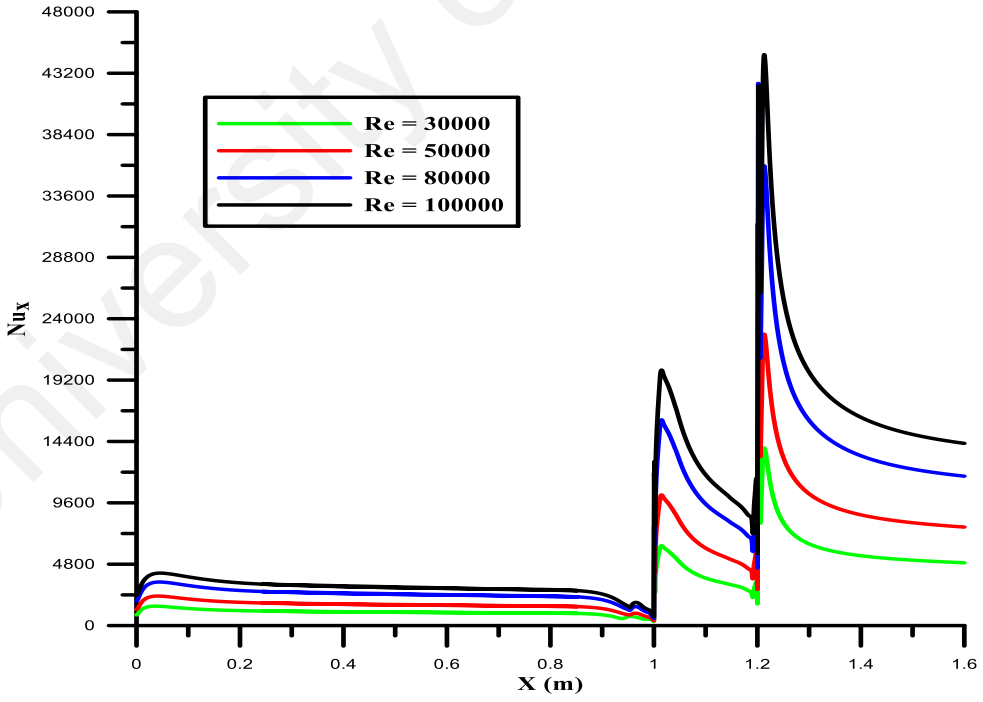

Figure 8.5: Distribution of local Nusselt number for case 3, with T=313 K and different Reynolds number.

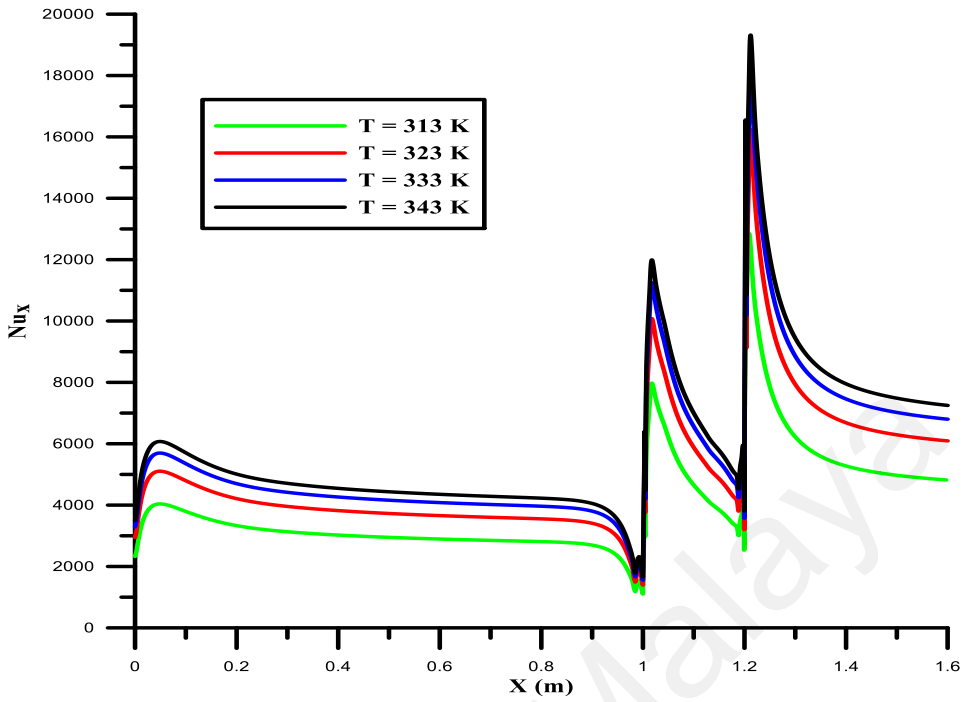

Figure 8.6: Local Nusselt number distribution for case 1, with Re=100,000 and different Temperatures

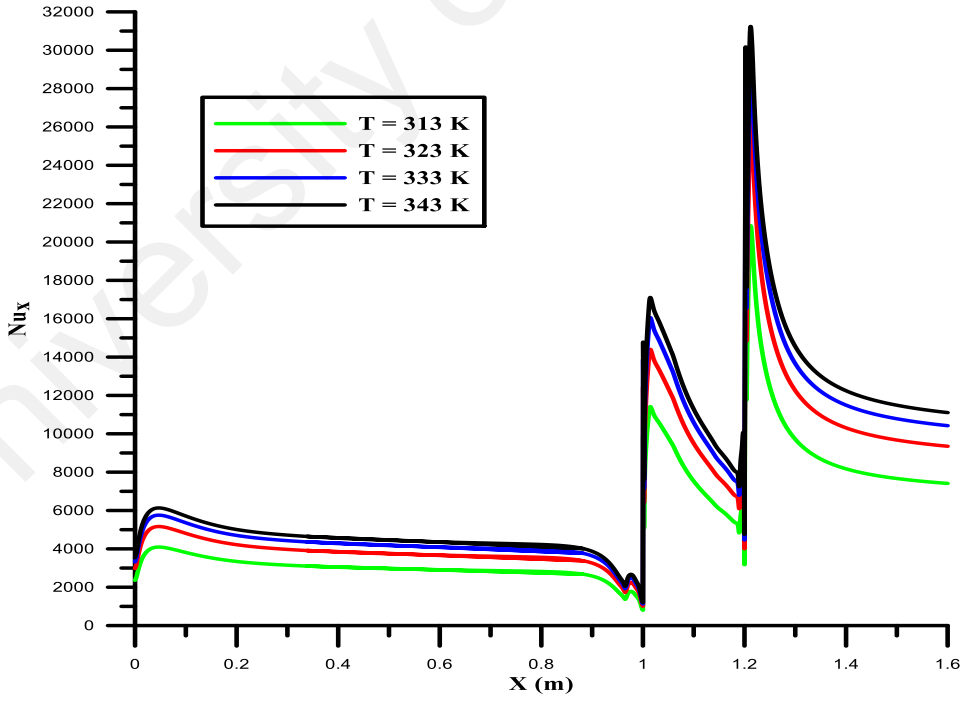

Figure 8.7: Local Nusselt number distribution for case 2, with Re=100,000 and different Temperatures.

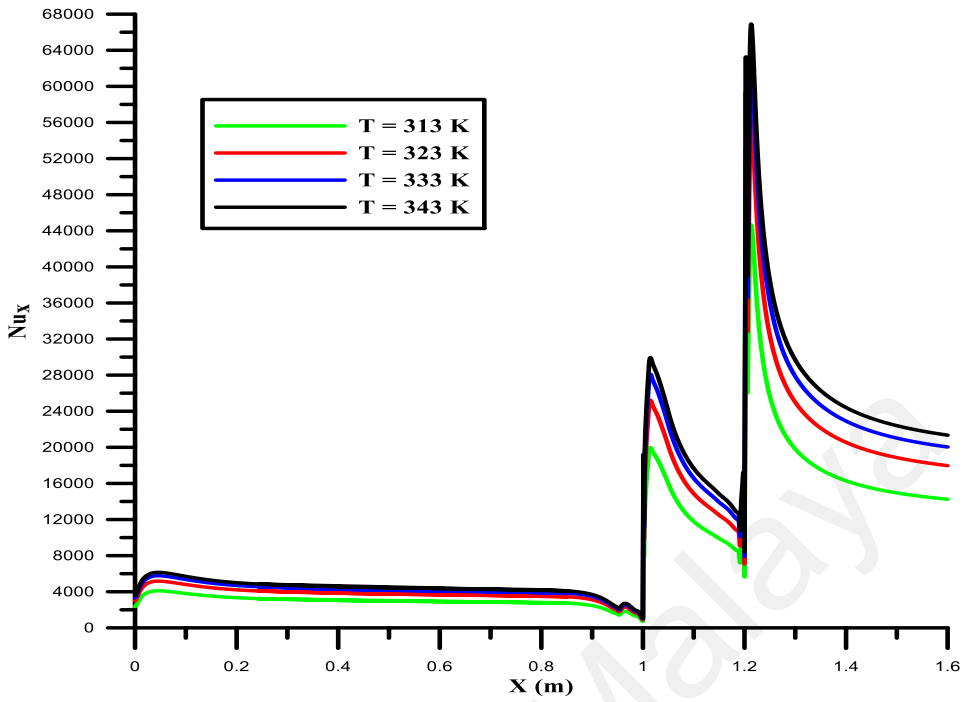

Figure 8.8: Local Nusselt number distribution for case 3, with Re=100,000 and different Temperatures.

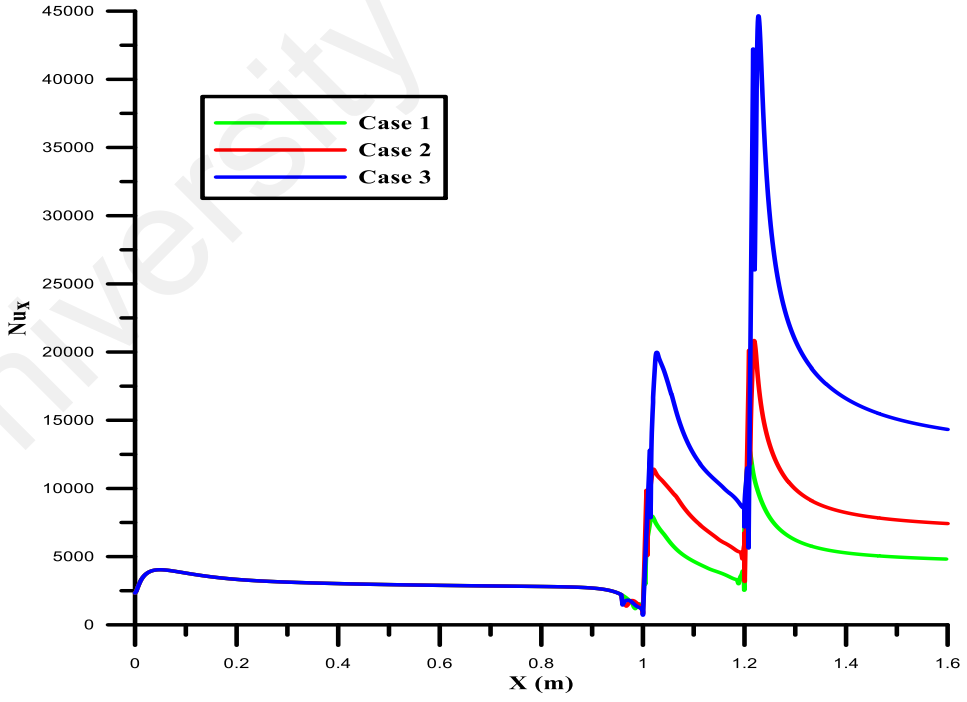

Figure 8.9: Effect step height on local Nusselt number for case 1, 2, and 3 at Re=100,000 and T=313 K.

B. *Flow visualization*

Figures 8.10-8.13 present the contour maps of the velocity field for case 1 at T=313 K and various Reynolds numbers. Generally, the recirculation zone is found before and after the first and second step, the recirculation zone around the first step being larger than that around the second step for a given Reynolds number and temperature. The recirculation zone also increased with Reynolds number for case 1 at T= 313 K. The effect of the step height on the recirculation zone is illustrated in Figures 8.14(A, B, C) and 8.15(A, B, C) for cases1, 2, and 3, Re= 100,000, and T=313 K. Increasing the step height increased the recirculation flow, and the largest recirculation zone was found at the first step for case 3, Re=100,000, and T=313 K relative to that observed in case 1 and 2.

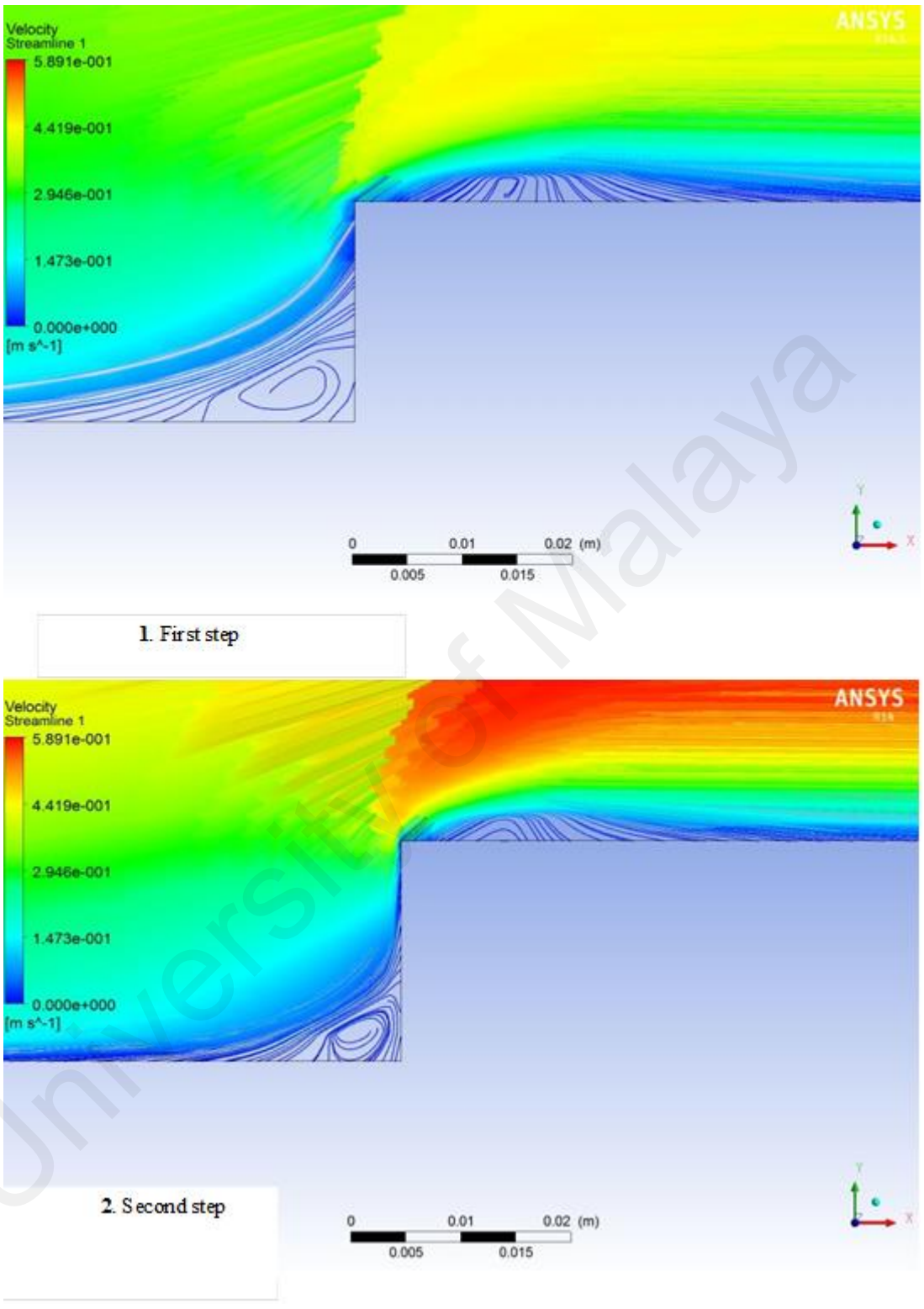

Figure 8.10: Velocity of streamline for case 1, with Re=30,000 and T=313 K.

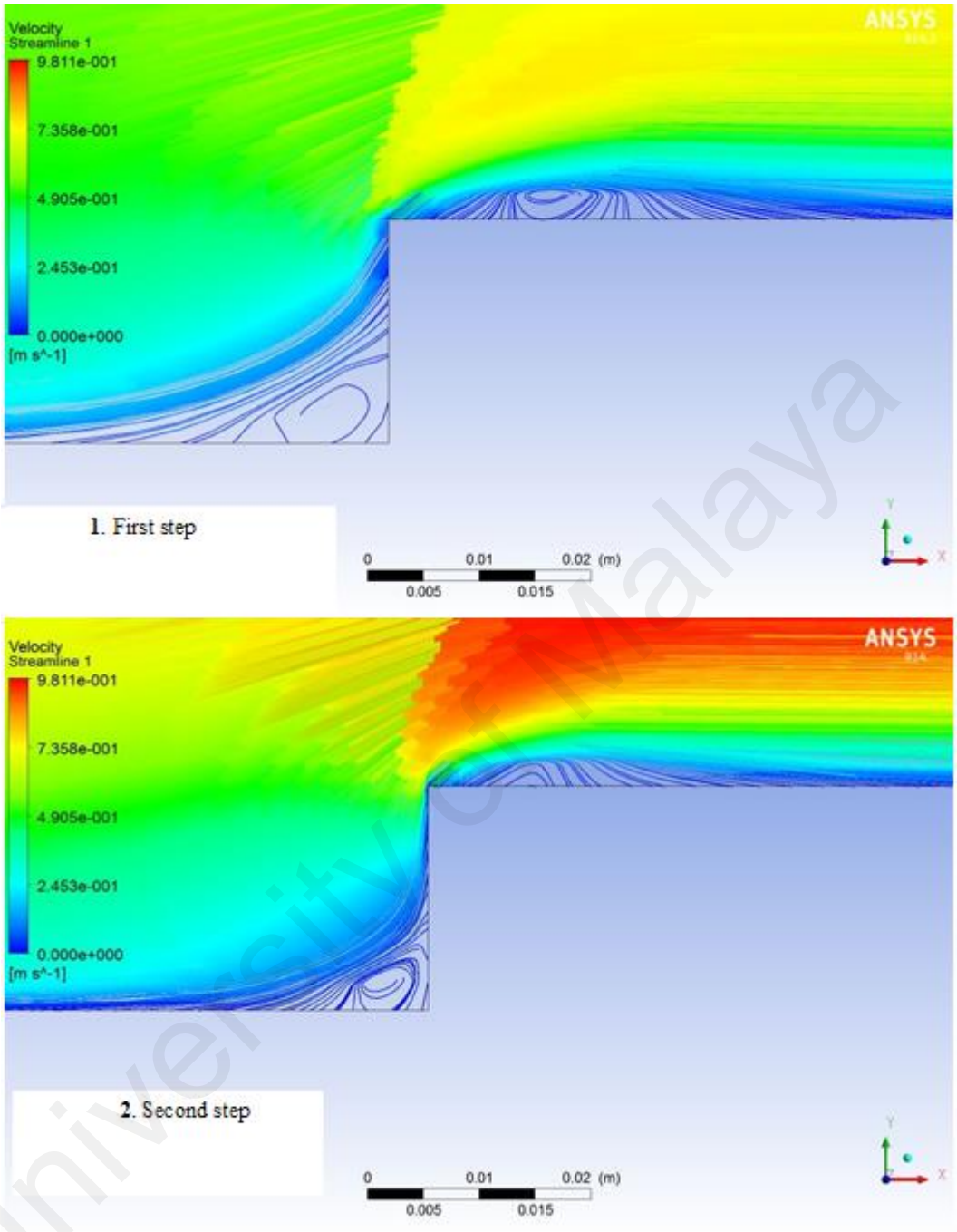

Figure 8.11: Velocity of streamline for case 1, with Re=50,000 and T=313 K.

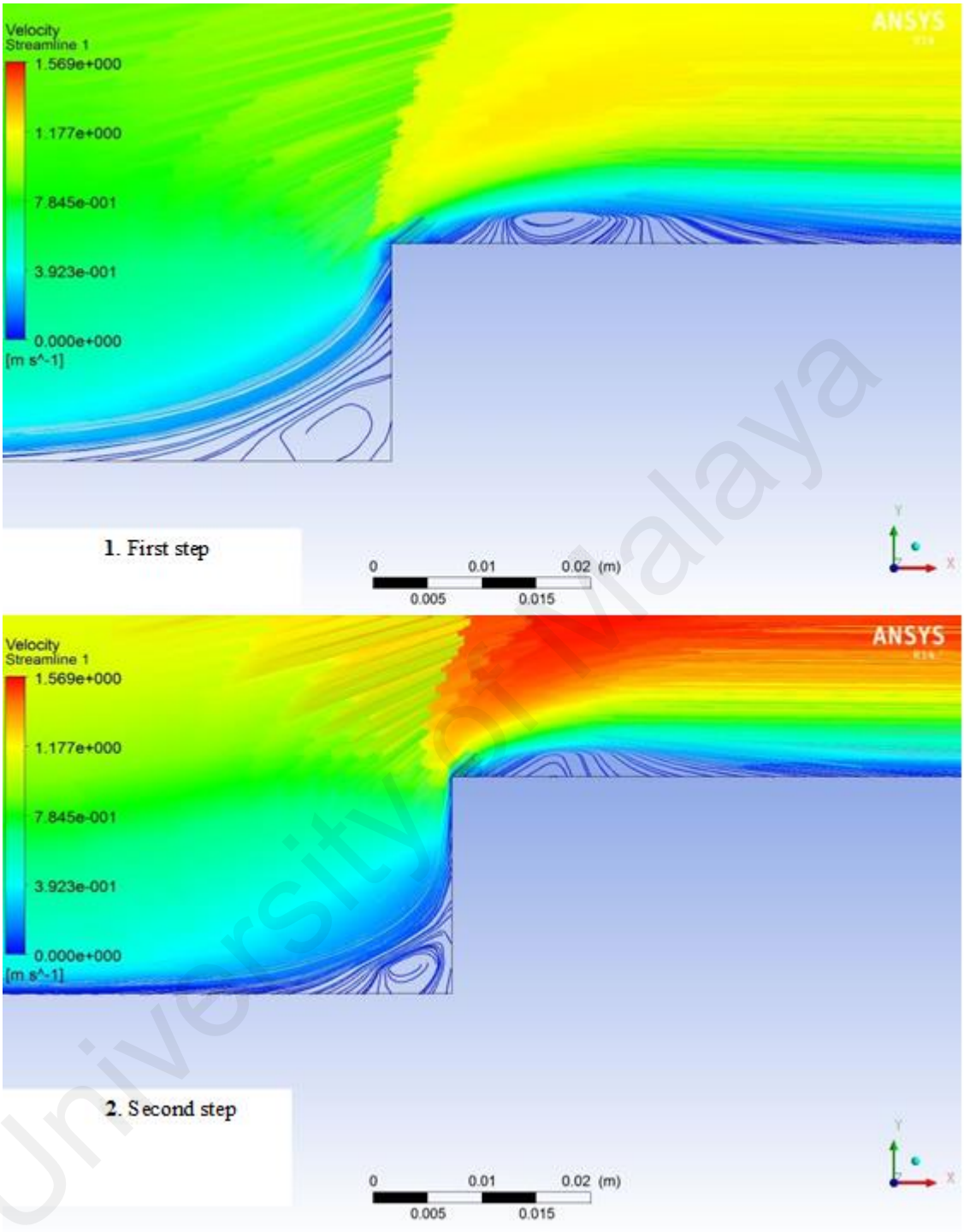

Figure 8.12: Velocity of streamline for case 1, with Re=80,000 and T=313 K.

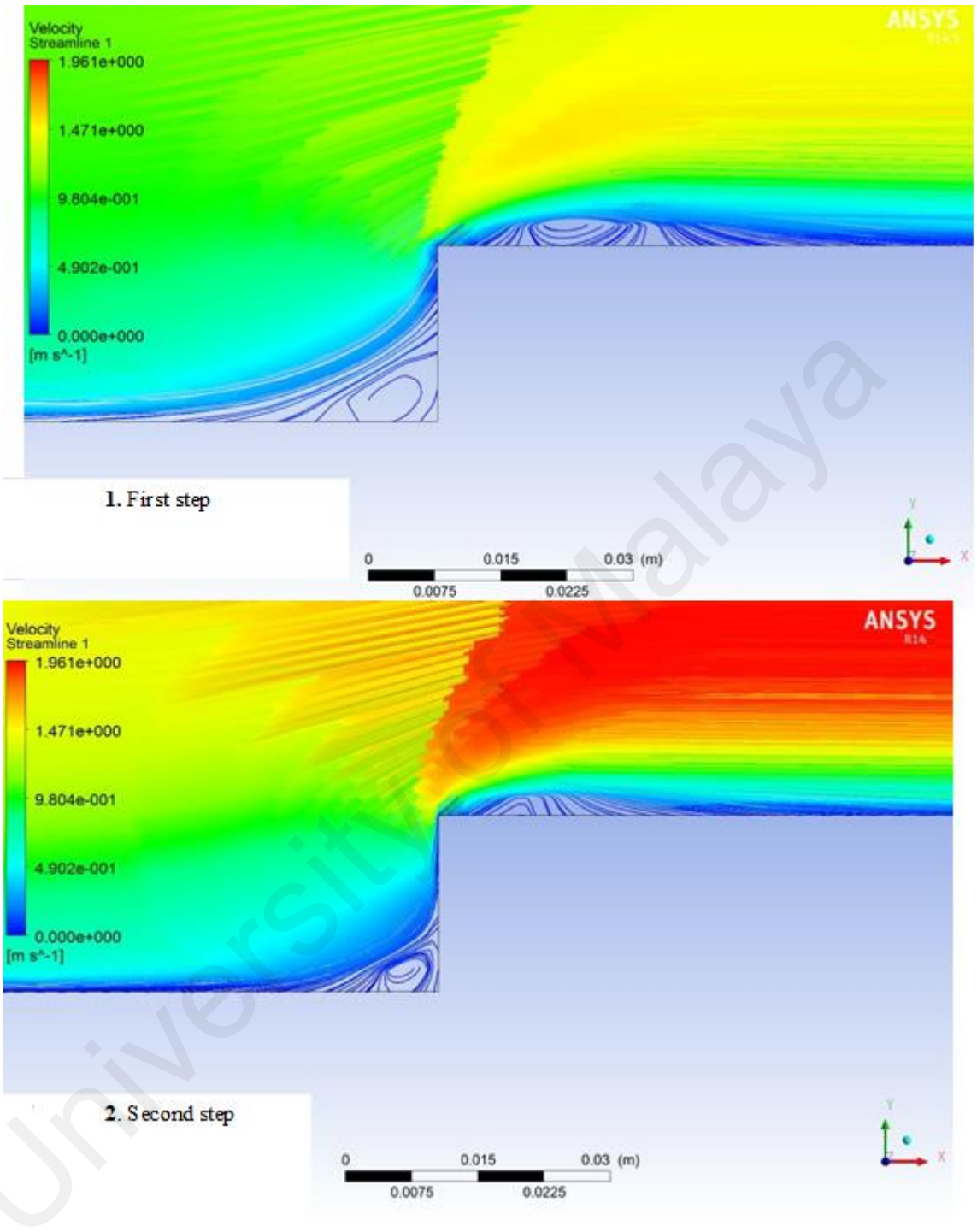

Figure 8.13: Velocity of streamline for case 1, with Re=100,000 and T=313 K.

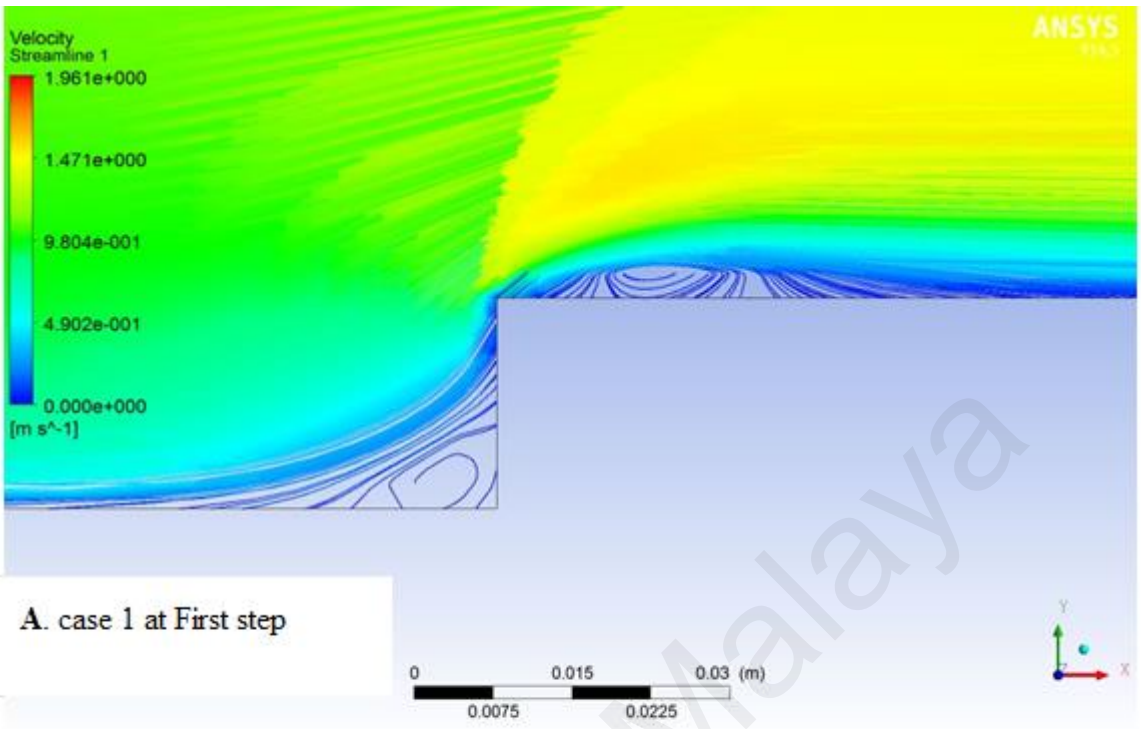

A. case 1 at First step

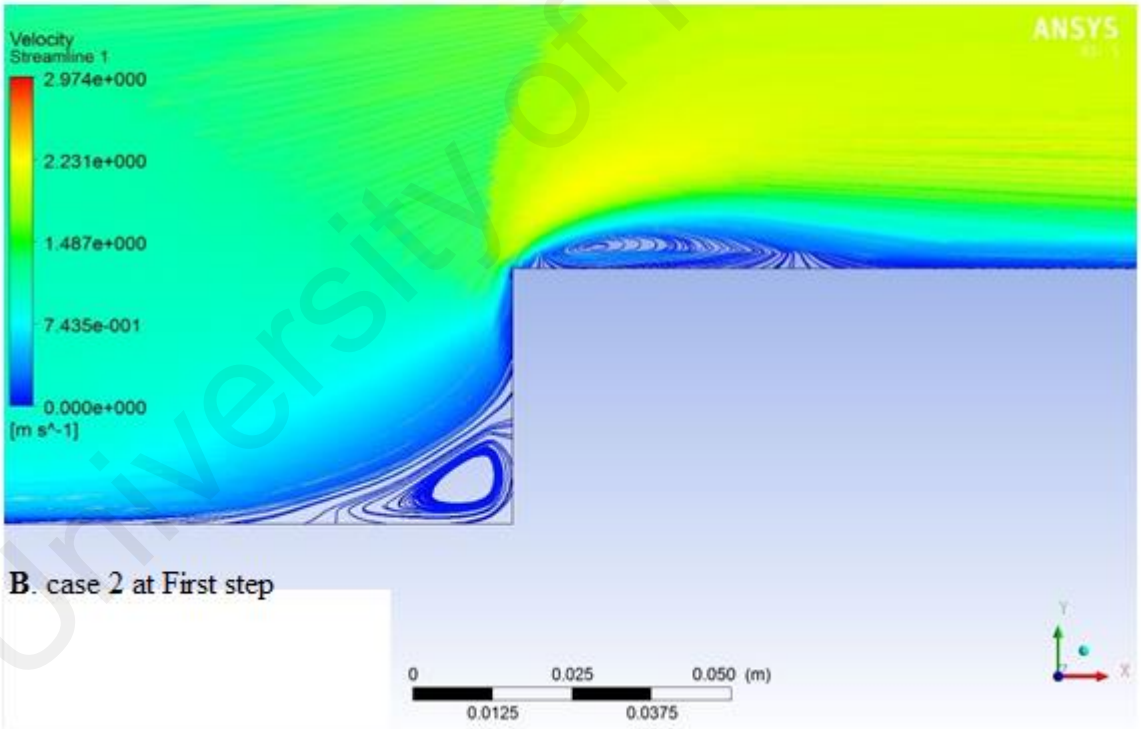

B. case 2 at First step

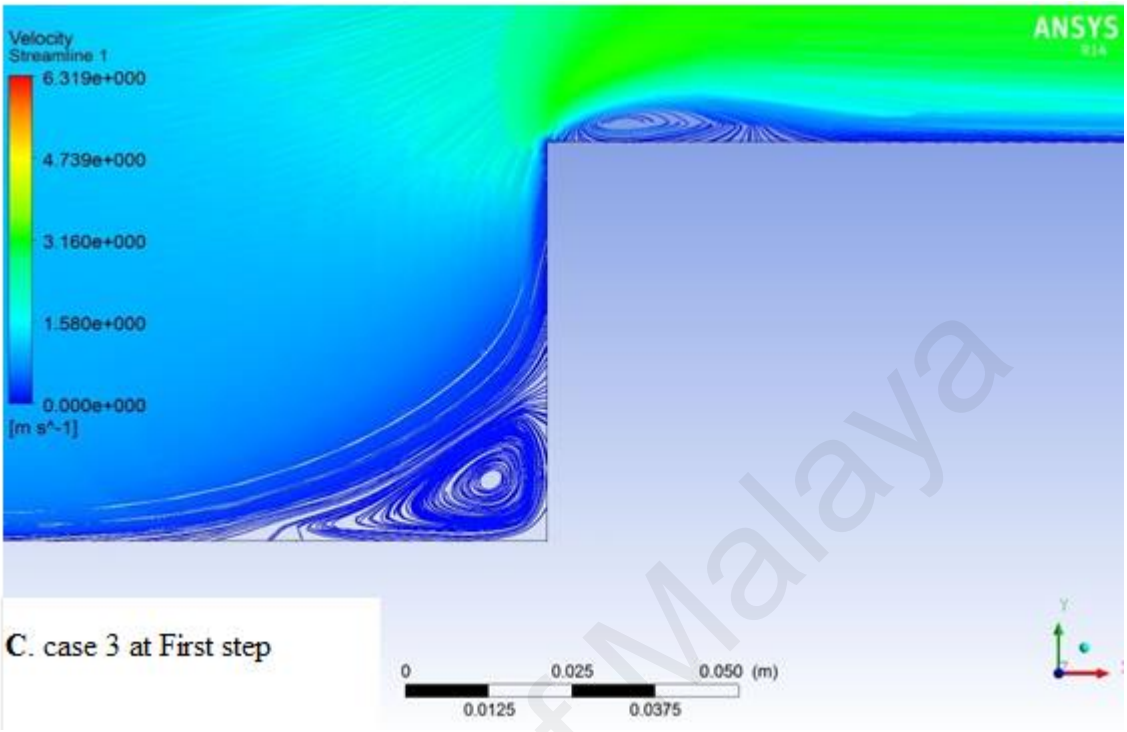

Figure 8.14: Effect step height (**First step**) on recirculation region for Re=100,000 and T=313 K.

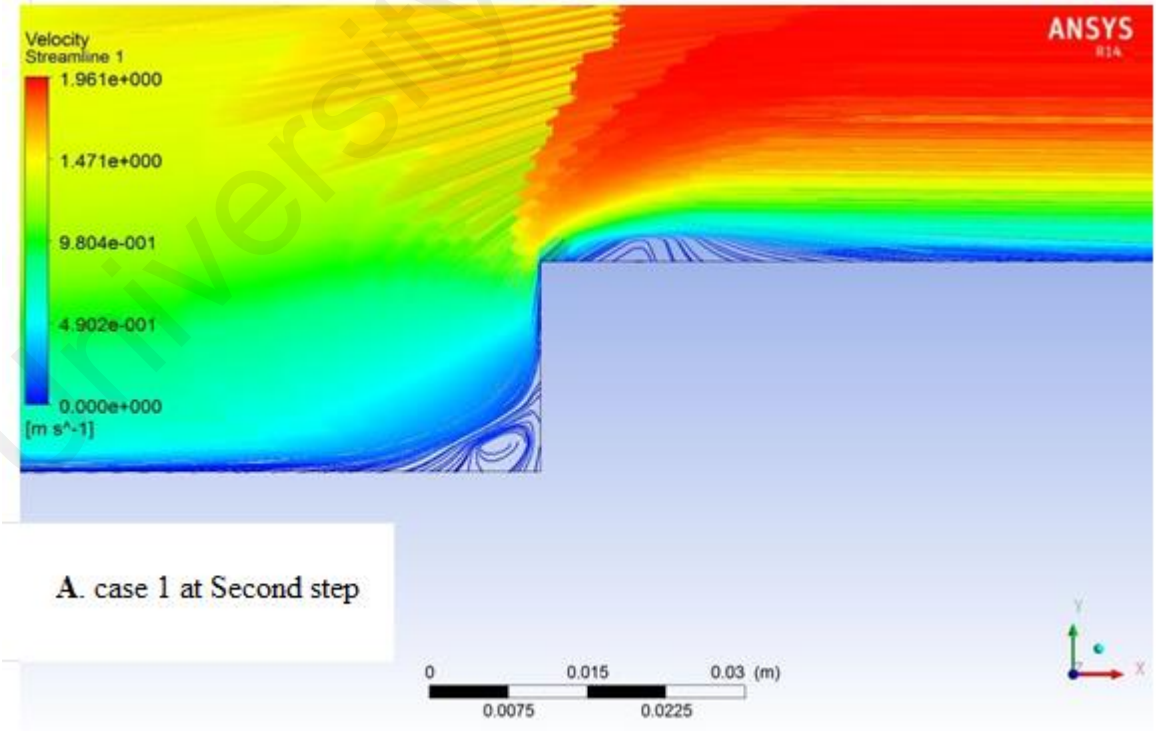

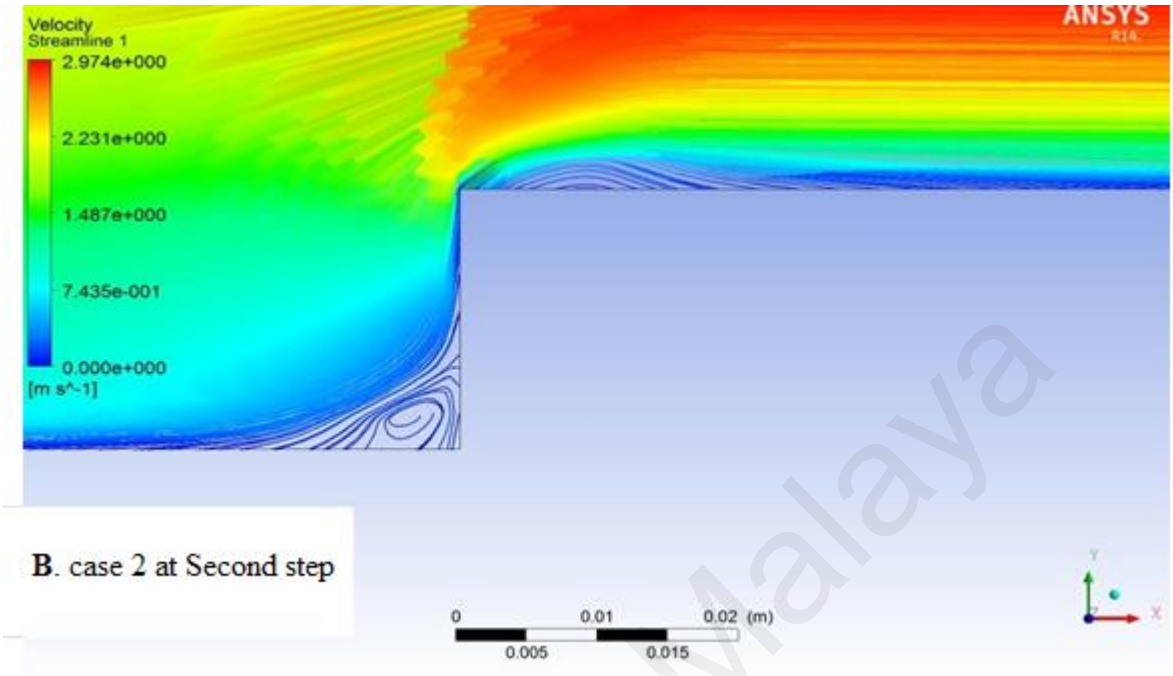

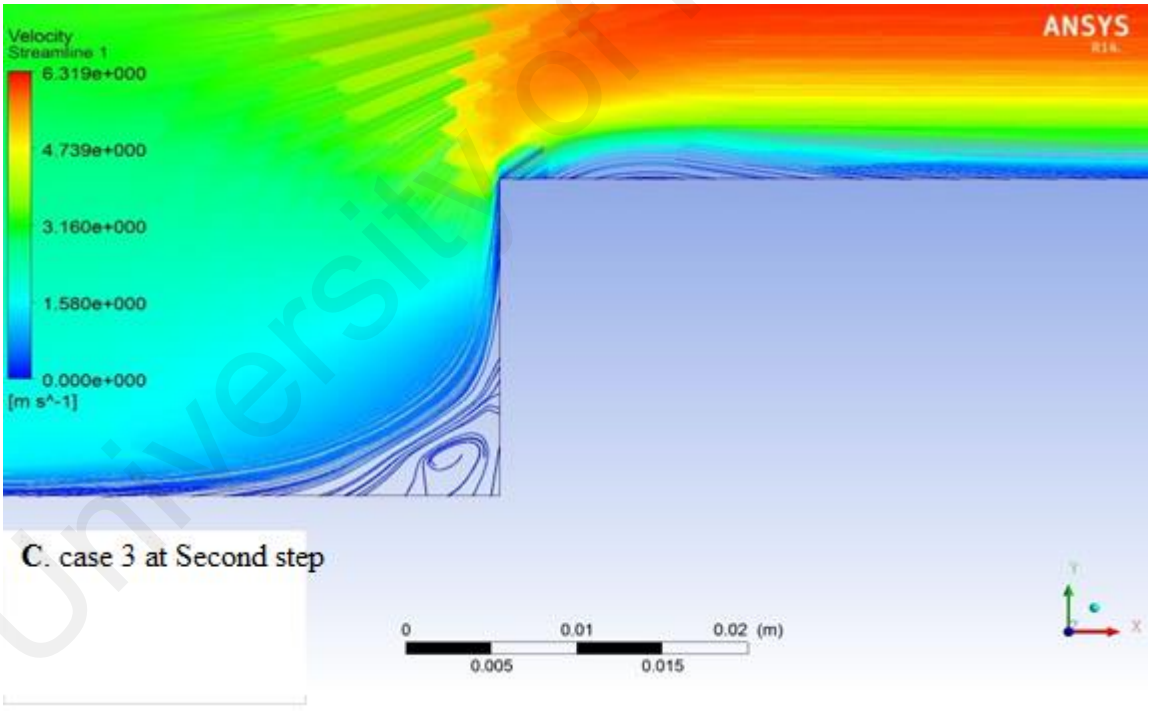

Figure 8.15: Effect step height (**Second step**) on recirculation region for Re=100,000 and T=313 K.

C. *Pressure coefficient*

Figure 7.16 shows the pressure coefficient along the x-axis for case 1 at T= 313 K and different Reynolds numbers. Increasing the Reynolds number led to an increase in the pressure coefficients, particularly at the first and second step, which in turn increased the recirculation flow and enhanced the heat transfer rate. Figure 8.17 presents the pressure coefficients at T=313 K and Re=100,000 for cases 1, 2, and 3. Case 3 shows the highest pressure coefficient and thus the largest increase in the Nusselt number.

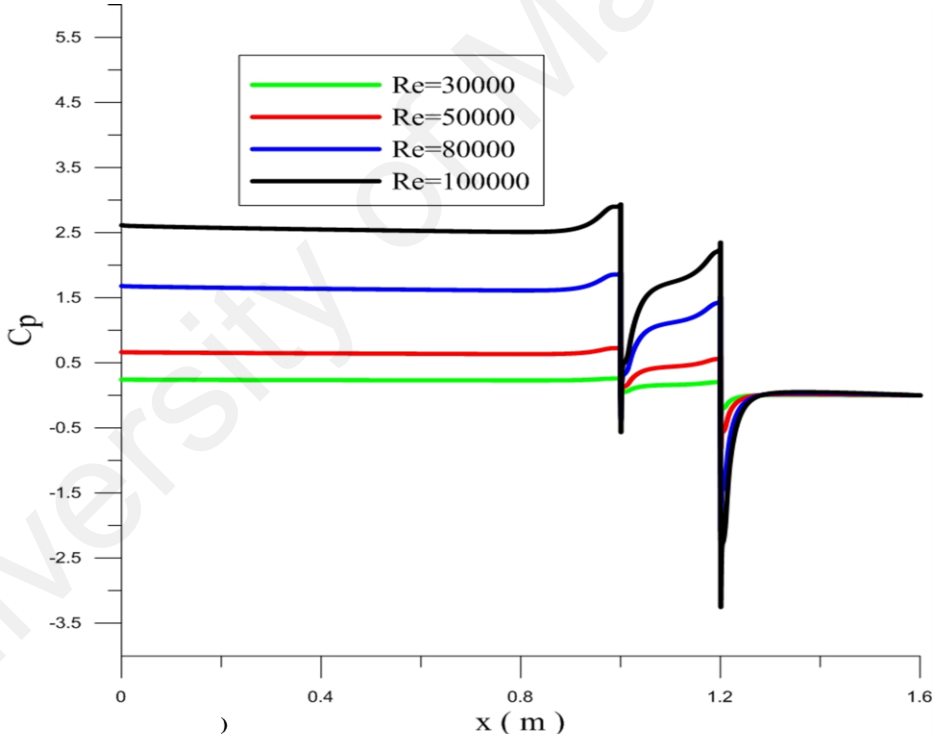

Figure 8.16: Variation of pressure coefficient for case 1, with T=313 K and different Reynolds number.

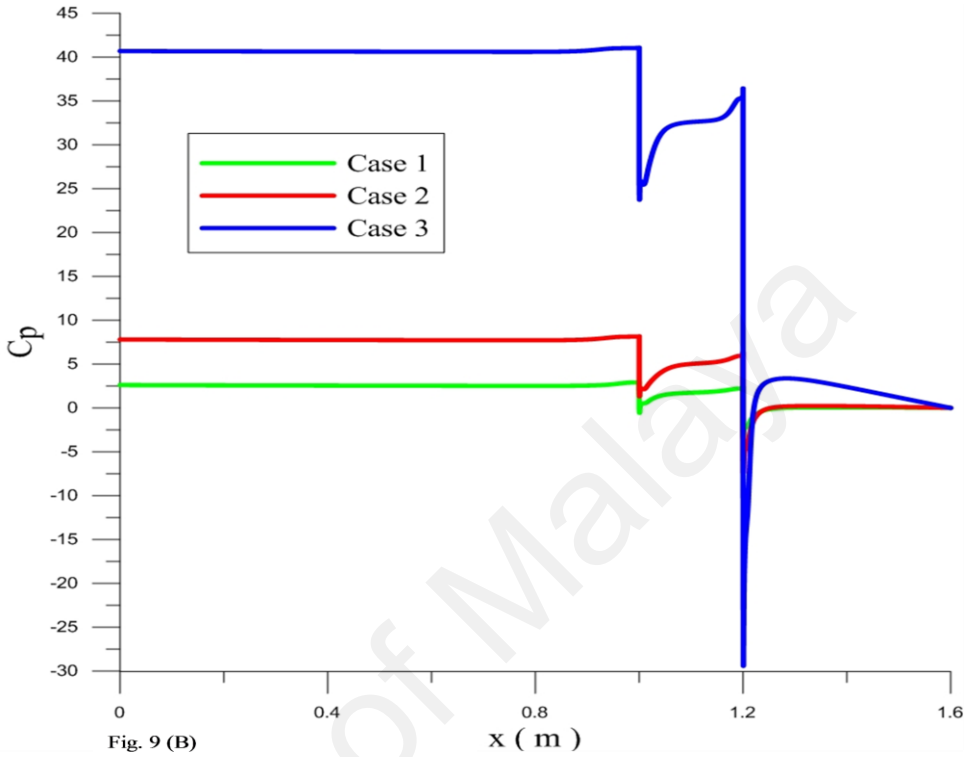

Figure 8.17: Effect step height on pressure coefficient at Re=100,000 and T=313 K.

Figure 8.18 compares the Nusselt number for case1, with Re= 30,000 and T= 313 K, with the values reported by (Gandjalikhan Nassab et al., 2009; Oztop et al., 2012). An acceptable agreement between the trends, especially at the step region, justifies the use of this computational approach. For more validation, compares the local Nusselt number for case 2, at Reynolds number of 30000 and T=313K with case 10 of Ref (Yılmaz & Öztop, 2006) presented in Figure 8.19.

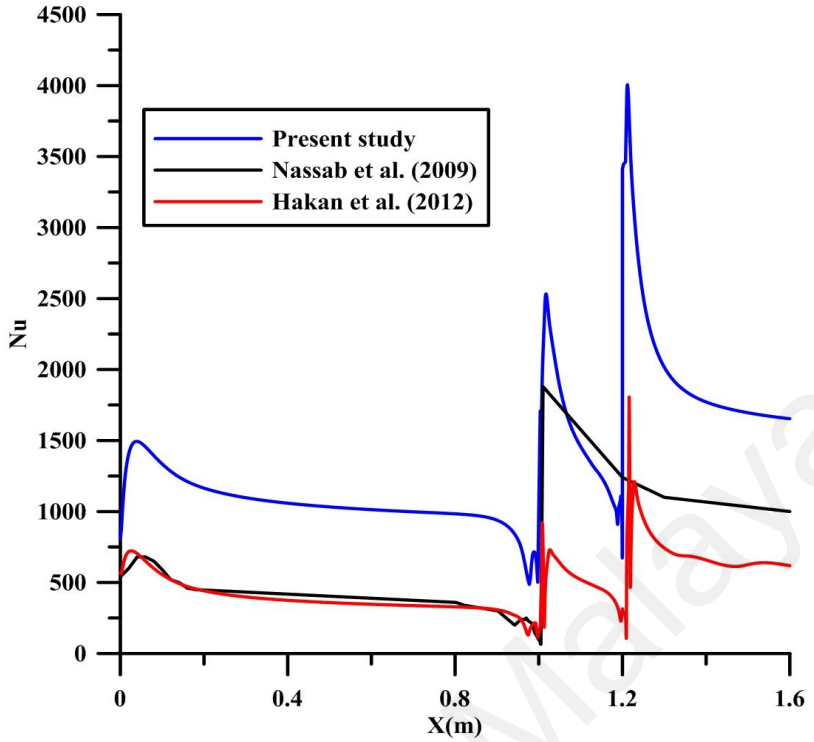

Figure 8.18: Comparison trend Nusselt number with (Nassab et al., 2009; Hakan et al., 2012) for case 1 Re=30,000 and T=313 K.

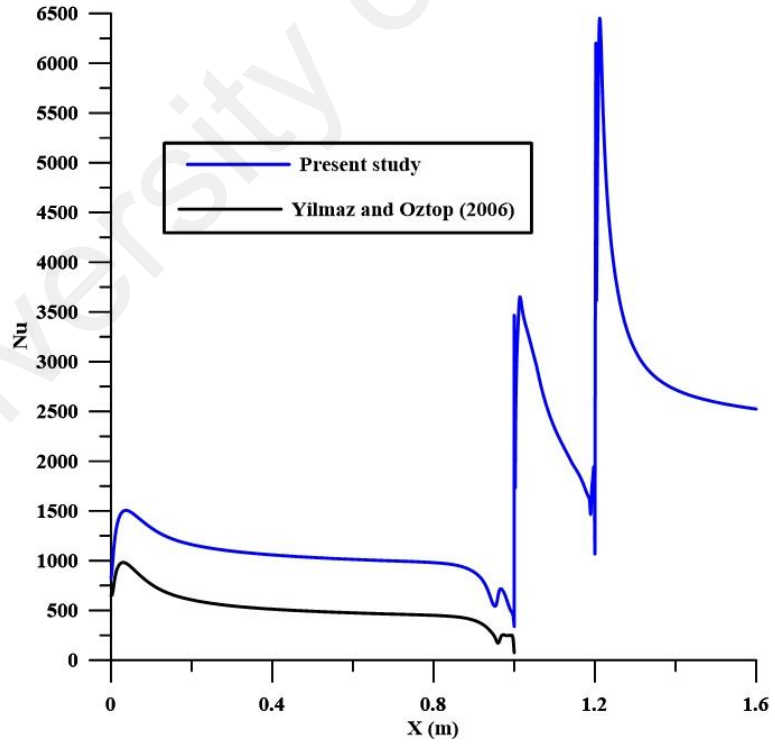

Figure 8.19: Comparison trend Nusselt number for case 2 Re=30,000 and T=313 K with Case10 of Ref (Yılmaz & Öztop, 2006).

8.3 Thermal performance of nanofluid in ducts with double forward-facing steps

Abstract

The turbulent heat transfer to nanofluid flow over double forward-facing steps was investigated numerically. The duct geometry and computational mesh were developed with ANSYS 14 ICEM. Two-dimensional governing equations were discretized and integrated using finite volume technique. The k-ε turbulence model was used in the analysis. Al_2O_3 and CuO nanoparticles at volume fractions varying from 1% to 4% with water as the base fluid were employed for turbulent flow in a passage with a double forward-facing step. The effects of volume fraction and step height were compared with the base fluid thermal performance. The obtained results showed an increase in Nusselt number with the increase in volume fraction of nanofluid, Reynolds number, and step height. A higher Nusselt number value was found at the second step compared to the first step for all cases. Velocity contours were developed to visualize the recirculation regions before and after the first and second steps. The results also demonstrated enhanced heat transfer with the increase of nanoparticle concentration, and the largest thermal enhancement factor occurred for the highest nanoparticle volume fraction (4%) of Al_2O_3 considered in this investigation.

Nomenclature

a	Length of bottom wall before the first step
b	Length of bottom wall after the first step
c	Length of bottom wall after the second step
$C1\varepsilon, C2\varepsilon, C3\varepsilon, \sigma k, \sigma\varepsilon$	Model constants
Cp	Specific heat
d_p	Diameter of nanofluid particles (nm)
d_f	Diameter of a base fluid molecule
H	Width of channel before the steps
$H1$	Width of channel after first step
$H2$	Width of channel after second step
$h1$	Height of first step
$h2$	Height of second step
L	Total length of channel
K	Turbulent energy
Nu	Nusselt number
P	Pressure
Pr	Prandtl number
Re	Reynolds number
T	Temperature
u, v	Axial velocity
X, Y	Cartesian coordinates

Greek symbols

ρ	Water density
ε	Turbulent dissipation
μ	Dynamic viscosity
β	Modeling function
μ_t	Turbulent viscosity
η	Thermal enhancement factor
ϕ	Volume fraction (%)

8.3.1 Introduction

Flow separations and recirculation flows occur due to sudden changes in the passage geometry. Such flows are found in a variety of applications, such as power plants, combustion furnaces, nuclear reactors, heat exchangers and cooling of electronic devices. Attempts to enhance the heat transfer rate in thermal systems have been reported in a number of studies over the past decades. Typical examples are introducing flow separation over a forward or backward-facing step, sudden expansion, and ribs channels. Separation due to a sudden contraction or a forward-facing step (FFS) in the passage not only developed in practical engineering applications but is also occurs in nature, such as lakes and rivers. Generally, the phenomena of separation and reattachment flow are addressed in numerous experimental and numerical studies (C. S. Oon et al., 2012; Hussein Togun, Tuqa Abdulrazzaq, S. N. Kazi, et al., 2013; Hussein Togun, Tuqa Abdulrazzaq, S.N. Kazi, et al., 2013; Hussein Togun et al., 2011; HusseinTogun et al., 2011; J. W. Baughn et al., 1984; Lee et al., 2011; Oon et al., 2013). Shakouchi and Kajino (Shakouchi & Kajino, 1994) presented an experimental study of heat transfer and fluid flow over single and double forward-facing steps using the laser Doppler anemometry technique. The effect of step height on heat transfer and flow characteristics showed a greater enhancement of heat transfer with the double forward-step compared to the single step. Yılmaz & Öztop, (2006) numerically studied airflow and heat transfer over a double forward-facing step using a standard k-ε turbulence model. They insulated the top wall and steps while the bottom wall before the step was heated. The obtained results indicated that the second step could serve as a control device for heating and fluid flow.

Recently, Tinney & Ukeiley, (2009) used particle image velocimetry to investigate turbulent oil flows over a double backward-facing step. They observed large turbulence at

the central region of the backward step. Laminar and turbulent convection flows over a vertical forward-facing step were numerically and empirically studied by (Abu-Mulaweh et al., 1996) and (Abu-Mulaweh, 2005), who found that increasing the step height leads to greater velocity turbulence and temperature variations. In contrast, (Wilhelm & Kleiser, 2002) and (Marino & Luchini, 2009) conducted a numerical study of laminar fluid flow over a horizontal forward-facing step. They discovered an increase in separation and reattachment length with an increase in the flow Reynolds number. The effects of forward and backward-facing steps on turbulent mixed convection flow over a flat plate were studied experimentally by (Abu-Mulaweh, 2009). Accordingly, the velocity turbulence intensity in the downstream area increased with the increase of forward–backward facing step height. For additional heat transfer enhancement, (Oztop et al., 2012) presented a numerical study of turbulent heat transfer and airflow over a double forward-facing step with obstacles. The results revealed superior heat transfer at an augmented aspect ratio of obstacle, step height and Reynolds number.

In recent years, studies of nanofluids have attracted attention due to their typically higher thermal conductivity compared to base fluids. The fluid commonly employed in heat exchangers, such as water, ethylene glycol or mineral oils, has limitations in transferring heat; therefore, nanofluids are expected to provide potentials for better thermal performance. Choi & Eastman, (1995) initiated the formulation of nanofluid by dispersing metallic or non-metallic nanometer-size particles in base liquids like water and ethylene glycol. Studies of nanofluid flow and heat transfer over forward and backward-facing steps are rather scarce. Abu-Nada, (2008) reported a numerical study on nanofluid flow and heat transfer over a backward-facing step. The nanoparticles in the study were Cu, Ag, Al_2O_3, CuO, and TiO_2 with volume fractions from 0.05 to 0.2 and a range of Reynolds numbers

from 200 to 600. Using finite volume method, the momentum and energy equations were solved and an enhancement in the Nusselt number at the top and bottom of the backward-facing step was observed. The investigation also identified effective high thermal conductivity regions outside the recirculation zones.

Santosh Christopher et al., (2012) preformed a numerical study on laminar Al_2O_3, Ag, Cu, SiO_2, and CuO nanofluid flows in sudden expansion. The same method as that of (Das & Kanna, 2007) was utilized to solve the sudden expansion flow and backward-facing flow with Reynolds numbers from 30 to 150 at nanoparticle volume fractions of 0.1, 0.2, and 0.05. According to the outcome, a decrease in reattachment length of roughly 1.3% was noted compared to the data of (Abu-Nada, 2008).

The performed literature survey showed that the nanofluid turbulent flow and heat transfer over a double forward-facing step has not been investigated as yet. In the present work flow and heat transfer in aluminum oxide–water and copper oxide-water nanofluids in a double forward –facing step under turbulent flow regime were simulated. Based on the recommended concentrations for Al_2O_3/water (Beck et al., 2010; Chandrasekar et al., 2010; Tavman & Turgut, 2010; Teng et al., 2010) and CuO/ Water (Aminossadati, 2013; Sarafraz & Hormozi, 2014; Wongcharee & Eiamsa-ard, 2012) nanofluids as effective coolant, volume concentrations of nanoparticles in the range of 1% to 4% were studied. Effects of volume concentration of nanofluids, step heights and flow Reynolds number on augmentation of heat transfer in the passage were analyzed. It was shown that the increase in heat transfer increases with nanoparticle concentration. Also for turbulent flow regime, the augmentation of heat transfer at the second step is larger than the first step.

8.3.2 Numerical model

A. *Geometry of the flow domain*

The duct geometry with double forward-facing step is presented schematically in Figure 8.20. The boundary conditions are denoted as the bottom of the figure. Accordingly, the steps are heated and kept at a constant temperature (T_h) and the top of the channel is insulated. The height of the first step is varied from 2 to 6cm while the second step was kept fixed at 2cm. The entrance width and channel length dimensions were 10cm and 1m, respectively. Three cases corresponding to the first step heights of 2cm, 4cm and 6cm as listed in Table 8.4 were simulated. In addition, two types of nanoparticles (Al_2O_3 and CuO) with different volume fractions were employed and the flow Reynolds numbers was varied from 30,000 to 100,000.

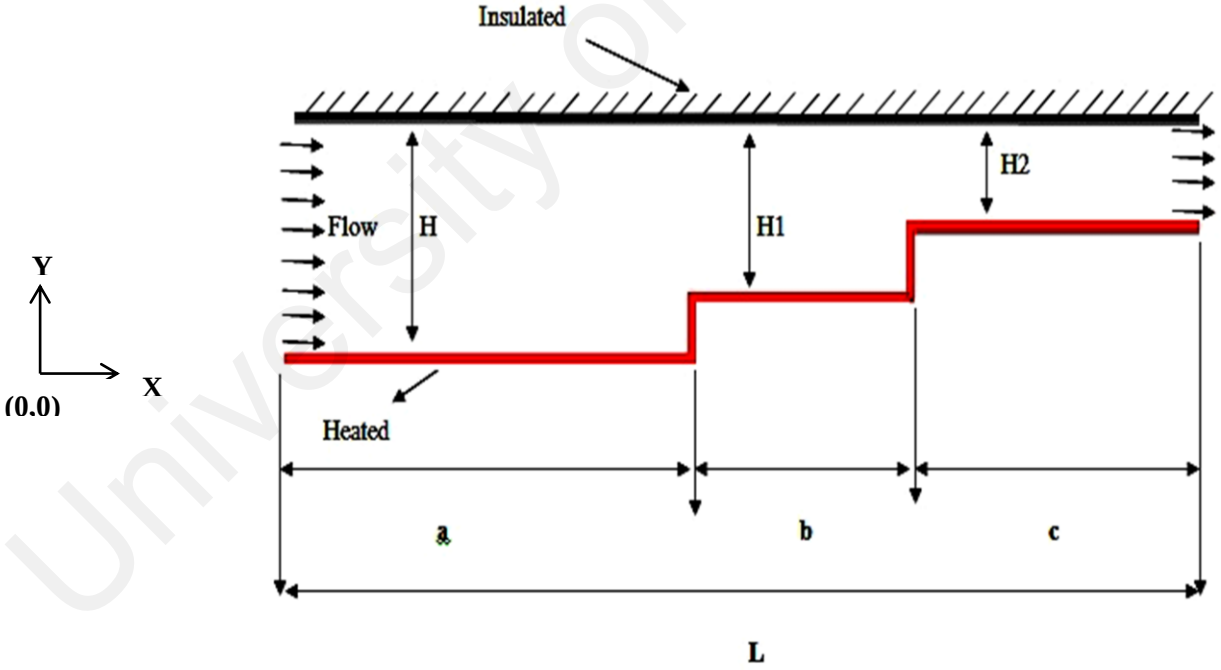

Figure 8.20: Dimensions of geometry.

Table 8. 4: Dimensions of geometry for three cases

Cases	H(cm)	h1=H-H1	h2=H1-H2	L(cm)	b(cm)	c(cm)
1	10	2	2	160	20	40
2	10	4	2	160	20	40
3	10	6	2	160	20	40

B. *Flow equations*

An incompressible two-dimensional turbulent flow with constant fluid properties is assumed. The governing equations of continuity, momentum and energy may be written as:

$$\frac{\partial U_i}{\partial x_i} = 0 \tag{8.9}$$

$$\frac{\partial (U_i U_j)}{\partial x_j} = -\frac{\partial p}{\partial x_i} + \frac{\partial}{\partial x_j}\left(\mu \frac{\partial U_i}{\partial x_j} - \overline{\rho u_i u_j}\right) \tag{8.10}$$

$$\frac{\partial (U_i T_j)}{\partial x_j} = -\frac{\partial}{\partial x_i}\left(\frac{\mu}{Pr}\frac{\partial T_i}{\partial x_j} - \overline{\rho u_i t_j}\right) \tag{8.11}$$

The Reynolds stresses and heat fluxes are, respectively, given as:

$$\overline{\rho u_i u_j} = -\mu_t \left(\frac{\partial U_i}{\partial x_j} + \frac{\partial U_j}{\partial x_i}\right) + \frac{2}{3}\delta_{ij} k\Big] \tag{8.12}$$

$$\overline{\rho u_i t_j} = -\frac{\mu_t}{\sigma_\theta}\frac{\partial T_i}{\partial x_j} \quad (8.13)$$

The standard k-ε model has two transport equations for the turbulence kinetic energy and energy dissipation that are solved together with the equations of balance by the finite volume method. The corresponding transport equations are,

$$\frac{\partial \rho k U_i}{\partial x_j} = -\frac{\partial}{\partial x_j} + \left[\left(\mu + \frac{\mu_t}{\sigma_k}\right)\frac{\partial k}{\partial x_j}\right] + \rho(G_b - \varepsilon) \quad (8.14)$$

$$\frac{\partial \rho \varepsilon U_i}{\partial x_j} = -\frac{\partial}{\partial x_j} + \left[\left(\mu + \frac{\mu_t}{\sigma_k}\right)\frac{\partial \varepsilon}{\partial x_j}\right] + \rho\frac{\varepsilon}{k}(c_{1\varepsilon}G_b - c_{2\varepsilon}\varepsilon) \quad (8.15)$$

$$G_b = \mu_t\left(\frac{\partial u_i}{\partial x_j} + \frac{\partial u_j}{\partial x_i}\right)\frac{\partial u_i}{\partial x_j} \quad (8.16)$$

$$\mu_t = \rho c_\mu \frac{k^2}{\varepsilon} \quad (8.17)$$

The standard constants used in the k-ε model are:

$$C_{1\varepsilon} = 1.44, C_{2\varepsilon} = 1.92, C_{3\varepsilon} = 0.09, \sigma_k = 1.0, \sigma_\varepsilon = 1.3, \text{and Pr} = 7.01.$$

In these simulations, a second-order scheme was used to obtain higher numerical accuracy. The residual sum was computed and sorted for each iteration and the convergence criterion was less than 10^{-6} for the continuity, and smaller than 10^{-8} for the momentum and energy equations.

8.3.3 Thermophysical properties of the nanofluid

The thermophysical properties of the nanofluid are calculated using specific correlations.

The effective density of nanofluid (ρ_{nf}) is given as (Vajjha & Das, 2009)),

$$\rho_{nf} = (1-\phi)\rho_f + \phi\rho_{np} \quad (8.18)$$

where ρ_f and ρ_{np} represent, respectively, the density of the base fluid and the solid nanoparticles.

The specific heat of the nanofluid is given by (Vajjha & Das, 2009)),

$$(\rho C_p)_{nf} = (1-\phi)(\rho C_p)_f + \phi(\rho C_p)_{np} \quad (8.19)$$

where $(\rho C_p)_f$ and $(\rho C_p)_{np}$ represent, respectively, the heat capacities of the base fluid and the nanoparticles,.

As noted by (Koo & Kleinstreuer, 2005), the effective thermal conductivity of nanofluid consists of static and Brownian effects, and could be calculated with the following empirical equations:

$$K_{eff} = K_{static} + K_{Brownian} \quad (8.20)$$

$$K_{static} = K_f\left[\frac{(K_{np}+2K_f)-2\phi(K_f-K_{np})}{(K_{np}+2K_f)+\phi(K_f+K_{np})}\right] \quad (8.21)$$

$$K_{Brownian} = 5\times10^4\beta\phi\rho_f C_{p,f}\sqrt{\frac{KT}{2\rho_{np}d_p}}f(T,\phi) \quad (8.22)$$

where k= 1.3809×10^{-23}J/K is the Boltzmann constant, and β is given as:

$$\beta = 8.4407(100\phi)^{-1.07304} \quad (8.23)$$

and $f(T,\phi)$ is given as

$$f(T,\phi) = (2.8217\times10^{-2}\phi + 3.917\times10^{-3})\left(\frac{T}{T_\circ}\right) + (-3.0669\times10^{-2}\phi - 3.91123\times10^{-3})(16)$$

The effective dynamic viscosity for the nanofluid may be calculated using the following correlations (Corcione, 2010):

$$\mu_{eff} = \mu_f \times \frac{1}{(1-34.87(d_p/d_f)^{-0.3}*\phi^{1.03})} \quad (8.24)$$

$$d_f = \left(\frac{6M}{N\pi\rho_{f0}}\right)^{1/3} \quad (8.25)$$

where d_p and d_f are, respectively, the diameter of the nanoparticles and equivalent diameter of a base fluid molecule; M is the molecular weight; N is the Avogadro number = 6.022×10^{23}mol^{-1}; and ρ_{f0} is the density of the base fluid found at Temperature=293K. Table 8.5 shows the physical properties of the nanofluid (Corcione, 2010) and water (Incropera, 2007).

The Nusselt number is defined as:

$$Nu = \frac{hd}{k} \quad (8.26)$$

where h is the heat transfer coefficient.

The heat transfer enhancement defined as:

$$\eta = \frac{Nu_{nf} - Nu_f}{Nu_f} \times 100\% \qquad (8.27)$$

Table 8. 5: Thermophysical properties of nanoparticles (Al_2O_3, CuO) and water at T=300 K.

Thermophysical properties	Al_2O_3 (Corcione, 2010)	CuO (Corcione, 2010)	Water (Incropera, 2007)
ρ (kg/m^3)	3600	6500	996.5
C_p(J/kg.k)	765	533	4181
K (W/m.k)	36	17.65	0.613
μ (Ns/m^2)	-	-	1E-03

8.3.4 Solution procedure

As noted before, the computation mesh was generated using ANSYS 14 ICEM software and the flow and heat transfer equations were solved with ANSYS-FLUENT 14 software. ICEM provides the tools needed to deal with complex geometry and to obtain a high-quality mesh. The standard k-ε model was used to analyze the turbulent heat transfer of nanofluids composed of suspended AL_2O_3 and CuO nanoparticles in water in a double forward-facing step passage.

A. *Grid-independent study*

A grid-independent study was performed by refining the grid size stepwise and comparing the results until the difference became negligibly small. For Re=30,000, with first step height of 2cm (case1), the grid sizes 9099, 37397, and 67117 were tested. The differences in Nusselt numbers obtained between the last two grids were less than 1% (Figure 8.21). Therefore, a grid of 37397 was used in the analysis.

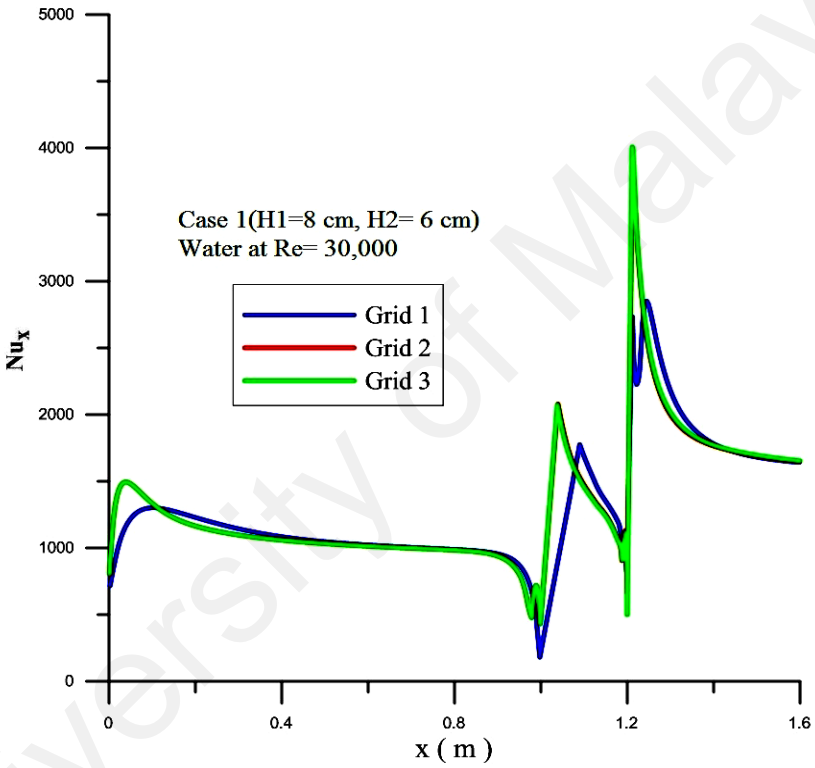

Figure 8.21: Variation of local Nusselt number with axial distance at different grid sizes.

B. *Code validation*

Since experimental data for turbulent flow and heat transfer of nanofluids in double forward-facing step passages has not been reported in the published literature, for validation of the present computational model simulations were performed for airflow in an inclined forward-facing step passage that was numerically studied by Gandjalikhan Nassab et al. (Gandjalikhan Nassab et al., 2009). For airflow at Reynolds number of 30,000, Figure 8.22 compares the present model predictions for the local Nusselt number with the earlier studies of (Gandjalikhan Nassab et al., 2009). It is seen that the present model predictions for the Nusselt number are in good agreement with the earlier numerical simulation of Nassab et al. (Gandjalikhan Nassab et al., 2009). In particular, the sharp increase of the local Nusselt number at the step due to formation of recirculating flow region and gradual decrease towards the end of the passage are well predicted by the present computational model and are good agreement with the simulations of (Gandjalikhan Nassab et al., 2009). A series of simulations for water, and Al_2O_3–water and CuO-water nanfluids were also performed for this configuration and the resulting Nusselt numbers are reproduced in Figure 8.22 for comparison. It is seen that the heat transfer for water is much larger than that for air, and the presence of nanoparticle further enhances the Nusselt numbers. In addition, higher local Nusselt number values are observed for the nanofluid with Al_2O_3 compared to the CuO nanofluid. Turbulent heat transfer to air flow in annular channel with sudden contraction was studied by Togun et al. (HusseinTogun et al., 2014). The present computational model was used and the thermal field for the configuration used in (HusseinTogun et al., 2014) was simulated. The corresponding simulation results are shown in Figure 8.23 and are compared simulation results of

(HusseinTogun et al., 2014) for contraction ratio CR = 2 and q = 4000W/m^2. It is seen the present model simulations are in good agreement with the earlier work (HusseinTogun et al., 2014).

For further validation of the present computational model, the experimental data for fluid flow and heat transfer over single Backward-facing step provided by Armaly et al. (Armaly et al., 2003) are used. The present model was applied to the configuration of the experimental passage of (Armaly et al., 2003). The corresponding velocity profiles at different distances from the step are evaluated. Figure 8.24 compares the present model predictions for the velocity profile with the experimental data of Armaly et al. (Armaly et al., 2003) for Re=343 at different distances form the step. In this figure, s is the step height. It is seen that the predicted velocity profiles are in good agreement with the experimental data, the peak velocity overestimated by a maximum of about 3% for some sections.

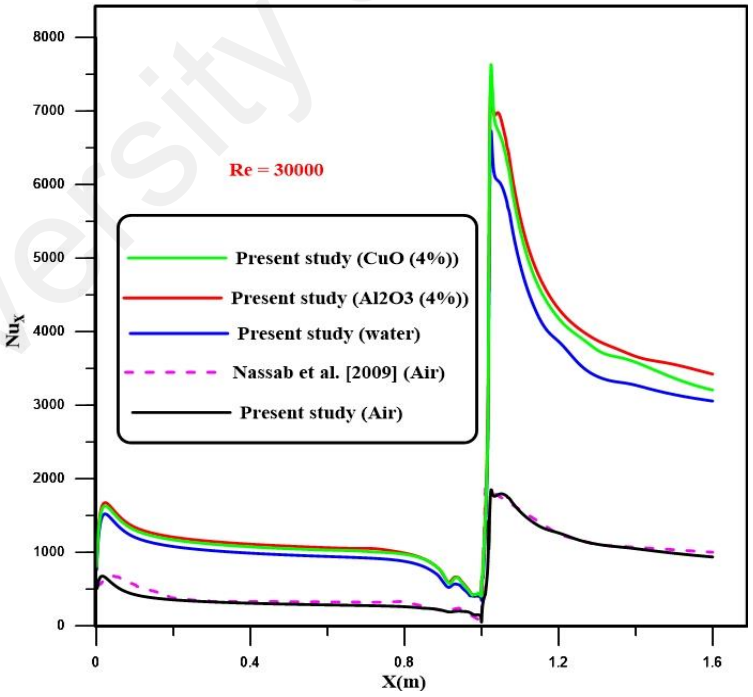

Figure 8.22: Comparison between local Nusslet number and Nassab et al. [2009] at Re=30,000.

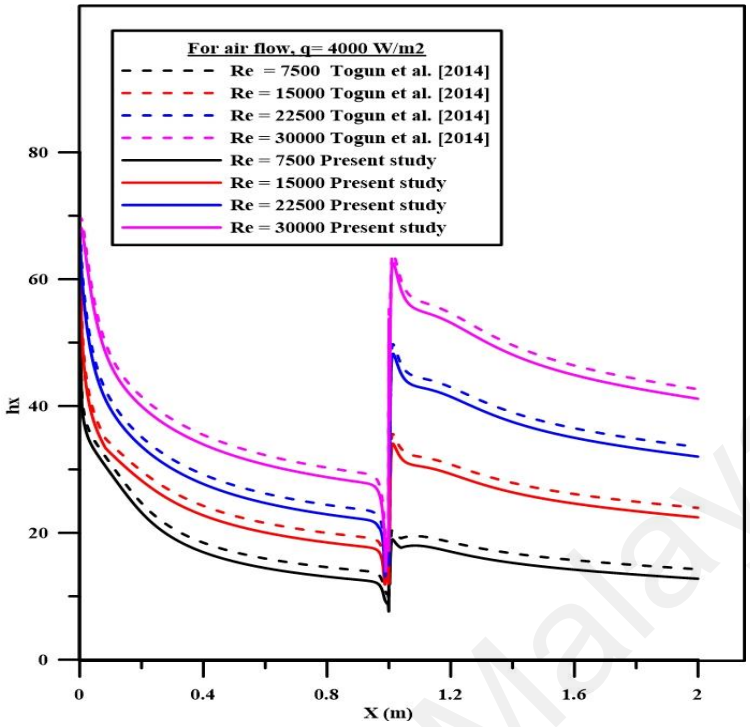

Figure 8.23: Comparison local heat transfer coefficient with Togun et al. [2014] at contraction ratio 2 and different Reynolds number.

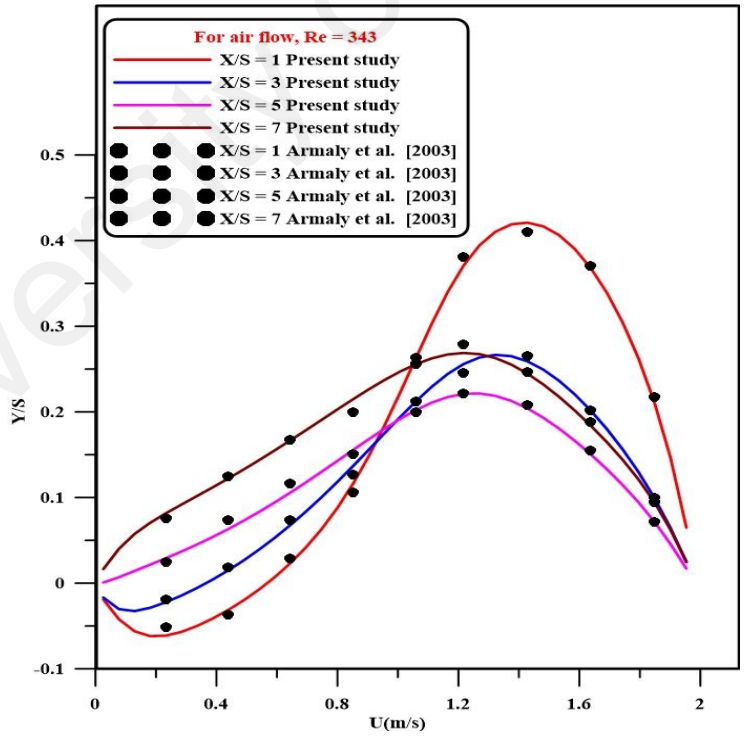

Figure 8.24: Comparison velocity profile with Armaly et al. [2003] for Re= 343 at different position.

8.3.5 Results and discussion

Simulations were conducted for turbulent heat transfer during nanofluid flow in a duct with double forward-facing steps. Two types of nanoparticles (namely Al_2O_3 and CuO) were used with volume fractions in the range of 1% to 4% and flow Reynolds numbers from 30,000 to 100,000 at a constant lower wall temperature of T=300K. Three different step heights were also studied in these simulations.

A. *Effect of nanofluid volume fraction*

Figures 8.25 and 8.26, respectively, show variations of the local Nusselt number with different volume fractions of Al_2O_3 and CuO for case 1(H1=8cm, H2=6cm) with Re= 30,000 and wall temperature of T=313K. For all cases, the local Nusselt number increases slightly with an increase in nanoparticle volume fraction due to the increase in the effective thermal conductivity of the nanofluid. The local Nusselt number profile presents two peaks at the first and second steps due to recirculation regions that form in these areas. These figures also show that the local Nusselt number for nanofluid with Al_2O_3 is roughly the same as the nanofluid with CuO nanoparticles with the same volume fraction. That is the effect of nanoparticle type and concentrations are small. This is because the turbulent transport overwhelms the heat transfer process and the effect of properties of the base fluid is not is as important. A close examination shows that the Al_2O_3 nanofluid has slightly higher Nu number in comparison to CuO nanofluid with the same volume fraction. This is perhaps due the higher heat conductivity and higher heat capacity of Al_2O_3 compared to CuO which affects the net heat transfer enhancement of the nanofluids.

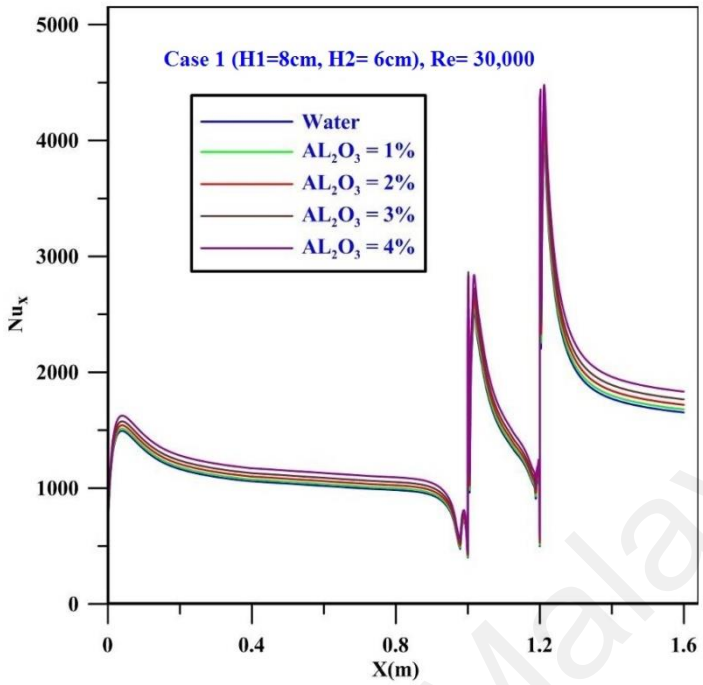

Figure 8.25: Variation of local Nusselt number with axial distance at different nanoparticle volume fractions for case 1 with Re= 30,000 and T=313K.

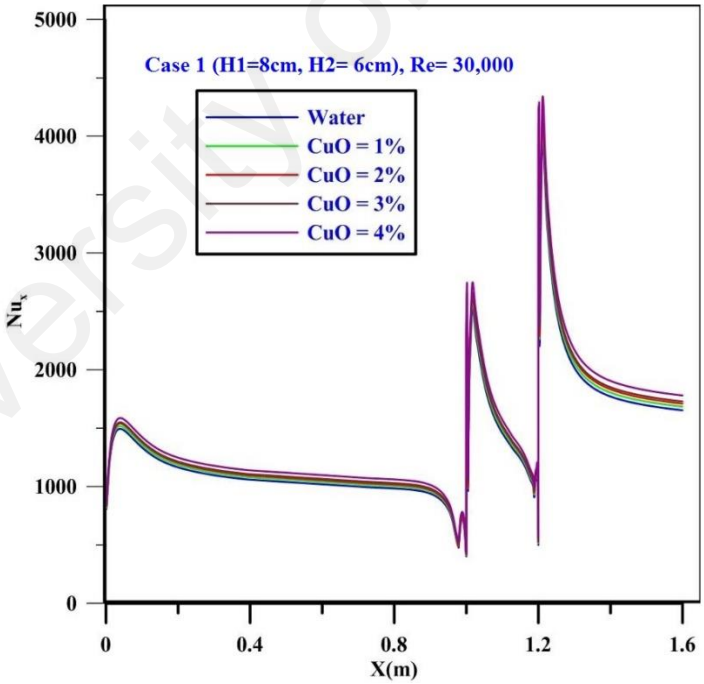

Figure 8.26: Variation of local Nusselt number with axial distance at different nanoparticle volume fractions for case 1 with Re= 30,000 and T=313K.

B. *Effect of Reynolds number*

The effects of flow Reynolds number on the local Nusselt number for Al_2O_3 and CuO nanofluids with volume fraction of ϕ=1% and inlet temperature of T=313K are presented, respectively, in Figures 8.27 and 8.28. Generally, a rise in Reynolds number leads to an increase in Nusselt number for both Al_2O_3 and CuO nanofluids. This is perhaps because the higher Re leads to higher level of turbulence and also generation of smaller fluctuation scales. Due to the hydrodynamics of the flow near the corners and passing sharp edges, recirculation regions before and after the steps are created, which significantly affect the heat transfer and the corresponding Nusselt number.

Comparing Figures 8.27 and 8.28, it appears that the Nusselt numbers for Al_2O_3 and CuO nanofluids are quite comparable, with the heat transfer for the Al_2O_3 nanfluid slightly higher. As noted before, this is because the turbulence transport essentially dominated the process and the effect of base fluid becomes secondary.

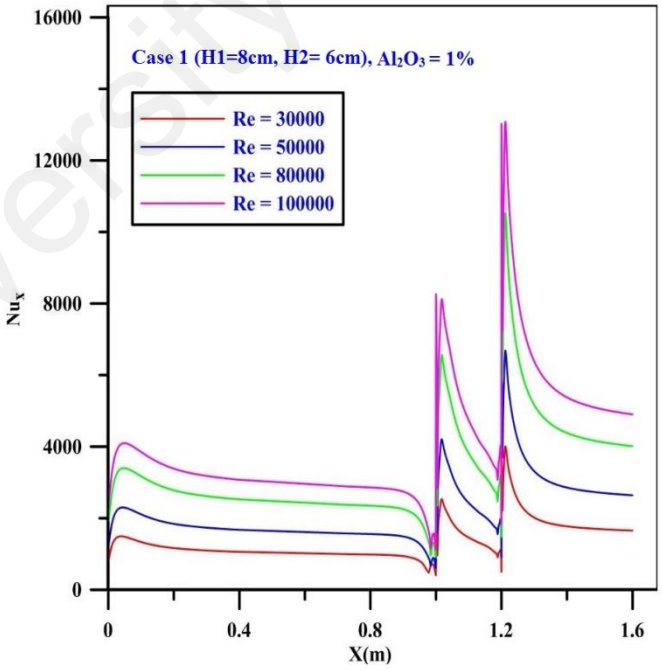

Figure 8.27: Variation of local Nusselt number with axial distance at different Reynolds numbers for case 1 with Al_2O_3=1% and T=313K.

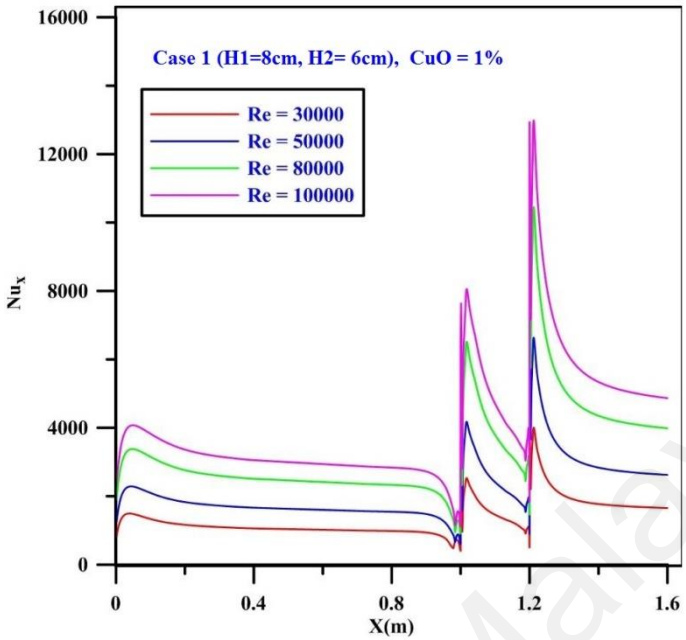

Figure 8.28: Variation of local Nusselt number with axial distance at different Reynolds numbers for case 1 with CuO=1% and T=313K.

C. *Effect of step height*

The local Nusselt number variation in the duct for first step heights of 2cm, 4cm and 6cm for Al_2O_3 and CuO nanofluids with 1% volume fraction and Re=30000 are presented in Figures 8.29 and 8.30. Note that the second step height is fixed at 2cm. It is seen that the local Nusselt number increases with the increase in the first step height; furthermore, the increment of the local Nusselt number observed at the second step is higher than that at the first step. This is because the increase of the first step height makes the channel narrower and the mean flow speed increases. The channel becomes even narrower at the second step and that leads to more intense recirculation region and enhances the heat transfer. The location of peak heat transfer after the step also shifts slightly to the right with increase of step height, which is consistent with stretching of the recirculation region with the increase of local velocity. Among the cases studied, the maximum local Nusselt number is observed

at the second step with the first step height of 6 cm (case 3) at Re=30,000. The results for the Al_2O_3 nanofluid and CuO nanofluid are comparable with the slightly higher heat transfer for the aluminum oxide nanofluid.

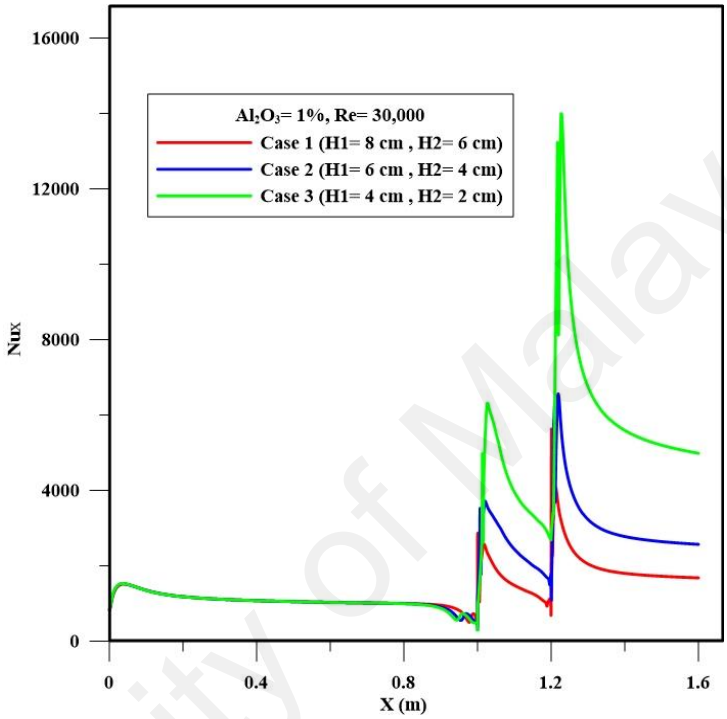

Figure 8.29: Profile of local Nusselt number at different step heights for Al2O3 at Re= 30,000 and T=313K.

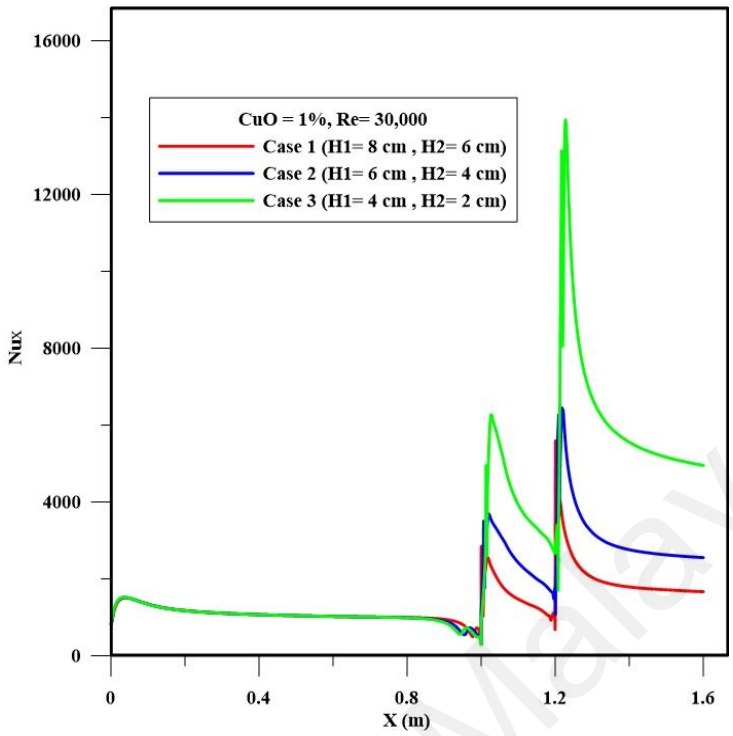

Figure 8.30: Profile of local Nusselt number at different step heights for CuO at Re= 30,000 and T=313K.

D. *Average of Nusselt numbers*

In this section, the mean heat transfer rates for nanofluid flowing through a duct with double forward-facing steps are presented. Figures 8.31, 8.32, and 8.33 show the variations of average Nusselt number for different flow Reynolds numbers and volume fractions of Al_2O_3 nanoparticles for different first step heights of 2cm (case 1), 4cm (case 2), and 6cm (case 3). The presented results indicate an increase in average Nusselt number with the increase of Reynolds number, first step height and nanoparticle volume fraction. For all cases studied, the largest enhancement of heat transfer was observed in case 3 with first step height of 6cm for Reynolds number of 100,000 and 4% solid volume fraction.

Similarly, the average Nusselt number for different step heights and with various Reynolds numbers and volume fractions of CuO are presented in Figures 8.34, 8.35, and 8.36. The trends are quite similar to those observed in Fig. 8. The heat trasnfer augmentation increases with increasing Reynolds number and volume fraction of CuO nanoparticles. Comparing Figures (8.31, 8.32, and 8.33 with Figures (8.34, 8.35, and 8.36), it is seen the heat transfer for aluminum oxide nanofluid is somwhat higher compared to the copper oxide nanofluid. As noted before, this is due to the higher thermal conductivity of the Al_2O_3 nanoparticles compared to CuO nanoparticles.

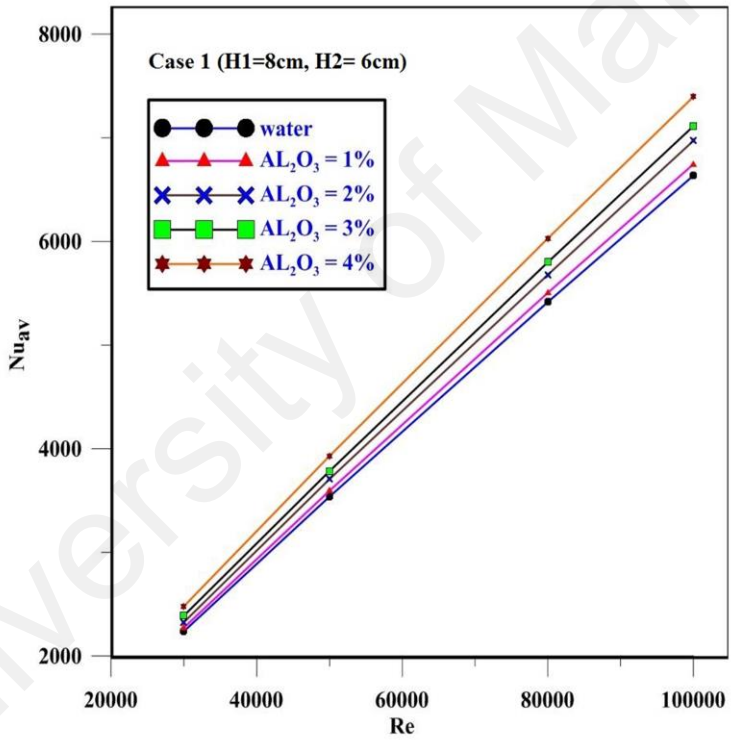

Figure 8.31: Average Nusselt number at different Reynolds numbers and volume concentrations of AL_2O_3 for Case 1.

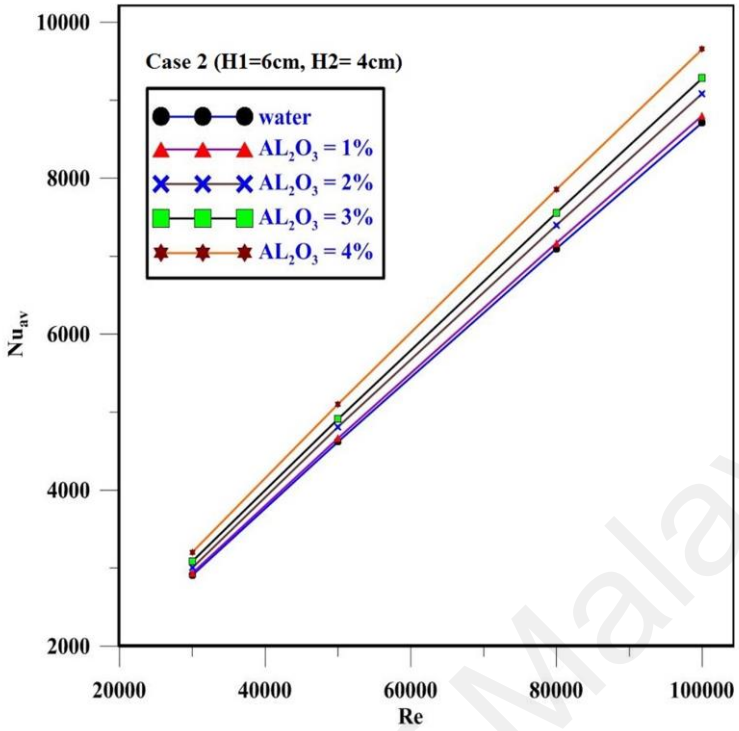

Figure 8.32: Average Nusselt number at different Reynolds numbers and volume concentrations of AL_2O_3 for Case 2.

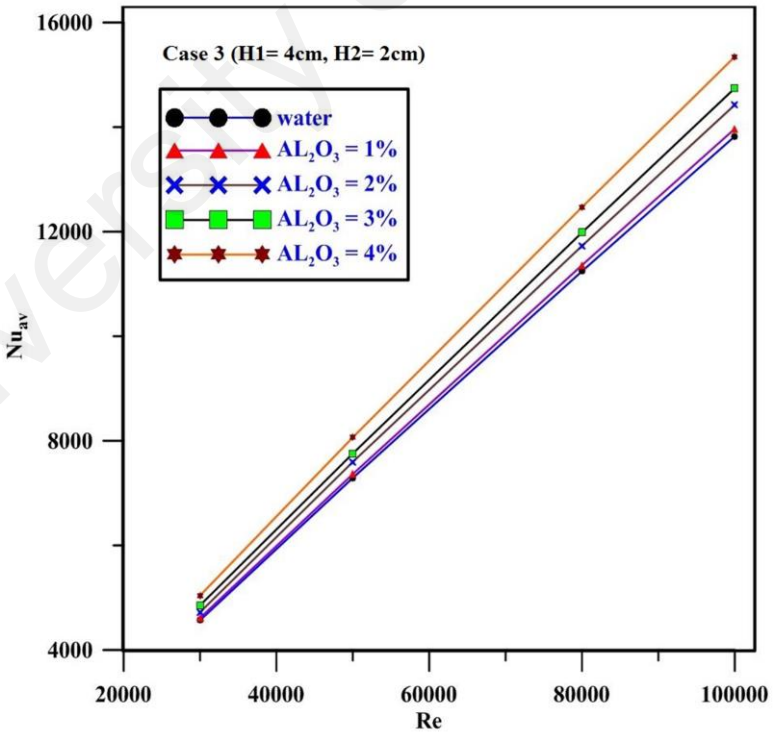

Figure 8.33: Average Nusselt number at different Reynolds numbers and volume concentrations of AL_2O_3 for Case 3.

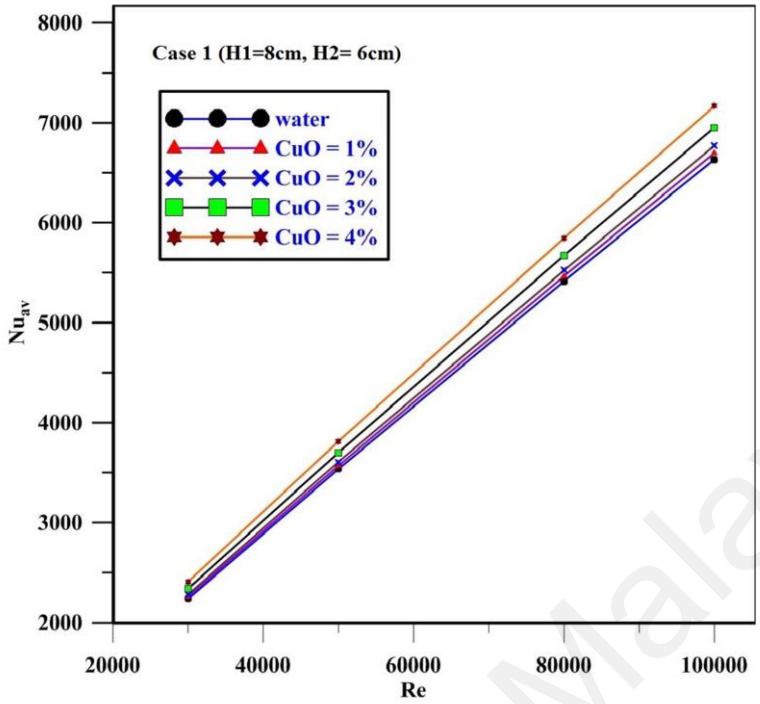

Figure 8.34: Average Nusselt number at different Reynolds numbers and volume concentrations of CuO for Case1.

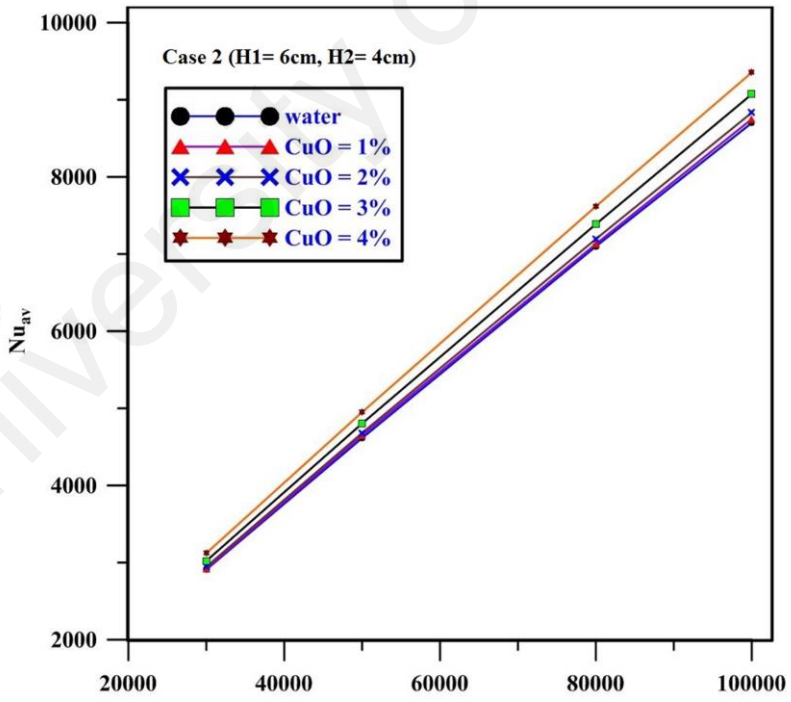

Figure 8.35: Average Nusselt number at different Reynolds numbers and volume concentrations of CuO for Case2.

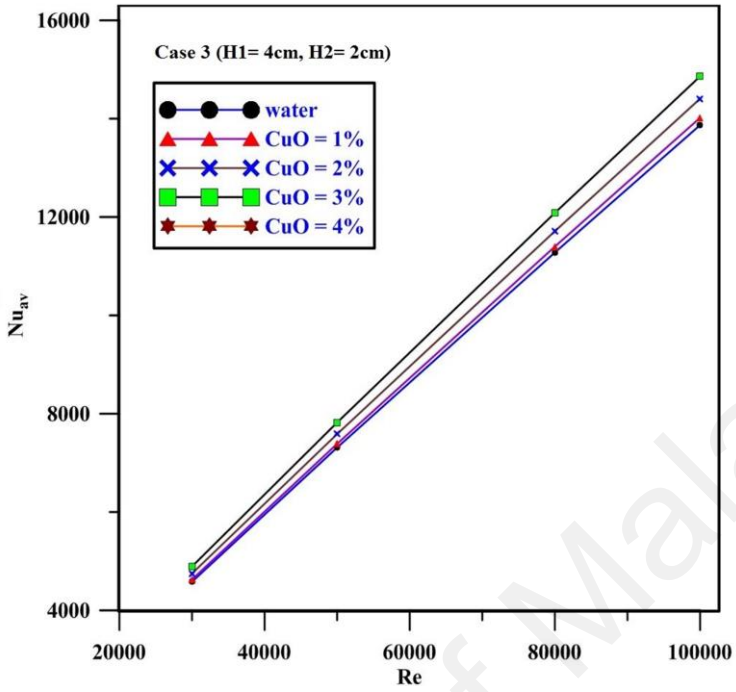

Figure 8.36: Average Nusselt number at different Reynolds numbers and volume concentrations of CuO for Case3.

E. *Thermal enhancement*

Figure 8.37 shows the variation of thermal enhancement factor (η) as defined by Equation (2) for both Al_2O_3 and CuO nanofluids for various first step heights at different Reynolds numbers and solid volume fractions. An increase of thermal enhancement is noticed with the increase of solid volume fraction and Reynolds number. The thermal enhancement is also higher for the aluminum oxide nanofluid compared to the copper oxide nanofluid. As noted before the heat transfer rate increases as the flow velocity increases. Figure 8.37 also shows that the highest thermal enhancement is obtained for the duct with first step height of 6 cm (case 3) for a nanofluid with 4% Al_2O_3 at Re=100,000 as compared to step heights of 2cm and 4 cm (cases 1 and 2).

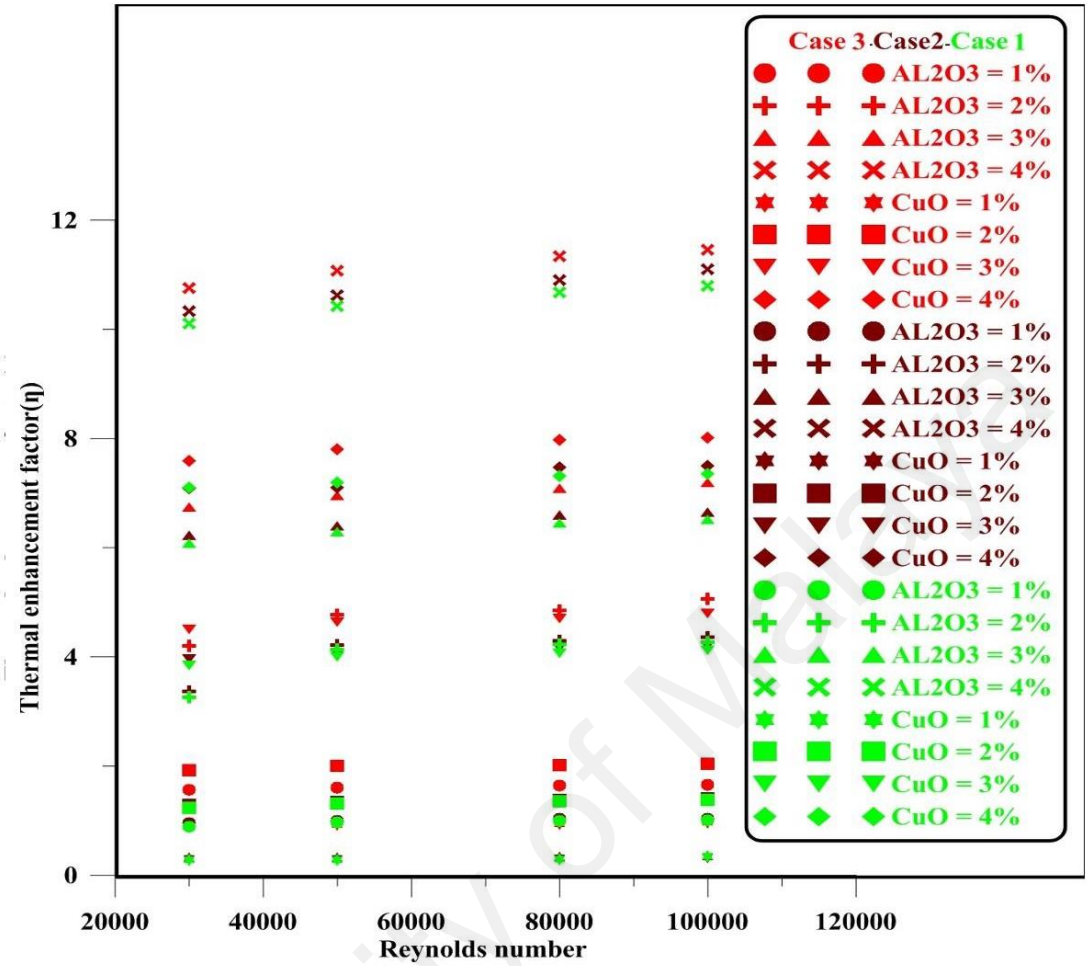

Figure 8.37: Variation of thermal enhancement factor at different Reynolds numbers and volume fractions of AL_2O_3 and CuO for cases 1, 2, and 3.

F. *Velocity Contours*

Figures 8.38-8.41 illustrate the axial velocity contours for Al_2O_3 nanofluid in case 1 with a 2cm first step and 4% solid volume fraction for different Reynolds numbers. Generally, for all cases there are two recirculation regions before and after each step which also affect the local thermal performance. The recirculation regions before and after the steps are clearly seen from these contour plots. Figures 8.38-8.41 also show that an increase in Reynolds number leads to enlargement of recirculation regions after the first and second steps, while the recirculation region before the first and second steps decreases. That is, as the flow velocity increases, the recirculation regions before steps are compressed, while the recirculation regions after step are stretched and enlarged. Figures 8.38-8.41 show that the largest recirculation region is after the second step, which corresponds to the region with the highest value of local Nusselt number.

Figure 8.42 shows the effect of step height on flow pattern and recirculation region after and before the first step for Reynolds number of 100000 and Al_2O_3 nanofluid. It is seen as the first step height increase, so does the size of the recirculation region before and after the first step. The reduction of passage cross-section area in the channel is higher after the second step; hence, the peak of local Nusselt number is larger at the second step compared to the first step due to the creation of larger recirculation region.

The corresponding turbulence kinetic energy contours are presented in Figure 8.43, where in increase in turbulence kinetic energy is observed after the second step with an increase in the first step height. The largest turbulence kinetic energy is seen after the second step of case 3 (with first step height of 6cm) compared with other step heights. It is conjectured that this is because the largest contraction of the flow passage occurs at the second step for case 3. Thus, the turbulence kinetic energy reaches to its highest value.

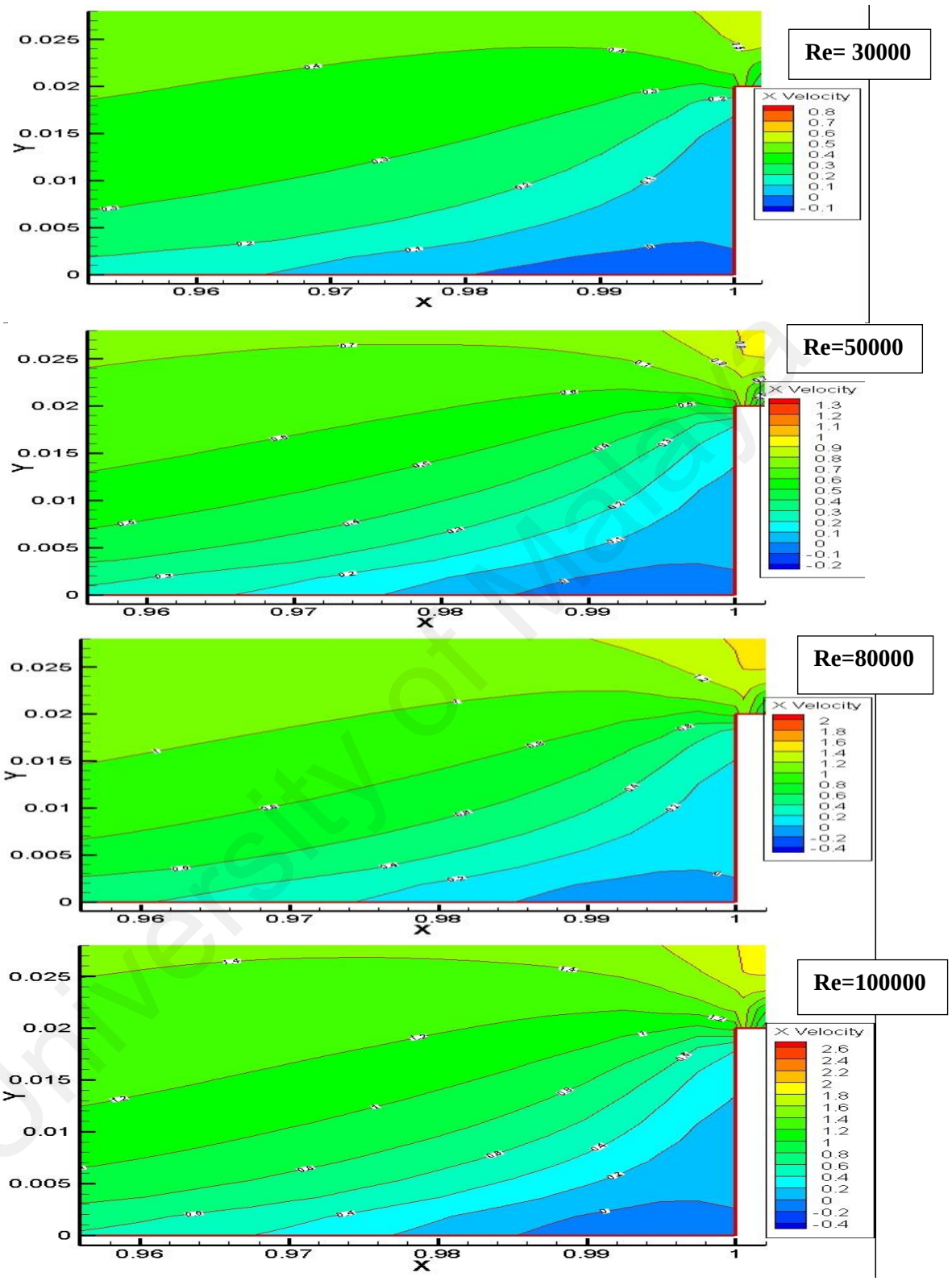

Figure 8.38: Effect of Reynolds number on size of recirculation region: case 1 at volume fraction AL_2O_3 4% **(Before first step**).

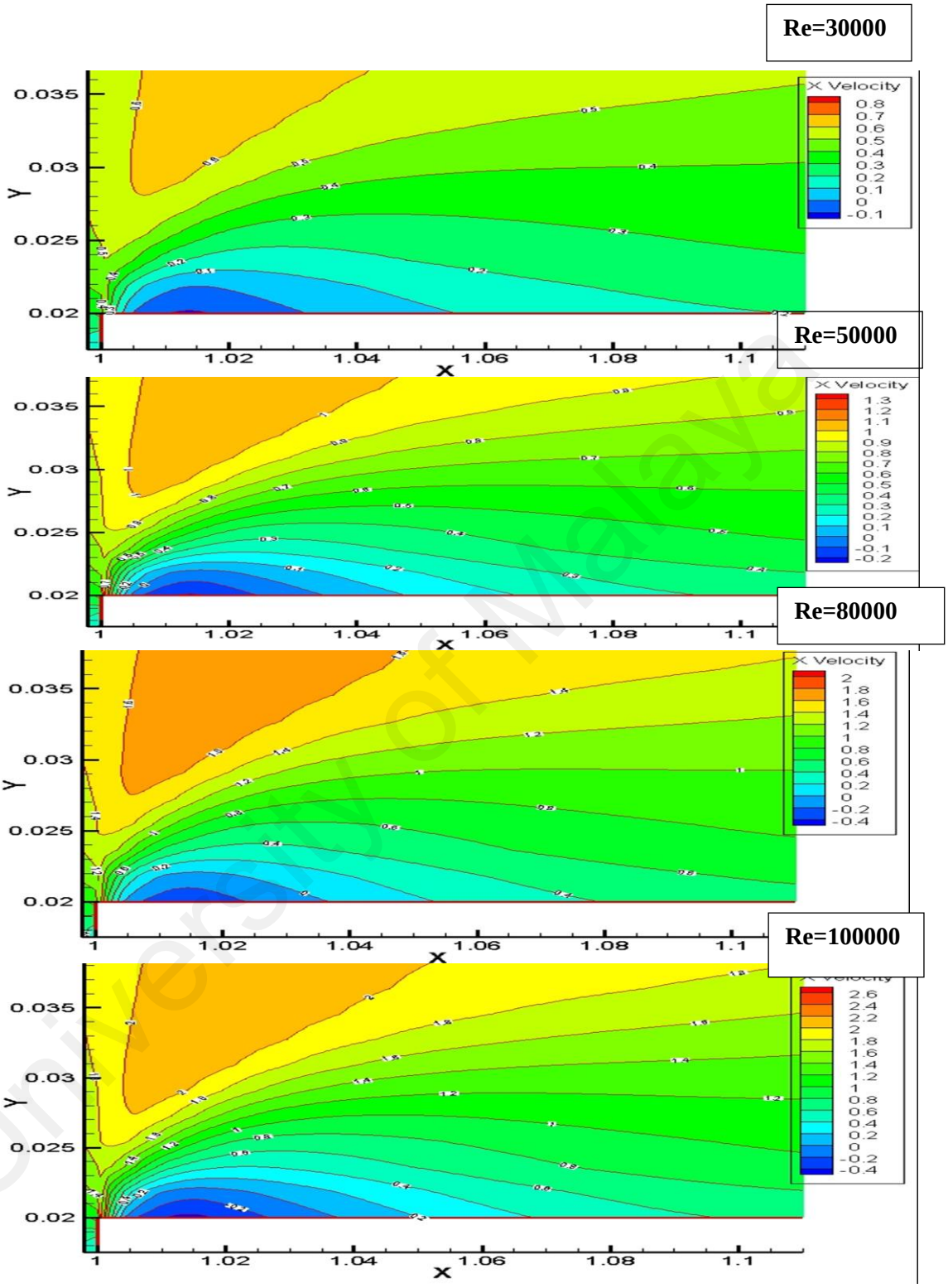

Figure 8.39: Effect of Reynolds number on size of recirculation region: case 1 at volume fraction AL_2O_3 4% **(After first step**).

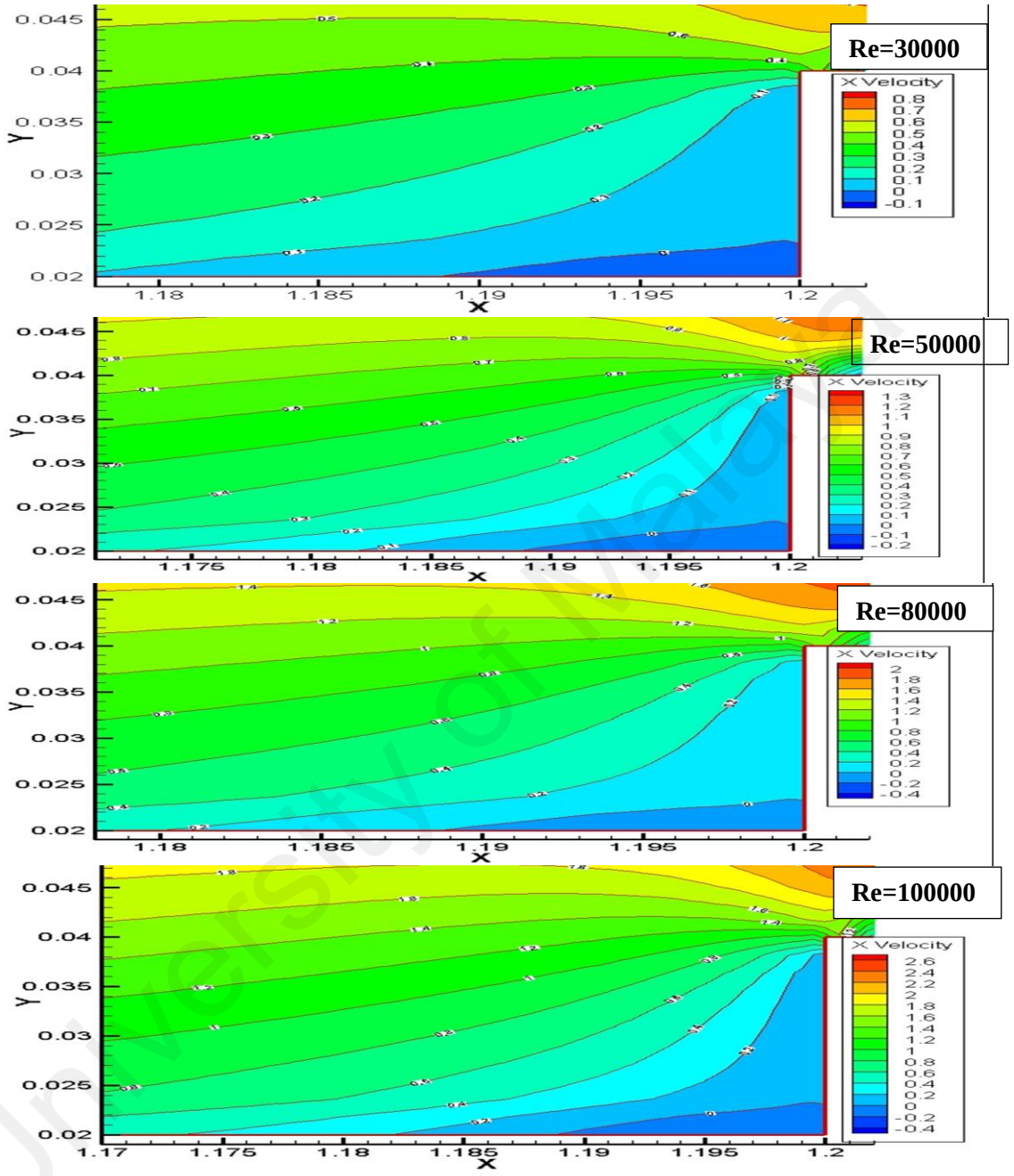

Figure 8.40: Effect of Reynolds number on size of recirculation region: case 1 at volume fraction AL_2O_3 4% **(Before second step**).

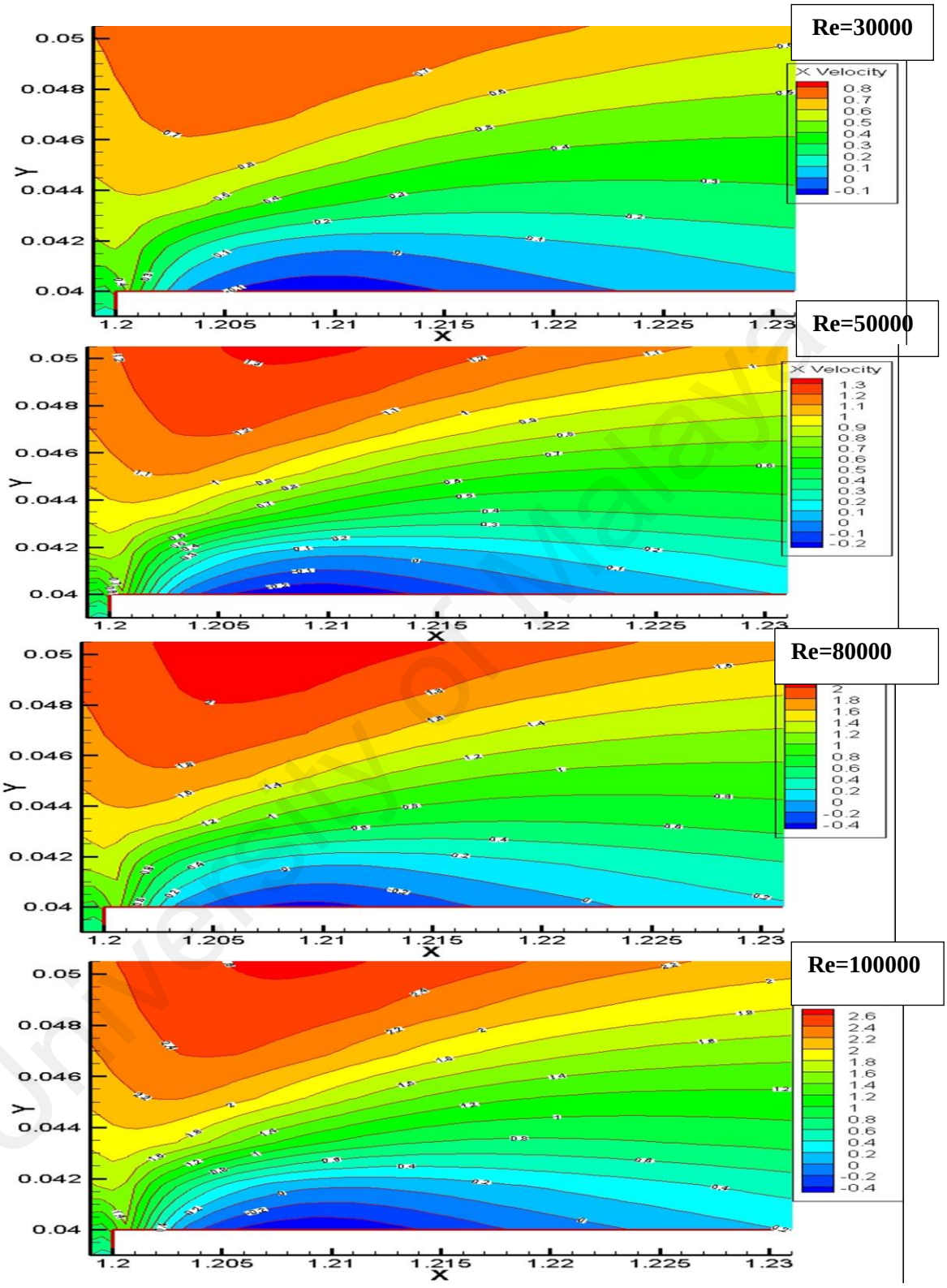

Figure 8.41: Effect of Reynolds number on size of recirculation region: case 1 at volume fraction Al_2O_3 4% **(After Second step)**.

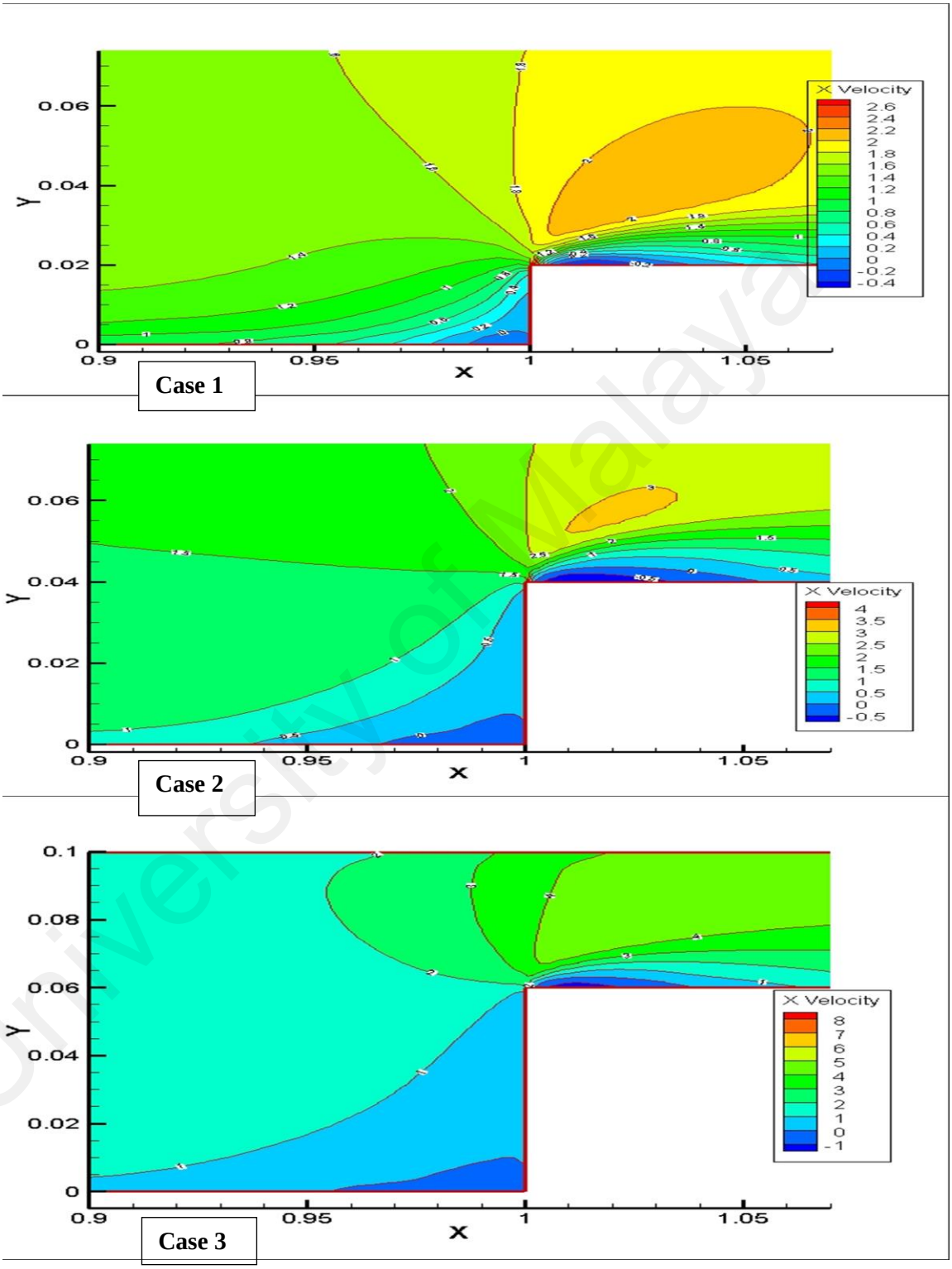

Figure 8.42: Effect step height on size of recirculation region at first step with Al_2O_3 (4%) ,Re=100,000 and T=313K for cases 1, 2, and 3.

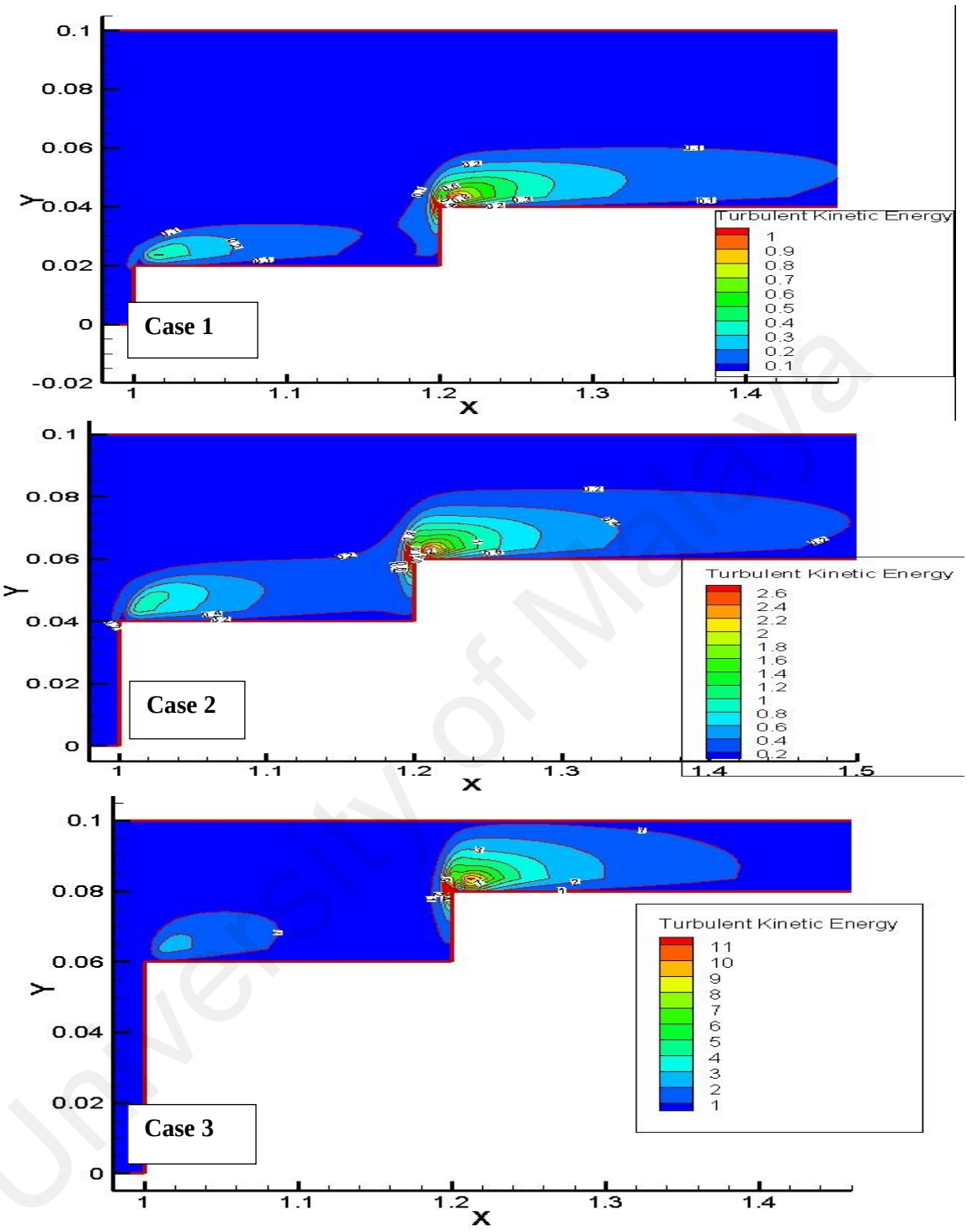

Figure 8.43: Contour of turbulent kinetic energy for case 1, 2 and 3 with Al_2O_3 (4%), Re=100,000.

8.4 Numerical simulation of laminar to turbulent nanofluid flow and heat transfer over a backward-facing step

Abstract

This paper presents a numerical study of heat transfer to turbulent and laminar Cu/water flow over a backward-facing step. Mathematical model based on Finite Volume Method with a FORTRAN code is used to solve the continuity, momentum, energy and turbulence equations. Turbulence was modeled by the shear stress transport (SST) K-ω Model. In this simulation, three volume fractions of nanofluid (0%, 2% and 4%), a varying Reynolds number from 50 to 200 for the laminar range and 5000 to 20000 for the turbulent range, an expansion ratio of 2 and constant heat flux of 4000W/m^2 were considered. The results show the effect of nanofluid volume fraction on enhancing the Nusselt number in the laminar and turbulent ranges. The effect of expansion ratio was clearly observed at the downstream inlet region where the peak of the Nusselt number profile was referred to as enhanced heat transfer due to the generated recirculation flow. An increase of pressure drop was evident with an increasing Reynolds number and decreasing nanofluid volume fraction, while the maximum pressure drop was detected in the downstream inlet region. A rising Reynolds number caused an increasing Nusselt number, and the highest heat transfer augmentation in the present investigation was about 26% and 36% for turbulent and laminar range respectively compared with pure water.

Nomenclature		Unit
C_p	Specific Heat Capacity	(J kg^{-1} K^{-1})
E	Total Energy	(J Kg^{-1})
h	Heat Transfer Coefficient	($Wm^{-2}K^{-1}$)
k	Turbulence Kinetic Energy	(m2 s-2)
Nu	Nusselt number	
P	Pressure	(Pa)
Pr	Prandtl number	
q	Heat Flux	(W m^{-2})
Re	Reynolds number	
T	Temperature	(K)
u	Velocity Component	(ms^{-1})
X,Y	Spatial Coordination	(m)
y	Distance to the Next Surface	(m)

Greek Symbols		
λ	Thermal conductivity	($Wm^{-1}K^{-1}$)
μ	Dynamic viscosity	(Pa s)
ν	Kinematic viscosity	(m^2s^{-1})
ρ	Density	(kg m^{-3})
σ	Turbulent Prandtl number	
τ	Wall Shear Stress	(Pa)

Subscripts	
eff	Effective
f	Base Fluid
i, j	Components
m	Mixture
P	Nanoparticles
t	Turbulent

8.4.1 Introduction

Flow over a backward-facing step generates recirculation zones and forms vortices due to the separation flow obtained from the adverse pressure gradients in the fluid flow. The phenomena of flow separation are found in different applications such as heat exchangers, nuclear reactors, power plants, cooling devices, etc. In the past decades, a number of works have been done on this phenomena and its effect on heat transfer rate. The pioneer investigators (Boelter et al., 1984), (Ede et al., 1956a), (Seban, 1959), (Abbot and Kline, 1962), (Seban, 1965), (Filetti and Kays, 1967), (Goldstein et al., 1970), (Durst and Whitelaw, 1971), and (Brederode and Bradshaw, 1972) developed experimental and theoretical methods of studying separation flow that takes place due to changes in the cross section of the passage. With advances in measurement devices and CFD software, the researchers have identified detailed information regarding the structure of separation flow and recirculation zone. Armaly et al., (1983) employed a Laser Doppler Anemometer to measure the velocity distribution and reattachment length for air flow over a backward-facing step. They investigated the laminar, transition, and turbulent range domains and the obtained results were in good agreement with the experimental and numerical findings. Particle tracking velocimetry was employed for studying the laminar separation flow in a forward-facing step by (Stuer et al., 1999). The experimental results demonstrated an increase in distance between the breakthroughs in span as the Reynolds number decreased. It was also noticed that the transverse direction of separation was slow, compared to the short time scale over flow visualization. The study of the fluid flow of two non-Newtonian liquids in sudden expansion with viscoelastic polyacrylamide (PAA) solutions and a purely viscous shear-thinning liquid performed by (Pak et al., 1990). The Reynolds number was varied from 10 to 35,000 with an expansion ratio of 2 to 2.667; according to the results

from the laminar range, the reattachment length of non-Newtonian fluid was shorter compared to the Newtonian fluid and two to three times shorter for the turbulent range than water. The effects of step height on heat transfer and turbulent flow characteristics were presented numerically by (Nie and Armaly, 2002). Uniform heat flux was maintained at the downstream region of the passage with Re = 28,000 It was found that an increase in step height caused the primary and secondary recirculation zones to enlarge. Increase Nusselt number noticed with increase blockage ratio and Reynolds number. Khanafer et al., (2008) carried out a numerical study on the heat transfer and laminar mixed convection of pulsatile flow over a backward-facing step with the help of the finite element method. Based on the results, by increasing the Reynolds number, the heat transfer rate amplified while the thickness of the thermal boundary layer reduced. In contrast, Chen et al., (2006) numerically studied heat transfer and turbulent forced convection flow over a backward-facing step. The results attained revealed enhanced heat transfer in response to an increase in step height. The effect of backward- and forward-facing steps on turbulent mixed-convection flow over a flat plate was investigated by (Abu-Mulaweh, 2009). Increased turbulence intensity occurred from the temperature fluctuations at the downstream region due to the introduction of the backward- and forward-facing steps. Hussein et al., (2011) presented experimental study of turbulent separation flow in concentric annular passage with sudden expansion. They found maximum augmentation of heat transfer about 18% at step height 18.5 mm in compared to without step. In general, separation and reattachment flow are adopted in several experimental and numerical studies (C. S. Oon et al., 2012; Hussein Togun, Tuqa Abdulrazzaq, S. N. Kazi, et al., 2013; Hussein Togun, Tuqa Abdulrazzaq, S.N. Kazi, et al., 2013; HusseinTogun et al., 2011; HusseinTogun et al., 2014; Oon et al., 2013; Togun et al., 2013).

More recently, the majority of studies have been utilizing nanofluid because of its higher thermal conductivity compared to normal fluid (Hassan et al., 2013). Abu-Nada, (2008) is a pioneer in research on laminar nanofluid flow over a backward-facing step with Cu, Ag, Al_2O_3, CuO, and TiO_2 nanofluid, volume fractions between 0.05 to 0.2 and Reynolds numbers ranging from 200 to 600. An investigation of findings signifies that the Nusselt number increased with the volume fraction and Reynolds number. Later, Kherbeet et al., (2012) presented a numerical investigation of heat transfer and laminar nanofluid flow over a micro-scale backward-facing step. The Reynolds numbers ranged from 0.01 to 0.5, nanoparticle types comprised Al_2O_3, CuO, SiO_2, and ZnO, and the expansion ratio was 2. An increasing Reynolds number and volume fraction seemed to lead to an increasing Nusselt number; the highest Nusselt number value was obtained with SiO_2.

Additional last investigations concern nanofluid flow over a backward-facing step for the laminar range (Al-aswadi et al., 2010; Amirhossein Heshmati, 2013; Hussein A. Mohammed, 2013; Kherbeet et al., 2014; Mohammed et al., 2014; Mohammed, Al-aswadi, Abu-Mulaweh, et al., 2011; Mohammed, Al-aswadi, Shuaib, et al., 2011; Mohammed et al., 2012), but such work with respect to the turbulent regime, in particular, is still not entirely understood. Due to the Cu has higher thermal conductivity and many experimental investigations done with good improvement in thermal performance then used in this simulation. The aim of the present paper is therefore to study the enhancement of heat transfer regarding both turbulent and laminar Cu/water flow over a backward-facing step.

8.4.2 Numerical Model

A. *Description of geometry*

The geometry and flow domain applied in this study are illustrated in Figure 8.44. The geometrical dimensions were 1.25cm inlet diameter, 200cm upstream length, 2.5cm outlet diameter and 150cm downstream length for an expansion ration of 2. The downstream wall was heated while all other walls were insulated. The Reynolds numbers varied from 50 to 200 for the laminar and 5000 to 20000 for the turbulent regimes. The working fluids were pure water or Cu/water at different volume fractions.

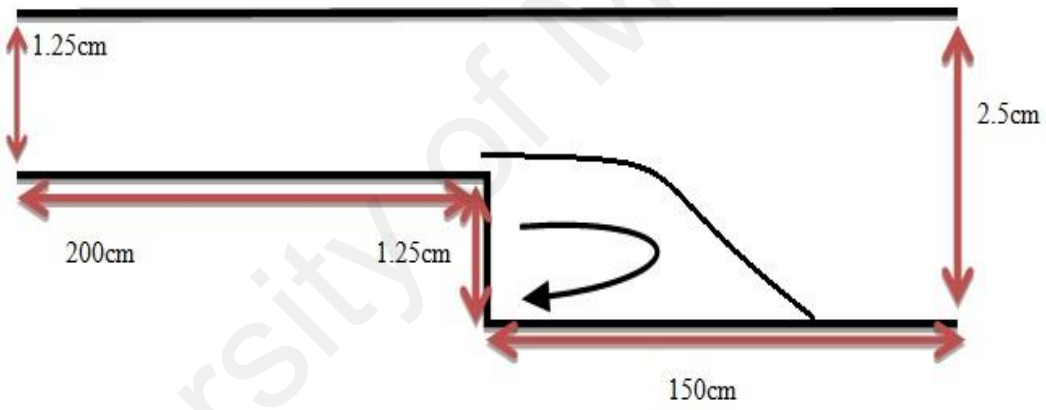

Figure 8.44: Geometry domain

B. *Governing equations*

The governing equations of continuity, momentum and energy were solved for turbulent flow at the rectangular coordinates under the hypotheses of steady-state, two-dimensional, incompressible, turbulent, and constant flow condition properties (Manca et al., 2012b):

$$\frac{\partial}{\partial x_i}(\rho u_i) = 0 \tag{8.28}$$

$$\frac{\partial}{\partial x_j}(\rho u_i u_j) = -\frac{\partial P}{\partial x_i} + \frac{\partial}{\partial x_i}\left[\mu\left(\frac{\partial u_i}{\partial x_j} + \frac{\partial u_j}{\partial x_i} - \frac{2}{3}\delta_{ij}\frac{\partial u_i}{\partial x_j}\right)\right] + \frac{\partial}{\partial x_j}\left(-\rho\overline{u_i' u_j'}\right) \tag{8.29}$$

$$\frac{\partial}{\partial x_i}[u_i(\rho E) + P] = \frac{\partial}{\partial x_j}\left[\left(\lambda + \frac{c_p \mu_t}{Pr_t}\right)\frac{\partial T}{\partial x_j} + u_i(\tau_{ij})_{eff}\right] \tag{8.30}$$

$E = C_p T + (u^2/2)$ and $(\tau_{ij})_{eff}$ represents the deviatoric stress tensor as determined by Eq. (8.31).

$$(\tau_{ij})_{eff} = \mu_{eff}\left(\frac{\partial u_j}{\partial x_i} + \frac{\partial u_i}{\partial x_j}\right) - \frac{2}{3}\mu_{eff}\frac{\partial u_i}{\partial x_j}\delta_{ij} \tag{8.31}$$

The SST K-ω Model equations, as developed by Menter (Menter, 1994), can be written as equations (8.32-8.33):

$$\frac{\partial}{\partial x_i}(\rho k u_i) = \frac{\partial}{\partial x_j}\left(\Gamma_k \frac{\partial k}{\partial x_j}\right) + \tilde{G}_k - Y_k + S_k \tag{8.32}$$

$$\frac{\partial}{\partial x_i}(\rho \omega k u_i) = \frac{\partial}{\partial x_j}\left(\Gamma_\omega \frac{\partial \omega}{\partial x_j}\right) + G_\omega - Y_\omega + D_\omega + S_\omega \tag{8.33}$$

where G_k is defined as the production of turbulent kinetic energy because of the mean velocity gradients, and G_ω is defined as the generation of ω.

$$\tilde{G}_k = min(G_k, 10\beta^* k_\omega) \tag{8.34}$$

For $G_k = -\rho\overline{u_i' u_j'}(\partial u_j/\partial x_i)$, where G_k is a function of G_ω.

$$G_\omega = \frac{\alpha}{v_t} G_k \tag{8.35}$$

where β^* is a model constant, and $\propto$ could be given by equation (8.36).

$$\propto = \propto_\infty \frac{(\propto_0^* + Re_t/R_\omega)}{(1 + Re_t/R_\omega)} \tag{8.36}$$

where R_ω=2.95, $\propto_\infty$is define by eq. (8.37):

$$\propto_{\infty} = F_1 \propto_{\infty,1} + (1 - F_1) \propto_{\infty,2} \quad (8.37)$$

$$\propto_{\infty,1} = \frac{\beta_{i,1}}{\beta_{\infty}^*} - \frac{\kappa^2}{\sigma_{\omega,1}\sqrt{\beta_{\infty}^*}} \quad (8.38)$$

$$\propto_{\infty,2} = \frac{\beta_{i,2}}{\beta_{\infty}^*} - \frac{\kappa^2}{\sigma_{\omega,2}\sqrt{\beta_{\infty}^*}} \quad (8.39)$$

The value of constants are κ=0.41 and β_i =0.072. $\propto = \propto_{\infty} = 1$, for high Reynolds number

The effective of diffusivity Γ_k and Γ_ω can be represented by equations (8.40-8.41):

$$\Gamma_k = \mu + \frac{\mu_t}{\sigma_k} \quad (8.40)$$

$$\Gamma_\omega = \mu + \frac{\mu_t}{\sigma_\omega} \quad (8.41)$$

The turbulent Prandtl numbers of k and ω are represented by equations 8.42 and 8.43:

$$\sigma_k = \frac{1}{F_1/\sigma_{k,1} + (1-F_1)/\sigma_{k,2}} \quad (8.42)$$

$$\sigma_\omega = \frac{1}{F_1/\sigma_{\omega,1} + (1-F_1)/\sigma_{\omega,2}} \quad (8.43)$$

where μ_t is given by eq. (8.44):

$$\mu_t = \propto^* \frac{\rho k}{\omega} \quad (8.44)$$

$\propto^*$is the coefficient for the damping of turbulent viscosity and is computed from:

$$\propto^* = \propto_{\infty}^* \frac{(\propto_0^* + Re_t/Re_k)}{(1 + Re_t/Re_k)} \quad (8.45)$$

The coefficients in eq. (8.46) are: $Re_t = \rho k/\mu\omega$, Re_k=6, $\propto_0^* = \beta_i/3$ and $\beta_i = 0.072$.

Also, for high Reynolds numbers$\propto^* = \propto_{\infty}^* = 1$.

The blending equation (F_1) is calculated by:

$$F_1 = \tan(\Phi_1^4) \quad (8.46)$$

$$\Phi_1 = \min\left[\max\left(\frac{\sqrt{k}}{0.09\omega y}\frac{500\mu}{\rho y^2 \omega}\right), \frac{4\rho k}{\sigma_{\omega,2} D_\omega^+ y^2}\right] \quad (8.47)$$

$$D_{\omega}^{+} = \max\left[2\rho\frac{1}{\sigma_{\omega,2}}\frac{1}{\omega}\frac{\partial k}{\partial x_i}\frac{\partial \omega}{\partial x_j}, 10^{-10}\right] \quad (8.48)$$

where D_{ω}^{+} is the positive portion of the cross-diffusion term. Y_k and Y_ω show the dissipation of k and ω due to turbulence:

$$Y_k = \rho\beta^* k\omega \quad (8.49)$$

$$Y_\omega = \rho\beta\omega^2 \quad (8.50)$$

$$\beta_i = F_1\beta_{i,1} + (1 - F_1)\beta_{i,2} \quad (8.51)$$

where S_k and S_ω correspond to the possible source terms and D_ω is defined as the cross-diffusion term and is computed from equation (8.52):

$$D_\omega = 2(1 - F_1)\rho\sigma_{\omega,2}\frac{1}{\omega}\frac{\partial k}{\partial x_j}\frac{\partial \omega}{\partial x_i} \quad (8.52)$$

The values of the constant model are shown in Table 8.6 as used by (Tseng et al., 2014).

Table 8. 6: The constant of K-ω Model (Tseng et al., 2014)

$\sigma_{k,1} = 1.176$	$\sigma_{k,2} = 1$	$\sigma_{\omega,1} = 2$	$\sigma_{\omega,2} = 1.168$	$\beta_i = 0.072$	$\alpha_0 = 1/9$
$\beta_{i,2} = 0.0828$	$\alpha_\infty^* = 1$	$\alpha_\infty = 0.52$	$\beta_\infty^* = 0.09$	$\sigma_k = 2$	$\alpha_\omega = 2$
$R_\beta = 8$	$R_k = 6$	$R_\omega = 2.95$	$\alpha_1 = 0.31$	$\beta_{i,1} = 0.075$	

For the two-dimensional conduction model and steady state with heated downstream wall, equation (8.53) may be used:

$$\frac{\partial}{\partial x_i}\left(\lambda\frac{\partial T}{\partial x_i}\right) = 0 \quad (8.53)$$

8.4.3 Thermophysical Properties of the Nanofluid

The thermophysical properties of the governing equations are as per (Ramiar et al., 2012), (Khanafer & Vafai, 2011) and (Cho et al., 2013).

$$\rho_m = \varphi\rho_p + (1-\varphi)\rho_f \tag{8.54}$$

An accurate equation for calculating the effective heat capacitance is ((Ramiar et al., 2012), (Khanafer & Vafai, 2011) and (Cho et al., 2013)):

$$\left(\rho c_p\right)_m = (1-\varphi)(\rho c_p)_f + \varphi(\rho c_p)_p \tag{8.55}$$

Chon et al.'s (Chon et al., 2005) correlation, which considers the Brownian motion and mean diameter of the nanoparticles, is used to calculate the effective thermal conductivity:

$$\frac{k_{nf}}{k_f} = 1 + 64.7\,\varphi^{0.746}\left(\frac{d_f}{d_p}\right)^{0.369}\left(\frac{k_p}{k_f}\right)^{0.7476}\mathrm{Pr}^{0.9955}\,\mathrm{Re}^{1.2321} \tag{8.56}$$

Pr and Re are defined as:

$$\mathrm{Pr} = \frac{\mu_f}{\rho_f \alpha_f} \text{ and } \mathrm{Re} = \frac{\rho_f k_b T}{3\pi\mu^2 l_f}$$

where L_f is the mean free path of water, k_b is the Boltzmann Constant ($1.3807\times10^{-23}\,\mathrm{JK^{-1}}$) and μ is the temperature-dependent viscosity of the base fluid as calculated with the following equation:

$$\mu = O\times10^{\frac{P}{T-Q}} \tag{8.57}$$

where *O*, *P*, and *Q* are constants. For water, these are equal to 2.414×10^{-5}, 247.8 and 140 respectively (Mintsa et al., 2009).

N Masoumi, (2009) have recently developed a new equation for predicting nanofluid effective viscosity that is a function of temperature, mean nanoparticle diameter, nanoparticle volume fraction, nanoparticle density and the base fluid's physical properties. Equation (8.58) is adopted for calculating the nanofluid effective viscosity:

$$\mu_{eff} = \mu_{bf} + \mu_{app} \tag{8.58}$$

where μ_{bf} and μ_{app} are the base fluid and apparent viscosity, respectively. The apparent viscosity is characterized by equation (8.59).

$$\mu_{app} = \frac{\rho_p V_B d_p^2}{72 C \delta} \tag{8.59}$$

where C depends on the base fluid's viscosity, the nanoparticles' mean diameter, d, depends on the mean diameter and volume fractions of the nanoparticles, and V_B is the Brownian velocity of the nanoparticles which depends on temperature, diameter and the density of particles equation (8.60).

$$C = \mu_{bf}^{-1}(c_1\varphi + c_2)\, d_p + (c_3\varphi + c_4) \tag{8.60}$$

where $c_1 = -1.133\times10^{-6}$, $c_2 = -2.771*10^{-6}$, $c_3 = 9.0\times10^{-8}$ and $c_4 = -3.93\times10^{-7}$

In this simulation, the nanofluid's thermophysical properties based on the properties of water (as base fluid) and copper (as nanoparticles) are calculated by equations (N Masoumi,

2009; S. V. Patankar, 1980; Safaei, Goodarzi, et al., 2011; Safaei, Goshayeshi, et al., 2011; Safaei et al., 2012; Safaei, Rahmanian, et al., 2011) corresponding to volume fractions φ =2% and φ =4% (Table 8.7) (Goodarzi et al., 2014). Volume fraction clearly has an influence on thermal conductivity due to increased surface area of nanoparticles dispersed in water. Furthermore, the base fluid viscosity apparently decreases with temperature, contributing to the intensifying Brownian motion along with temperature (Mintsa et al., 2009).

Table 8. 7: Properties of nanofluid (Goodarzi et al., 2014).

Property	Water	Cu
Cp (J/KgK)	4179	3830
ρ (Kg/m^3)	997.1	8954
K(W/mK)	0.6	400
μ(Pa.s)	8.91×10^{-4}	-
α (K^{-1})	2.1×10^{-4}	1.67×10^{-5}

The dimensionless pumping power is calculated by the nanofluid flow rate and the pressure drop across the passage.

$$P_{Pump} = \frac{Q.\Delta P}{\mu^3 \rho^{-2} d_h^{-1}} \quad (8.61)$$

Where μ and ρ are represent viscosity and density of nanofluid, respectively, Q is the flow rate and ΔP pressure drop across the passage, d_h hydraulic diameter.

The Nusselt number can be determined using the equation 8.62.

$$Nu = \frac{h_{nf}\, d_h}{k_{nf}} \tag{8.62}$$

Where h_{nf} and k_{nf} are define the heat transfer coefficient and thermal conductivity of nanofluid respectively.

8.4.4 Numerical Procedure

The governing equations were solved with a computer program using FORTRAN code according to associated boundary and initial conditions. The Finite Volume Method [28, 29] was applied to discretize the governing equations within the computational domain, while the SIMPLE algorithm [30-32] assisted with linking the pressure and velocity fields. The diffusion terms in the momentum equations and convective terms were estimated by selecting the Second Order Central Difference and Second Order Upwind differencing, respectively, resulting in greater solution stability.

Non-uniform quadrilateral grids were utilized for meshing the solution domain. The meshing process strategy was highly concentrated near the step and step corners in order to ensure numerical simulation accuracy and to conserve both grid size and computational time. The residual sum for each variable was computed and stored after each iteration, thus recording the convergence history. The convergence criterion necessitated that the maximum relative mass residual based on the inlet mass be smaller than 1×10^{-3}.

8.4.5 Grid Independence

Structured non-uniform grid distributions were performed to discretize the computation domain. Due to the significance that velocity and temperature gradients have near the walls,

the number of elements increased there. Different grid sizes were adopted, and Tables 8.8 and 8.9 show two cases of investigations performed for selected grids in this simulation.

Table 8. 8: Grid independency tests for laminar regime.

Number of grids	3000×8	4000×9	5000×10
Average Nusselt number for Re=50 and pure water $(\phi = 0)$	115.64018	115.61147	115.60996

Table 8. 9: Grid independency tests for the turbulence RNG k-ε model.

Number of grids	5000×10	6000×12	7000×14
Average Nusselt number for Re=5000 and pure water $(\phi = 0)$	2483.3585	2483.3635	2483.3621

8.4.6 Numerical Procedure Validation

A. *Laminar forced convection validation*

The laminar forced convection of single-phase nanofluids in a 2D horizontal backward-facing step at an expansion ratio of 2 and step height of 4.8mm was studied by Al-Aswadi et al. (Al-aswadi et al., 2010).

Calculations were done for $50 \le \mathrm{Re} \le 175$ while the volume fraction of nanoparticles was kept fixed at $\phi = 0.05$. The computed X-velocity of Cu/water nanofluid at Re=175 was contrasted with the work of Al-aswadi et al. (Al-aswadi et al., 2010) in Figure 8.45. The

present results demonstrate very good agreement with the results of Al-aswadi et al. (Al-aswadi et al., 2010). Therefore, the current numerical procedure can be used with confidence to simulate laminar forced convection flows.

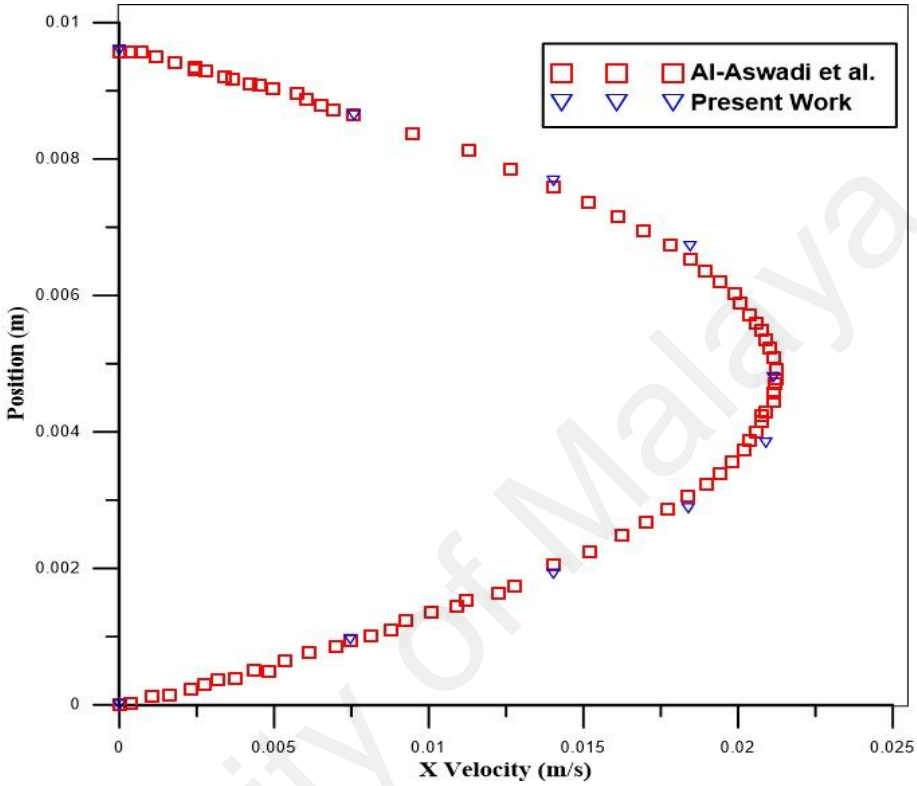

Figure 8.45: Variation of X-velocity at X=207.44 mm, Re =175

B. *Turbulent forced convection validation*

The present numerical procedure for solving turbulent forced convection was validated against the existing results of Jongebloed (Jongebloed, 2008) for turbulent forced convection in a backward-facing step. In this work, laminar and turbulent forced convection heat transfer of air in a backward-facing step with an expansion ratio of 1.942 and step height of 4.9 m was studied numerically by finite volume method. Investigations were done at $400 \le \mathrm{Re} \le 1200$ for the laminar regime and $6600 \le \mathrm{Re} \le 15000$ for the turbulent regime. For Re = 7000, 11400 and 17799, the predicted reattachment length /step height

(X_1/S) is shown in Table 4 and the results were compared to Jongebloed's (Jongebloed, 2008). Table 8.10 indicates reasonable agreement between the results of the present work and those of (Jongebloed, 2008). The small discrepancies seen in this table may be due to the differences between the turbulence models used. For more validation results, investigation study of heat transfer and fluid flow over vertical double forward facing step which conducted by (Tuqa et al., 2014) used. In Figure 8.46 the present results compared with the simulation results of (Tuqa et al., 2014) for case 1 at T=310 K where satisfy agreement found with our code.

Table 8. 10: Comparison of the separation points with (Jongebloed, 2008)

Re	Reattachment length/step height (Jongebloed (2008) work, RNG K— ε turbulence model)	Reattachment length/step height (present work, K-w turbulence model)
7000	6.92	6.87
11,400	7.01	6.98
17,799	8.00	7.99

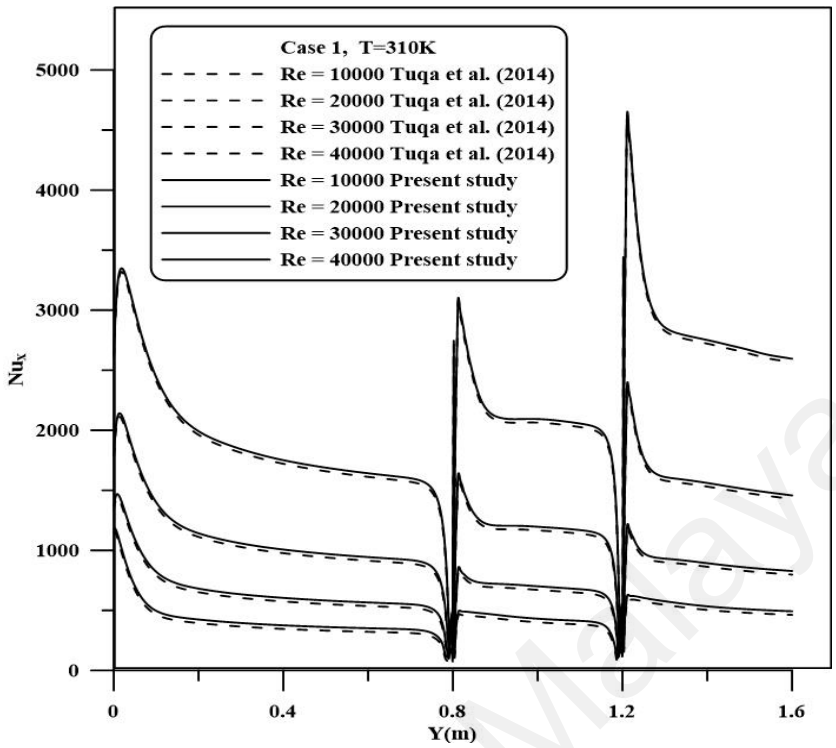

Figure 8.46: Comparison Nusselt number with (Tuqa et al., 2014)

8.4.7 Results and Discussion

A. *Effect of nanofluid volume fraction*

Figures 8.47-8.49 show the variation in surface Nusselt number for the laminar range of Reynolds numbers 50, 100, and 200 and the volume fractions of Cu 0%, 2%, and 4%. The Nusselt number profile increased suddenly at the downstream inlet region and then decreased gradually up to the exit due to the recirculation flow created by the backward-facing step. It is also clear that the Nusselt number increased at higher nanofluid volume fractions due to increase of thermal conductivity of fluid by disperse nanoparticles. Nusselt number variations in the turbulent range at Reynolds numbers 5000, 10000, and 20000, and various nanofluid volume fractions are presented in Figures 8.50-8.52. Generally, the results portray a rise in Nusselt number at the downstream inlet region, and it was also

observed that an increasing nanofluid volume fraction caused the Nusselt number to increase

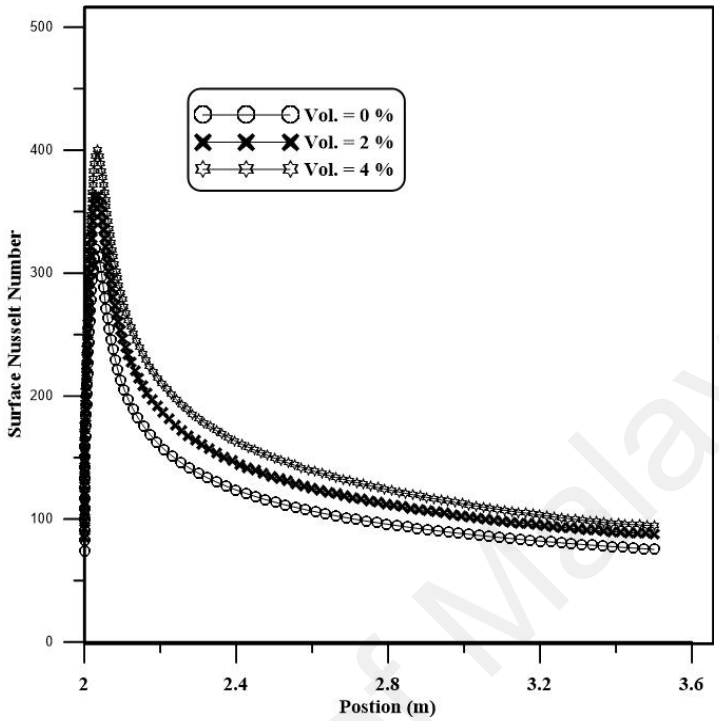

Figure 8.47: Distribution of surface Nusselt number at different volume fraction and **Re= 50**.

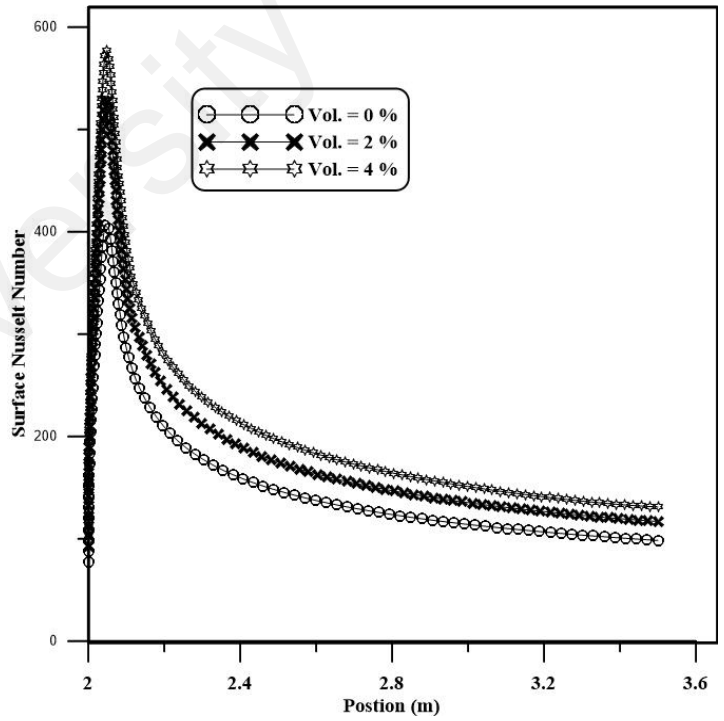

Figure 8.48: Distribution of surface Nusselt number at different volume fraction and **Re= 100.**

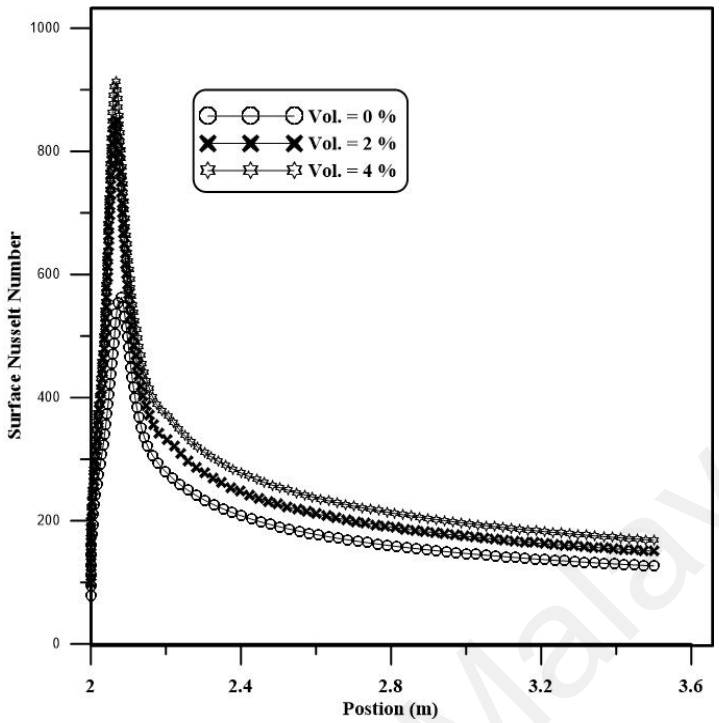

Figure 8.49: Distribution of surface Nusselt number at different volume fraction and **Re= 200.**

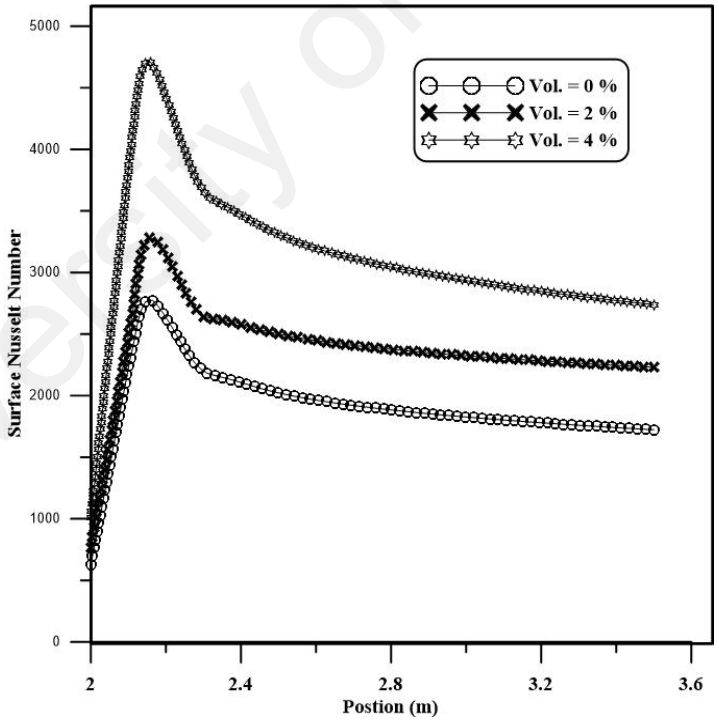

Figure 8.50: Distribution of surface Nusselt number at different volume fraction and **Re= 5000.**

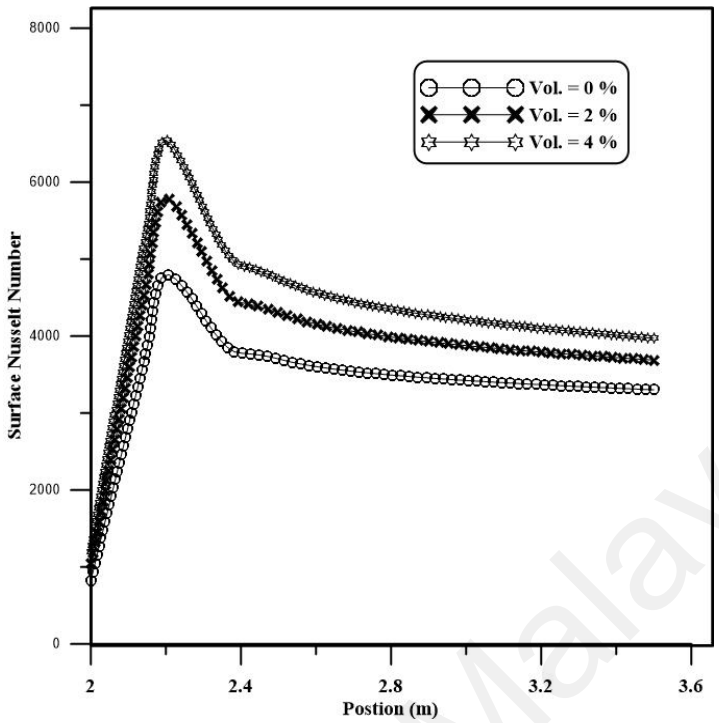

Figure 8.51: Distribution of surface Nusselt number at different volume fraction and **Re= 10000.**

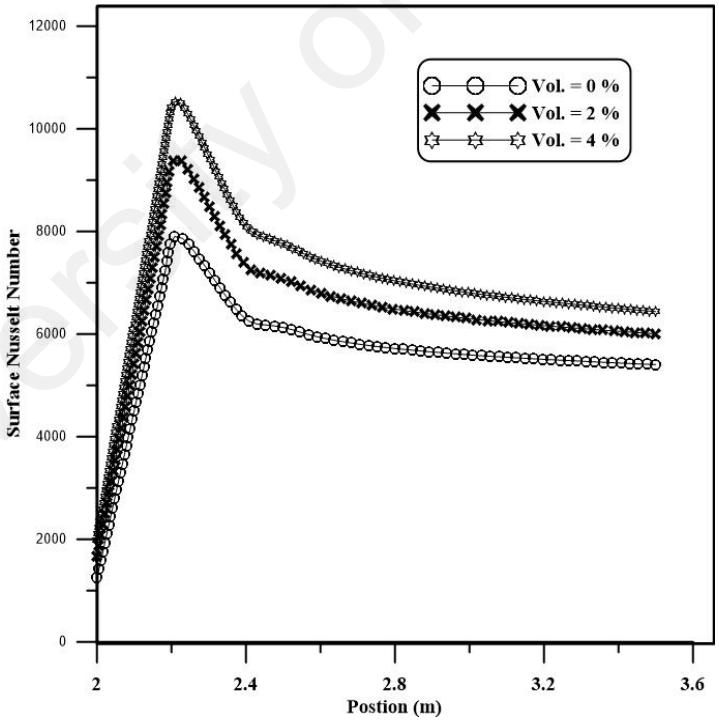

Figure 8.52: Distribution of surface Nusselt number at different volume fraction and **Re= 20000.**

B. *Effect of the Reynolds number*

The effects of the Reynolds number on the local Nusselt number for the laminar and turbulent ranges are presented in Figures 8.53 -8.55, and Figures 8.56-8.58, respectively. With the increase of Reynolds number, the Nusselt number increased in the laminar and turbulent ranges. For pure water, the effect of the Reynolds number in the turbulent regime is obvious because clearly, the difference in Nusselt number at various Re values is significant in comparison with nanofluid for the laminar range.

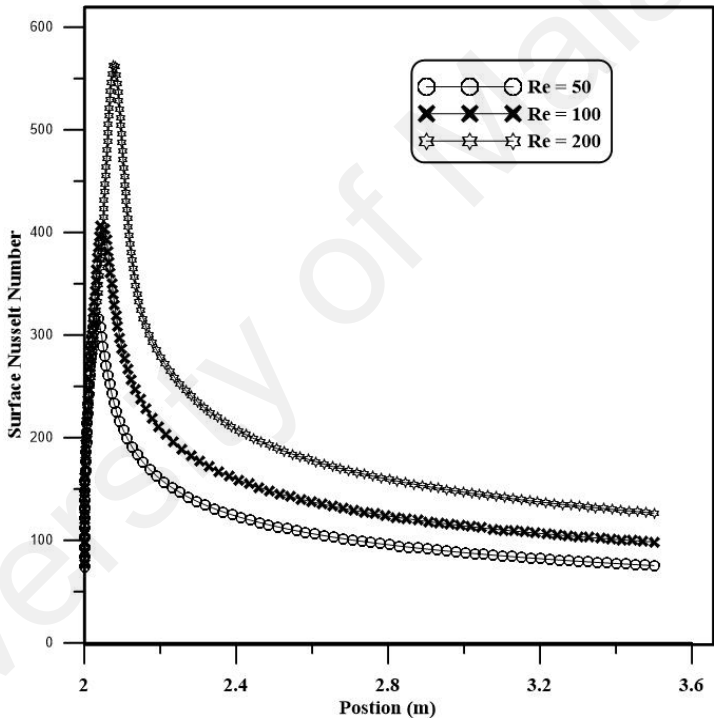

Figure 8.53: Effect of laminar Reynolds number on surface Nusselt number for **Vol. = 0%.**

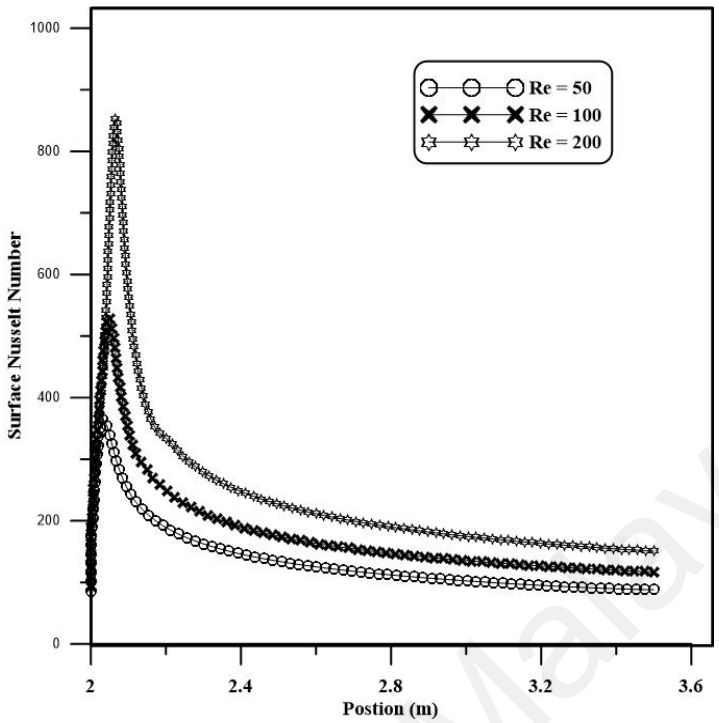

Figure 8.54: Effect of laminar Reynolds number on surface Nusselt number for **Vol. = 2%.**

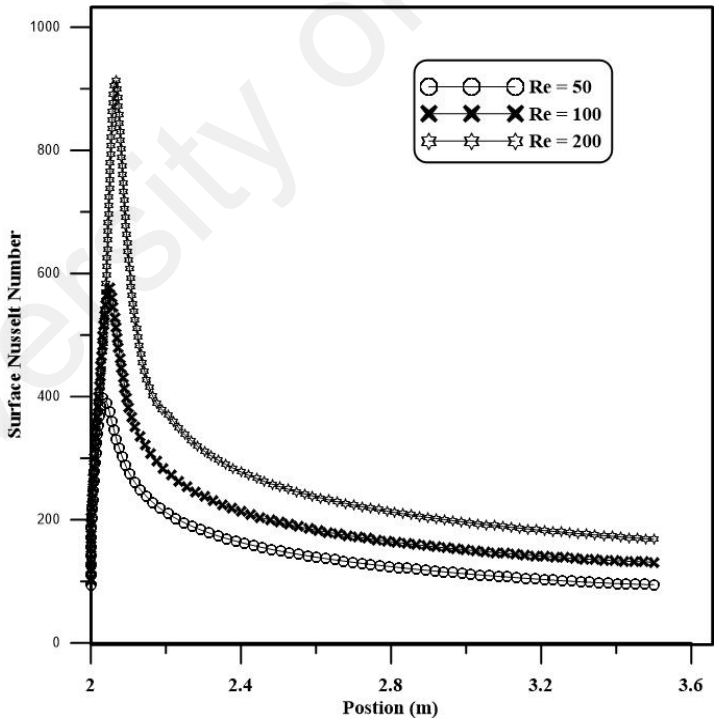

Figure 8.55: Effect of laminar Reynolds number on surface Nusselt number for **Vol. = 4%.**

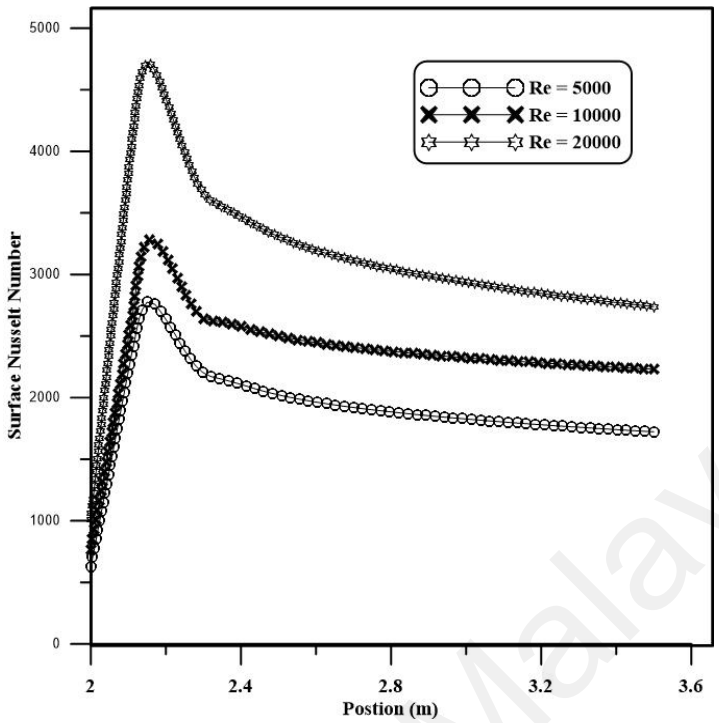

Figure 8.56: Effect of turbulent Reynolds number on surface Nusselt number for **Vol. = 0%.**

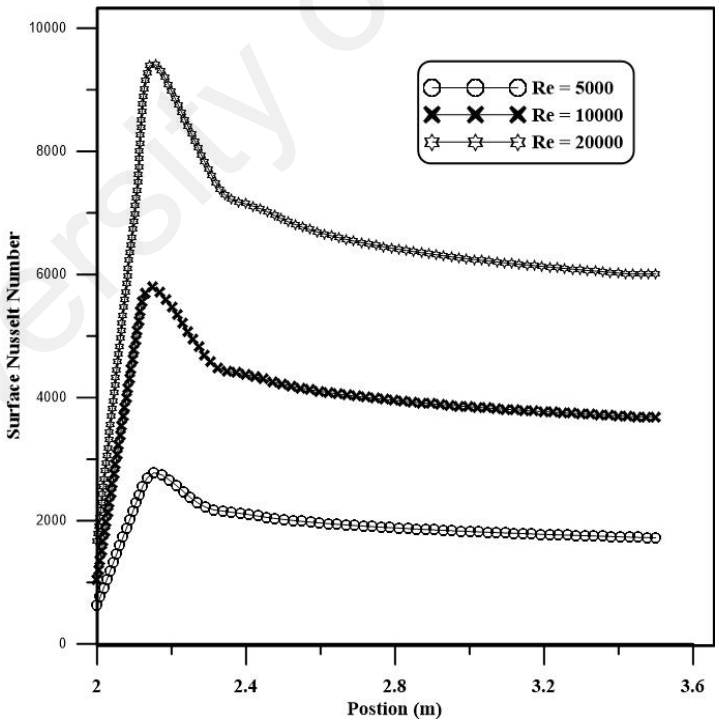

Figure 8.57: Effect of turbulent Reynolds number on surface Nusselt number for **Vol. = 2%**.

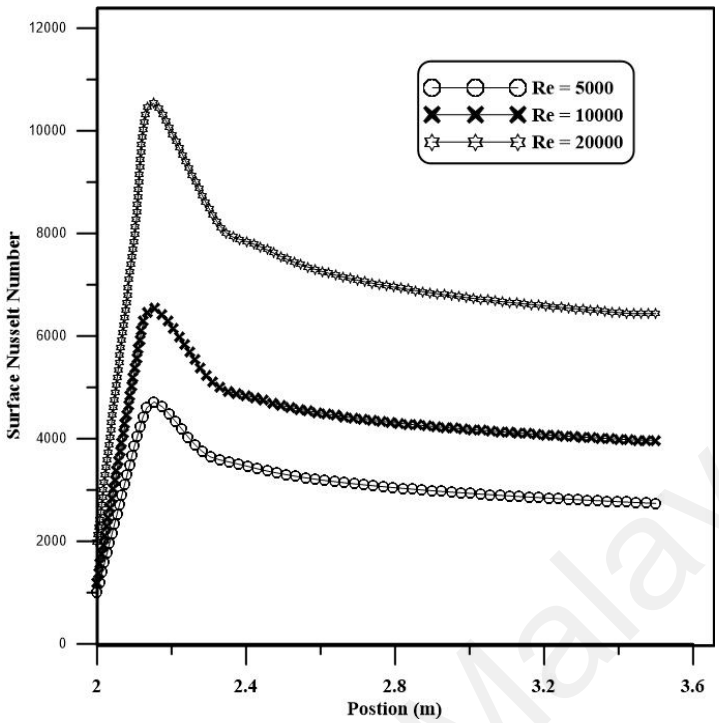

Figure 8.58 : Effect of turbulent Reynolds number on surface Nusselt number for **Vol. = 4%.**

C. *Average Nusselt number*

In Figures 8.59 and 8.60 the variation of average Nusselt number with the Reynolds number at different nanofluid volume fractions can be seen. For all cases, the average Nusselt number augmented as the Reynolds number and nanofluid volume fractions increased. The highest Nusselt number was obtained at 4% volume fraction and 20,000 Reynolds number. Generally, the maximum ratio of enhancement heat transfer to nanofluid was about 26% and 36% for turbulent and laminar range respectively compared with pure water due to increase of intensity convection of enhanced conductivity nanofluid.

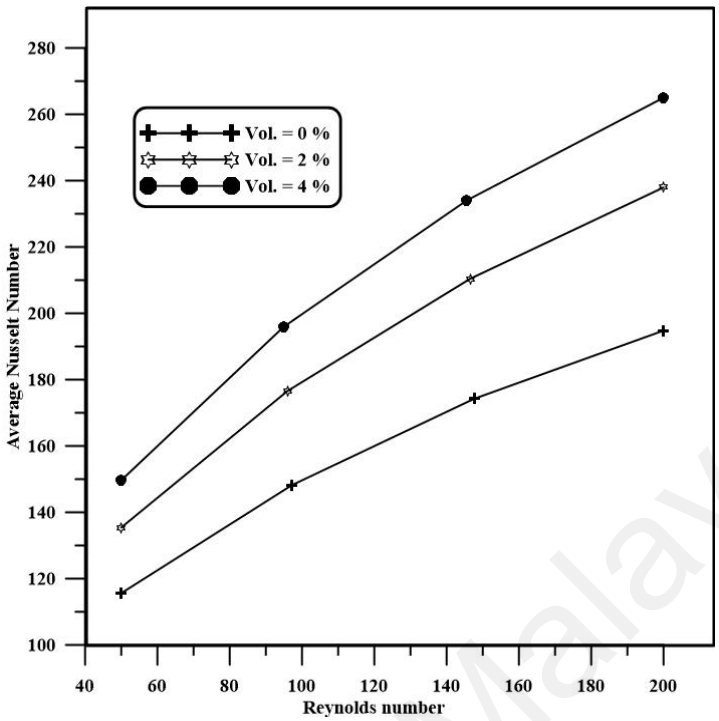

Figure 8.59: Average Nusselt number with different Reynolds number for laminar range.

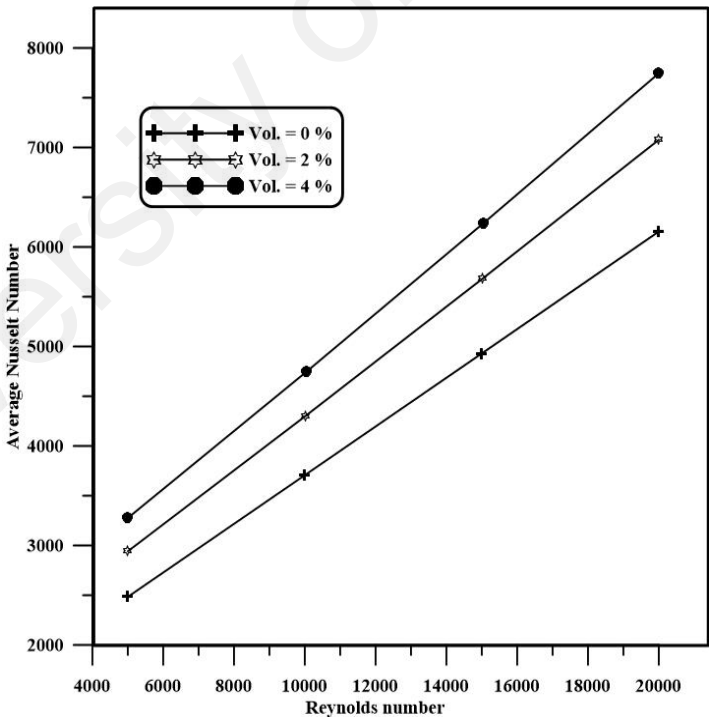

Figure 8.60: Average Nusselt number with different Reynolds number for turbulent range.

D. *Streamlines*

The streamlines at the beginning of expansion for the laminar and turbulent regimes at 4% volume fraction and Reynolds number ranging from 50 to 200 and 5000 to 20000, respectively, are presented in Figures 8.61-8.63 and 8.64-8.66. Obviously, the recirculation region expanded with the increase of Reynolds number for the laminar and turbulent ranges, while the largest recirculation region was obtained at Re=20000, which corresponds to the greatest heat transfer improvement. For more clarification, isothermal streamlines are presented in Figures 8.67-8.69 and 8.70-8.72 Reynolds number ranging from 50 to 200 and 5000 to 20000, respectively.

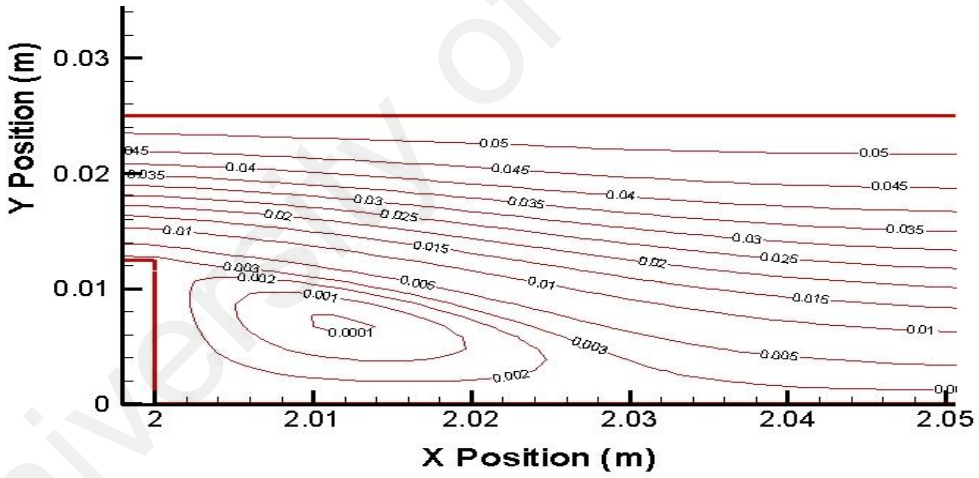

Figure 8.61: Streamline of velocity at expansion ratio 2 with volume fraction 4% and **Re=50.**

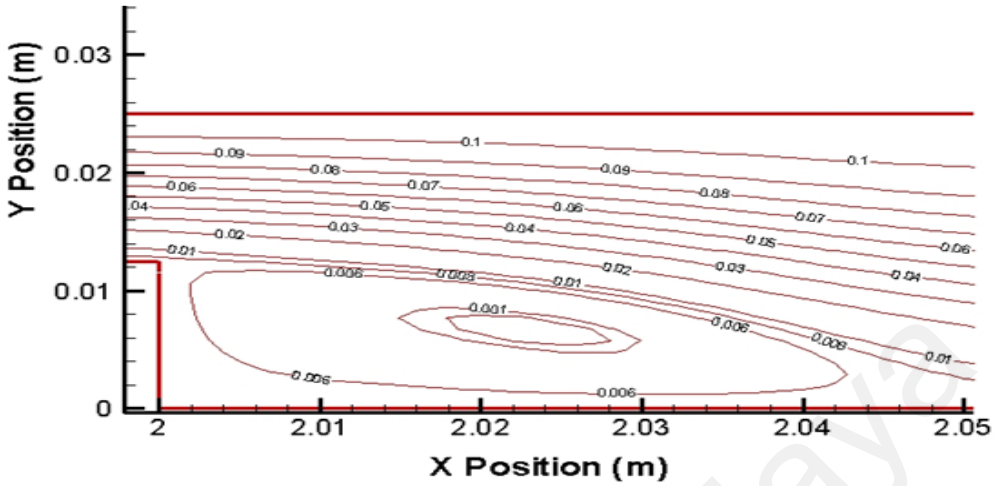

Figure 8.62: Streamline of velocity at expansion ratio 2 with volume fraction 4% and **Re=100.**

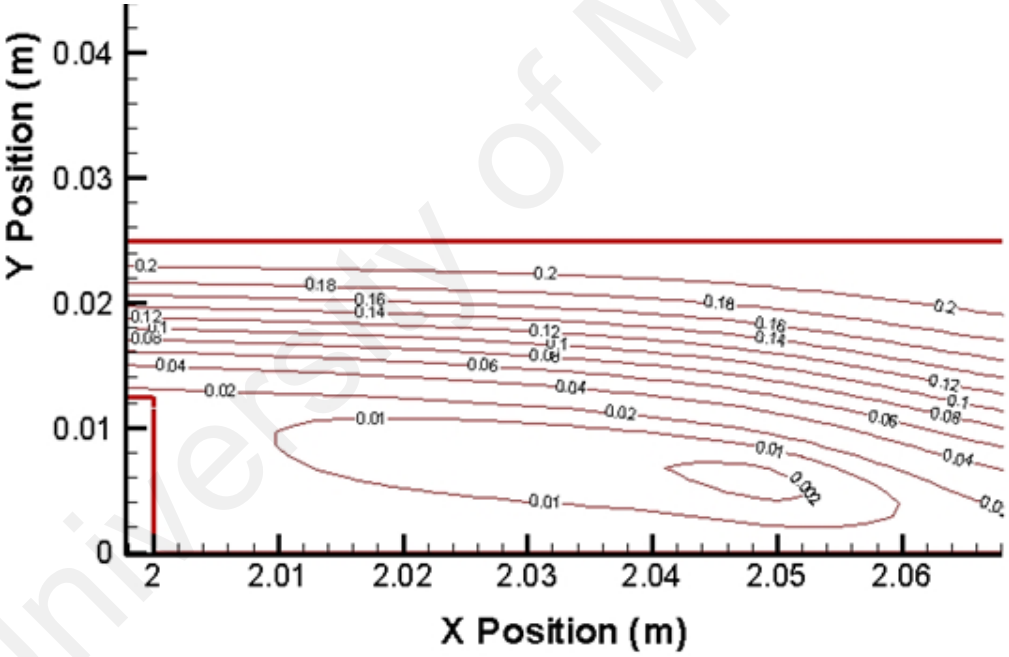

Figure 8.63: Streamline of velocity at expansion ratio 2 with volume fraction 4% and **Re=200.**

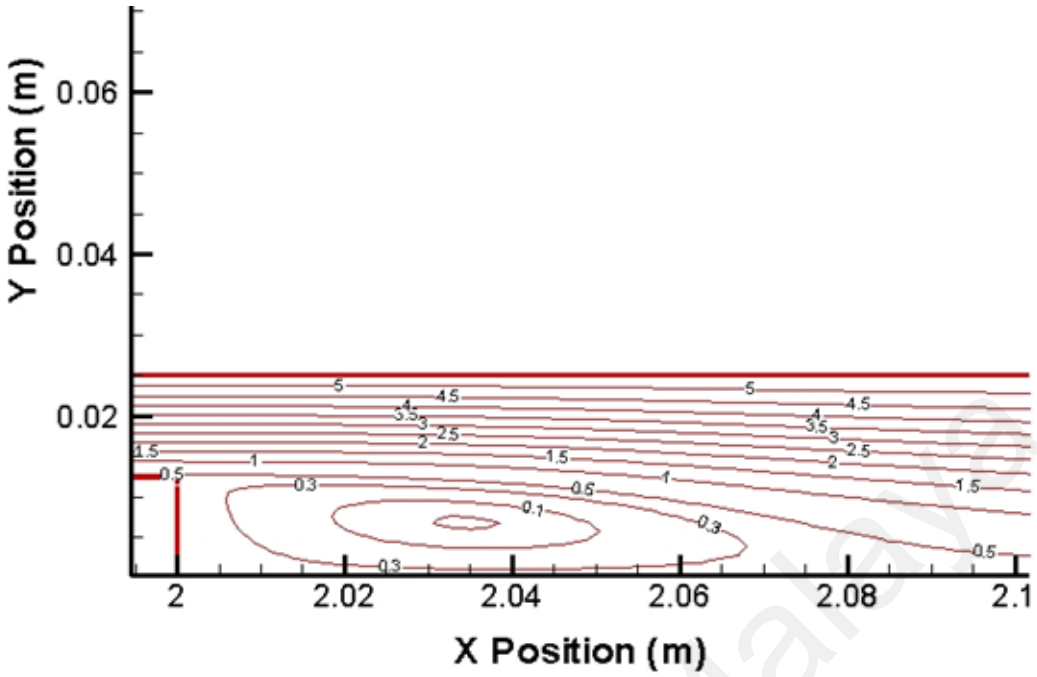

Figure 8.64: Streamline of velocity at expansion ratio 2 with volume fraction 4% and **Re = 5000.**

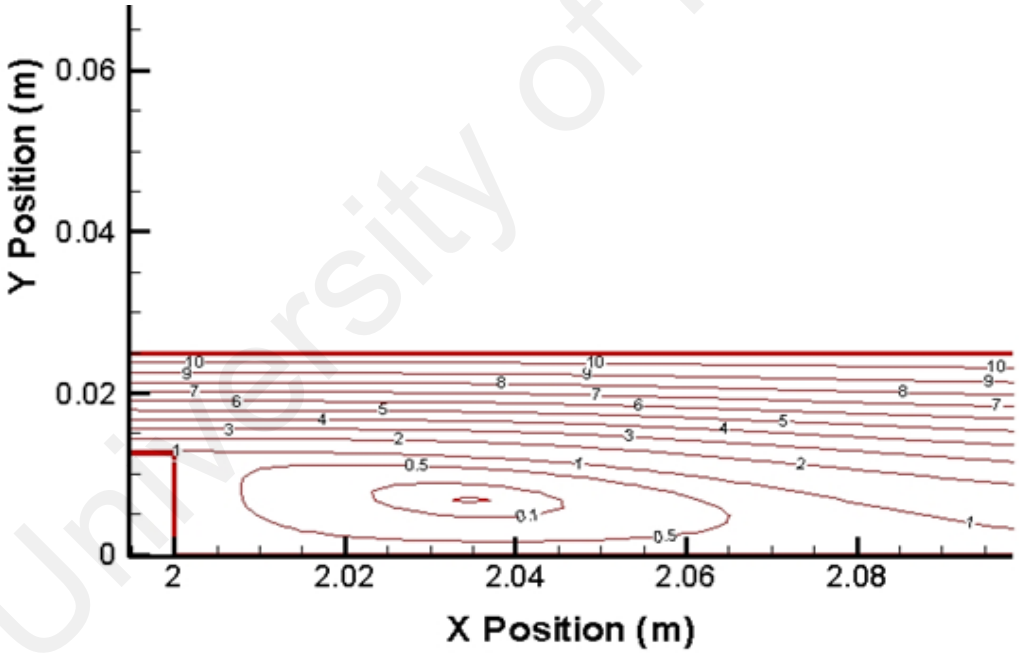

Figure 8.65: Streamline of velocity at expansion ratio 2 with volume fraction 4% and **Re = 10000.**

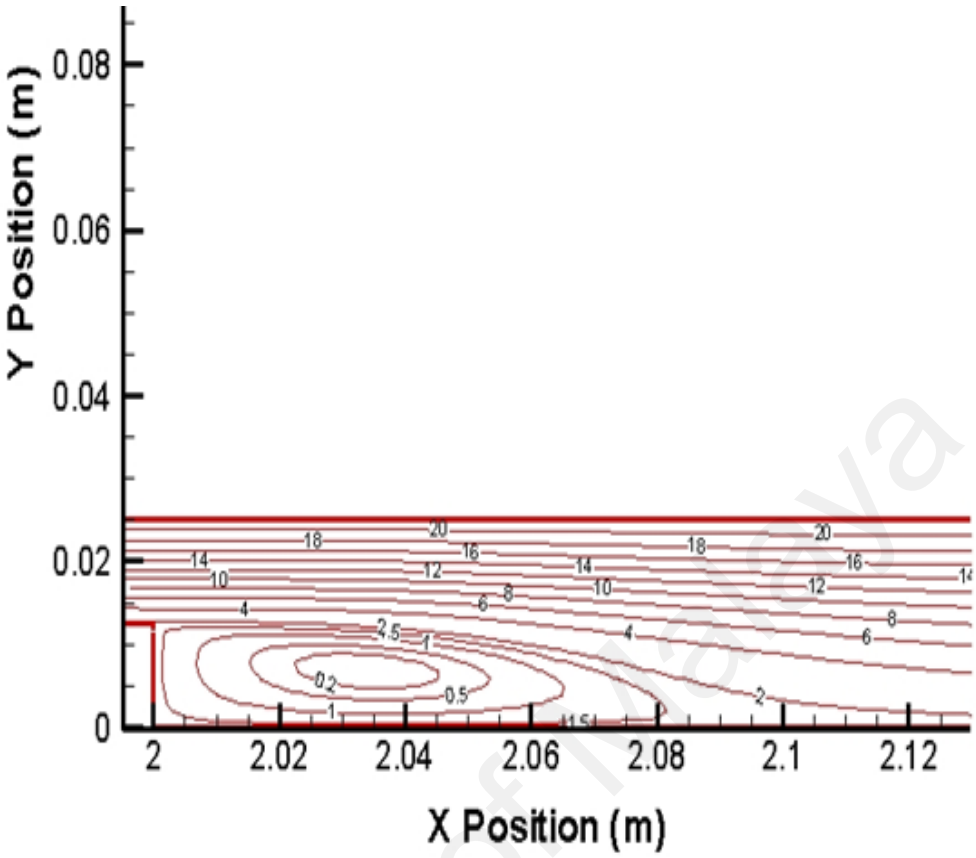

Figure 8.66: Streamline of velocity at expansion ratio 2 with volume fraction 4% and **Re = 20000.**

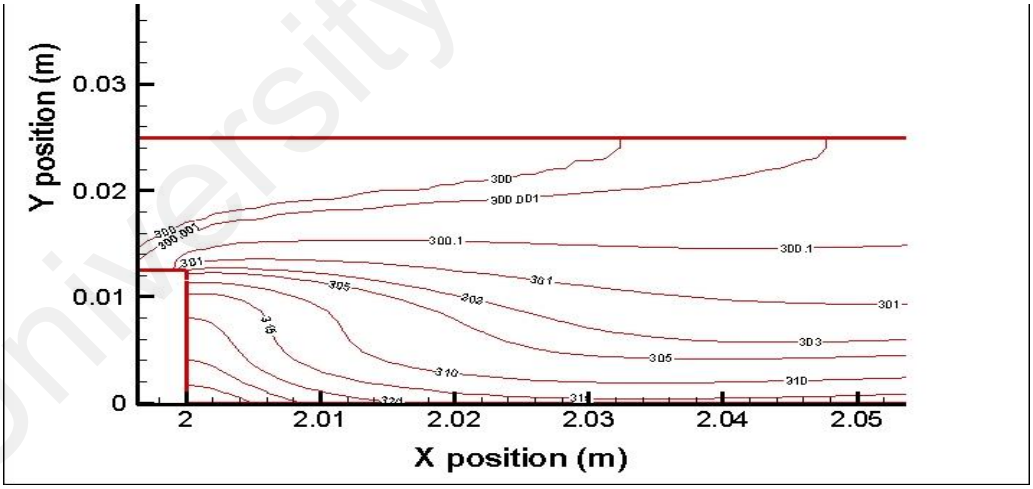

Figure 8.67: Isothermal Streamline at expansion ratio 2 with volume fraction 4% and **Re=50.**

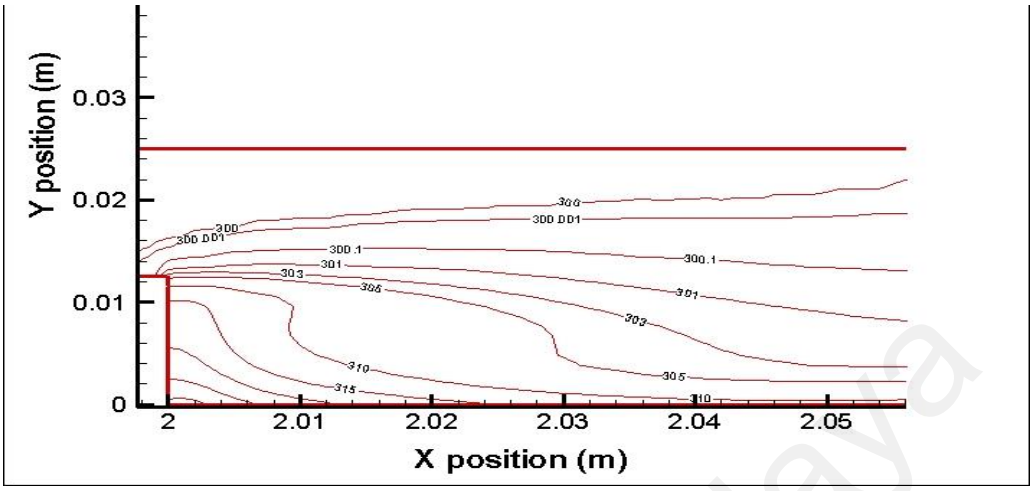

Figure 8.68: Isothermal Streamline at expansion ratio 2 with volume fraction 4% and **Re=100.**

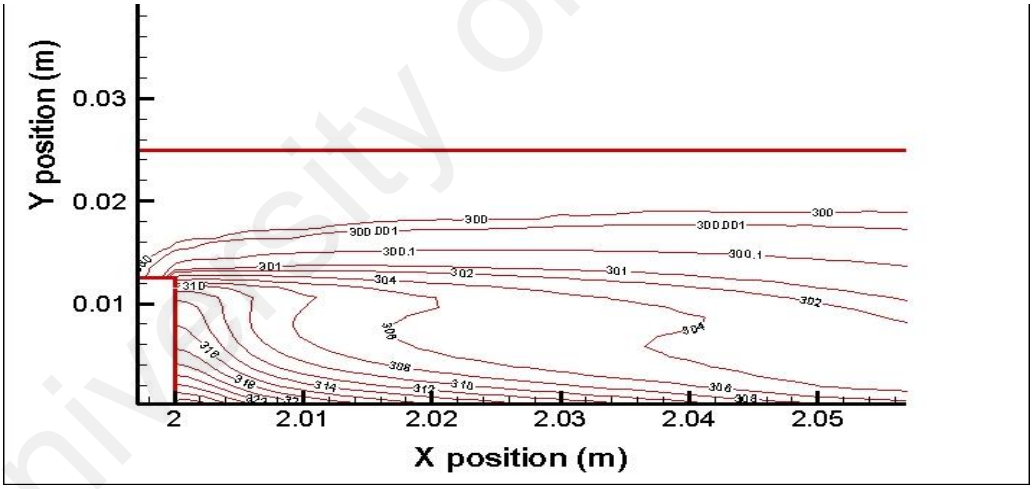

Figure 8.69 : Isothermal Streamline at expansion ratio 2 with volume fraction 4% and **Re=200.**

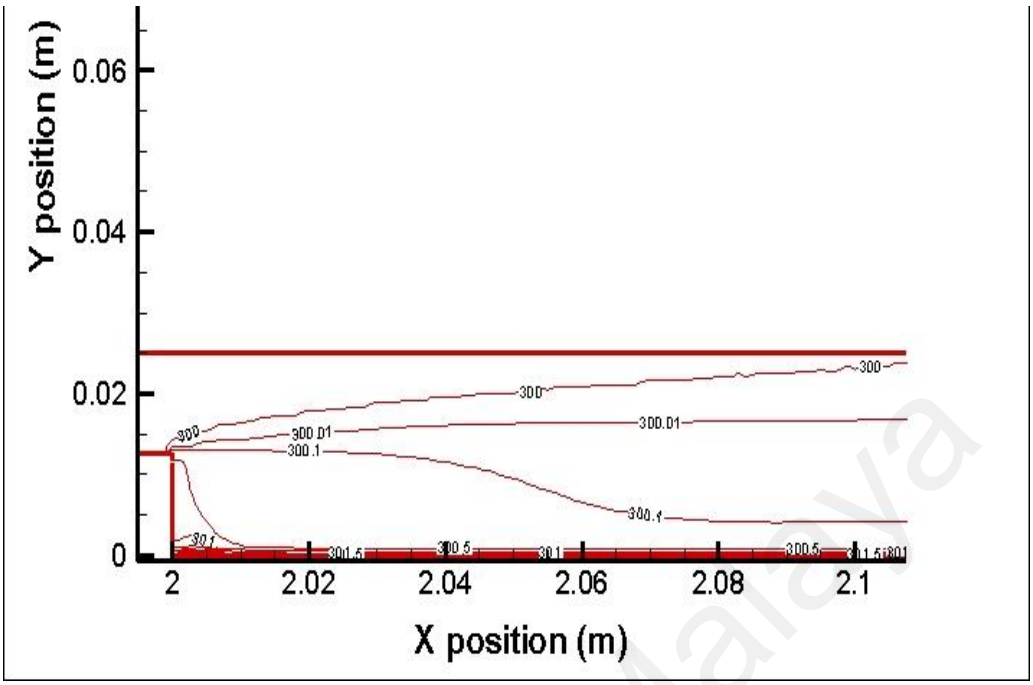

Figure 8.70: Isothermal Streamline at expansion ratio 2 with volume fraction 4% and **Re=5000.**

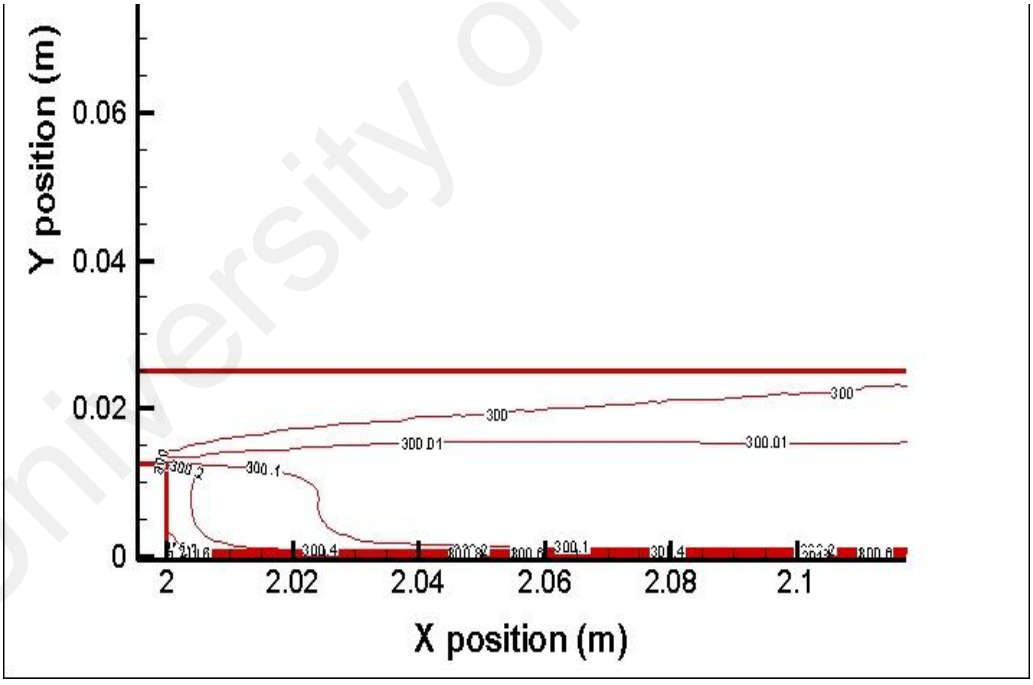

Figure 8.71: Isothermal Streamline at expansion ratio 2 with volume fraction 4% and **Re=10000.**

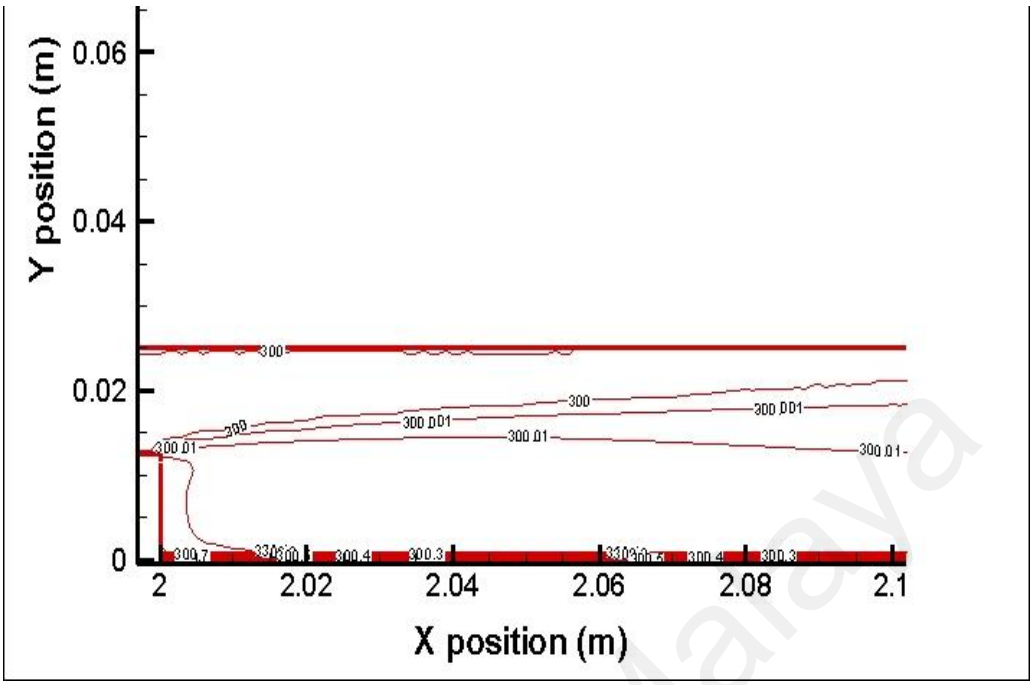

Figure 8.72: Isothermal Streamline at expansion ratio 2 with volume fraction 4% and **Re=20000.**

E. *Pressure drop*

The pressure drop variation with axial distance for different Reynolds numbers and nanofluid volume fractions is presented in Figure 8.73 and 8.74. According to the results, the pressure drop intensified as the Reynolds number increased and nanofluid volume fraction declined. Generally, the highest pressure drop occurred at the downstream inlet region due to recirculation flow which caused the improvement of heat transfer.

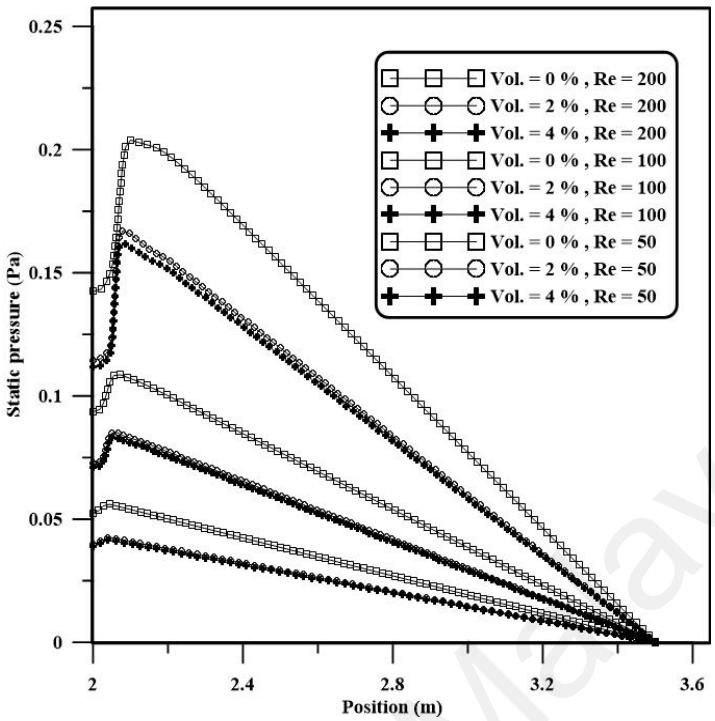

Figure 8.73: Pressure drop with different Reynolds number and volume fraction for laminar range.

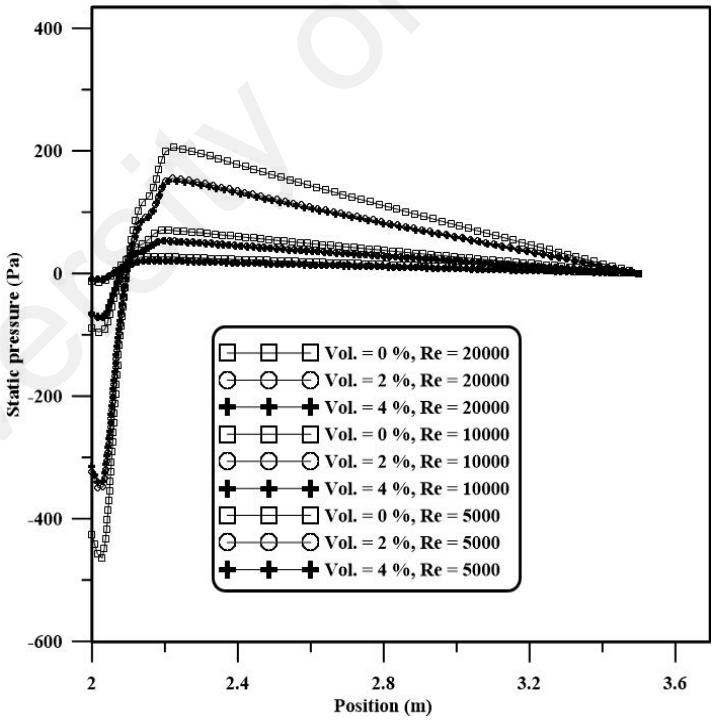

Figure 8.74: Pressure drop with different Reynolds number and volume fraction for turbulent range.

8.5 Conclusions (extended studies)

Turbulent forced convection and heat transfer over a double forward-facing step was studied. Three cases, corresponding to three different step heights, were investigated at four Reynolds numbers and four temperatures. The results show that increasing the Reynolds number and temperature increased the Nusselt number for all cases. The enhancement of the Nusselt number occurred at the first and second steps due to separation flow, and the highest augmentation was observed at the second step for case 3 relative to the values observed in case 1 and 2. The effect of step height on the recirculation zone increased the separation length at the same Reynolds number and temperature, which increases the Nusselt number. In addition, the obtained results indicate an increased in the pressure coefficient with increasing Reynolds number and step height.

The two-dimensional turbulent flow and heat transfer of nanofluids in passages with double forward-facing step were studied using a computational modeling approach. The simulation results were presented for three cases with different step heights and flow Reynolds numbers ranging from 30,000 to 100,000 for two types of nanofluid with solid volume fractions from 1% to 4%. Based on the presented results, it is concluded that the Nusselt number increases with flow Reynolds number and nanofluid solid volume fraction. Increasing the step height also amplifies the heat transfer rate due to the enhancement of recirculation flow regions. The peak local Nusselt number was observed at the second step, which is significantly larger than the first step. Among the cases studied, the largest thermal enhancement was obtained for first step height of 2cm for nanofluid with 4% volume fraction of Al_2O_3 and flow Reynolds number of 100,000, which are the highest solid volume fraction and flow Reynolds number studied.

The heat transfer of turbulent and laminar Cu/water nanofluid flow over a backward-facing step was numerically studied. A shear stress transport (SST) K-ω Model with boundary conditions, three nanofluid volume fractions and Reynolds numbers ranging from 50 to 200 for the laminar regime and 5000 to 20000 for the turbulent regime, at a constant heat flux of $4000W/m^2$ and an expansion ratio fixed at 2, was considered. Calculations show that the heat transfer augmented when the volume fraction and Reynolds number were increased. It was additionally observed that the recirculation flow as created by the backward-facing step enhanced heat transfer. The velocity streamline illustrated the recirculation and separation region. The maximum heat transfer increase was obtained at 4% volume fraction and Reynolds number of 20000, while the greatest pressure drop at the downstream inlet region indicated the heat transfer improvement.

List of Publications and Awards

Academic Journals

1- An experimental study of heat transfer to turbulent separation fluid flow in an annular passage, International Journal of Heat and Mass Transfer 54 (4), 766-773, **2011**.

2- A Review of Experimental Study of Turbulent Heat Transfer in Separated Flow Australian Journal of Basic and Applied Sciences 5 (10), 489-505, **2011**.

3- Numerical simulation of heat transfer to separation air flow in an annular pipe, International Communications in Heat and Mass Transfer 39 (8), 1176–1180, **2012**.

4- CFD Simulation of Heat Transfer and Turbulent Fluid Flow Over a Double Forward-Facing Step, Mathematical Problems in Engineering, vol. 2013 page 1-10 , **2013**.

5- Computational simulation of heat transfer to separation fluid flow in an annular passage, International Communications in Heat and Mass Transfer 1, 92–96, **2013**.

6- A 3D numerical study of heat transfer in a single-phase micro-channel heat sink using graphene, aluminum and silicon as substrates, International Communications in Heat and Mass Transfer, Vol.48 pp. 108-115, **2013**.

7- Numerical Study of Turbulent Heat Transfer in Separated Flow: Review, International Review of Mechanical Engineering (IREME) 7 (2), 337-349, **2013**.

8- Heat Transfer to Laminar Flow over a Double Backward-Facing Step, World Academy of Science Engineering and Technology 80, 1001-1006, **2013**.

9- A CFD study of turbulent heat transfer and fluid flow through the channel with semicircle rib IEEE, 291-295, **2013**.

10- Enhancements of Heat Transfer Nanofluid Flow In Circular Pipe with Twisted Tape Inserts: Review Australian Journal of Basic and Applied Sciences, 7 (9), 97-102 **2013**.

11- Numerical Simulation on Heat Transfer Enhancement in Channel by Triangular Ribs World Academy of Science, Engineering and Technology 80, 430-434 **2013**.

12- Sustainability and environmental impact of ethanol as a biofuel, Reviews in Chemical Engineering, DE GRUYTER, page 1-22, **2013**.

13- Numerical simulation of laminar to turbulent nanofluid flow and heat transfer over a backward-facing step, Applied Mathematics and Computation 239, 153–170, **2014**.

14- - Investigation of Heat Transfer Enhancement In A Forward-Facing Contracting Channel Using Fmwcnt Nanofluids Numerical Heat Transfer, Part A, Vol. 66, Issue 12, pp.1321–1340, **2014**.

15- Numerical study of turbulent heat transfer in annular pipe with sudden contraction Applied mechanics and materials, Vol.(465-466), PP 461-466, **2014**.

16- Heat Transfer and Turbulent Fluid Flow over Vertical Double Forward-Facing Step International Journal of Mechanical, Industrial Science and Engineering Vol:8 No:2, page 2016-220, **2014**.

17- Preparation, characterization, viscosity, and thermal conductivity of nitrogen-doped graphene aqueous nanofluids, Journal of Materials Science, pp.1-16, **2014**

18- A theoretical model to predict gas permeability for slip flow through a porous medium, Applied Thermal Engineering, Vol. 70, issue , pp. 271-76, **2014**.

19- Numerical Study of Heat Transfer and Laminar Flow over a Backward Facing Step with and without Obstacle, International Journal of Mechanical, Industrial Science and Engineering, Vol. 8, issu2 , pp. 377-381, **2014.**

20- An experimental study on thermal conductivity and viscosity of nanofluids containing carbon nanotubes, Nanoscale research letters, Vol. 9 page 151, **2014**.

21- A Review of studies on forced, natural and mixed heat transfer to fluid flow in an annular passage, Renewable and Sustainable Energy Reviews, Vol. 39, Pages 835-856, **2014**.

22- 23- Augmented of Turbulent Heat Transfer in an Annular Pipe with Abrupt Expansion, Thermal Science, OnLine-First Issue 00, Pages: 138-138, doi:10.2298/TSCI140816138T **2014**.

23- 22- Thermal performance of nanofluid in ducts with double forward-facing steps. Journal of the Taiwan Institute of Chemical Engineers, DOI 10.1016/j.jtice.2014.10.009, **2014.**

24- An experimental and numerical investigation of heat transfer enhancement for graphene nanoplatelets nanofluids in turbulent flow conditions, International Journal of Heat and Mass Transfer Vol. 81, 41–51, **2015**.

25- Turbulent Three-Dimensional Numerical Study of Heat Transfer and Separation Al_2O_3/Nanofluid Flow through Coaxial Annular Pipe Journal of the Taiwan Institute of Chemical Engineers, **Submitted.**

26- Enhancement of heat transfer and nanofluid flow through an annular channel with abrupt contraction. International Communications in Heat and Mass Transfer, **Submitted.**

27- Influence of laminar separation flow and nanofluids on heat transfer enhancement with different configurations: A Review, Renewable and Sustainable Energy Reviews, **Submitted.**

Book

1-Chapter of Book An Overview of Heat Transfer Phenomena "Heat Transfer to Separation Flow in Heat Exchangers", InTech 2012.

2- Chapter of Book of Heat Transfer "Heat transfer and nanofluid flow through different geometries" InTech 2014 (**Accept**).

Proceedings

1- An experimental study of turbulent heat transfer separation external in an annular passage, Universiti Malaysia Perlis (UniMAP) 2009, Malaysia.

2- Effects of fiber orientations and fiber types of composite laminated plates, Universiti Malaysia Perlis (UniMAP) 2009, Malaysia.

3- A computational simulation of heat transfer to separation air flow in a concentric pipe, Universiti Malaysia Perlis (UniMAP) 2012, Malaysia.

4- A CFD study of turbulent heat transfer and fluid flow through the channel with semicircle rib, Clean Energy and Technology (CEAT), 2013 IEEE, Malaysia.

5- Numerical Simulation on Heat Transfer Enhancement in Channel by Triangular Ribs WASET 2013 Italy.

6- 6-Heat Transfer to Laminar Flow over a Double Backward-Facing Step, WASET 2013 Italy.

7- Guidelines for Implementing Total Quality Management in Higher Education. Organization, First Management and Engineering Congress (MECON) /Singapore 2013.

8- Heat transfer enhancement of laminar fluid flow in separated region using nanofluid: A Review, 2nd International Conference on Mechanical, Automotive and Aerospace Engineering (ICMAAE 2013). Malaysia.

9- Numerical study of nanofluid heat transfer performance in closed conduit turbulent flow, 2nd International Conference on Mechanical, Automotive and Aerospace Engineering (ICMAAE 2013). Malaysia.

10- Heat Transfer and Turbulent Fluid Flow over Vertical Double Forward-Facing Step, International Conference on Mathematics and Computational Mechanics 2014 BARCELONA, ESPANA.

11- Numerical Study of Heat Transfer and Laminar Flow over a Backward Facing Step with and without Obstacle, International Conference on Mathematics and Computational Mechanics 2014 BARCELONA, ESPANA.

Patent

1. ENHANCEMENT OF HEAT TRANSFER TO WATER FLOW OVER DOUBLE FORWARD FACING STEP, **Submitted.**

2. ASSESSING THERMAL PERFORMANCE OF NANOFLUID IN DUCTS WITH DOUBLE FORWARD-FACING STEPS, **Submitted.**

3. IMPROVEMENT OF HEAT TRANSFER AND NANOFLUID FLOW THROUGH AN ANNULAR CHANNEL WITH ABRUPT CONTRACTION, Submitted

4. AUGMENTATION OF SEPARATION NANOFLUID FLOW THROUGH COAXIAL ANNULAR PIPE, **Submitted.**

Awards & certificates or letters of appreciation:

1-Medal and Certificate of Appreciation for Publishing Research in High Impact Factor International Journal/ Scientists and Innovators Department / Research &Development Office/ Ministry of Higher Educational & Scientific Research/Iraq/2011.

2- Top 25 hottest articles in the International Communications in Heat and Mass Transfer for the paper "Numerical simulation of heat transfer to separation air flow in an annular pipe" Volume 39, Issue 8, October 2012, Pages 1176–1180.

3- Top 25 hottest articles in Applied Mathematics and Computation "Numerical simulation of laminar to turbulent nanofluid flow and heat transfer over a backward-facing step" Applied Mathematics and Computation Volume 239, 15 July 2014, Pages 153–170

References

A. Boughamoura, S. B. N. (2004). Piston-driven turbulent flow and heat transfer in a pipe with a sudden expansion. International Journal of Heat and Technology 22(2), 31-40.

A. Li, & Armaly, B. F. (2000). Mixed convection adjacent to 3D backward facing step. Proceedings of the ASMEIMECE conference, ASME HTD366-2, New York 51-58.

A. M. Gooray, C. B. W. a. W. A. (1985). Turbulent heat transfer computations for rearward-facing steps and sudden pipe expansions. J. Heat Transfe, 107, 70-76.

A.C., R. Forced convection heat transfer in passages with varying roughness and heat flux around the perimeter. TRG Report 1963; 519.

A.L., M. Liquid turbulence in a gas-liquid absorption system. Ph.D. Thesis, Carnegie Institute of Technology, Pittsburgh, PA, 1951.

Abbott, D. E. K., S. J. . (1962). Experimental investigations of subsonic turbulent flow over single and double backward-facing steps. Trans. ASME D: journal fluids engineering, 84(3), 317-325.

Abdeleghani, Z. Computational study of simultaneous heat and mass transfer in turbulent separated flow. PhD Engineering thesis Stevens Institute of Technology, USA1993.

Abe, K., Kondoh, T., & Nagano, Y. (1994). A new turbulence model for predicting fluid flow and heat transfer in separating and reattaching flows—I. Flow field calculations. International Journal of Heat and Mass Transfer, 37(1), 139-151. doi: http://dx.doi.org/10.1016/0017-9310(94)90168-6

Abe, K., Kondoh, T., & Nagano, Y. (1995). A new turbulence model for predicting fluid flow and heat transfer in separating and reattaching flows—II. Thermal field calculations. International Journal of Heat and Mass Transfer, 38(8), 1467-1481. doi: http://dx.doi.org/10.1016/0017-9310(94)00252-Q

Abu-Mulaweh, H. I. (2002). Effects of backward- and forward-facing steps on turbulent natural convection flow along a vertical flat plate. International Journal of Thermal Sciences, 41(4), 376-385. doi: http://dx.doi.org/10.1016/S1290-0729(02)01328-5

Abu-Mulaweh, H. I. (2003). A review of research on laminar mixed convection flow over backward- and forward-facing steps. International Journal of Thermal Sciences, 42(9), 897-909. doi: http://dx.doi.org/10.1016/S1290-0729(03)00062-0

Abu-Mulaweh, H. I. (2005). Turbulent mixed convection flow over a forward-facing step—the effect of step heights. International Journal of Thermal Sciences, 44(2), 155-162. doi: http://dx.doi.org/10.1016/j.ijthermalsci.2004.08.001

Abu-Mulaweh, H. I. (2009). Investigations on the Effect of Backward-Facing and Forward-Facing Steps on Turbulent Mixed-Convection Flow Over a Flat Plate. Experimental Heat Transfer, 22(2), 117-127. doi: 10.1080/08916150902805927

Abu-Mulaweh, H. I., Armaly, B. F., & Chen, T. S. (1996). Laminar natural convection flow over a vertical forward-facing step. Journal of Thermophysics and Heat Transfer, 10(3), 517-523. doi: 10.2514/3.819

Abu-Mulaweh, H. I., Chen, T. S., & Armaly, B. F. (2002). Turbulent mixed convection flow over a backward-facing step—the effect of the step heights. International Journal of Heat and Fluid Flow, 23(6), 758-765. doi: http://dx.doi.org/10.1016/S0142-727X(02)00191-1

Abu-Nada, E. (2008). Application of nanofluids for heat transfer enhancement of separated flows encountered in a backward facing step. International Journal of Heat and Fluid Flow, 29(1), 242-249. doi: http://dx.doi.org/10.1016/j.ijheatfluidflow.2007.07.001

Abu-Nada, E. (2009). Effects of variable viscosity and thermal conductivity of Al2O3–water nanofluid on heat transfer enhancement in natural convection. International Journal of Heat and Fluid Flow, 30(4), 679-690. doi: http://dx.doi.org/10.1016/j.ijheatfluidflow.2009.02.003
Addad, Y., Laurence, D., Talotte, C., & Jacob, M. C. (2003). Large eddy simulation of a forward–backward facing step for acoustic source identification. International Journal of Heat and Fluid Flow, 24(4), 562-571. doi: http://dx.doi.org/10.1016/S0142-727X(03)00050-X
Afshin Goharzadeh, P. R. (2009). Experimental measurement of laminar axisymmetric flow through confined annular geometries with sudden inward expansion. Journal of Fluids Engineering, 131, 124501 (124504 pages).
Agelinchaab, M., & Tachie, M. F. (2008). PIV Study of Separated and Reattached Open Channel Flow Over Surface Mounted Blocks. Journal of Fluids Engineering, 130(6), 061206-061206. doi: 10.1115/1.2911677
Ahmet Eraslan N., T. O. A. (2003). Assessment of flow and heat transfer characteristics for proposed solid density distribution in dilute laminar slurry upflow through a concentric annulus. Chemical Engineering Science, 58, 4055-4069.
Ahn, S. W., & Kim, K. C. (1998). Fully developed fluid flow and heat transfer in rough annuli. International Communications in Heat and Mass Transfer, 25(4), 501-510. doi: http://dx.doi.org/10.1016/S0735-1933(98)00037-2
Al-Arabi, M., El-Shaarawi, M. A. I., & Khamis, M. (1987). Natural convection in uniformly heated vertical annuli. International Journal of Heat and Mass Transfer, 30(7), 1381-1389. doi: http://dx.doi.org/10.1016/0017-9310(87)90170-0
Al-aswadi, A. A., Mohammed, H. A., Shuaib, N. H., & Campo, A. (2010). Laminar forced convection flow over a backward facing step using nanofluids. International Communications in Heat and Mass Transfer, 37(8), 950-957. doi: http://dx.doi.org/10.1016/j.icheatmasstransfer.2010.06.007
Albadr, J., Tayal, S., & Alasadi, M. (2013). Heat transfer through heat exchanger using Al2O3 nanofluid at different concentrations. Case Studies in Thermal Engineering, 1(1), 38-44. doi: http://dx.doi.org/10.1016/j.csite.2013.08.004
Alemasov, V. E., Glebov, G.A., Kozlov, A.P., . (1989). Thermo-anemometric methods for studying flows with separation. Kazan'Branch of the USSR Academy of Sciences, Kazan, 178s.
Ali, A., Vafai, K., & Khaled, A. R. A. (2003). Comparative study between parallel and counter flow configurations between air and falling film desiccant in the presence of nanoparticle suspensions. International Journal of Energy Research, 27(8), 725-745. doi: 10.1002/er.908
Alizad, K., Vafai, K., & Shafahi, M. (2012). Thermal performance and operational attributes of the startup characteristics of flat-shaped heat pipes using nanofluids. International Journal of Heat and Mass Transfer, 55(1–3), 140-155. doi: http://dx.doi.org/10.1016/j.ijheatmasstransfer.2011.08.050
Amin Kashani, D. J.-V., Siamak Hossainpour. (2013). Numerical Study of Laminar Forced Convection of Water/Al2o3 Nanofluid in an Annulus with Constant Wall Temperature. IIUM Engineering Journal, 14(1), 76-91.
Aminossadati, S. M. (2013). Hydromagnetic natural cooling of a triangular heat source in a triangular cavity with water–CuO nanofluid. International Communications in Heat and

Mass Transfer, 43(0), 22-29. doi: http://dx.doi.org/10.1016/j.icheatmasstransfer.2013.02.009
Amirhossein Heshmati, H. A. M., Mohammad Parsazadeh, Farshid Fathinia, Mazlan A. Wahid, Mohsin M. Sies, Aminuddin Saat. (2013). Effect of Vertical Baffle Installation on Forced Convective Heat Transfer in Channel Having a Backward Facing Step. Applied Mechanics and Materials, 388, 169-175.
Amrollahi, A., Rashidi, A. M., Lotfi, R., Emami Meibodi, M., & Kashefi, K. (2010). Convection heat transfer of functionalized MWNT in aqueous fluids in laminar and turbulent flow at the entrance region. International Communications in Heat and Mass Transfer, 37(6), 717-723. doi: http://dx.doi.org/10.1016/j.icheatmasstransfer.2010.03.003
Armaly, B. F., Durst, F., Pereira, J. C. F., & Schönung, B. (1983). Experimental and theoretical investigation of backward-facing step flow. Journal of Fluid Mechanics, 127, 473-496. doi: doi:10.1017/S0022112083002839
Armaly, B. F., Li, A., & Nie, J. H. (2003). Measurements in three-dimensional laminar separated flow. International Journal of Heat and Mass Transfer, 46(19), 3573-3582. doi: http://dx.doi.org/10.1016/S0017-9310(03)00153-4
Aung, W. (1983). An experimental study of laminar heat transfer downstream of backstep. J. Heat Transfer, 105, 823–829.
Avancha, R. V. R., & Pletcher, R. H. (2002). Large eddy simulation of the turbulent flow past a backward-facing step with heat transfer and property variations. International Journal of Heat and Fluid Flow, 23(5), 601-614. doi: http://dx.doi.org/10.1016/S0142-727X(02)00156-X
Avcı, M., & Aydın, O. (2008). Laminar forced convection slip-flow in a micro-annulus between two concentric cylinders. International Journal of Heat and Mass Transfer, 51(13–14), 3460-3467. doi: http://dx.doi.org/10.1016/j.ijheatmasstransfer.2007.10.036
Aya Kitoh, K. S., Hiroyuki Yoshikawa. (2007). Expansion ratio effects on three-dimensional separated flow and heat transfer around backward-facing-steps. J. Heat Transfer, 129(9), 1141-1156.
B.-X. Wang, H. L., X.F. Peng. (2000). Research on the heat-conduction enhancement for liquid with nano-particle suspensions. General Paper (G-1), International Symposium on Thermal Science and Engineering (TSE2002), Beijing.
B.E. Launder, B. I. S. (1974). Application of the energy-dissipation model of turbulence to the calculation of flow near a spinning disc. Lett. Heat Mass Transfer, 1, 131-138.
Barbosa-Saldaña, J. G., & Anand, N. K. (2007). Flow Over a Three-Dimensional Horizontal Forward-Facing Step. Numerical Heat Transfer, Part A: Applications, 53(1), 1-17. doi: 10.1080/10407780701446473
Barton, I. E. (1997). Laminar flow over a backward-facing step with a stream of hot particles. International Journal of Heat and Fluid Flow, 18(4), 400-410. doi: http://dx.doi.org/10.1016/S0142-727X(97)00019-2
Baughn, J. W., Hoffman, M. A., Takahashi, R. K., & Launder, B. E. (1984). Local Heat Transfer Downstream of an Abrupt Expansion in a Circular Channel With Constant Wall Heat Flux. Journal of Heat Transfer, 106(4), 789-796. doi: 10.1115/1.3246753
Baughn, J. W., M.A. Hoffman, B.E. Launder, D. Lee and C. Yap. (1989). Heat transfer, temperature, and velocity measurements downstream of an abrupt expansion in a circular tube at a uniform wall temperature. J Heat Transfer, 111, 870-876.
Baughn, J. W., M.A. Hoffman, D. Lee and C. Yap. (1987a-a). Turbulent velocity and temperature profiles downstream of an abrupt expansion in a circular duct with a constant

wall temperature. In the Proceedings of the 1986a ASME-JSME Thermal Eng Conference, 449-454.
Baughn, J. W., M.A. Hoffman, D. Lee and C. Yap. (1987a-b). Turbulent velocity and temperature profiles downstream of an abrupt expansion in a circular duct with a constant wall temperature. In the Proceedings of the ASME-JSME Thermal Eng Conference, 1986a, 449-454.
Baughn, J. W., M.A. Hoffman, R.K. Takahashi and B.E. Launder. (1984). Local heat transfer downstream of an abrupt expansion in a circular channel with constant wall heat flux. J Heat Transfer, 106, 789-796.
Beck, M., Yuan, Y., Warrier, P., & Teja, A. (2010). The thermal conductivity of alumina nanofluids in water, ethylene glycol, and ethylene glycol + water mixtures. Journal of Nanoparticle Research, 12(4), 1469-1477. doi: 10.1007/s11051-009-9716-9
Boelter, L. M. K., G. Young and H.W. Iversen. (1948). An investigation of Aircraft Heaters XXVII -Distribution of heat transfer rate in the entrance section of a circular tub. NACA, TN-1451.
Boelter, L. M. K. Y., G; Iversen, H W (1948). An investigation of aircraft heaters XXVII : distribution of heat-transfer rate in the entrance section of a circular tube. NACA-TN-1451.
Boughamoura, A., Belmabrouk, H., & Ben Nasrallah, S. (2003). Numerical study of a piston-driven laminar flow and heat transfer in a pipe with a sudden expansion. International Journal of Thermal Sciences, 42(6), 591-604. doi: http://dx.doi.org/10.1016/S1290-0729(03)00025-5
Bozorgan, N., Mafi, M., & Bozorgan, N. (2012). Performance Evaluation of /Water Nanofluid as Coolant in a Double-Tube Heat Exchanger Flowing under a Turbulent Flow Regime. Advances in Mechanical Engineering, 2012, 8. doi: 10.1155/2012/891382
Brinkman, H. C. (1952). The Viscosity of Concentrated Suspensions and Solutions. The Journal of Chemical Physics, 20(4), 571-571. doi: doi:http://dx.doi.org/10.1063/1.1700493
C. Berner, F. D., D.M. McEligot, . (1984). Flow around baffles. ASME Journal of Heat Transfer, 106, 743-749.
C. S., O., Hussein, T., Kazi, S. N., Badarudin, A., Zubir, M. N. M., & Sadeghinezhad, E. (2012). Numerical simulation of heat transfer to separation air flow in an annular pipe. International Communications in Heat and Mass Transfer, 39(8), 1176-1180. doi: http://dx.doi.org/10.1016/j.icheatmasstransfer.2012.06.019
C. S. Oon, Hussein Togun, S. N. Kazi, A. Badarudin, M. N. M. Zubir, & E. Sadeghinezhad. (2012). Numerical simulation of heat transfer to separation air flow in an annular pipe. International Communications in Heat and Mass Transfer, 39(8), 1176-1180. doi: http://dx.doi.org/10.1016/j.icheatmasstransfer.2012.06.019
C. S. Oon, Hussein Togun, S. N. Kazi, A. Badarudin, M. N. M. Zubir, & E. Sadeghinezhad. (2013). Computational simulation of heat transfer to separation fluid flow in an annular passage. International Communications in Heat and Mass Transfer, 46(0), 92-96. doi: http://dx.doi.org/10.1016/j.icheatmasstransfer.2013.05.005
C.K.G. Lam, K. A. B. (1981a). Modified form of the k-ϵ model for predicting wall turbulence. ASME J. Fluids Engng., 103, 456-460.
C.K.G. Lam, K. A. B. (1981b). Modified form of the k-ϵ model for predicting wall turbulence. ASME J. Fluids Engng., 103, 456-460.
Camussi, R., Felli, M., Pereira, F., Aloisio, G., & Di Marco, A. (2008). Statistical properties of wall pressure fluctuations over a forward-facing step. Physics of Fluids (1994-present), 20(7), -. doi: doi:http://dx.doi.org/10.1063/1.2959172

Chandrasekar, M., Suresh, S., & Chandra Bose, A. (2010). Experimental investigations and theoretical determination of thermal conductivity and viscosity of Al2O3/water nanofluid. Experimental Thermal and Fluid Science, 34(2), 210-216. doi: http://dx.doi.org/10.1016/j.expthermflusci.2009.10.022
Chang, P. K. (1976). Control of flow separation. McGraw-Hill, New York.
Chen, J. C., & Yu, W. S. (1970). Entrance region and variable heat flux effects in turbulent heat transfer to liquid metals flowing in concentric annuli. International Journal of Heat and Mass Transfer, 13(4), 667-680. doi: http://dx.doi.org/10.1016/0017-9310(70)90041-4
Chen, Y. T., Nie, J. H., Armaly, B. F., & Hsieh, H. T. (2006). Turbulent separated convection flow adjacent to backward-facing step—effects of step height. International Journal of Heat and Mass Transfer, 49(19–20), 3670-3680. doi: http://dx.doi.org/10.1016/j.ijheatmasstransfer.2006.02.024
Chiang, T. P., Sheu, T. W. H., & Wang, S. K. (2000). Side wall effects on the structure of laminar flow over a plane-symmetric sudden expansion. Computers & Fluids, 29(5), 467-492. doi: http://dx.doi.org/10.1016/S0045-7930(99)00018-3
Chien, K. Y. (1982). Prediction of channel and boundary-layer flows with a low-Reynolds-number turbulence model. AIAA J., 20 33-38.
Chieng, C. C., & Launder, B. E. (1980). On the calculation of turbulent heat transport downstream from an abrupt pipe expansion. Numerical Heat Transfer, 3(2), 189-207. doi: 10.1080/01495728008961754
Cho, C.-C., Chen, C.-L., & Chen, C. o.-K. (2013). Natural convection heat transfer and entropy generation in wavy-wall enclosure containing water-based nanofluid. International Journal of Heat and Mass Transfer, 61(0), 749-758. doi: http://dx.doi.org/10.1016/j.ijheatmasstransfer.2013.02.044
Choi, S. U. S., & Eastman, J. A. (1995). Enhancing thermal conductivity of fluids with nanoparticles. International mechanical engineering congress and exhibition, San Francisco, CA (United States).
Chon, C. H., Kihm, K. D., Lee, S. P., & Choi, S. U. S. (2005). Empirical correlation finding the role of temperature and particle size for nanofluid (Al2O3) thermal conductivity enhancement. Applied Physics Letters, 87(15), 153107-153107-153103. doi: 10.1063/1.2093936
Chung, B. T. F., & Jia, S. (1995). A turbulent near-wall model on convective heat transfer from an abrupt expansion tube. Heat and Mass Transfer, 31(1-2), 33-40. doi: 10.1007/bf02537419
Chung, S. Y., Rhee, G. H., & Sung, H. J. (2002). Direct numerical simulation of turbulent concentric annular pipe flow: Part 1: Flow field. International Journal of Heat and Fluid Flow, 23(4), 426-440. doi: http://dx.doi.org/10.1016/S0142-727X(02)00140-6
Chung, S. Y., & Sung, H. J. (2003). Direct numerical simulation of turbulent concentric annular pipe flow: Part 2: Heat transfer. International Journal of Heat and Fluid Flow, 24(3), 399-411. doi: http://dx.doi.org/10.1016/S0142-727X(03)00017-1
Churchill, S. W., & Chan, C. (1995). Turbulent flow in channels in terms of turbulent shear and normal stresses. AIChE Journal, 41(12), 2513-2521. doi: 10.1002/aic.690411202
Corcione, M. (2010). Heat transfer features of buoyancy-driven nanofluids inside rectangular enclosures differentially heated at the sidewalls. International Journal of Thermal Sciences, 49(9), 1536-1546. doi: http://dx.doi.org/10.1016/j.ijthermalsci.2010.05.005

D.B. Carrington, D. W. P. (2002). Convective heat transfer downstream of a 3-D backward-facing-step. Numer. Heat Transfer Pt. A-Appl., 41, 555-578.
Dalle Donne M., B. F. H. Experimental local heat transfer and friction coefficients for subsonic laminar, transitional and turbulent flow of air or helium in a tube at high temperatures. Dragon Project Report 184, April 1963.
Das, M. K., & Kanna, P. R. (2007). Application of an ADI scheme for steady and periodic solutions in a lid-driven cavity problem. International Journal of Numerical Methods for Heat & Fluid Flow, 17(8), 799-822. doi: 10.1108/09615530710825783
Davis G., T. R. (1969). Natural convection between concentric vertical cylinders. Phys. Fluids 12, 198-207.
De Brederode, V., & Bradshaw, P. (1972). Three-dimensional Flow in Nominally Two-dimensional Separation Bubbles: Flow behind a rearward-facing step. I: Department of Aeronautics, Imperial College of Science and Technology.
De Zilwa S.R., S. S. a. J. H. W. (1997). Active control of isothermal and combusting flows in plane sudden-expansions. Proc. Transport Phenomena in Thermal Sci and Process Eng. , 325-330.
Demir, H., Dalkilic, A. S., Kürekci, N. A., Duangthongsuk, W., & Wongwises, S. (2011). Numerical investigation on the single phase forced convection heat transfer characteristics of TiO2 nanofluids in a double-tube counter flow heat exchanger. International Communications in Heat and Mass Transfer, 38(2), 218-228. doi: http://dx.doi.org/10.1016/j.icheatmasstransfer.2010.12.009
Donne, M. D., & Meerwald, E. (1966). Experimental local heat-transfer and average friction coefficients for subsonic turbulent flow of air in an annulus at high temperatures. International Journal of Heat and Mass Transfer, 9(12), 1361-1376. doi: http://dx.doi.org/10.1016/0017-9310(66)90134-7
Donne, M. D., & Meerwald, E. (1973). Heat transfer and friction coefficients for turbulent flow of air in smooth annuli at high temperatures. International Journal of Heat and Mass Transfer, 16(4), 787-809. doi: http://dx.doi.org/10.1016/0017-9310(73)90091-4
Duangthongsuk, W., & Wongwises, S. (2010). An experimental study on the heat transfer performance and pressure drop of TiO2-water nanofluids flowing under a turbulent flow regime. International Journal of Heat and Mass Transfer, 53(1–3), 334-344. doi: http://dx.doi.org/10.1016/j.ijheatmasstransfer.2009.09.024
Durst, F., Melling, A., & Whitelaw, J. H. (1974). Low Reynolds number flow over a plane symmetric sudden expansion. Journal of Fluid Mechanics, 64(01), 111-128. doi: doi:10.1017/S0022112074002035
Durst, F. W., J. H. . (1971). Aerodynamic properties of separated gas flows: existing measurements techniques and new optical geometry for the laser-Doppler anemometer. Progress Heat and Mass Transfer 4, 311.
Dutta, R., Dewan, A., & Srinivasan, B. (2013). Comparison of various integration to wall (ITW) RANS models for predicting turbulent slot jet impingement heat transfer. International Journal of Heat and Mass Transfer, 65(0), 750-764. doi: http://dx.doi.org/10.1016/j.ijheatmasstransfer.2013.06.056
E. Fiorentini, M. Felli, F. Pareira, R. Camussi, & Marco, A. D. (2007). Wall Pressure Fluctuations Over a Forward-Facing Step. 13th AIAA/CEAS Aeroacoustics Conference, Rome: AIAA.51, 1-10.
E.M. Sparrow, O. B. (1985). Heat transfer coefficient on the downstream face of an abrupt enlargement or inlet constriction in a pipe. ASME Journal of Heat Transfer, 102, 408-414.

Ede, A., C.I. Hislop and R. Morris. (1956a). Effect of the local heat transfer coefficient in a pipe of an abrupt disturbance of the fluid flow: abrupt convergence and divergence of diameter ratio 2:1. Proc Inst Mech Engrs, 1113-1130.
Ede, A., C.I. Hislop and R. Morris. (1956b). Effect of the local heat transfer coefficient in a pipe of an abrupt disturbance of the fluid flow: abrupt convergence and divergence of diameter ratio 2:1. Proc Inst Mech Engrs., 170, 1113-1130.
Farajollahi, B., Etemad, S. G., & Hojjat, M. (2010). Heat transfer of nanofluids in a shell and tube heat exchanger. International Journal of Heat and Mass Transfer, 53(1–3), 12-17. doi: http://dx.doi.org/10.1016/j.ijheatmasstransfer.2009.10.019
Fearn, R. M., Mullin, T., & Cliffe, K. A. (1990). Nonlinear flow phenomena in a symmetric sudden expansion. Journal of Fluid Mechanics, 211, 595-608. doi: doi:10.1017/S0022112090001707
Filetti, E. G. a. W. M. K. (1967). Heat transfer in separated, reattached and redeveloped regions behind a double step at entrance to flat duct. . Journal of Heat Transfer, 89, 163-168.
Gandjalikhan Nassab, S. A., Moosavi, R., & Hosseini Sarvari, S. M. (2009). Turbulent forced convection flow adjacent to inclined forward step in a duct. International Journal of Thermal Sciences, 48(7), 1319-1326. doi: http://dx.doi.org/10.1016/j.ijthermalsci.2008.10.003
Gasset, N., Poitras, G., Gagnon, Y., & Brothers, C. (2005). Study of atmospheric boundary layer flows over a coastal cliff. Wind Engineering, 29(1), 3-24. doi: 10.1260/0309524054353719
Gavara, M., & Kanna, P. R. (2012). Study of conjugate natural convection between vertical coaxial rectangular cylinders. International Communications in Heat and Mass Transfer, 39(7), 904-912. doi: http://dx.doi.org/10.1016/j.icheatmasstransfer.2012.06.001
Goldstein, R. J., Eriksenv,. L., Olsonr, M. & Eckerte, . R. G. (1970). Laminar separation, reattachment and transition of flow over a downstream facing step. ASME Journal of Fluids Engineering 92(4), 732-739.
Goodarzi, M., Safaei, M. R., Vafai, K., Ahmadi, G., Dahari, M., Kazi, S. N., & Jomhari, N. (2014). Investigation of nanofluid mixed convection in a shallow cavity using a two-phase mixture model. International Journal of Thermal Sciences, 75(0), 204-220. doi: http://dx.doi.org/10.1016/j.ijthermalsci.2013.08.003
Guj, G., & Stella, F. (1995). NATURAL CONVECTION IN HORIZONTAL ECCENTRIC ANNULI: NUMERICAL STUDY. Numerical Heat Transfer, Part A: Applications, 27(1), 89-105. doi: 10.1080/10407789508913690
Guo, Z.-Y., Li, D.-Y., & Liang, X.-G. (1996). Thermal effect on the recirculation zone in sudden-expansion gas flows. International Journal of Heat and Mass Transfer, 39(13), 2619-2624. doi: http://dx.doi.org/10.1016/0017-9310(95)00371-1
H. K. Myong, N. K. (1990a). A new approach to improved of k-ϵ turbulence model for wall bounded shear flows. JSMEJ. Ser. , H33, 63-72.
H. K. Myong, N. K. (1990b). A new approach to improved of k-ϵ turbulence model for wall bounded shear flows. JSMEJ. Ser., H33, 63-72.
H. R. Ashorynejad, M. S. a. E. F. (2013). Lattice Boltzmann Simulation of Nanofluids Natural Convection Heat Transfer in Concentric Annulus (TECHNICAL NOTE). International Journal of Engineering Transactions B, 26, 895-904.

Habib, M. A., A.M. Attya and M.M. Khalifa. (1992). Measurements of augmented heat transfer downstream of an abrupt rectangular channel expansion. J. Modeling, Measurement & Control B, 44(1), 33-46.
Habib, M. A., A.M. Mobarak, A.E. Attya and A. Aly. (1992). An experimental investigation of heat transfer and flow in channels with streamwise-periodic flow. Journal of Energy, 17(11), 1049-1058.
Habib, M. A., Mobarak, A. M., Abdel Hadi, E. A., Affify, R. I., & Sallak, M. A. (1994). Experimental Investigation of Heat Transfer and Flow Over Baffles of Different Heights. Journal of Heat Transfer, 116(2), 363-368. doi: 10.1115/1.2911408
Habibi Matin, M., & Pop, I. (2013). Natural convection flow and heat transfer in an eccentric annulus filled by Copper nanofluid. International Journal of Heat and Mass Transfer, 61(0), 353-364. doi: http://dx.doi.org/10.1016/j.ijheatmasstransfer.2013.01.061
Han, J. C., & Park, J. S. (1988). Developing heat transfer in rectangular channels with rib turbulators. International Journal of Heat and Mass Transfer, 31(1), 183-195. doi: http://dx.doi.org/10.1016/0017-9310(88)90235-9
Hassan, M., Sadri, R., Ahmadi, G., Dahari, M., Kazi, S., Safaei, M., & Sadeghinezhad, E. (2013). Numerical Study of Entropy Generation in a Flowing Nanofluid Used in Micro- and Minichannels. Entropy, 15(1), 144-155.
Hattori, H., & Nagano, Y. (2010). Investigation of turbulent boundary layer over forward-facing step via direct numerical simulation. International Journal of Heat and Fluid Flow, 31(3), 284-294. doi: http://dx.doi.org/10.1016/j.ijheatfluidflow.2010.02.027
Heikal, M. R. F., & Hatton, A. P. (1978). Predictions and measurements of non-axisymmetric turbulent diffusion in an annular channel. International Journal of Heat and Mass Transfer, 21(7), 841-848. doi: http://dx.doi.org/10.1016/0017-9310(78)90175-8
Herrmann Schlichting, K. G. (2000). Boundary-Layer Theory. Springer- Science - 799 pages.
Heyerichs, K., & Pollard, A. (1996). Heat transfer in separated and impinging turbulent flows. International Journal of Heat and Mass Transfer, 39(12), 2385-2400. doi: http://dx.doi.org/10.1016/0017-9310(95)00347-9
Ho, C. J., & Lin, Y. H. (1989). Thermal convection heat transfer of air/water layers enclosed in horizontal annuli with mixed boundary conditions. Wärme - und Stoffübertragung, 24(4), 211-224. doi: 10.1007/bf01625497
Holman, J. P. (2002). Heat Transfer. McGraw Hill, New York, Ninth Edition
Hong J.K., L. K. M., Choi Y.D. (1983). Analysis of turbulent heat in a concentric annular pipe with artificial roughness. J. KSME 7(3), 301-3012.
Hosseini, R., Ramezani, M., & Mazaheri, M. R. (2009). Experimental study of turbulent forced convection in vertical eccentric annulus. Energy Conversion and Management, 50(9), 2266-2274. doi: http://dx.doi.org/10.1016/j.enconman.2009.05.002
Hsieh, W. D., & Chang, K. C. (1996). Calculation of wall heat transfer in pipeexpansion turbulent flows. International Journal of Heat and Mass Transfer, 39(18), 3813-3822. doi: http://dx.doi.org/10.1016/0017-9310(96)00061-0
Hussein A. Mohammed, M. G., K.M. Munisamy, Mazlan A. Wahid. (2013). Combined Convection Heat Transfer of Nanofluids Flow over Forward Facing Step in a Channel Having a Blockage. Applied Mechanics and Materials, 388, 185-191.
Hussein, T., Abdulrazzaq, T., Kazi, S. N., Badarudin, A., & Ariffin, M. K. A. (2014). Numerical study of turbulent heat transfer in annular pipe with sudden contraction. Applied mechanics and materials. , 465-466, 461-466.

Hussein, T., S.N., K., & Ahmed, B. (2011). A Review of Experimental Study of Turbulent Heat Transfer in Separated Flow. Australian Journal of Basic and Applied Sciences, 5(10), 489-505.
Hussein, T., Shkarah, A. J., Kazi, S. N., & Badarudin, A. (2013). CFD Simulation of Heat Transfer and Turbulent Fluid Flow over a Double Forward-Facing Step. Mathematical Problems in Engineering, 2013, 10. doi: 10.1155/2013/895374
Hussein Togun, Tuqa Abdulrazzaq, S. N. Kazi, A. Badarudin, & Ariffin, M. K. A. (2013). Heat Transfer to Laminar Flow over a Double Backward-Facing Step International Journal of Mechanical, Industrial Science and Engineering, World Academy of Science, Engineering and Technology, 80, 971 - 977.
Hussein Togun, Tuqa Abdulrazzaq, S.N. Kazi, Abdul Amir H. Kadhum, Ahmed Badarudin, M.K.A. Ariffin, & Sadeghinezhad, E. (2013). Numerical Study of Turbulent Heat Transfer in Separated Flow: Review. International Review of Mechanical Engineering (IREME), 7(2), 337-349.
Hussein Togun, Y. K. Salman, Hakim S. Sultan Aljibori, & Kazi, S. N. (2011). An experimental study of heat transfer to turbulent separation fluid flow in an annular passage. International Journal of Heat and Mass Transfer, 54(4), 766-773. doi: http://dx.doi.org/10.1016/j.ijheatmasstransfer.2010.10.031
Hussein Togun, Y. K. S., Hakim S. Sultan Aljibori, S. N. Kazi, . (2011). An experimental study of heat transfer to turbulent separation fluid flow in an annular passage. International Journal of Heat and Mass Transfer, 54(4), 766-773. doi: http://dx.doi.org/10.1016/j.ijheatmasstransfer.2010.10.031
HusseinTogun, S.N. Kazi, & Badarudin, A. (2011). A Review of Experimental Study of Turbulent Heat Transfer in Separated Flow. Australian Journal of Basic and Applied Sciences, 5(10), 489-505.
HusseinTogun, Tuqa Abdulrazzaq, S. N. Kazi, A. Badarudin, & Ariffin, M. K. A. (2014). Numerical study of turbulent heat transfer in annular pipe with sudden contraction. Applied mechanics and materials, 465 - 466, 461-466.
Iguchi, M. a. T. S. (1988). Study on the flow near the wall of the larger pipe, downstream of a sudden expansion. Trans JSME B, 54(507), 3010-3015.
Incropera, F. P. (2007). Fundamentals of heat and mass transfer. John Wiley.
Izadi, M., Behzadmehr, A., & Jalali-Vahida, D. (2009). Numerical study of developing laminar forced convection of a nanofluid in an annulus. International Journal of Thermal Sciences, 48(11), 2119-2129. doi: http://dx.doi.org/10.1016/j.ijthermalsci.2009.04.003
J. H., N., & B. F., A. (2002). Reattachment of Three-Dimensional Flow Adjacent to Backward-Facing Step 8th AIAA/ASME Joint Thermophysics and Heat Transfer Conference: American Institute of Aeronautics and Astronautics.
J. W. Baughn, M.A. Hoffman, R.K. Takahash, & Launder, B. E. (1984). Local heat transfer downstream of an abrupt expansion in a circular channel with constant wall heat flux. Journal of Heat Transfer, 106, 789-796.
J.G. Barbosa Saldana, N.K. Anand, & Sarin, V. (2005). Numerical simulation of mixed convective flow over a three-dimensional horizontal backward facing-step. Journal of Heat Transfer 127, 1027–1036.
J.G. Barbosa Saldana, N. K. A., V. Sarin (2005). Numerical simulation of mixed convective flow over a three dimensional horizontal backward facing step. J. Heat Transfer 127, 1027-1036.

J.K. Eaton, J. P. J. (1980). Turbulent flow reattachment: An experimental study of the flow and structure behind a backward- facing step. Report MD-39, department of mechanical engineering Stanford University

J.S., K. Experiment of turbulent heat transfer on the annular pipes with ring and spiral artificial roughness. Master's Thesis, Korea University (1983).

Jayatilleke, C. L. (1969). The influence of prandtl number and surface roughness on the resistances of the laminar sub-layer to momentum and heat transfer. Prog. Heat Mass Transfer, 1, 193-329.

Jongebloed, L. Numerical Study Using FLUENT of the Separation and Reattachment Points for Backwards-Facing Step Flow. M. Sc. Thesis, Rensselaer Polytechnic Institute, 2008.

Jongebloed, L. (2008). Numerical Study using FLUENT of the Separation and Reattachment Points for Backwards-Facing Step Flow. M. Sc. Thesis, Rensselaer Polytechnic Institute, Hartford, Connecticut, U. S.A.

K. Sakuraba, K. F., M. Sano. (2004). Control of turbulent channel flow over a backward-facing-step by suction or injection. Heat Transfer – Asian Research, 33(8), 490–504.

K. Sugawara, H. Y., T. Ota. (2004). LES of three-dimensional separated flow and heat transfer in a symmetric expansion plane channel. J. Nippon Dennetsu Shinpojiumu Koen Ronbunshu, 1, 103-104.

K. Sugawara, H. Y., T. Ota. (2005). LES of turbulent separated flow, heat transfer in a symmetric expansion plane channel. Journal of Fluids Engineering, Transactions of the ASME, 127, 865–871.

K.J, H. (1998). Experimental and computational study of laminar axisymmetric recirculating flows of Newtonian and viscoplastic non-Newtonian fluids. PhD dissertation, Polytechnic University, New York.

K.M., L. The experiment of turbulent heat transfer in annular pipe with artificial roughness. Master's Thesis, Korea University (1982).

Kader, B. A. (1981). Temperature and concentration profiles in fully turbulent boundary layers. Int. J. Heat Mass Transfer, 24, 1541-1544. doi: 10.1016/0017-9310(81)90220-9

Kang J.S., C. Y. D. (1985). Study on the effects of artificial roughness on the turbulent heat transfer of concentric annular pipes. J. KSME 9(3), 335-344.

Kanna, P. R., & Das, M. K. (2006). Heat Transfer Study of Two-Dimensional Laminar Incompressible Wall Jet over Backward-Facing Step. Numerical Heat Transfer, Part A: Applications, 50(2), 165-187. doi: 10.1080/10407780500506857

Kaufmann, W., and Smarr. (1993). Supercomputing and the Transformation of Science. ScienScientific American Library, New York.

Kawamura, T., A. Yamamori, J. Mimatsu and M. Kumada. (1991). Time and spatial characteristics of heat transfer at the reattachment region of a two-dimensional backward-facing step. Proc. of the ASME-JSME Thermal Eng Conf.3 197-204.

Kawamura, T., S. Tanaka, I. Mabuchi and M. Kumada. (1987-88). Temporal and spatial characteristics of heat transfer at the reattachment region of a backward-facing step. Exp Heat Transfer, X, 299-313.

Kawamura, T., Tanaka, S., Mabuchi, I., & Kumada, M. (1987). TEMPORAL AND SPATIAL CHARACTERISTICS OF HEAT TRANSFER AT THE REATTACHMENT REGION OF A BACKWARD-FACING STEP. Experimental Heat Transfer, 1(4), 299-313. doi: 10.1080/08916158708946348

Kawamura, T., Yamamori, A., Mimatsu, J., Kumada, M., . (1991). Time and spatial characteristics of heat transfer at the reattachment region of a two-dimensional backward-facing step. Proc. of the 1991 ASME-JSME Thermal Eng Conf.3, 197-204.
Kays, E. G. F. a. W. M. (1967). Heat Transfer in Separated, Reattached and Redevelopment Regions behind a Double Step at Entrance to a Flat Duct. ASME Journal Heat Transfer, 89 163–168.
Kays, W. M., & Leung, E. Y. (1963). Heat transfer in annular passages—hydrodynamically developed turbulent flow with arbitrarily prescribed heat flux. International Journal of Heat and Mass Transfer, 6(7), 537-557. doi: http://dx.doi.org/10.1016/0017-9310(63)90012-7
KC Chang, WD Hsieh, & Chen, C. (1995). A modified low-Reynolds number turbulence model applicable to recirculating flow in pipe expansion. J. Fluids Eng., 117, 417-423.
KC Chang, W. H., CS Chen. (1995). A modified low-Reynolds number turbulence model applicable to recirculating flow in pipe expansion. J. Fluids Eng, , 117, 417-423.
Khaled J. Hammad, G. C. V., , M. Volkan Otugen. (2001). Laminar flow of a Hershel-Bulkley fluid over an axisymmetric sudden expansion. Journal of Fluids Engineering, 123, 588-594.
Khanafer, K., Al-Azmi, B., Al-Shammari, A., & Pop, I. (2008). Mixed convection analysis of laminar pulsating flow and heat transfer over a backward-facing step. International Journal of Heat and Mass Transfer, 51(25–26), 5785-5793. doi: http://dx.doi.org/10.1016/j.ijheatmasstransfer.2008.04.060
Khanafer, K., & Vafai, K. (2011). A critical synthesis of thermophysical characteristics of nanofluids. International Journal of Heat and Mass Transfer, 54(19–20), 4410-4428. doi: http://dx.doi.org/10.1016/j.ijheatmasstransfer.2011.04.048
Kherbeet, A. S., Mohammed, H. A., Munisamy, K. M., & Salman, B. H. (2014). The effect of step height of microscale backward-facing step on mixed convection nanofluid flow and heat transfer characteristics. International Journal of Heat and Mass Transfer, 68(0), 554-566. doi: http://dx.doi.org/10.1016/j.ijheatmasstransfer.2013.09.050
Kherbeet, A. S., Mohammed, H. A., & Salman, B. H. (2012). The effect of nanofluids flow on mixed convection heat transfer over microscale backward-facing step. International Journal of Heat and Mass Transfer, 55(21–22), 5870-5881. doi: http://dx.doi.org/10.1016/j.ijheatmasstransfer.2012.05.084
Khezzar, L., De Zilwa, S. R. N., & Whitelaw, J. H. (1999). Combustion of premixed fuel and air downstream of a plane sudden-expansion. Experiments in Fluids, 27(4), 296-309. doi: 10.1007/s003480050354
Klinzing, W. P., & Sparrow, E. M. (2009). Evaluation of Turbulence Models for External Flows. Numerical Heat Transfer, Part A: Applications, 55(3), 205-228. doi: 10.1080/10407780802629001
Koo, J., & Kleinstreuer, C. (2005). Impact analysis of nanoparticle motion mechanisms on the thermal conductivity of nanofluids. International Communications in Heat and Mass Transfer, 32(9), 1111-1118. doi: http://dx.doi.org/10.1016/j.icheatmasstransfer.2005.05.014
Koram, K. K. a. E. M. S. (1978). Turbulent heat transfer downstream of an unsymmetric blockage in a tube. J. Heat Transfer, 100, 588-594.
Krall, K. M. a. E. M. S. (1966). Turbulent heat transfer in the separated, reattachment, and redevelopment regions of a circular tube. J. Heat Transfer, 88, 131-136.
Kwang –Yong Kim, Y. J.-L. (1994). Prediction of turbulent heat transfer downstream of an abrupt pipe expansion. KSME Journal, 8, 248-254.

L.I., P. B. S. a. R. (1965). Heat exchange and friction resistance in pipes and channels of various geometrical shapes. Heat and Mass Transfer I Nauka i Tekhnika Mink

Lancial, N., Beaubert, F., Harmand, S., & Rolland, G. (2013). Effects of a turbulent wall jet on heat transfer over a non-confined backward-facing step. International Journal of Heat and Fluid Flow, 44(0), 336-347. doi: http://dx.doi.org/10.1016/j.ijheatfluidflow.2013.07.003

Largeau, J. F., & Moriniere, V. (2007). Wall pressure fluctuations and topology in separated flows over a forward-facing step. Experiments in Fluids, 42(1), 21-40. doi: 10.1007/s00348-006-0215-9

Launder, B. E., & Spalding, D. B. (1974). The numerical computation of turbulent flows. Computer Methods in Applied Mechanics and Engineering, 3(2), 269-289. doi: http://dx.doi.org/10.1016/0045-7825(74)90029-2

Lee, B. K., Cho, N. H., & Choi, Y. D. (1988). Analysis of periodically fully developed turbulent flow and heat transfer by k-ε equation model in artificially roughened annulus. International Journal of Heat and Mass Transfer, 31(9), 1797-1806. doi: http://dx.doi.org/10.1016/0017-9310(88)90194-9

Lee, D., Lee, J., Park, H., & Kim, M. (2011). Experimental and numerical study of heat transfer downstream of an axisymmetric abrupt expansion and in a cavity of a circular tube. Journal of Mechanical Science and Technology, 25(2), 395-401. doi: 10.1007/s12206-010-1222-6

Lee, T., & Mateescu, D. (1998). Experimental and numerical investigation of 2-d backward-facing step flow. Journal of Fluids and Structures, 12(6), 703-716. doi: http://dx.doi.org/10.1006/jfls.1998.0166

Lima, R. C., Andrade, C. R., & Zaparoli, E. L. (2008). Numerical study of three recirculation zones in the unilateral sudden expansion flow. International Communications in Heat and Mass Transfer, 35(9), 1053-1060. doi: http://dx.doi.org/10.1016/j.icheatmasstransfer.2008.07.004

Lundberg R.E., R. W. C., Kays W.M. . (1961). Heat transfer with laminar flow in concentric annuli with constant and variable wall temperature and heat flux. Thermosciences Division, Dept. Mech. Engng. Report AHT-2, Stanford University 1961.

M. R. Safaei, H. R. G., B. S. Razavi and M. Goodarzi. (2011). Numerical investigation of laminar and turbulent mixed convection in a shallow water-filled enclosure by various turbulence methods. Scientific Research and Essays, 6, 4826-4838.

M. R. Safaei, M. G. a. M. M. (2011). Numerical modeling of turbulence mixed convection heat transfer in air filled enclosures by finite volume method. The International Journal of Multiphysics, 5, 307-324.

M.A. Habib, A. M. A., D.M. McEligot,. (1988). Calculation of turbulent flow and heat transfer in channels with streamwise periodic flow. ASME Winter Annual Meeting in Boston, and ASME J. of Turbomachinery, 110, 405-411.

M.A. Habib., F. D., D.M. McEligot. (1984). Streamwise-Periodic Flow Around Baffles. Proc. 2nd Int. Conference on Applications of Laser Anemometry to Fluid Mechanics, Lisbon, Portugal.

M.M. Rashidi, E. Erfani, The modified differential transform method for investigating Nano boundary- layer over stretching surfaces, International Journal of Numerical methods for heat and fluid flow 21 (7) (2011) 864-883.

M.M. Rashidi, N. Fridoonimehr, A. Hosseini, O. Anwar Beg, T.-K. Hung, Homotopy simulation of nanofluids dynamics from a Nono-linearly stretching isothermal permeable sheet with transpiration, Meccanica 49 (2) 2014) 469-482.
M.M. Rashidi,, N. Vishnu Ganesh, A.K. Abdul Hakeem, B. Ganga, Buoyancy effect on MHD flow of nanofluids over a stretching sheet in the presence of thermal radiation, Journal of Molecular Liquids 198 (2014) 234-238
M.F., D. R. G. a. T. Analysis of fully developed turbulent heat transfer and flow in an annulus with various eccentricities. NACA-TN3451 (1955).
Mabuchi, I., Murata, T., Kumada, M., . (1986). Effect of free-stream turbulence on heat transfer characteristics in the reattachment region on the bottom surface of a backward-facing step (For different angles of separation). . Trans JSME., B52, 2619-2625.
Mabuchi, I., T. Murata and M. Kumada. (1986). Effect of free-stream turbulence on heat transfer characteristics in the reattachment region on the bottom surface of a backward-facing step (For different angles of separation). Trans JSME B52, 2619-2625.
Macagno, E. O., and Hung T. K. (1967). Computational and experimental study of a captive annular eddy. J. Fluid Mech., 28, 43-64.
Mahmoudi, A. H., Shahi, M., & Talebi, F. (2012). Entropy Generation Due to Natural Convection in a Partially Open Cavity with a Thin Heat Source Subjected to a Nanofluid. Numerical Heat Transfer, Part A: Applications, 61(4), 283-305. doi: 10.1080/10407782.2012.647990
Manca, O., Nardini, S., & Ricci, D. (2011). Numerical Analysis of Water Forced Convection in Channels with Differently Shaped Transverse Ribs. Journal of Applied Mathematics, 2011. doi: 10.1155/2011/323485
Manca, O., Nardini, S., & Ricci, D. (2012a). A numerical study of nanofluid forced convection in ribbed channels. Applied Thermal Engineering, 37(0), 280-292. doi: http://dx.doi.org/10.1016/j.applthermaleng.2011.11.030
Manca, O., Nardini, S., & Ricci, D. (2012b). A numerical study of nanofluid forced convection in ribbed channels. Applied Thermal Engineering, 37, 280-292.
Manzar, M. A. a. S., S. N. (2009). Particle Distribution and Erosion During the Flow of Newtonian and Non-Newtonian Slurries in Straight and Coiled Pipes. Engineering Applications of Computational Fluid Mechanics, 3, 296-320.
Marino, L., & Luchini, P. (2009). Adjoint analysis of the flow over a forward-facing step. Theoretical and Computational Fluid Dynamics, 23(1), 37-54. doi: 10.1007/s00162-008-0090-5
Mehrez, Z., Bouterra, M., El Cafsi, A., Belghith, A., & Quere, P. (2009). The influence of the periodic disturbance on the local heat transfer in separated and reattached flow. Heat and Mass Transfer, 46(1), 107-112. doi: 10.1007/s00231-009-0548-z
Mehrizi, A. A., Farhadi, M., & Shayamehr, S. (2013). Natural convection flow of Cu–Water nanofluid in horizontal cylindrical annuli with inner triangular cylinder using lattice Boltzmann method. International Communications in Heat and Mass Transfer, 44(0), 147-156. doi: http://dx.doi.org/10.1016/j.icheatmasstransfer.2013.03.001
Menter, F. R. (1993). Zonal Two Equation k- Turbulence Models for Aerodynamic Flows. AIAA Paper #93-2906, 24th Fluid Dynamics Conference, July 1993.
Menter, F. R. (1994). Two-equation eddy-viscosity turbulence models for engineering applications. AIAA Journal, 32(8), 1598-1605. doi: 10.2514/3.12149
Miller P., B. J. J., Benforado D.M. (1995). Heat transfer to water in an annulus. AIChE J. , 1(4), 501-504.

Minaev, B. N. S., E. I.; Frolikov, I. I. (1977). Effect of free convection on heat transfer in a horizontal eccentric annular channel. High Temperature Science. High Temperature Science, 15, 280-284.
Mintsa, H. A., Roy, G., Nguyen, C. T., & Doucet, D. (2009). New temperature dependent thermal conductivity data for water-based nanofluids. International Journal of Thermal Sciences, 48(2), 363-371. doi: http://dx.doi.org/10.1016/j.ijthermalsci.2008.03.009
Miranda J.P., P. F. T., Oliveira P.J. (2003). Local loss coefficient in sudden expansion laminar flows of inelastic shear thinning fluids. . 17th International Congress of Mechanical Engineering November 10-14, (2003).
Moffat, R. J. (1985). Using Uncertainty Analysis in the Planning of an Experiment. Journal of Fluids Engineering, 107(2), 173-178. doi: 10.1115/1.3242452
Moffat, R. J. (1988). Describing the uncertainties in experimental results. Experimental Thermal and Fluid Science, 1(1), 3-17. doi: http://dx.doi.org/10.1016/0894-1777(88)90043-X
Mohammed, H. A., Al-Aswadi, A. A., Abu-Mulaweh, H. I., Hussein, A. K., & Kanna, P. R. (2014). Mixed Convection Over a Backward-Facing Step in a Vertical Duct Using Nanofluids—Buoyancy Opposing Case. Journal of Computational and Theoretical Nanoscience, 11(3), 860-872. doi: 10.1166/jctn.2014.3339
Mohammed, H. A., Al-aswadi, A. A., Abu-Mulaweh, H. I., & Shuaib, N. H. (2011). Influence of nanofluids on mixed convective heat transfer over a horizontal backward-facing step. Heat Transfer—Asian Research, 40(4), 287-307. doi: 10.1002/htj.20344
Mohammed, H. A., Al-aswadi, A. A., Shuaib, N. H., & Saidur, R. (2011). Convective heat transfer and fluid flow study over a step using nanofluids: A review. Renewable and Sustainable Energy Reviews, 15(6), 2921-2939. doi: http://dx.doi.org/10.1016/j.rser.2011.02.019
Mohammed, H. A., Al-aswadi, A. A., Yusoff, M. Z., & Saidur, R. (2012). Buoyancy-assisted mixed convective flow over backward-facing step in a vertical duct using nanofluids. Thermophysics and Aeromechanics, 19(1), 33-52. doi: 10.1134/S0869864312010040
Mohanty, A. K., & Dubey, M. R. (1996). Buoyancy induced flow and heat transfer through a vertical annulus. International Journal of Heat and Mass Transfer, 39(10), 2087-2093. doi: http://dx.doi.org/10.1016/0017-9310(95)00280-4
Mokhtari Moghari, R., Akbarinia, A., Shariat, M., Talebi, F., & Laur, R. (2011). Two phase mixed convection Al2O3–water nanofluid flow in an annulus. International Journal of Multiphase Flow, 37(6), 585-595. doi: http://dx.doi.org/10.1016/j.ijmultiphaseflow.2011.03.008
Mori, Y., Uchida, Y., Sakai, K. (1986). A study of the time and spatial micro- structure of heat transfer performance near the reattaching point of separated flows. Trans JSME. , B52, 3353-3361.
Mori, Y., Y. Uchida and K. Sakai. (1986). A study of the time and spatial micro- structure of heat transfer performance near the reattaching point of separated flows. Trans JSME B52, 3353-3361.
Moss, K. J. (1998). Heat and Mass transfer in Building services design Kindle Edition.
Munakata, T. A. (1962). Calculation on laminar heat transfer in tube (in Japanese). Chem. Engng. Tokyo 26, 1085-1088.
N Masoumi, N. S. a. A. B. (2009). A new model for calculating the effective viscosity of nanofluids. Journal of Physics D: Applied Physics, 42(5), 055501-055506.

Nag D., D. A. (2007). On the eddy characteristics of laminar axisymmetric flows through confined annular geometries with inward expansion. Proc. Inst. Mech. Eng. Part C J. Mech. Sci., 221, 213-226.
Neary, V. S., & Sotiropoulos, F. (1996). Numerical investigation of laminar flows through 90-degree diversions of rectangular cross-section. Computers & Fluids, 25(2), 95-118. doi: http://dx.doi.org/10.1016/0045-7930(95)00030-5
Nie, J. H., & Armaly, B. F. (2002). Three-dimensional convective flow adjacent to backward-facing step - effects of step height. International Journal of Heat and Mass Transfer, 45(12), 2431-2438. doi: http://dx.doi.org/10.1016/S0017-9310(01)00345-3
O. Labbe, P. S., E. Montreuil. (2002). Large-eddy simulation of heat transfer over a backward-facing-step. Numer. Heat Transfer Pt. A, 42, 73–90.
Ogugbue, C. C., and Shah, S. N. (2011). Laminar and Turbulent Friction Factors for Annular Flow of Drag Reducing Polymer Solutions in Coiled-Tubing Operations. SPE Drilling & Completions, 26(4), 506-518.
Ohori Yuki, N. A., Yoshikawa Hiroyuki and Ota Terukazu. (2004). Turbulent Heat Transfer in a Symmetric Sudden Expansion Channel. Proceedings of the Thermal Engineering Conference, 409-410.
Oliveira, P. J. (2003). Asymmetric flows of viscoelastic fluids in symmetric planar expansion geometries. Journal of Non-Newtonian Fluid Mechanics, 114(1), 33-63. doi: http://dx.doi.org/10.1016/S0377-0257(03)00117-4
Oliveira, P. J., & Pinho, F. T. (1997). Pressure drop coefficient of laminar Newtonian flow in axisymmetric sudden expansions. International Journal of Heat and Fluid Flow, 18(5), 518-529. doi: http://dx.doi.org/10.1016/S0142-727X(97)80010-0
Oon, C. S., Togun, H., Kazi, S. N., Badarudin, A., & Sadeghinezhad, E. (2013). Computational simulation of heat transfer to separation fluid flow in an annular passage. International Communications in Heat and Mass Transfer, 46(0), 92-96. doi: http://dx.doi.org/10.1016/j.icheatmasstransfer.2013.05.005
Ota, T., N. Nakamura and T. Hirayama. (1995). Turbulent separated and reattached flow around an inclined downward step. Turbul. Heat Mass Transfer, 1, 286-293.
Ota Terukazu, Y. H., Shibuya Kazuki, Nakajima Madoka, Yoshikawa Hiroyuki. (2002). Numerical Analysis of Separated Flow and Heat Transfer in an Enlarged Channel. Transactions of the Japan Society of Mechanical Engineers, B 66, 2109-2116.
Ould-Rouiss, M., Redjem-Saad, L., & Lauriat, G. (2009). Direct numerical simulation of turbulent heat transfer in annuli: Effect of heat flux ratio. International Journal of Heat and Fluid Flow, 30(4), 579-589. doi: http://dx.doi.org/10.1016/j.ijheatfluidflow.2009.02.018
Oyakawa, K., I. Teruya, I. Senaha, M. Yaga and I. Mabuchi. (1996). Evaluation of thermal performance on heat transfer enhancement by passive and active methods at downstream region of backward-facing step. Trans JSME B62, 1104-1110.
Oyakawa, K., Saitoh, T., Teruya, I., Mabuchi, I. (1995). Heat transfer enhancement using slat at reattachment region downstream of backward facing step. Trans JSME, B61, 4426-4431.
Oyakawa, K., T. Saitoh, I. Teruya and I. Mabuchi. (1995). Heat transfer enhancement using slat at reattachment region downstream of backward facing step. Trans JSME B61, 4426-4431.

Oyakawa, K., T. Taira and E. Yamazato. (1994). Studies of heat transfer control by jet discharge at reattachment region downstream of a backward facing step. Trans JSME B60, 248-254.
Oyakawa, K., Taira, T., Yamazato, E. (1994). Studies of heat transfer control by jet discharge at reattachment region downstream of a backward facing step. Trans JSME, B60, 248-254.
Özbelge, T. A. (2001). Heat transfer enhancement in turbulent upward flows of liquid–solid suspensions through vertical annuli. International Journal of Heat and Mass Transfer, 44(17), 3373-3379. doi: http://dx.doi.org/10.1016/S0017-9310(00)00366-5
Oztop, H. F., Mushatet, K. S., & Yılmaz, İ. (2012). Analysis of turbulent flow and heat transfer over a double forward facing step with obstacles. International Communications in Heat and Mass Transfer, 39(9), 1395-1403. doi: http://dx.doi.org/10.1016/j.icheatmasstransfer.2012.07.011
Pak, B., Cho, Y. I., & Choi, S. U. S. (1990). Separation and reattachment of non-newtonian fluid flows in a sudden expansion pipe. Journal of Non-Newtonian Fluid Mechanics, 37(2–3), 175-199. doi: http://dx.doi.org/10.1016/0377-0257(90)90004-U
Park, S.-K., & Ota, T. (2010). An experimental approach to turbulent heat transfer using a symmetric expanded plane channel. Journal of Mechanical Science and Technology, 24(4), 857-863. doi: 10.1007/s12206-010-0218-6
Park, T. S., & Sung, H. J. (1995). A nonlinear low-Reynolds-number κ-ε model for turbulent separated and reattaching flows—I. Flow field computations. International Journal of Heat and Mass Transfer, 38(14), 2657-2666. doi: http://dx.doi.org/10.1016/0017-9310(95)00009-X
Parsazadeh, M., Mohammed, H. A., & Fathinia, F. (2013). Influence of nanofluid on turbulent forced convective flow in a channel with detached rib-arrays. International Communications in Heat and Mass Transfer, 46(0), 97-105. doi: http://dx.doi.org/10.1016/j.icheatmasstransfer.2013.05.006
Patankar, S. (1980). Numerical Heat Transfer and Fluid Flow. Taylor & Francis.
Patankar, S. V. (1980). Numerical heat transfer and fluid flow: Taylor & Francis.
Patankar, S. V., & Spalding, D. B. (1972). A calculation procedure for heat, mass and momentum transfer in three-dimensional parabolic flows. International Journal of Heat and Mass Transfer, 15(10), 1787-1806. doi: http://dx.doi.org/10.1016/0017-9310(72)90054-3
Pereira, F. A. R., Barrozo, M. A. S., & Ataíde, C. H. (2007). CFD predictions of drilling fluid velocity and pressure profiles in laminar helical flow. Associação Brasileira de Engenharia Química, 24(4), 587-595. doi: 10.1590/S0104-66322007000400011
Peyghambarzadeh, S. M., Hashemabadi, S. H., Naraki, M., & Vermahmoudi, Y. (2013). Experimental study of overall heat transfer coefficient in the application of dilute nanofluids in the car radiator. Applied Thermal Engineering, 52(1), 8-16. doi: http://dx.doi.org/10.1016/j.applthermaleng.2012.11.013
Pinho, F. T., Oliveira, P. J., & Miranda, J. P. (2003). Pressure losses in the laminar flow of shear-thinning power-law fluids across a sudden axisymmetric expansion. International Journal of Heat and Fluid Flow, 24(5), 747-761. doi: http://dx.doi.org/10.1016/S0142-727X(03)00083-3
Pletcher, E. J. H. a. R. H. (1985). Application of a viscous – Invisced Interaction procedure to predict separated flows with heat transfer. J. Heat transfer, 107, 557-563.

Popiel, C. O., & Wojtkowiak, J. (1998). Simple Formulas for Thermophysical Properties of Liquid Water for Heat Transfer Calculations (from 0°C to 150°C). Heat Transfer Engineering, 19(3), 87-101. doi: 10.1080/01457639808939929
Prakash, C., & Renzoni, P. (1985). Effect of buoyancy on laminar fully developed flow in a vertical annular passage with radial internal fins. International Journal of Heat and Mass Transfer, 28(5), 995-1003. doi: http://dx.doi.org/10.1016/0017-9310(85)90281-9
Quarmby, A. (1967). Some measurements of turbulent heat transfer in the thermal entrance region of concentric annuli. International Journal of Heat and Mass Transfer, 10(3), 267-276. doi: http://dx.doi.org/10.1016/0017-9310(67)90144-5
Quarmby A, A. R. (1970). Turbulent Heat Transfer in Concentric Annuli With Constant Wall Temperatures. J. Heat Transfer, 92(1), 33-45.
R.P. Durrett, W.H. Stevenson, & Thompson, H. D. (1988). Radial and axial turbulent flow measurements with an LDV in an axisymmetric sudden expansion air flow. Journal of Fluids Engineering, 110, 367-372.
Rahgoshay, M., Ranjbar, A. A., & Ramiar, A. (2012). Laminar pulsating flow of nanofluids in a circular tube with isothermal wall. International Communications in Heat and Mass Transfer, 39(3), 463-469. doi: http://dx.doi.org/10.1016/j.icheatmasstransfer.2011.12.008
Rahimi-Esbo, M., Ranjbar, A. A., Ramiar, A., Rahgoshay, M., & Arya, A. (2012). Numerical Study of the Turbulent Forced Convection Jet Flow of Nanofluid in a Converging Duct. Numerical Heat Transfer, Part A: Applications, 62(1), 60-79. doi: 10.1080/10407782.2012.677368
Ramiar, A., Ranjbar, A. A., & Hosseinizadeh, S. F. (2012). Effect of axial conduction and variable properties on two dimensional conjugate heat transfer of AL2O3-EG/Water mixture nanofluid in microchannel. Journal of Applied Fluid Mechanics (JAFM), 5(3), 79-87.
Rhee, G. H., & Sung, H. J. (1996). A nonlinear low-Reynolds-number k-ε model for turbulent separated and reattaching flows—II. Thermal field computations. International Journal of Heat and Mass Transfer, 39(16), 3465-3474. doi: http://dx.doi.org/10.1016/0017-9310(96)00007-5
RJ., K. T. a. G. (1978). An Experimental Study of Natural Convection Heat Transfer in Concentric and Eccentric Horizontal Cylindrical Annuli. J. Heat Transfer, 100(4), 635-640.
Robinson, D. P., & Walker, V. (1978). Mass transfer for turbulent flow in an annulus with non-axisymmetric boundary conditions. International Journal of Heat and Mass Transfer, 21(10), 1299-1308. doi: http://dx.doi.org/10.1016/0017-9310(78)90021-2
Roschina, N. A., Uvarov, A. V., & Osipov, A. I. (2005). Natural convection in an annulus between coaxial horizontal cylinders with internal heat generation. International Journal of Heat and Mass Transfer, 48(21–22), 4518-4525. doi: http://dx.doi.org/10.1016/j.ijheatmasstransfer.2005.05.035
Rouizi, Y., Favennec, Y., Ventura, J., & Petit, D. (2009). Numerical model reduction of 2D steady incompressible laminar flows: Application on the flow over a backward-facing step. J. Comput. Phys., 228(6), 2239-2255. doi: 10.1016/j.jcp.2008.12.001
Runchal, A. K. (1976). Mass transfer investigation in turbulent flow downstream of sudden enlargement of a circular pipe for very high Schmidt numbers. Int. J. Heat Mass Transfer, 14, 781-792.
S Dutta, S. A. (1993). Heat transfer and flow past a backstep with the nonlinear k-ϵ turbulence model and the modified k-ϵ turbulence model. Numer Heat Transfer, A23, 281-301.

S.A., N. (2008). Experimental investigation of natural convection heat transfer in horizontal and inclined annular fluid layers. Heat Mass Transfer 44, 929-936.
S.A.M. Said, M. A. H., M.O. Iqbal. (2003). Heat transfer to pulsating turbulent flow in an abrupt pipe expansion. Int. J. Numer. Methods Heat Fluid Flow, 13(2-3), 286–308.
S.O., W. N. W. a. M. (1968). An analysis of heat transfer for fully developed turbulent flow in concentric annuli. Journal of Heat Mass Transfer, 90(1), 43-50.
Safaei, M. R., Goodarzi, M., & Mohammadi, M. (2011). Numerical modeling of turbulence mixed convection heat transfer in air filled enclosures by finite volume method. The International Journal of Multiphysics, 5(4), 307-324. doi: 10.1260/1750-9548.5.4.307
Safaei, M. R., Goshayeshi, H. R., Razavi, B. S., & Goodarzi, M. (2011). Numerical investigation of laminar and turbulent mixed convection in a shallow water-filled enclosure by various turbulence methods. Scientific Research and Essays, 6(22), 4826-4838.
Safaei, M. R., Maghmoumi, Y., & Karimipour, A. (2012). Numerical investigation of turbulence mixed convection heat transfer of water and drilling mud inside a square enclosure by finite volume method. Paper presented at the AIP Conference Proceedings.
Safaei, M. R., Rahmanian, B., & Goodarzi, M. (2011). Numerical study of laminar mixed convection heat transfer of power-law non-Newtonian fluids in square enclosures by finite volume method. International Journal of the Physical Sciences, 6 (33), 7456 - 7470. doi: DOI: 10.5897/IJPS11.1092
Saidur, R., Leong, K. Y., & Mohammad, H. A. (2011). A review on applications and challenges of nanofluids. Renewable and Sustainable Energy Reviews, 15(3), 1646-1668. doi: http://dx.doi.org/10.1016/j.rser.2010.11.035
Sambamurthy, N. B., Shaija, A., Narasimham, G. S. V. L., & Murthy, M. V. K. (2008). Laminar conjugate natural convection in horizontal annuli. International Journal of Heat and Fluid Flow, 29(5), 1347-1359. doi: http://dx.doi.org/10.1016/j.ijheatfluidflow.2008.04.003
Sano Masatoshi, S. I., Sakuraba Kenichiro,. (2009). Control of turbulent channel flow over a backward-facing step by suction. Journal of Fluid Science and Technology, 4(1), 188-199.
Santosh Christopher, D., Kanna, P. R., Madhusudhana, G. R., Venkumar, P., & Mohammed, H. A. (2012). Numerical Investigation of Heat Transfer from a Two-Dimensional Sudden Expansion Flow Using Nanofluids. Numerical Heat Transfer, Part A: Applications, 61(7), 527-546. doi: 10.1080/10407782.2012.666933
Sarafraz, M. M., & Hormozi, F. (2014). Scale formation and subcooled flow boiling heat transfer of CuO–water nanofluid inside the vertical annulus. Experimental Thermal and Fluid Science, 52(0), 205-214. doi: http://dx.doi.org/10.1016/j.expthermflusci.2013.09.012
Seban, R. A. (1959). Heat Transfer to Separated and Reattached Subsonic Turbulent Flows Obtained Downstream of a Surface Step. Journal of the Aerospace Sciences, 26(12), 809-814. doi: 10.2514/8.8324
Seban, R. A. (1966). . The effect of suction and injection on the heat transfer and flow in a turbulent separated air flow. Transaction of the ASME, 276-284.
Seban, R. A. (1966). The Effect of Suction and Injection on the Heat Transfer and Flow in a Turbulent Separated Airflow. Journal of Heat Transfer, 88(3), 276-282. doi: 10.1115/1.3691536
Seban, R. A., A. Emery and A. Levy. (1959). Heat transfer to separated and reattached subsonic turbulent flows obtained downstream of a surface step. Journal of Aerospace Science, 2, 809-814.

Seban, R. A., & American Society of Mechanical, E. (1965). The effect of suction and injection on the heat transfer and flow in a turbulent separated airflow. New York, N.Y.: ASME.
Seban, R. A., Emery, A., Levy, A. (1959). Heat transfer to separated and reattached subsonic turbulent flows obtained downstream of a surface step. J. Aerospace Science, 2, 809-814.
Seki, N., S. Fukusako and T. Hirata. (1976a). Effect of stall length on heat transfer in reattachment region behind a double step at entrance to an enlarged flat duct. . Int. J. Heat Mass Transfer, 19, 700-702.
Seki, N., S. Fukusako and T. Hirata. (1976b). Turbulent fluctuations and heat transfer for separated flow associated with a double step at entrance to an enlarged flat duct. ASME J. Heat Transfer, 98, 588-593.
Sellars J.R., T. M., Klein J.S (1956). Heat transfer to laminar flow in a around tube or flat conduit-the Graetz problem extend. Trans. Am. Soc. Mech. Engrs., 78, 441-448.
Shafahi, M., Bianco, V., Vafai, K., & Manca, O. (2010). Thermal performance of flat-shaped heat pipes using nanofluids. International Journal of Heat and Mass Transfer, 53(7–8), 1438-1445. doi: http://dx.doi.org/10.1016/j.ijheatmasstransfer.2009.12.007
Shah, S. N., Singhal, N. and Jain, S. (2004). Determination of Friction Pressure Losses in Straight and Coiled Tubing by CFD Simulations. AIAA / ASME symposium held in Oklahoma City.
Shahi, M., Mahmoudi, A. H., & Talebi, F. (2011). A numerical investigation of conjugated-natural convection heat transfer enhancement of a nanofluid in an annular tube driven by inner heat generating solid cylinder. International Communications in Heat and Mass Transfer, 38(4), 533-542. doi: http://dx.doi.org/10.1016/j.icheatmasstransfer.2010.12.022
Shahraki, F. (2002). MODELING OF BUOYANCY-DRIVEN FLOW AND HEAT TRANSFER FOR AIR IN A HORIZONTAL ANNULUS: EFFECTS OF VERTICAL ECCENTRICITY AND TEMPERATURE-DEPENDENT PROPERTIES. Numerical Heat Transfer, Part A: Applications, 42(6), 603-621. doi: 10.1080/10407780290059729
Shakouchi, T., & Kajino, I. (1994). Flow and forced-convection heat transfer over forward-facing double steps (effects of step ratio). Journal Name: Heat Transfer - Japanese Research; (United States); Journal Volume: 22:7, Medium: X; Size: Pages: 716-730.
Sheriff, N., & Gumley, P. (1966). Heat-transfer and friction properties of surfaces with discrete roughnesses. International Journal of Heat and Mass Transfer, 9(12), 1297-1320. doi: http://dx.doi.org/10.1016/0017-9310(66)90130-X
Shi, Y., Zhao, T. S., & Guo, Z. L. (2006). Finite difference-based lattice Boltzmann simulation of natural convection heat transfer in a horizontal concentric annulus. Computers & Fluids, 35(1), 1-15. doi: http://dx.doi.org/10.1016/j.compfluid.2004.11.003
Smyth, R. (1974). Heat transfer in turbulent separated flow. Journal of Nuclear Science and Technology, 1(12), 545-553.
Smyth, R. (1979). Turbulent flow over plane symmetric sudden expansion J. Heat Transfer ASME Trans, 101 348-353.
Sogin, H. H. (1964). A Summary of Experiments on Local Heat Transfer From the Rear of Bluff Obstacles to a Low Speed Airstream. Journal of Heat Transfer, 86(2), 200-202. doi: 10.1115/1.3687094
Soong, C. Y., & Hsueh, W. C. (1993). Mixed convection in a suddenly-expanded channel with effects of cold fluid injection. International Journal of Heat and Mass Transfer, 36(6), 1477-1484. doi: http://dx.doi.org/10.1016/S0017-9310(05)80058-4

Sorgun M., O. R. E., Ozbayoglu M.E., Ozbayoglu A.M. (2013). An Experimental and numerical study of Two-Phase flow in horizontal eccentric annuli. Energy Sources Part A. 2013; 35:891-8., 35, 891-899.
Sparrow, E. M., Chuck, W. (1987). PC solutions for the heat transfer and fluid flow downstream of an abrupt asymmetric enlargement in a channel. Numer. Heat Transfer, 12, 19–40.
Stein, R. P., & Begell, W. (1958). Heat transfer to water in turbulent flow in internally heated annuli. AIChE Journal, 4(2), 127-131. doi: 10.1002/aic.690040203
Stüer, H., Gyr, A., & Kinzelbach, W. (1999). Laminar separation on a forward facing step. European Journal of Mechanics - B/Fluids, 18(4), 675-692. doi: http://dx.doi.org/10.1016/S0997-7546(99)00104-1
Stuer H., G. A., Kinzelbach W., . (1999). Laminar separation on a forward facing step. Eur. J. Mech. B\Fluids 18 657-692.
Suzuki, H., K. Suzuki, S. Kida and T. Nakamae. (1991). Heat transfer augmentation in the region downstream of a backward-facing step (Effects of a cylinder mounted near the top comer of the step). Trans JSME S7B, 1410-1415.
Suzuki, K., Y.M. Kang, T. Sugimoto and T. Sato. (1982). Heat transfer in the downstream region of an orifice in a tube. Trans JSME B48, 132-140.
Tavman, I., & Turgut, A. (2010). An Investigation on Thermal Conductivity and Viscosity of Water Based Nanofluids. In S. Kakaç, B. Kosoy, D. Li & A. Pramuanjaroenkij (Eds.), Microfluidics Based Microsystems (pp. 139-162): Springer Netherlands.
Teng, T.-P., Hung, Y.-H., Teng, T.-C., Mo, H.-E., & Hsu, H.-G. (2010). The effect of alumina/water nanofluid particle size on thermal conductivity. Applied Thermal Engineering, 30(14–15), 2213-2218. doi: http://dx.doi.org/10.1016/j.applthermaleng.2010.05.036
Terekhov, V. I., N.I., Y., & R.F., Z. (2003). Some features of a turbulent separated flow and heat transfer behind a step and a rib 2-Heat transfer in a separated flow. Journal of applied Mechanics and Technical Physics, 44, 522-531.
Terekhov, V. I., & Pakhomov, M. A. (2009). Predictions of turbulent flow and heat transfer in gas–droplets flow downstream of a sudden pipe expansion. International Journal of Heat and Mass Transfer, 52(21–22), 4711-4721. doi: http://dx.doi.org/10.1016/j.ijheatmasstransfer.2009.06.018
Terekhov, V. I., Yarygina, N. I., & Zhdanov, R. F. (2003). Heat transfer in turbulent separated flows in the presence of high free-stream turbulence. International Journal of Heat and Mass Transfer, 46(23), 4535-4551. doi: http://dx.doi.org/10.1016/S0017-9310(03)00291-6
Terhaar, S., Velazquez, A., Arias, J. R., & Sanchez-Sanz, M. (2010). Experimental study on the unsteady laminar heat transfer downstream of a backwards facing step. International Communications in Heat and Mass Transfer, 37(5), 457-462. doi: http://dx.doi.org/10.1016/j.icheatmasstransfer.2010.01.009
Thiruvengadam, M., Armaly, B. F., & Drallmeier, J. A. (2009). Three dimensional mixed convection in plane symmetric-sudden expansion: Symmetric flow regime. International Journal of Heat and Mass Transfer, 52(3–4), 899-907. doi: http://dx.doi.org/10.1016/j.ijheatmasstransfer.2008.06.028
Tinney, C. E., & Ukeiley, L. S. (2009). A study of a 3-D double backward-facing step. Experiments in Fluids, 47(3), 427-438. doi: 10.1007/s00348-009-0675-9

Togun, H., Shkarah, A. J., Kazi, S. N., & Badarudin, A. (2013). CFD Simulation of Heat Transfer and Turbulent Fluid Flow over a Double Forward-Facing Step. Mathematical Problems in Engineering, 2013, 10. doi: 10.1155/2013/895374
Tseng, Y. S., Ferng, Y. M., & Lin, C. H. (2014). Investigating flow and heat transfer characteristics in a fuel bundle with split-vane pair grids by CFD methodology. Annals of Nuclear Energy, 64(0), 93-99. doi: http://dx.doi.org/10.1016/j.anucene.2013.09.037
Tsou, F. K., S.J. Chen and W. Aung. (1991). Starting flow and heat transfer downstream of a backward-facing step. Journal of Heat Transfer, 113, 583-589.
Tun-Ping Teng, Y.-H. H., Tun-Chien Teng, Jyun-Hong Chen. (2011). Performance evaluation on an air-cooled heat exchanger for alumina nanofluid under laminar flow. Nanoscale Research Letters, 6(1), 488-499.
Tuqa, A., Hussein, T., Ariffin, M. K. A., Kazi, S. N., Badarudin, A., Adam, N. M., & Masuri, S. (2014). Heat Transfer and Turbulent Fluid Flow over Vertical Double Forward-Facing Step. World Academy of Science, Engineering and Technology, 86, 722-726.
Uruba, V., Jonáš, P., & Mazur, O. (2007). Control of a channel-flow behind a backward-facing step by suction/blowing. International Journal of Heat and Fluid Flow, 28(4), 665-672. doi: http://dx.doi.org/10.1016/j.ijheatfluidflow.2007.04.002
V Scherer, S. W. (1991). The influence of the recirculation region: a comparison of the convective heat transfer downstream of a backward facing-step and behind a jet in a cross flow. J. Eng Gas Turbines and Power, 113, 126-134.
V.I. Terekhov, T. V. B. (2008). Effect of boundary layer thickness before the flow separation on aerodynamic characteristic and heat transfer behind an abrupt expansion in a round tube. J. thermophysics and Aeromechanics, 15, 91-97.
Vajjha, R. S., & Das, D. K. (2009). Experimental determination of thermal conductivity of three nanofluids and development of new correlations. International Journal of Heat and Mass Transfer, 52(21–22), 4675-4682. doi: http://dx.doi.org/10.1016/j.ijheatmasstransfer.2009.06.027
Velazquez, A., Arias, J. R., & Mendez, B. (2008). Laminar heat transfer enhancement downstream of a backward facing step by using a pulsating flow. International Journal of Heat and Mass Transfer, 51(7–8), 2075-2089. doi: http://dx.doi.org/10.1016/j.ijheatmasstransfer.2007.06.009
Vogel, J. C., & Eaton, J. K. (1985). Combined Heat Transfer and Fluid Dynamic Measurements Downstream of a Backward-Facing Step. Journal of Heat Transfer, 107(4), 922-929. doi: citeulike-article-id:10521008
doi: 10.1115/1.3247522
Vogel, J. C. a. J. K. E. (1985). Combined heat transfer and fluid dynamic measurements downstream of a backward–facing step. J. of heat transfer ASME Trans., 107, 922-929.
W. Aung, R. J. G. (1972). Heat transfer in turbulent separated flow downstream of a rearward-facing step. Israel J. of Tech., 10, 35-41.
W.D. Moss, S. B. (1980). Re-Circulating flows associated with two dimensional steps. The Aeronautical Q. , 31, 151-172
Waheed, M. A. (2007). An Approach to the Simulation of Natural-Convective Heat Transfer between Two Concentric Horizontal Cylindrical Annuli. Numerical Heat Transfer, Part A: Applications, 53(3), 323-340. doi: 10.1080/10407780701632510
Warren Rohsenow M., J. H. P., Young Cho I. (1998). Handbook of Heat transfer Third Edition New York, 1998 , pp.5.32.

Wilhelm, D., & Kleiser, L. (2002). Application of a Spectral Element Method to Two-Dimensional Forward-Facing Step Flow. Journal of Scientific Computing, 17(1-4), 619-627. doi: 10.1023/A:1015178831786
Wolfshtein, M. (1969). The velocity and temperature distribution in one-dimensional flow with turbulence augmentation and pressure gradient. International Journal of Heat and Mass Transfer, 12(3), 301-318. doi: http://dx.doi.org/10.1016/0017-9310(69)90012-X
Wongcharee, K., & Eiamsa-ard, S. (2012). Heat transfer enhancement by using CuO/water nanofluid in corrugated tube equipped with twisted tape. International Communications in Heat and Mass Transfer, 39(2), 251-257. doi: http://dx.doi.org/10.1016/j.icheatmasstransfer.2011.11.010
Worsøe-Schmidt, P. M. (1967). Heat transfer in the thermal entrance region of circular tubes and annular passages with fully developed laminar flow. International Journal of Heat and Mass Transfer, 10(4), 541-551. doi: http://dx.doi.org/10.1016/0017-9310(67)90173-1
Xuan, Y., & Roetzel, W. (2000). Conceptions for heat transfer correlation of nanofluids. International Journal of Heat and Mass Transfer, 43(19), 3701-3707. doi: http://dx.doi.org/10.1016/S0017-9310(99)00369-5
Y-T Yang, M. L. H. (1998). Numerical studies of heat transfer characteristics by using jet discharge at downstream of a backward-facing-step. J. Acta Mechanica, 128, 29-37.
Y Yin, Y. N., M Tagawa. (1992). Numerical prediction of turbulent heat transfer in high-Prandtl-number fluids. Trans JSME, B58, 2254-2260.
Y. Nagano, M. H. (1987). Improved form of k-ϵ model for wall turbulent shear flows. ASME J. Fluids Engng. , 109, 156-160.
Y. Nagano, M. T. (1990). An improved k-ϵ model for boundary layer flows. ASME J. Fluids Engng., 112, 33-39.
Y. Nagano, M. T. a. T. T. (1991). An Improved Two-Equation Heat Transfer Model for Wall Turbulent Shear Flows. Proceedings of 3rd ASME/JSME Thermal Engineering Joint Conference, 3, 233-240.
Y.L. Tsay, T. S. C., J.C. Cheng. (2005). Heat transfer enhancement of backward facing-step flow in a channel by using baffle installation on the channel wall. Acta Mechanica, 174, 63-76.
Yang C.S., J. D. Z., Tang U.H., Gau C. . (2009). Flow and heat transfer of natural convection in horizontal annulus with a heating element on inner cylinder J. Heat Transfer 131(8), 082502.082501 - 082502.082506.
Yang, J.-T., & Tsai, C.-H. (1996). High temperature heat transfer of separated flow over a sudden-expansion with base mass injection. International Journal of Heat and Mass Transfer, 39(11), 2293-2301. doi: http://dx.doi.org/10.1016/0017-9310(95)00309-6
Yang, Y., Zhang, Z. G., Grulke, E. A., Anderson, W. B., & Wu, G. (2005). Heat transfer properties of nanoparticle-in-fluid dispersions (nanofluids) in laminar flow. International Journal of Heat and Mass Transfer, 48(6), 1107-1116. doi: http://dx.doi.org/10.1016/j.ijheatmasstransfer.2004.09.038
Yılmaz, I. l., & Öztop, H. F. (2006). Turbulence forced convection heat transfer over double forward facing step flow. International Communications in Heat and Mass Transfer, 33(4), 508-517. doi: http://dx.doi.org/10.1016/j.icheatmasstransfer.2005.08.015
Yoshikawa Hiroyuki, I. K., Ota Terukazu. (2004). Numerical Simulation of Three-Dimensional Separated Flow and Heat Transfer in an Enlarged Rectangular Channel. J. Nippon Dennetsu Shinpojiumu Koen Ronbunshu. J. Nippon Dennetsu Shinpojiumu Koen Ronbunshu, 41, 221-222.

Yoshikawa Hiroyuki, Y. M., Ota Terukazu. (2002). Numerical Simulation of Heat Transfer in Unsteady Separated and Reattached Flow Around a Symmetric Sudden Expansion Channel. J. Nippon Dennetsu Shinpojiumu Koen Ronbunshu 39, 15-16.
Yu, B., Kawaguchi, Y., Kaneda, M., Ozoe, H., & Churchill, S. W. (2005). The computed characteristics of turbulent flow and convection in concentric circular annuli. Part II. Uniform heating on the inner surface. International Journal of Heat and Mass Transfer, 48(3–4), 621-634. doi: http://dx.doi.org/10.1016/j.ijheatmasstransfer.2004.08.022
Z. Mehrez, M. Bouterra, A. El Cafsi, A. Belghith, & Quéré, P. L. (2010). Simulation of the Periodically Perturbed Separated and Reattaching Flow over a Backward-Facing Step. Journal of Applied Fluid Mechanics, 3(2), 1-8.
Z. Yang, H. T. S. (1993). New time scale based k-ϵ model for near-wall turbulence. AIAA J. , 31, 1191-1198.
Zamzamian, A., Oskouie, S. N., Doosthoseini, A., Joneidi, A., & Pazouki, M. (2011). Experimental investigation of forced convective heat transfer coefficient in nanofluids of Al2O3/EG and CuO/EG in a double pipe and plate heat exchangers under turbulent flow. Experimental Thermal and Fluid Science, 35(3), 495-502. doi: http://dx.doi.org/10.1016/j.expthermflusci.2010.11.013
Zemanick, P. P. a. R. S. (1970). Local heat transfer downstream of abrupt circular channel expansion. J. Heat Transfer, 92, 53-60.
Zhang, C. X. (1994). Numerical predictions of turbulent recirculating flows with a κ-ϵ model. Journal of Wind Engineering and Industrial Aerodynamics, 51(2), 177-201. doi: http://dx.doi.org/10.1016/0167-6105(94)90003-5
Zouhaier Mehrez, Mourad Bouterra, Afif El Cafsi, Ali Belghith, & Quere, P. L. (2010). Heat transfer control of separated and reattaching flow by local forcing – effect of Richardson number. Journal of applied science in the thermodynamics and fluid mechanics, 4, 1802-9388.

APPENDIX A

UNCERTAINTY ANALYSIS

Introduction

In order to determine the accuracy for the non-dimensional parameters such as the Reynolds and Nusselt numbers, the heat transfer parameter, the uncertainty of the heat transferred, the energy balance obtained, mass flow rates, inlet, outlet and wall temperatures will be analyzed.

Theory

The result R of the experiment is calculated from a set of measurements using a group of equations. The result R is a function of several variables and is given by Moffat (Moffat, 1985) as:

$$R = f\,cn(x_1, x_2, \ldots, x_n) \tag{B.1}$$

Hence the effect of the uncertainty in a single measurement on the calculated result, if only that one measurement were in error would be:

$$\delta R = \frac{\partial R}{\partial x_i} \cdot \delta x_i \tag{B.2}$$

The partial derivative of R with respect to x_i is the sensitivity coefficient for the result R with respect to the measurement x_i. For several independent variables, the uncertainty of R can be found by a root-sum-square method. Hence for several independent variables the uncertainty of R is described by Moffat (1988) as:

$$\delta R = \left[\sum_{i=1}^{n} \left(\frac{\partial R}{\partial x_i} \cdot \delta x_i\right)^2\right]^{0.5} \tag{B.3}$$

Terms in the uncertainty equations that 3 times smaller than the largest term are suppressed by the root-sum-square method. Hence small terms have very small effects Moffat (1988).

Uncertainties

Uncertainties of the instrumentation

Instrumentation that is used in the current study includes thermocouples, magnetic flow meters, pressure transducers and the power supply. The uncertainty falls within the 95% confidence region.

Heat transfer uncertainties

Inlet and outlet and station temperatures

Since only one thermocouple was used to measure inlet temperature and one thermocouple to measure the outlet thermocouple the uncertainty of the measurement remains 0.1℃. For the stations also only one thermocouple was used and here the uncertainty is 0.1℃.

Fluid properties

All fluid properties and their uncertainties were calculated from the formulations obtained by (Popiel & Wojtkowiak, 1998). The uncertainties of the properties are given in Table 0..

Table 0.1 Uncertainties of fluid properties

Property	Uncertainty
Specific heat	2%
Thermal conductivity	5%
Dynamic viscosity	1%

Heat transfer coefficient

The heat transfer coefficient is calculated from

$$h(x) = \frac{\dot{q}}{T_w(x) - T_b(x)} \tag{B.4}$$

with its uncertainty given by

$$\delta h(x) = \left[\left(\frac{\partial h(x)}{\partial \dot{q}} \cdot \delta \dot{q}\right)^2 + \left(\frac{\partial h(x)}{\partial T_w} \cdot \delta T_w\right)^2 + \left(\frac{\partial h(x)}{\partial T_b} \cdot \delta T_b\right)^2\right]^{0.5} \tag{B.5}$$

$$\delta h(x) = \left[\left(\frac{\delta \dot{q}}{T_w(x) - T_b(x)}\right)^2 + \left(\frac{-\dot{q}}{(T_w(x) - T_b(x))^2} \cdot \delta T_w\right)^2 + \left(\frac{-\dot{q}}{T_w(x) - T_b(x)} \cdot \delta T_m\right)^2\right]^{0.5} \tag{B.6}$$

The wall temperatures are measured at 13 stations, and between each station the local heat transfer coefficient is calculated. The average heat transfer coefficient was obtained by adding all the local heat transfer coefficients and then dividing the result by 12.

$$h_{avg} = \frac{1}{n} \cdot (h(x_1) + \cdots + h(x_n)) \tag{B.7}$$

$$\delta h_{avg} = \left[\left(\frac{\partial h_{avg}}{\partial h(x_1)} \cdot \delta h(x_1)\right)^2 + \cdots + \left(\frac{\partial h_{avg}}{\partial h(x_n)} \cdot \delta h(x_n)\right)^2\right]^{0.5} \tag{B.8}$$

hence the uncertainty of the average heat transfer coefficient is determined by equation B.9

$$\delta h_{avg} = \frac{1}{n} \cdot (\delta h(x_1)^2 + \cdots + \delta h(x_n)^2)^{0.5} \tag{B.9}$$

Heat flux

The heat flux is calculated from

$$\dot{q}_{in} = \dot{Q}_{in}/A_s \tag{B.10}$$

with its uncertainty given by

$$\delta\dot{q}_{in} = \left[\left(\frac{\partial \dot{q}_{in}}{\partial \dot{Q}_{in}} \cdot \delta\dot{Q}_{in}\right)^2 + \left(\frac{\partial \dot{q}_{in}}{\partial A_s} \cdot \delta A_s\right)^2\right]^{0.5} \tag{B.11}$$

$$\delta\dot{q}_{in} = \left[\left(\frac{\partial \dot{Q}_{in}}{A_s}\right)^2 + \left(-\frac{\dot{Q}_{in}}{A_s^2} \cdot \delta A_s\right)^2\right]^{0.5} \tag{B.12}$$

Heat transfer

The input heat transfer uncertainty is calculated from

$$\dot{Q} = V \cdot I \tag{B.13}$$

with the uncertainty given by

$$\delta\dot{Q} = \left[\left(\frac{\partial \dot{Q}}{\partial V} \cdot \delta V\right)^2 + \left(\frac{\partial \dot{Q}}{\partial I} \cdot \delta I\right)^2\right]^{0.5} \tag{B.14}$$

$$\delta\dot{Q} = [(I \cdot \delta V)^2 + (V \cdot \delta I)^2]^2 \tag{B.15}$$

Heat transfer area

The heat transfer area is calculated from

$$A_s = \pi \cdot D \cdot L \tag{B.16}$$

with its uncertainty given by

$$\delta A_s = \left[\left(\frac{\partial A_s}{\partial D} \cdot \delta D\right)^2 + \left(\frac{\partial A_s}{\partial L} \cdot \delta L\right)^2\right]^{0.5} \tag{B.17}$$

$$\delta A_s = [(\pi \cdot \delta D \cdot L)^2 + (\pi \cdot D \cdot \delta L)^2]^{0.5} \tag{B.18}$$

Perimeter of test section

The perimeter of the test section is calculated from

$$P = \pi \cdot D \tag{B.20}$$

with its uncertainty given by

$$\delta P = \left[\left(\frac{\partial P}{\partial D} \cdot \delta D\right)^2\right]^{0.5} \tag{B.21}$$

$$\delta P = \pi \cdot \delta D \tag{B.22}$$

Dimensionless parameters

Since all fluid flow and heat transfer equations are in terms of dimensionless parameters, the uncertainties of these parameters are determined. The Nusselt, Reynolds and Prandtl number are mainly used in the study of heat transfer their respective uncertainties are shown below.

$$Nu_{avg} = \frac{h_{avg} \cdot D}{k} \tag{B.23}$$

with its uncertainty given by

$$\delta Nu_{avg} = \left[\left(\frac{\partial Nu_{avg}}{\partial h_{avg}} \cdot \delta h_{avg}\right)^2 + \left(\frac{\partial Nu_{avg}}{\partial D} \cdot \delta D\right)^2 + \left(\frac{\partial Nu_{avg}}{\partial k} \cdot \delta k\right)^2\right]^{0.5} \tag{B.24}$$

$$\delta Nu_{avg} = \left[\left(\frac{D}{k} \cdot \delta h_{avg}\right)^2 + \left(\frac{h_{avg}}{k} \cdot \delta D\right)^2 + \left(-\frac{h_{avg}}{k^2} \cdot \delta k\right)^2\right]^{0.5} \tag{B.25}$$

$$Re = \frac{4 \cdot \dot{m}}{\mu \cdot D \cdot \pi} \tag{B.26}$$

with its uncertainty given by

$$\delta Re = \left[\left(\frac{\partial Re}{\partial \dot{m}} \cdot \delta \dot{m}\right)^2 + \left(\frac{\partial Re}{\partial \mu} \cdot \delta \mu\right)^2 + \left(\frac{\partial Re}{\partial D} \cdot \delta D\right)^2\right]^{0.5} \tag{B.27}$$

$$\delta Re = \left[\left(\frac{4}{\mu \cdot D \cdot \pi} \cdot \delta \dot{m}\right)^2 + \left(-\frac{4 \cdot \dot{m}}{\mu^2 \cdot D \cdot \pi} \cdot \delta \mu\right)^2 + \left(-\frac{4 \cdot \dot{m}}{\mu \cdot D^2 \cdot \pi} \cdot \delta D\right)^2\right]^{0.5} \tag{B.28}$$

APPENDIX B

NUMERICAL DATA FOR SURFACE HEAT TRANSFER COEFFICIENT

Table B1: Surface heat transfer coefficient for Al_2O_3 nanofluids at ER=1.67

Axial Position , Z(m)	Re= 50,000	Re= 40,000	Re= 30,000	Re= 20,000
1.502	875.81	829.582	783.354	737.126
1.50401	846.774	716.987	587.2	457.413
1.50601	864.679	681.279	497.879	314.479
1.50802	1028.68	845.192	661.704	478.216
1.51002	1281.78	1069.042	856.304	643.566
1.51202	1518.38	1249.69	981	712.31
1.51403	1723.89	1411.73	1099.57	787.41
1.51603	1910.6	1573.92	1237.24	900.56
1.51804	2085.01	1726.66	1368.31	1009.96
1.52004	2249.79	1864.96	1480.13	1095.3
1.52204	2406.59	1993.48	1580.37	1167.26
1.52405	2556.45	2114.82	1673.19	1231.56
1.52605	2699.95	2229.94	1759.93	1289.92
1.52806	2837.39	2339.35	1841.31	1343.27
1.53006	2968.96	2443.38	1917.8	1392.22
1.53206	3094.79	2542.19	1989.59	1436.99
1.53407	3215.04	2635.9	2056.76	1477.62
1.53607	3329.84	2724.71	2119.58	1514.45
1.53808	3439.27	2808.83	2178.39	1547.95
1.54008	3543.48	2888.27	2233.06	1577.85
1.54208	3642.57	2963.05	2283.53	1604.01
1.54409	3736.71	3033.5	2330.29	1627.08
1.54609	3826.02	3099.82	2373.62	1647.42
1.5481	3910.65	3161.86	2413.07	1664.28
1.5501	3990.88	3220.15	2449.42	1678.69
1.5521	4067.03	3275.15	2483.27	1691.39
1.55411	4139.62	3327.1	2514.58	1702.06
1.55611	4209.09	3376.47	2543.85	1711.23
1.55812	4276.09	3424.1	2572.11	1720.12
1.56012	4341.71	3471.01	2600.31	1729.61
1.56212	4407.74	3518.98	2630.22	1741.46

1.56413	4473.26	3567.18	2661.1	1755.02
1.56613	4535.68	3612.96	2690.24	1767.52
1.56814	4594.19	3655.45	2716.71	1777.97
1.57014	4648.71	3694.56	2740.41	1786.26
1.57214	4699.08	3730.12	2761.16	1792.2
1.57415	4745.31	3761.81	2778.31	1794.81
1.57615	4787.36	3789.98	2792.6	1795.22
1.57816	4825.41	3814.73	2804.05	1793.37
1.58016	4860.38	3836.74	2813.1	1789.46
1.58216	4892.76	3856.6	2820.44	1784.28
1.58417	4922.73	3874.2	2825.67	1777.14
1.58617	4950.33	3889.07	2827.81	1766.55
1.58818	4975.72	3901.75	2827.78	1753.81
1.59018	4998.96	3913.07	2827.18	1741.29
1.59218	5019.94	3922.75	2825.56	1728.37
1.59419	5038.68	3930.64	2822.6	1714.56
1.59619	5055.46	3937.13	2818.8	1700.47
1.5982	5070.35	3942.17	2813.99	1685.81
1.6002	5083.3	3945.84	2808.38	1670.92
1.6022	5094.73	3948.64	2802.55	1656.46
1.60421	5104.77	3950.48	2796.19	1641.9
1.60621	5113.41	3951.36	2789.31	1627.26
1.60822	5120.78	3951.46	2782.14	1612.82
1.61022	5126.99	3950.98	2774.97	1598.96
1.61222	5132.03	3950.18	2768.33	1586.48
1.61423	5135.8	3948.74	2761.68	1574.62
1.61623	5138.54	3946.68	2754.82	1562.96
1.61824	5140.28	3944.41	2748.54	1552.67
1.62024	5140.81	3941.22	2741.63	1542.04
1.62224	5140.46	3936.76	2733.06	1529.36
1.62425	5139.32	3931.69	2724.06	1516.43
1.62625	5137.01	3925.6	2714.19	1502.78
1.62826	5133.76	3919.11	2704.46	1489.81
1.63026	5129.82	3912.34	2694.86	1477.38
1.63226	5124.98	3905.01	2685.04	1465.07
1.63427	5119.3	3896.83	2674.36	1451.89
1.63627	5112.71	3887.76	2662.81	1437.86
1.63828	5105.52	3878.9	2652.28	1425.66
1.64028	5097.75	3869.68	2641.61	1413.54
1.64228	5097.75	3869.06	2640.37	1411.68
1.64429	5089.26	3860.47	2631.68	1402.89
1.64629	5080.14	3851.46	2622.78	1394.1

1.6483	5070.29	3841.82	2613.35	1384.88
1.6503	5059.82	3831.89	2603.96	1376.03
1.6523	5048.81	3821.34	2593.87	1366.4
1.65431	5037.27	3809.97	2582.67	1355.37
1.65631	5025.24	3798.59	2571.94	1345.29
1.65832	5012.92	3787.43	2561.94	1336.45
1.66032	5000.16	3776	2551.84	1327.68
1.66232	4987.2	3764.52	2541.84	1319.16
1.66433	4974.09	3753.49	2532.89	1312.29
1.66633	4960.19	3741.94	2523.69	1305.44
1.66834	4942.45	3726.52	2510.59	1294.66
1.67034	4919.73	3706.46	2493.19	1279.92
1.67234	4901.11	3690.75	2480.39	1270.03
1.67234	4889.86	3679.5	2469.14	1258.78
1.67435	4878.38	3670.94	2463.5	1256.06
1.67635	4862.55	3658.2	2453.85	1249.5
1.67836	4841.95	3640.84	2439.73	1238.62
1.68036	4817.9	3620.56	2423.22	1225.88
1.68236	4792.41	3599.45	2406.49	1213.53
1.68437	4766.7	3578.43	2390.16	1201.89
1.68637	4741.4	3558.06	2374.72	1191.38
1.68838	4716.65	3538.19	2359.73	1181.27
1.69038	4692.11	3518.46	2344.81	1171.16
1.69238	4667.67	3499.17	2330.67	1162.17
1.69439	4643.63	3480.44	2317.25	1154.06
1.69639	4619.74	3462.01	2304.28	1146.55
1.6984	4595.88	3443.85	2291.82	1139.79
1.7004	4572.04	3425.73	2279.42	1133.11
1.7024	4548.18	3407.43	2266.68	1125.93
1.70441	4524.38	3387.6	2250.82	1114.04
1.70641	4500.63	3367.5	2234.37	1101.24
1.70842	4476.94	3353.16	2229.38	1105.6
1.71042	4453.25	3341.2	2229.15	1117.1
1.71242	4429.39	3325.06	2220.73	1116.4
1.71443	4405.37	3305.73	2206.09	1106.45
1.71643	4381.5	3284.56	2187.62	1090.68
1.71844	4357.55	3264.7	2171.85	1079
1.72044	4333.73	3248.06	2162.39	1076.72
1.72244	4309.96	3232.96	2155.96	1078.96
1.72445	4285.94	3218.1	2150.26	1082.42
1.72645	4262.07	3203.42	2144.77	1086.12
1.72846	4238.3	3188.75	2139.2	1089.65

1.73046	4214.62	3174.21	2133.8	1093.39
1.73246	4191.05	3159.84	2128.63	1097.42
1.73447	4167.61	3145.48	2123.35	1101.22
1.73647	4144.37	3131.28	2118.19	1105.1
1.73848	4121.32	3117.37	2113.42	1109.47
1.74048	4098.48	3103.61	2108.74	1113.87
1.74248	4075.95	3090.13	2104.31	1118.49
1.74449	4053.74	3077.09	2100.44	1123.79
1.74649	4031.65	3064.1	2096.55	1129
1.7485	4009.79	3051.33	2092.87	1134.41
1.7505	3988.31	3039.1	2089.89	1140.68
1.7525	3967.16	3027.18	2087.2	1147.22
1.75451	3946.24	3015.5	2084.76	1154.02
1.75651	3925.53	3004.47	2083.41	1162.35
1.75852	3905.06	2993.75	2082.44	1171.13
1.76052	3884.76	2983.09	2081.42	1179.75
1.76252	3864.58	2972.68	2080.78	1188.88
1.76453	3844.53	2962.52	2080.51	1198.5
1.76653	3824.57	2952.54	2080.51	1208.48
1.76854	3804.6	2942.59	2080.58	1218.57
1.77054	3784.6	2932.73	2080.86	1228.99
1.77255	3764.58	2922.8	2081.02	1239.24
1.77455	3744.45	2912.76	2081.07	1249.38
1.77655	3744.45	2922.79	2101.13	1279.47
1.77856	3724.3	2912.48	2100.66	1288.84
1.78056	3704.09	2902.02	2099.95	1297.88
1.78257	3683.79	2891.38	2098.97	1306.56
1.78457	3663.32	2880.51	2097.7	1314.89
1.78657	3642.71	2869.32	2095.93	1322.54
1.78858	3622.04	2857.97	2093.9	1329.83
1.79058	3601.18	2846.35	2091.52	1336.69
1.79058	3580.35	2825.52	2070.69	1315.86
1.79259	3559.61	2813.9	2068.19	1322.48
1.79459	3538.76	2801.96	2065.16	1328.36
1.79659	3518.08	2789.89	2061.7	1333.51
1.7986	3497.58	2778.03	2058.48	1338.93
1.8006	3477.13	2766.01	2054.89	1343.77
1.80261	3456.96	2753.96	2050.96	1347.96
1.80461	3437.11	2742.21	2047.31	1352.41
1.80661	3417.63	2730.66	2043.69	1356.72
1.80862	3398.51	2719.19	2039.87	1360.55
1.81062	3379.81	2707.94	2036.07	1364.2

1.81263	3361.68	2697.23	2032.78	1368.33
1.81463	3344.12	2686.99	2029.86	1372.73
1.81663	3327.14	2677.06	2026.98	1376.9
1.81864	3310.78	2667.52	2024.26	1381
1.82064	3294.98	2658.41	2021.84	1385.27
1.82265	3279.8	2649.69	2019.58	1389.47
1.82465	3265.25	2641.37	2017.49	1393.61
1.82665	3251.25	2633.48	2015.71	1397.94
1.82866	3237.8	2625.96	2014.12	1402.28
1.83066	3224.87	2618.83	2012.79	1406.75
1.83267	3212.31	2612.05	2011.79	1411.53
1.83467	3200.14	2605.55	2010.96	1416.37
1.83667	3188.37	2599.22	2010.07	1420.92
1.83868	3176.88	2593.11	2009.34	1425.57
1.84068	3165.56	2587.01	2008.46	1429.91
1.84269	3154.42	2580.92	2007.42	1433.92
1.84469	3143.31	2574.79	2006.27	1437.75
1.84669	3132.27	2568.58	2004.89	1441.2
1.8487	3121.2	2562.2	2003.2	1444.2
1.8507	3110.03	2555.59	2001.15	1446.71
1.85271	3098.87	2548.87	1998.87	1448.87
1.85471	3087.52	2541.86	1996.2	1450.54
1.85671	3076.07	2534.68	1993.29	1451.9
1.85872	3064.53	2527.35	1990.17	1452.99
1.86072	3052.71	2519.63	1986.55	1453.47
1.86273	3040.8	2511.77	1982.74	1453.71
1.86473	3028.84	2503.75	1978.66	1453.57
1.86673	3016.68	2495.38	1974.08	1452.78
1.86874	3004.38	2486.79	1969.2	1451.61
1.87074	2992.04	2478.1	1964.16	1450.22
1.87275	2979.57	2469.2	1958.83	1448.46
1.87475	2967.01	2460.12	1953.23	1446.34
1.87675	2954.41	2450.92	1947.43	1443.94
1.87876	2941.73	2441.59	1941.45	1441.31
1.88076	2929.01	2432.18	1935.35	1438.52
1.88277	2916.35	2422.69	1929.03	1435.37
1.88477	2903.75	2413.24	1922.73	1432.22
1.88677	2891.12	2403.7	1916.28	1428.86
1.88878	2878.54	2394.14	1909.74	1425.34
1.89078	2866.03	2384.56	1903.09	1421.62
1.89279	2853.59	2375.01	1896.43	1417.85
1.89479	2841.24	2365.5	1889.76	1414.02

1.89679	2828.99	2356.02	1883.05	1410.08
1.8988	2816.84	2346.59	1876.34	1406.09
1.9008	2804.8	2337.22	1869.64	1402.06
1.90281	2792.88	2327.93	1862.98	1398.03
1.90481	2781.08	2318.67	1856.26	1393.85
1.90681	2769.39	2309.5	1849.61	1389.72
1.90882	2769.39	2311.98	1854.57	1397.16
1.91082	2757.79	2302.84	1847.89	1392.94
1.91283	2746.42	2293.89	1841.36	1388.83
1.91483	2735.27	2285.02	1834.77	1384.52
1.91683	2724.21	2276.22	1828.23	1380.24
1.91884	2713.27	2267.53	1821.79	1376.05
1.92084	2702.48	2258.96	1815.44	1371.92
1.92084	2691.83	2248.31	1804.79	1361.27
1.92285	2681.39	2240.05	1798.71	1357.37
1.92485	2671.11	2231.93	1792.75	1353.57
1.92685	2660.96	2223.89	1786.82	1349.75
1.92886	2651	2215.94	1780.88	1345.82
1.93086	2641.13	2208.08	1775.03	1341.98
1.93287	2631.42	2200.35	1769.28	1338.21
1.93487	2621.84	2192.7	1763.56	1334.42
1.93687	2612.34	2185.09	1757.84	1330.59
1.93888	2603.02	2177.58	1752.14	1326.7
1.94088	2593.87	2170.25	1746.63	1323.01
1.94289	2584.86	2163.04	1741.22	1319.4
1.94489	2575.97	2155.87	1735.77	1315.67
1.94689	2567.2	2148.8	1730.4	1312
1.9489	2558.56	2141.84	1725.12	1308.4
1.9509	2550.07	2135.02	1719.97	1304.92
1.95291	2541.68	2128.3	1714.92	1301.54
1.95491	2533.39	2121.6	1709.81	1298.02
1.95691	2525.27	2115.08	1704.89	1294.7
1.95892	2517.23	2108.64	1700.05	1291.46
1.96092	2509.28	2102.22	1695.16	1288.1
1.96293	2501.43	2095.88	1690.33	1284.78
1.96493	2493.68	2089.62	1685.56	1281.5
1.96693	2486.11	2083.51	1680.91	1278.31
1.96894	2478.63	2077.43	1676.23	1275.03
1.97094	2471.18	2071.43	1671.68	1271.93
1.97295	2463.86	2065.56	1667.26	1268.96
1.97495	2456.68	2059.75	1662.82	1265.89
1.97695	2449.59	2053.97	1658.35	1262.73

1.97896	2442.51	2048.23	1653.95	1259.67
1.98096	2435.53	2042.58	1649.63	1256.68
1.98297	2428.7	2037.05	1645.4	1253.75
1.98497	2421.93	2031.58	1641.23	1250.88
1.98697	2415.26	2026.15	1637.04	1247.93
1.98898	2408.66	2020.73	1632.8	1244.87
1.99098	2402.12	2015.39	1628.66	1241.93
1.99299	2395.62	2010.08	1624.54	1239
1.99499	2389.21	2004.83	1620.45	1236.07
1.99699	2382.87	1999.67	1616.47	1233.27
1.999	2376.57	1994.52	1612.47	1230.42
2.001	2370.36	1989.43	1608.5	1227.57
2.00301	2364.22	1984.38	1604.54	1224.7
2.00501	2358.15	1979.42	1600.69	1221.96
2.00701	2352.14	1974.49	1596.84	1219.19
2.00902	2346.17	1969.6	1593.03	1216.46
2.01102	2340.27	1964.75	1589.23	1213.71
2.01303	2334.45	1959.93	1585.41	1210.89
2.01503	2328.64	1955.13	1581.62	1208.11
2.01703	2322.82	1950.31	1577.8	1205.29
2.01904	2317.09	1945.58	1574.07	1202.56
2.02104	2311.47	1940.95	1570.43	1199.91
2.02305	2305.88	1936.31	1566.74	1197.17
2.02505	2300.29	1931.66	1563.03	1194.4
2.02705	2294.78	1927.08	1559.38	1191.68
2.02906	2289.35	1922.53	1555.71	1188.89
2.03106	2283.93	1917.99	1552.05	1186.11
2.03307	2278.55	1913.54	1548.53	1183.52
2.03507	2273.23	1909.16	1545.09	1181.02
2.03707	2267.92	1904.74	1541.56	1178.38
2.03908	2262.67	1900.34	1538.01	1175.68
2.04108	2257.49	1895.99	1534.49	1172.99
2.04309	2252.34	1891.68	1531.02	1170.36
2.04509	2247.25	1887.43	1527.61	1167.79
2.04709	2242.18	1883.18	1524.18	1165.18
2.0491	2237.15	1878.94	1520.73	1162.52
2.0511	2232.16	1874.74	1517.32	1159.9
2.05311	2227.26	1870.65	1514.04	1157.43
2.05511	2222.4	1866.59	1510.78	1154.97
2.05511	2217.57	1861.76	1505.95	1150.14
2.05711	2212.78	1857.74	1502.7	1147.66
2.05912	2208.06	1853.77	1499.48	1145.19

2.06112	2203.37	1849.85	1496.33	1142.81
2.06313	2198.66	1845.92	1493.18	1140.44
2.06513	2194.02	1842.04	1490.06	1138.08
2.06713	2189.55	1838.33	1487.11	1135.89
2.06914	2185.15	1834.69	1484.23	1133.77
2.07114	2180.59	1830.86	1481.13	1131.4
2.07315	2175.98	1827	1478.02	1129.04
2.07515	2171.4	1823.11	1474.82	1126.53
2.07715	2171.4	1823.7	1476	1128.3
2.07916	2166.87	1819.76	1472.65	1125.54
2.08116	2162.32	1815.81	1469.3	1122.79
2.08317	2157.75	1811.87	1465.99	1120.11
2.08517	2153.29	1808.03	1462.77	1117.51
2.08717	2148.94	1804.29	1459.64	1114.99
2.08918	2144.69	1800.59	1456.49	1112.39
2.09118	2140.56	1797.01	1453.46	1109.91
2.09319	2136.45	1793.53	1450.61	1107.69
2.09519	2132.35	1790.09	1447.83	1105.57
2.09719	2128.33	1786.77	1445.21	1103.65
2.0992	2124.3	1783.43	1442.56	1101.69
2.1012	2120.29	1780.05	1439.81	1099.57
2.10321	2116.35	1776.75	1437.15	1097.55
2.10521	2112.41	1773.41	1434.41	1095.41
2.10721	2108.51	1770.11	1431.71	1093.31
2.10922	2104.69	1766.92	1429.15	1091.38
2.11122	2100.87	1763.72	1426.57	1089.42
2.11323	2097.07	1760.55	1424.03	1087.51
2.11523	2093.35	1757.43	1421.51	1085.59
2.11723	2089.66	1754.37	1419.08	1083.79
2.11924	2086.02	1751.35	1416.68	1082.01
2.12124	2082.41	1748.33	1414.25	1080.17
2.12325	2078.82	1745.31	1411.8	1078.29
2.12525	2075.27	1742.36	1409.45	1076.54
2.12725	2071.76	1739.42	1407.08	1074.74
2.12926	2068.3	1736.52	1404.74	1072.96
2.13126	2064.88	1733.65	1402.42	1071.19
2.13327	2061.46	1730.76	1400.06	1069.36
2.13527	2058.04	1727.84	1397.64	1067.44
2.13727	2054.69	1724.99	1395.29	1065.59
2.13928	2051.35	1722.15	1392.95	1063.75
2.14128	2048.02	1719.31	1390.6	1061.89
2.14329	2044.75	1716.53	1388.31	1060.09

2.14529	2041.52	1713.79	1386.06	1058.33
2.14729	2038.3	1711.07	1383.84	1056.61
2.1493	2035.11	1708.35	1381.59	1054.83
2.1513	2031.94	1705.66	1379.38	1053.1
2.15331	2028.78	1702.98	1377.18	1051.38
2.15531	2025.66	1700.31	1374.96	1049.61
2.15731	2022.58	1697.7	1372.82	1047.94
2.15932	2019.55	1695.14	1370.73	1046.32
2.16132	2016.54	1692.58	1368.62	1044.66
2.16333	2013.52	1690.02	1366.52	1043.02
2.16533	2010.54	1687.51	1364.48	1041.45
2.16733	2007.59	1685	1362.41	1039.82
2.16934	2004.72	1682.57	1360.42	1038.27
2.17134	2001.84	1680.12	1358.4	1036.68
2.17335	1998.95	1677.69	1356.43	1035.17
2.17535	1996.11	1675.3	1354.49	1033.68
2.17735	1993.33	1672.94	1352.55	1032.16
2.17936	1990.55	1670.59	1350.63	1030.67
2.18136	1987.8	1668.27	1348.74	1029.21
2.18337	1985.06	1665.97	1346.88	1027.79
2.18537	1982.36	1663.72	1345.08	1026.44
2.18737	1979.69	1661.48	1343.27	1025.06
2.18938	1977.03	1659.24	1341.45	1023.66
2.19138	1974.4	1657.03	1339.66	1022.29
2.19339	1971.84	1654.88	1337.92	1020.96
2.19539	1969.29	1652.72	1336.15	1019.58
2.19739	1966.72	1650.56	1334.4	1018.24
2.1994	1964.21	1648.47	1332.73	1016.99
2.2014	1961.74	1646.41	1331.08	1015.75
2.20341	1959.27	1644.37	1329.47	1014.57
2.20541	1956.82	1642.33	1327.84	1013.35
2.20741	1954.44	1640.34	1326.24	1012.14
2.20942	1952.06	1638.32	1324.58	1010.84
2.20942	1949.69	1635.95	1322.21	1008.47
2.21142	1947.36	1634.04	1320.72	1007.4
2.21343	1945.06	1632.16	1319.26	1006.36
2.21543	1945.06	1632.54	1320.02	1007.5
2.21743	1942.77	1630.64	1318.51	1006.38
2.21944	1940.51	1628.75	1316.99	1005.23
2.22144	1938.29	1626.9	1315.51	1004.12
2.22345	1936.06	1625.05	1314.04	1003.03
2.22545	1933.86	1623.2	1312.54	1001.88

2.22745	1931.71	1621.4	1311.09	1000.78
2.22946	1929.52	1619.59	1309.66	999.73
2.23146	1927.35	1617.78	1308.21	998.64
2.23347	1925.25	1616.01	1306.77	997.53
2.23547	1923.15	1614.25	1305.35	996.45
2.23747	1921.05	1612.49	1303.93	995.37
2.23948	1919	1610.8	1302.6	994.4
2.24148	1916.94	1609.11	1301.28	993.45
2.24349	1914.9	1607.43	1299.96	992.49
2.24549	1912.89	1605.78	1298.67	991.56
2.24749	1910.89	1604.12	1297.35	990.58
2.2495	1908.94	1602.51	1296.08	989.65
2.2515	1906.99	1600.88	1294.77	988.66
2.25351	1905.06	1599.27	1293.48	987.69
2.25551	1903.18	1597.74	1292.3	986.86
2.25751	1901.29	1596.19	1291.09	985.99
2.25952	1899.42	1594.64	1289.86	985.08
2.26152	1897.58	1593.12	1288.66	984.2
2.26353	1895.74	1591.59	1287.44	983.29
2.26553	1893.92	1590.1	1286.28	982.46
2.26753	1892.12	1588.62	1285.12	981.62
2.26954	1890.34	1587.14	1283.94	980.74
2.27154	1888.56	1585.68	1282.8	979.92
2.27355	1886.8	1584.23	1281.66	979.09
2.27555	1885.08	1582.8	1280.52	978.24
2.27755	1883.37	1581.38	1279.39	977.4
2.27956	1881.64	1579.95	1278.26	976.57
2.28156	1879.96	1578.58	1277.2	975.82
2.28357	1878.32	1577.24	1276.16	975.08
2.28557	1876.68	1575.87	1275.06	974.25
2.28758	1875.04	1574.52	1274	973.48
2.28958	1873.44	1573.22	1273	972.78
2.29158	1871.87	1571.95	1272.03	972.11
2.29359	1870.29	1570.65	1271.01	971.37
2.29559	1868.71	1569.34	1269.97	970.6
2.2976	1867.14	1568.05	1268.96	969.87
2.2996	1865.6	1566.79	1267.98	969.17
2.3016	1864.1	1565.56	1267.02	968.48
2.30361	1862.6	1564.33	1266.06	967.79
2.30561	1861.11	1563.11	1265.11	967.11
2.30762	1859.64	1561.9	1264.16	966.42
2.30962	1858.19	1560.73	1263.27	965.81

2.31162	1856.75	1559.57	1262.39	965.21
2.31363	1855.3	1558.41	1261.52	964.63
2.31563	1853.84	1557.21	1260.58	963.95
2.31764	1852.46	1556.1	1259.74	963.38
2.31964	1851.07	1554.98	1258.89	962.8
2.32164	1849.65	1553.84	1258.03	962.22
2.32365	1848.28	1552.74	1257.2	961.66
2.32565	1846.92	1551.62	1256.32	961.02
2.32766	1845.57	1550.55	1255.53	960.51
2.32966	1844.24	1549.51	1254.78	960.05
2.33166	1842.9	1548.43	1253.96	959.49
2.33367	1841.57	1547.35	1253.13	958.91
2.33567	1840.25	1546.3	1252.35	958.4
2.33768	1838.96	1545.25	1251.54	957.83
2.33968	1837.71	1544.25	1250.79	957.33
2.34168	1836.43	1543.23	1250.03	956.83
2.34369	1835.14	1542.2	1249.26	956.32
2.34569	1833.9	1541.2	1248.5	955.8
2.3477	1832.67	1540.22	1247.77	955.32
2.3497	1832.67	1540.46	1248.25	956.04
2.3497	1831.44	1539.23	1247.02	954.81
2.3517	1830.24	1538.25	1246.26	954.27
2.35371	1829.01	1537.25	1245.49	953.73
2.35571	1827.81	1536.3	1244.79	953.28
2.35772	1826.65	1535.4	1244.15	952.9
2.35972	1825.47	1534.46	1243.45	952.44
2.36172	1824.29	1533.5	1242.71	951.92
2.36373	1823.15	1532.61	1242.07	951.53
2.36573	1822.01	1531.72	1241.43	951.14
2.36774	1820.85	1530.79	1240.73	950.67
2.36974	1819.71	1529.88	1240.05	950.22
2.37174	1818.63	1529.02	1239.41	949.8
2.37375	1817.56	1528.16	1238.76	949.36
2.37575	1816.46	1527.28	1238.1	948.92
2.37776	1815.36	1526.38	1237.4	948.42
2.37976	1814.29	1525.52	1236.75	947.98
2.38176	1813.23	1524.68	1236.13	947.58
2.38377	1812.15	1523.84	1235.53	947.22
2.38577	1811.13	1523.03	1234.93	946.83
2.38778	1810.12	1522.22	1234.32	946.42
2.38978	1809.1	1521.42	1233.74	946.06
2.39178	1808.09	1520.6	1233.11	945.62

2.39379	1807.07	1519.79	1232.51	945.23
2.39579	1806.05	1518.98	1231.91	944.84
2.3978	1805.04	1518.18	1231.32	944.46
2.3998	1804.04	1517.38	1230.72	944.06
2.4018	1803.05	1516.59	1230.13	943.67
2.40381	1802.04	1515.77	1229.5	943.23
2.40581	1801.05	1514.98	1228.91	942.84
2.40782	1800.09	1514.22	1228.35	942.48
2.40982	1799.11	1513.43	1227.75	942.07
2.41182	1798.14	1512.66	1227.18	941.7
2.41383	1797.21	1511.94	1226.67	941.4
2.41583	1796.27	1511.22	1226.17	941.12
2.41784	1795.33	1510.46	1225.59	940.72
2.41984	1794.39	1509.71	1225.03	940.35
2.42184	1793.46	1508.99	1224.52	940.05
2.42385	1792.55	1508.3	1224.05	939.8
2.42585	1791.64	1507.59	1223.54	939.49
2.42786	1790.73	1506.88	1223.03	939.18
2.42986	1789.82	1506.16	1222.5	938.84
2.43186	1788.93	1505.45	1221.97	938.49
2.43387	1788.05	1504.77	1221.49	938.21
2.43587	1787.17	1504.08	1220.99	937.9
2.43788	1786.3	1503.43	1220.56	937.69
2.43988	1785.43	1502.76	1220.09	937.42
2.44188	1784.58	1502.1	1219.62	937.14
2.44389	1783.7	1501.41	1219.12	936.83
2.44589	1782.85	1500.76	1218.67	936.58
2.4479	1782.01	1500.09	1218.17	936.25
2.4499	1781.15	1499.38	1217.61	935.84
2.4519	1780.29	1498.72	1217.15	935.58
2.45391	1779.46	1498.06	1216.66	935.26
2.45591	1778.63	1497.38	1216.13	934.88
2.45792	1777.8	1496.73	1215.66	934.59
2.45992	1776.96	1496.04	1215.12	934.2
2.46192	1776.13	1495.37	1214.61	933.85
2.46393	1775.31	1494.72	1214.13	933.54
2.46593	1774.48	1494.05	1213.62	933.19
2.46794	1773.67	1493.4	1213.13	932.86
2.46994	1772.87	1492.76	1212.65	932.54
2.47194	1772.06	1492.12	1212.18	932.24
2.47395	1771.27	1491.49	1211.71	931.93
2.47595	1770.49	1490.85	1211.21	931.57

2.47796	1769.69	1490.21	1210.73	931.25
2.47996	1768.89	1489.57	1210.25	930.93
2.48196	1768.14	1488.99	1209.84	930.69
2.48397	1767.37	1488.39	1209.41	930.43
2.48597	1766.57	1487.72	1208.87	930.02
2.48798	1765.78	1487.06	1208.34	929.62
2.48998	1764.99	1486.42	1207.85	929.28
2.49198	1764.21	1485.79	1207.37	928.95
2.49399	1763.42	1485.11	1206.8	928.49
2.49599	1762.65	1484.47	1206.29	928.11
2.498	1761.87	1483.86	1205.85	927.84
2.5	1761.47	1483.55	1205.63	927.71

Table B2: Surface heat transfer coefficient for CuO nanofluids at ER=1.67

Axial Position , Z(m)	Re= 50,000	Re= 40,000	Re= 30,000	Re= 20,000
1.502	868.557	861.304	854.051	846.798
1.50401	838.898	831.022	823.146	815.27
1.50601	852.834	840.989	829.144	817.299
1.50802	1011.71	994.74	977.77	960.8
1.51002	1261.25	1240.72	1220.19	1199.66
1.51202	1494.09	1469.8	1445.51	1421.22
1.51403	1696.13	1668.37	1640.61	1612.85
1.51603	1879.58	1848.56	1817.54	1786.52
1.51804	2050.89	2016.77	1982.65	1948.53
1.52004	2212.7	2175.61	2138.52	2101.43
1.52204	2366.7	2326.81	2286.92	2247.03
1.52405	2513.9	2471.35	2428.8	2386.25
1.52605	2654.79	2609.63	2564.47	2519.31
1.52806	2789.68	2741.97	2694.26	2646.55
1.53006	2918.77	2868.58	2818.39	2768.2
1.53206	3042.2	2989.61	2937.02	2884.43
1.53407	3160.23	3105.42	3050.61	2995.8
1.53607	3272.87	3215.9	3158.93	3101.96
1.53808	3380.27	3321.27	3262.27	3203.27
1.54008	3482.57	3421.66	3360.75	3299.84
1.54208	3579.75	3516.93	3454.11	3391.29
1.54409	3672.06	3607.41	3542.76	3478.11
1.54609	3759.68	3693.34	3627	3560.66
1.5481	3842.74	3774.83	3706.92	3639.01
1.5501	3921.55	3852.22	3782.89	3713.56
1.5521	3996.37	3925.71	3855.05	3784.39
1.55411	4067.56	3995.5	3923.44	3851.38
1.55611	4135.65	4062.21	3988.77	3915.33
1.55812	4201.43	4126.77	4052.11	3977.45
1.56012	4265.97	4190.23	4114.49	4038.75
1.56212	4330.83	4253.92	4177.01	4100.1
1.56413	4395.02	4316.78	4238.54	4160.3
1.56613	4456.1	4376.52	4296.94	4217.36
1.56814	4513.42	4432.65	4351.88	4271.11
1.57014	4567.04	4485.37	4403.7	4322.03
1.57214	4616.55	4534.02	4451.49	4368.96
1.57415	4661.78	4578.25	4494.72	4411.19
1.57615	4703.04	4618.72	4534.4	4450.08

1.57816	4740.49	4655.57	4570.65	4485.73
1.58016	4774.91	4689.44	4603.97	4518.5
1.58216	4806.83	4720.9	4634.97	4549.04
1.58417	4836.36	4749.99	4663.62	4577.25
1.58617	4863.58	4776.83	4690.08	4603.33
1.58818	4888.5	4801.28	4714.06	4626.84
1.59018	4911.32	4823.68	4736.04	4648.4
1.59218	4932.06	4844.18	4756.3	4668.42
1.59419	4950.52	4862.36	4774.2	4686.04
1.59619	4966.95	4878.44	4789.93	4701.42
1.5982	4981.68	4893.01	4804.34	4715.67
1.6002	4994.56	4905.82	4817.08	4728.34
1.6022	5005.93	4917.13	4828.33	4739.53
1.60421	5015.94	4927.11	4838.28	4749.45
1.60621	5024.54	4935.67	4846.8	4757.93
1.60822	5032.04	4943.3	4854.56	4765.82
1.61022	5038.37	4949.75	4861.13	4772.51
1.61222	5043.29	4954.55	4865.81	4777.07
1.61423	5047.13	4958.46	4869.79	4781.12
1.61623	5050.07	4961.6	4873.13	4784.66
1.61824	5051.7	4963.12	4874.54	4785.96
1.62024	5052.21	4963.61	4875.01	4786.41
1.62224	5051.8	4963.14	4874.48	4785.82
1.62425	5050.43	4961.54	4872.65	4783.76
1.62625	5048.1	4959.19	4870.28	4781.37
1.62826	5044.82	4955.88	4866.94	4778
1.63026	5040.8	4951.78	4862.76	4773.74
1.63226	5036.03	4947.08	4858.13	4769.18
1.63427	5030.47	4941.64	4852.81	4763.98
1.63627	5024.13	4935.55	4846.97	4758.39
1.63828	5017.04	4928.56	4840.08	4751.6
1.64028	5009.28	4920.81	4832.34	4743.87
1.64228	5009.28	4920.81	4832.34	4743.87
1.64429	5000.96	4912.66	4824.36	4736.06
1.64629	4992.03	4903.92	4815.81	4727.7
1.6483	4982.48	4894.67	4806.86	4719.05
1.6503	4972.36	4884.9	4797.44	4709.98
1.6523	4961.71	4874.61	4787.51	4700.41
1.65431	4950.53	4863.79	4777.05	4690.31
1.65631	4938.71	4852.18	4765.65	4679.12
1.65832	4926.49	4840.06	4753.63	4667.2
1.66032	4914.16	4828.16	4742.16	4656.16

1.66232	4901.55	4815.9	4730.25	4644.6
1.66433	4888.61	4803.13	4717.65	4632.17
1.66633	4874.95	4789.71	4704.47	4619.23
1.66834	4857.4	4772.35	4687.3	4602.25
1.67034	4835.36	4750.99	4666.62	4582.25
1.67234	4817.48	4733.85	4650.22	4566.59
1.67234	4806.46	4723.06	4639.66	4556.26
1.67435	4794.9	4711.42	4627.94	4544.46
1.67635	4779.07	4695.59	4612.11	4528.63
1.67836	4758.69	4675.43	4592.17	4508.91
1.68036	4735.16	4652.42	4569.68	4486.94
1.68236	4710.32	4628.23	4546.14	4464.05
1.68437	4685.05	4603.4	4521.75	4440.1
1.68637	4660.1	4578.8	4497.5	4416.2
1.68838	4635.65	4554.65	4473.65	4392.65
1.69038	4611.59	4531.07	4450.55	4370.03
1.69238	4587.78	4507.89	4428	4348.11
1.69439	4564.12	4484.61	4405.1	4325.59
1.69639	4540.62	4461.5	4382.38	4303.26
1.6984	4517.17	4438.46	4359.75	4281.04
1.7004	4493.76	4415.48	4337.2	4258.92
1.7024	4470.35	4392.52	4314.69	4236.86
1.70441	4446.96	4369.54	4292.12	4214.7
1.70641	4423.62	4346.61	4269.6	4192.59
1.70842	4400.27	4323.6	4246.93	4170.26
1.71042	4377.03	4300.81	4224.59	4148.37
1.71242	4353.79	4278.19	4202.59	4126.99
1.71443	4330.38	4255.39	4180.4	4105.41
1.71643	4306.9	4232.3	4157.7	4083.1
1.71844	4283.41	4209.27	4135.13	4060.99
1.72044	4259.97	4186.21	4112.45	4038.69
1.72244	4236.58	4163.2	4089.82	4016.44
1.72445	4213.25	4140.56	4067.87	3995.18
1.72645	4189.93	4117.79	4045.65	3973.51
1.72846	4166.5	4094.7	4022.9	3951.1
1.73046	4143.19	4071.76	4000.33	3928.9
1.73246	4120.17	4049.29	3978.41	3907.53
1.73447	4097.25	4026.89	3956.53	3886.17
1.73647	4074.42	4004.47	3934.52	3864.57
1.73848	4051.79	3982.26	3912.73	3843.2
1.74048	4029.44	3960.4	3891.36	3822.32
1.74248	4007.31	3938.67	3870.03	3801.39

1.74449	3985.42	3917.1	3848.78	3780.46
1.74649	3963.85	3896.05	3828.25	3760.45
1.7485	3942.53	3875.27	3808.01	3740.75
1.7505	3921.43	3854.55	3787.67	3720.79
1.7525	3900.66	3834.16	3767.66	3701.16
1.75451	3880.16	3814.08	3748	3681.92
1.75651	3859.82	3794.11	3728.4	3662.69
1.75852	3839.67	3774.28	3708.89	3643.5
1.76052	3819.74	3754.72	3689.7	3624.68
1.76252	3800	3735.42	3670.84	3606.26
1.76453	3780.35	3716.17	3651.99	3587.81
1.76653	3760.79	3697.01	3633.23	3569.45
1.76854	3741.27	3677.94	3614.61	3551.28
1.77054	3721.71	3658.82	3595.93	3533.04
1.77255	3702.1	3639.62	3577.14	3514.66
1.77455	3682.47	3620.49	3558.51	3496.53
1.77655	3682.47	3620.49	3558.51	3496.53
1.77856	3662.83	3601.36	3539.89	3478.42
1.78056	3643.08	3582.07	3521.06	3460.05
1.78257	3623.17	3562.55	3501.93	3441.31
1.78457	3603.1	3542.88	3482.66	3422.44
1.78657	3582.93	3523.15	3463.37	3403.59
1.78858	3562.65	3503.26	3443.87	3384.48
1.79058	3542.19	3483.2	3424.21	3365.22
1.79058	3521.77	3463.19	3404.61	3346.03
1.79259	3501.29	3442.97	3384.65	3326.33
1.79459	3480.78	3422.8	3364.82	3306.84
1.79659	3460.47	3402.86	3345.25	3287.64
1.7986	3440.32	3383.06	3325.8	3268.54
1.8006	3420.3	3363.47	3306.64	3249.81
1.80261	3400.48	3344	3287.52	3231.04
1.80461	3380.96	3324.81	3268.66	3212.51
1.80661	3361.83	3306.03	3250.23	3194.43
1.80862	3343.01	3287.51	3232.01	3176.51
1.81062	3324.61	3269.41	3214.21	3159.01
1.81263	3306.76	3251.84	3196.92	3142
1.81463	3289.44	3234.76	3180.08	3125.4
1.81663	3272.71	3218.28	3163.85	3109.42
1.81864	3256.62	3202.46	3148.3	3094.14
1.82064	3241.06	3187.14	3133.22	3079.3
1.82265	3226.08	3172.36	3118.64	3064.92
1.82465	3211.62	3157.99	3104.36	3050.73

1.82665	3197.7	3144.15	3090.6	3037.05
1.82866	3184.36	3130.92	3077.48	3024.04
1.83066	3171.6	3118.33	3065.06	3011.79
1.83267	3159.29	3106.27	3053.25	3000.23
1.83467	3147.25	3094.36	3041.47	2988.58
1.83667	3135.61	3082.85	3030.09	2977.33
1.83868	3124.28	3071.68	3019.08	2966.48
1.84068	3113.16	3060.76	3008.36	2955.96
1.84269	3102.19	3049.96	2997.73	2945.5
1.84469	3091.33	3039.35	2987.37	2935.39
1.84669	3080.53	3028.79	2977.05	2925.31
1.8487	3069.67	3018.14	2966.61	2915.08
1.8507	3058.71	3007.39	2956.07	2904.75
1.85271	3047.69	2996.51	2945.33	2894.15
1.85471	3036.62	2985.72	2934.82	2883.92
1.85671	3025.46	2974.85	2924.24	2873.63
1.85872	3014.16	2963.79	2913.42	2863.05
1.86072	3002.7	2952.69	2902.68	2852.67
1.86273	2991.07	2941.34	2891.61	2841.88
1.86473	2979.3	2929.76	2880.22	2830.68
1.86673	2967.44	2918.2	2868.96	2819.72
1.86874	2955.44	2906.5	2857.56	2808.62
1.87074	2943.28	2894.52	2845.76	2797
1.87275	2931.09	2882.61	2834.13	2785.65
1.87475	2918.81	2870.61	2822.41	2774.21
1.87675	2906.42	2858.43	2810.44	2762.45
1.87876	2894.02	2846.31	2798.6	2750.89
1.88076	2881.62	2834.23	2786.84	2739.45
1.88277	2869.25	2822.15	2775.05	2727.95
1.88477	2856.93	2810.11	2763.29	2716.47
1.88677	2844.6	2798.08	2751.56	2705.04
1.88878	2832.28	2786.02	2739.76	2693.5
1.89078	2820	2773.97	2727.94	2681.91
1.89279	2807.81	2762.03	2716.25	2670.47
1.89479	2795.7	2750.16	2704.62	2659.08
1.89679	2783.68	2738.37	2693.06	2647.75
1.8988	2771.76	2726.68	2681.6	2636.52
1.9008	2759.92	2715.04	2670.16	2625.28
1.90281	2748.23	2703.58	2658.93	2614.28
1.90481	2736.65	2692.22	2647.79	2603.36
1.90681	2725.17	2680.95	2636.73	2592.51
1.90882	2725.17	2680.95	2636.73	2592.51

1.91082	2713.84	2669.89	2625.94	2581.99
1.91283	2702.62	2658.82	2615.02	2571.22
1.91483	2691.57	2647.87	2604.17	2560.47
1.91683	2680.67	2637.13	2593.59	2550.05
1.91884	2669.92	2626.57	2583.22	2539.87
1.92084	2659.36	2616.24	2573.12	2530
1.92084	2648.95	2606.07	2563.19	2520.31
1.92285	2638.69	2595.99	2553.29	2510.59
1.92485	2628.56	2586.01	2543.46	2500.91
1.92685	2618.55	2576.14	2533.73	2491.32
1.92886	2608.69	2566.38	2524.07	2481.76
1.93086	2598.97	2556.81	2514.65	2472.49
1.93287	2589.43	2547.44	2505.45	2463.46
1.93487	2579.99	2538.14	2496.29	2454.44
1.93687	2570.67	2529	2487.33	2445.66
1.93888	2561.53	2520.04	2478.55	2437.06
1.94088	2552.52	2511.17	2469.82	2428.47
1.94289	2543.67	2502.48	2461.29	2420.1
1.94489	2534.9	2493.83	2452.76	2411.69
1.94689	2526.21	2485.22	2444.23	2403.24
1.9489	2517.72	2476.88	2436.04	2395.2
1.9509	2509.35	2468.63	2427.91	2387.19
1.95291	2501.08	2460.48	2419.88	2379.28
1.95491	2492.97	2452.55	2412.13	2371.71
1.95691	2484.96	2444.65	2404.34	2364.03
1.95892	2477.08	2436.93	2396.78	2356.63
1.96092	2469.3	2429.32	2389.34	2349.36
1.96293	2461.57	2421.71	2381.85	2341.99
1.96493	2453.97	2414.26	2374.55	2334.84
1.96693	2446.51	2406.91	2367.31	2327.71
1.96894	2439.14	2399.65	2360.16	2320.67
1.97094	2431.85	2392.52	2353.19	2313.86
1.97295	2424.68	2385.5	2346.32	2307.14
1.97495	2417.57	2378.46	2339.35	2300.24
1.97695	2410.53	2371.47	2332.41	2293.35
1.97896	2403.63	2364.75	2325.87	2286.99
1.98096	2396.78	2358.03	2319.28	2280.53
1.98297	2390.01	2351.32	2312.63	2273.94
1.98497	2383.35	2344.77	2306.19	2267.61
1.98697	2376.78	2338.3	2299.82	2261.34
1.98898	2370.26	2331.86	2293.46	2255.06
1.99098	2363.81	2325.5	2287.19	2248.88

1.99299	2357.5	2319.38	2281.26	2243.14
1.99499	2351.21	2313.21	2275.21	2237.21
1.99699	2344.92	2306.97	2269.02	2231.07
1.999	2338.76	2300.95	2263.14	2225.33
2.001	2332.68	2295	2257.32	2219.64
2.00301	2326.62	2289.02	2251.42	2213.82
2.00501	2320.61	2283.07	2245.53	2207.99
2.00701	2314.71	2277.28	2239.85	2202.42
2.00902	2308.83	2271.49	2234.15	2196.81
2.01102	2303.02	2265.77	2228.52	2191.27
2.01303	2297.26	2260.07	2222.88	2185.69
2.01503	2291.51	2254.38	2217.25	2180.12
2.01703	2285.81	2248.8	2211.79	2174.78
2.01904	2280.21	2243.33	2206.45	2169.57
2.02104	2274.63	2237.79	2200.95	2164.11
2.02305	2269.06	2232.24	2195.42	2158.6
2.02505	2263.57	2226.85	2190.13	2153.41
2.02705	2258.14	2221.5	2184.86	2148.22
2.02906	2252.77	2216.19	2179.61	2143.03
2.03106	2247.4	2210.87	2174.34	2137.81
2.03307	2242.06	2205.57	2169.08	2132.59
2.03507	2236.82	2200.41	2164	2127.59
2.03707	2231.6	2195.28	2158.96	2122.64
2.03908	2226.4	2190.13	2153.86	2117.59
2.04108	2221.29	2185.09	2148.89	2112.69
2.04309	2216.2	2180.06	2143.92	2107.78
2.04509	2211.13	2175.01	2138.89	2102.77
2.04709	2206.14	2170.1	2134.06	2098.02
2.0491	2201.21	2165.27	2129.33	2093.39
2.0511	2196.31	2160.46	2124.61	2088.76
2.05311	2191.47	2155.68	2119.89	2084.1
2.05511	2186.65	2150.9	2115.15	2079.4
2.05511	2181.86	2146.15	2110.44	2074.73
2.05711	2177.11	2141.44	2105.77	2070.1
2.05912	2172.39	2136.72	2101.05	2065.38
2.06112	2167.75	2132.13	2096.51	2060.89
2.06313	2163.17	2127.68	2092.19	2056.7
2.06513	2158.61	2123.2	2087.79	2052.38
2.06713	2154.18	2118.81	2083.44	2048.07
2.06914	2149.82	2114.49	2079.16	2043.83
2.07114	2145.36	2110.13	2074.9	2039.67
2.07315	2140.83	2105.68	2070.53	2035.38

2.07515	2136.32	2101.24	2066.16	2031.08
2.07715	2136.32	2101.24	2066.16	2031.08
2.07916	2131.85	2096.83	2061.81	2026.79
2.08116	2127.37	2092.42	2057.47	2022.52
2.08317	2122.83	2087.91	2052.99	2018.07
2.08517	2118.4	2083.51	2048.62	2013.73
2.08717	2114.05	2079.16	2044.27	2009.38
2.08918	2109.83	2074.97	2040.11	2005.25
2.09118	2105.72	2070.88	2036.04	2001.2
2.09319	2101.58	2066.71	2031.84	1996.97
2.09519	2097.49	2062.63	2027.77	1992.91
2.09719	2093.47	2058.61	2023.75	1988.89
2.0992	2089.46	2054.62	2019.78	1984.94
2.1012	2085.52	2050.75	2015.98	1981.21
2.10321	2081.64	2046.93	2012.22	1977.51
2.10521	2077.75	2043.09	2008.43	1973.77
2.10721	2073.89	2039.27	2004.65	1970.03
2.10922	2070.12	2035.55	2000.98	1966.41
2.11122	2066.35	2031.83	1997.31	1962.79
2.11323	2062.59	2028.11	1993.63	1959.15
2.11523	2058.91	2024.47	1990.03	1955.59
2.11723	2055.29	2020.92	1986.55	1952.18
2.11924	2051.68	2017.34	1983	1948.66
2.12124	2048.09	2013.77	1979.45	1945.13
2.12325	2044.54	2010.26	1975.98	1941.7
2.12525	2041.04	2006.81	1972.58	1938.35
2.12725	2037.54	2003.32	1969.1	1934.88
2.12926	2034.07	1999.84	1965.61	1931.38
2.13126	2030.68	1996.48	1962.28	1928.08
2.13327	2027.3	1993.14	1958.98	1924.82
2.13527	2023.93	1989.82	1955.71	1921.6
2.13727	2020.59	1986.49	1952.39	1918.29
2.13928	2017.29	1983.23	1949.17	1915.11
2.14128	2014.01	1980	1945.99	1911.98
2.14329	2010.78	1976.81	1942.84	1908.87
2.14529	2007.56	1973.6	1939.64	1905.68
2.14729	2004.36	1970.42	1936.48	1902.54
2.1493	2001.22	1967.33	1933.44	1899.55
2.1513	1998.1	1964.26	1930.42	1896.58
2.15331	1995	1961.22	1927.44	1893.66
2.15531	1991.93	1958.2	1924.47	1890.74
2.15731	1988.87	1955.16	1921.45	1887.74

2.15932	1985.85	1952.15	1918.45	1884.75
2.16132	1982.85	1949.16	1915.47	1881.78
2.16333	1979.87	1946.22	1912.57	1878.92
2.16533	1976.91	1943.28	1909.65	1876.02
2.16733	1973.98	1940.37	1906.76	1873.15
2.16934	1971.08	1937.44	1903.8	1870.16
2.17134	1968.22	1934.6	1900.98	1867.36
2.17335	1965.4	1931.85	1898.3	1864.75
2.17535	1962.62	1929.13	1895.64	1862.15
2.17735	1959.82	1926.31	1892.8	1859.29
2.17936	1957.05	1923.55	1890.05	1856.55
2.18136	1954.32	1920.84	1887.36	1853.88
2.18337	1951.61	1918.16	1884.71	1851.26
2.18537	1948.9	1915.44	1881.98	1848.52
2.18737	1946.25	1912.81	1879.37	1845.93
2.18938	1943.62	1910.21	1876.8	1843.39
2.19138	1941.01	1907.62	1874.23	1840.84
2.19339	1938.47	1905.1	1871.73	1838.36
2.19539	1935.93	1902.57	1869.21	1835.85
2.19739	1933.42	1900.12	1866.82	1833.52
2.1994	1930.95	1897.69	1864.43	1831.17
2.2014	1928.47	1895.2	1861.93	1828.66
2.20341	1926.01	1892.75	1859.49	1826.23
2.20541	1923.59	1890.36	1857.13	1823.9
2.20741	1921.19	1887.94	1854.69	1821.44
2.20942	1918.82	1885.58	1852.34	1819.1
2.20942	1916.46	1883.23	1850	1816.77
2.21142	1914.12	1880.88	1847.64	1814.4
2.21343	1911.84	1878.62	1845.4	1812.18
2.21543	1911.84	1878.62	1845.4	1812.18
2.21743	1909.57	1876.37	1843.17	1809.97
2.21944	1907.32	1874.13	1840.94	1807.75
2.22144	1905.11	1871.93	1838.75	1805.57
2.22345	1902.87	1869.68	1836.49	1803.3
2.22545	1900.67	1867.48	1834.29	1801.1
2.22745	1898.55	1865.39	1832.23	1799.07
2.22946	1896.39	1863.26	1830.13	1797
2.23146	1894.22	1861.09	1827.96	1794.83
2.23347	1892.14	1859.03	1825.92	1792.81
2.23547	1890.08	1857.01	1823.94	1790.87
2.23747	1888	1854.95	1821.9	1788.85
2.23948	1885.94	1852.88	1819.82	1786.76

2.24148	1883.89	1850.84	1817.79	1784.74
2.24349	1881.87	1848.84	1815.81	1782.78
2.24549	1879.88	1846.87	1813.86	1780.85
2.24749	1877.91	1844.93	1811.95	1778.97
2.2495	1875.95	1842.96	1809.97	1776.98
2.2515	1874.01	1841.03	1808.05	1775.07
2.25351	1872.09	1839.12	1806.15	1773.18
2.25551	1870.21	1837.24	1804.27	1771.3
2.25751	1868.31	1835.33	1802.35	1769.37
2.25952	1866.4	1833.38	1800.36	1767.34
2.26152	1864.57	1831.56	1798.55	1765.54
2.26353	1862.74	1829.74	1796.74	1763.74
2.26553	1860.9	1827.88	1794.86	1761.84
2.26753	1859.1	1826.08	1793.06	1760.04
2.26954	1857.32	1824.3	1791.28	1758.26
2.27154	1855.52	1822.48	1789.44	1756.4
2.27355	1853.76	1820.72	1787.68	1754.64
2.27555	1852.03	1818.98	1785.93	1752.88
2.27755	1850.32	1817.27	1784.22	1751.17
2.27956	1848.62	1815.6	1782.58	1749.56
2.28156	1846.96	1813.96	1780.96	1747.96
2.28357	1845.34	1812.36	1779.38	1746.4
2.28557	1843.69	1810.7	1777.71	1744.72
2.28758	1842.05	1809.06	1776.07	1743.08
2.28958	1840.47	1807.5	1774.53	1741.56
2.29158	1838.88	1805.89	1772.9	1739.91
2.29359	1837.27	1804.25	1771.23	1738.21
2.29559	1835.71	1802.71	1769.71	1736.71
2.2976	1834.18	1801.22	1768.26	1735.3
2.2996	1832.66	1799.72	1766.78	1733.84
2.3016	1831.11	1798.12	1765.13	1732.14
2.30361	1829.59	1796.58	1763.57	1730.56
2.30561	1828.1	1795.09	1762.08	1729.07
2.30762	1826.61	1793.58	1760.55	1727.52
2.30962	1825.13	1792.07	1759.01	1725.95
2.31162	1823.69	1790.63	1757.57	1724.51
2.31363	1822.24	1789.18	1756.12	1723.06
2.31563	1820.82	1787.8	1754.78	1721.76
2.31764	1819.44	1786.42	1753.4	1720.38
2.31964	1818.03	1784.99	1751.95	1718.91
2.32164	1816.6	1783.55	1750.5	1717.45
2.32365	1815.24	1782.2	1749.16	1716.12

2.32565	1813.87	1780.82	1747.77	1714.72
2.32766	1812.51	1779.45	1746.39	1713.33
2.32966	1811.18	1778.12	1745.06	1712
2.33166	1809.85	1776.8	1743.75	1710.7
2.33367	1808.52	1775.47	1742.42	1709.37
2.33567	1807.19	1774.13	1741.07	1708.01
2.33768	1805.89	1772.82	1739.75	1706.68
2.33968	1804.63	1771.55	1738.47	1705.39
2.34168	1803.35	1770.27	1737.19	1704.11
2.34369	1802.07	1769	1735.93	1702.86
2.34569	1800.83	1767.76	1734.69	1701.62
2.3477	1799.58	1766.49	1733.4	1700.31
2.3497	1799.58	1766.49	1733.4	1700.31
2.3497	1798.36	1765.28	1732.2	1699.12
2.3517	1797.13	1764.02	1730.91	1697.8
2.35371	1795.89	1762.77	1729.65	1696.53
2.35571	1794.68	1761.55	1728.42	1695.29
2.35772	1793.52	1760.39	1727.26	1694.13
2.35972	1792.34	1759.21	1726.08	1692.95
2.36172	1791.16	1758.03	1724.9	1691.77
2.36373	1790.03	1756.91	1723.79	1690.67
2.36573	1788.88	1755.75	1722.62	1689.49
2.36774	1787.74	1754.63	1721.52	1688.41
2.36974	1786.6	1753.49	1720.38	1687.27
2.37174	1785.46	1752.29	1719.12	1685.95
2.37375	1784.39	1751.22	1718.05	1684.88
2.37575	1783.3	1750.14	1716.98	1683.82
2.37776	1782.19	1749.02	1715.85	1682.68
2.37976	1781.15	1748.01	1714.87	1681.73
2.38176	1780.1	1746.97	1713.84	1680.71
2.38377	1779.04	1745.93	1712.82	1679.71
2.38577	1778	1744.87	1711.74	1678.61
2.38778	1776.96	1743.8	1710.64	1677.48
2.38978	1775.93	1742.76	1709.59	1676.42
2.39178	1774.93	1741.77	1708.61	1675.45
2.39379	1773.9	1740.73	1707.56	1674.39
2.39579	1772.88	1739.71	1706.54	1673.37
2.3978	1771.87	1738.7	1705.53	1672.36
2.3998	1770.87	1737.7	1704.53	1671.36
2.4018	1769.88	1736.71	1703.54	1670.37
2.40381	1768.89	1735.74	1702.59	1669.44
2.40581	1767.92	1734.79	1701.66	1668.53

2.40782	1766.97	1733.85	1700.73	1667.61
2.40982	1765.99	1732.87	1699.75	1666.63
2.41182	1765.03	1731.92	1698.81	1665.7
2.41383	1764.12	1731.03	1697.94	1664.85
2.41583	1763.16	1730.05	1696.94	1663.83
2.41784	1762.21	1729.09	1695.97	1662.85
2.41984	1761.3	1728.21	1695.12	1662.03
2.42184	1760.37	1727.28	1694.19	1661.1
2.42385	1759.47	1726.39	1693.31	1660.23
2.42585	1758.57	1725.5	1692.43	1659.36
2.42786	1757.65	1724.57	1691.49	1658.41
2.42986	1756.76	1723.7	1690.64	1657.58
2.43186	1755.87	1722.81	1689.75	1656.69
2.43387	1754.99	1721.93	1688.87	1655.81
2.43587	1754.12	1721.07	1688.02	1654.97
2.43788	1753.24	1720.18	1687.12	1654.06
2.43988	1752.37	1719.31	1686.25	1653.19
2.44188	1751.51	1718.44	1685.37	1652.3
2.44389	1750.65	1717.6	1684.55	1651.5
2.44589	1749.8	1716.75	1683.7	1650.65
2.4479	1748.98	1715.95	1682.92	1649.89
2.4499	1748.14	1715.13	1682.12	1649.11
2.4519	1747.3	1714.31	1681.32	1648.33
2.45391	1746.48	1713.5	1680.52	1647.54
2.45591	1745.66	1712.69	1679.72	1646.75
2.45792	1744.83	1711.86	1678.89	1645.92
2.45992	1743.99	1711.02	1678.05	1645.08
2.46192	1743.16	1710.19	1677.22	1644.25
2.46393	1742.37	1709.43	1676.49	1643.55
2.46593	1741.58	1708.68	1675.78	1642.88
2.46794	1740.78	1707.89	1675	1642.11
2.46994	1740.01	1707.15	1674.29	1641.43
2.47194	1739.21	1706.36	1673.51	1640.66
2.47395	1738.42	1705.57	1672.72	1639.87
2.47595	1737.65	1704.81	1671.97	1639.13
2.47796	1736.85	1704.01	1671.17	1638.33
2.47996	1736.07	1703.25	1670.43	1637.61
2.48196	1735.31	1702.48	1669.65	1636.82
2.48397	1734.52	1701.67	1668.82	1635.97
2.48597	1733.75	1700.93	1668.11	1635.29
2.48798	1733.01	1700.24	1667.47	1634.7
2.48998	1732.25	1699.51	1666.77	1634.03

2.49198	1731.48	1698.75	1666.02	1633.29
2.49399	1730.72	1698.02	1665.32	1632.62
2.49599	1729.98	1697.31	1664.64	1631.97
2.498	1729.22	1696.57	1663.92	1631.27
2.5	1728.82	1696.17	1663.52	1630.87

Table B3: Surface heat transfer coefficient for TiO_2 nanofluids at ER=1.67

Axial Position , Z(m)	Re= 50,000	Re= 40,000	Re= 30,000	Re= 20,000
1.502	860.355	853.102	844.9	836.698
1.50401	830.975	823.099	815.176	807.253
1.50601	844.372	832.527	824.065	815.603
1.50802	1001.22	984.25	973.76	963.27
1.51002	1248.18	1227.65	1214.58	1201.51
1.51202	1478.64	1454.35	1438.9	1423.45
1.51403	1678.65	1650.89	1633.41	1615.93
1.51603	1860.27	1829.25	1809.94	1790.63
1.51804	2029.86	1995.74	1974.71	1953.68
1.52004	2190.04	2152.95	2130.29	2107.63
1.52204	2342.51	2302.62	2278.43	2254.24
1.52405	2488.22	2445.67	2419.99	2394.31
1.52605	2627.71	2582.55	2555.47	2528.39
1.52806	2761.19	2713.48	2684.99	2656.5
1.53006	2888.97	2838.78	2808.98	2779.18
1.53206	3011.26	2958.67	2927.73	2896.79
1.53407	3128.05	3073.24	3041.06	3008.88
1.53607	3239.48	3182.51	3149.12	3115.73
1.53808	3345.75	3286.75	3252.23	3217.71
1.54008	3446.94	3386.03	3350.4	3314.77
1.54208	3543.17	3480.35	3443.77	3407.19
1.54409	3634.54	3569.89	3532.37	3494.85
1.54609	3721.25	3654.91	3616.48	3578.05
1.5481	3803.47	3735.56	3696.29	3657.02
1.5501	3881.49	3812.16	3772.1	3732.04
1.5521	3955.47	3884.81	3843.91	3803.01
1.55411	4025.9	3953.84	3912.18	3870.52
1.55611	4093.36	4019.92	3977.63	3935.34
1.55812	4158.41	4083.75	4040.73	3997.71
1.56012	4222.17	4146.43	4102.63	4058.83
1.56212	4286.39	4209.48	4165.04	4120.6
1.56413	4349.93	4271.69	4226.6	4181.51
1.56613	4410.29	4330.71	4284.9	4239.09
1.56814	4467.04	4386.27	4339.89	4293.51
1.57014	4519.87	4438.2	4391.03	4343.86
1.57214	4568.74	4486.21	4438.4	4390.59
1.57415	4613.73	4530.2	4482.15	4434.1

1.57615	4654.75	4570.43	4522.14	4473.85
1.57816	4691.91	4606.99	4558.41	4509.83
1.58016	4725.97	4640.5	4591.56	4542.62
1.58216	4757.46	4671.53	4622.16	4572.79
1.58417	4786.48	4700.11	4650.23	4600.35
1.58617	4813.46	4726.71	4676.59	4626.47
1.58818	4838.35	4751.13	4700.98	4650.83
1.59018	4860.96	4773.32	4722.96	4672.6
1.59218	4881.43	4793.55	4742.92	4692.29
1.59419	4900	4811.84	4761.32	4710.8
1.59619	4916.58	4828.07	4777.7	4727.33
1.5982	4931.14	4842.47	4791.93	4741.39
1.6002	4943.91	4855.17	4804.52	4753.87
1.6022	4955.07	4866.27	4815.41	4764.55
1.60421	4964.9	4876.07	4825.03	4773.99
1.60621	4973.52	4884.65	4833.63	4782.61
1.60822	4980.82	4892.08	4840.86	4789.64
1.61022	4986.86	4898.24	4846.73	4795.22
1.61222	4991.79	4903.05	4851.55	4800.05
1.61423	4995.72	4907.05	4855.64	4804.23
1.61623	4998.65	4910.18	4858.76	4807.34
1.61824	5000.2	4911.62	4860.12	4808.62
1.62024	5000.58	4911.98	4860.35	4808.72
1.62224	5000.2	4911.54	4859.94	4808.34
1.62425	4998.91	4910.02	4858.5	4806.98
1.62625	4996.72	4907.81	4856.43	4805.05
1.62826	4993.58	4904.64	4853.4	4802.16
1.63026	4989.47	4900.45	4849.12	4797.79
1.63226	4984.6	4895.65	4844.22	4792.79
1.63427	4979.04	4890.21	4838.78	4787.35
1.63627	4972.74	4884.16	4832.77	4781.38
1.63828	4965.77	4877.29	4826.02	4774.75
1.64028	4958.35	4869.88	4818.95	4768.02
1.64228	4958.35	4869.88	4818.95	4768.02
1.64429	4950.3	4862	4811.34	4760.68
1.64629	4941.48	4853.37	4802.82	4752.27
1.6483	4932.07	4844.26	4793.85	4743.44
1.6503	4921.95	4834.49	4784.08	4733.67
1.6523	4911.25	4824.15	4773.69	4723.23
1.65431	4900.08	4813.34	4762.89	4712.44
1.65631	4888.52	4801.99	4751.8	4701.61
1.65832	4876.47	4790.04	4740.02	4690

1.66032	4863.94	4777.94	4727.72	4677.5
1.66232	4851.23	4765.58	4715.26	4664.94
1.66433	4838.4	4752.92	4702.71	4652.5
1.66633	4825.02	4739.78	4689.85	4639.92
1.66834	4807.78	4722.73	4673.11	4623.49
1.67034	4785.69	4701.32	4651.65	4601.98
1.67234	4767.78	4684.15	4634.45	4584.75
1.67234	4756.88	4673.48	4623.9	4574.32
1.67435	4745.43	4661.95	4612.48	4563.01
1.67635	4730.02	4646.54	4597.49	4548.44
1.67836	4710.1	4626.84	4578.25	4529.66
1.68036	4686.64	4603.9	4555.38	4506.86
1.68236	4661.8	4579.71	4531.19	4482.67
1.68437	4636.88	4555.23	4507.06	4458.89
1.68637	4612.3	4531	4483.2	4435.4
1.68838	4588.12	4507.12	4459.59	4412.06
1.69038	4564.41	4483.89	4436.71	4389.53
1.69238	4541.21	4461.32	4414.75	4368.18
1.69439	4518	4438.49	4392.37	4346.25
1.69639	4494.65	4415.53	4369.56	4323.59
1.6984	4471.53	4392.82	4347.18	4301.54
1.7004	4448.45	4370.17	4324.86	4279.55
1.7024	4425.35	4347.52	4302.52	4257.52
1.70441	4402.35	4324.93	4280.32	4235.71
1.70641	4379.28	4302.27	4257.93	4213.59
1.70842	4356.08	4279.41	4235.22	4191.03
1.71042	4333.02	4256.8	4212.79	4168.78
1.71242	4309.93	4234.33	4190.47	4146.61
1.71443	4286.71	4211.72	4168.05	4124.38
1.71643	4263.46	4188.86	4145.42	4101.98
1.71844	4240.2	4166.06	4122.85	4079.64
1.72044	4216.96	4143.2	4100.19	4057.18
1.72244	4193.73	4120.35	4077.5	4034.65
1.72445	4170.58	4097.89	4055.22	4012.55
1.72645	4147.45	4075.31	4032.83	3990.35
1.72846	4124.37	4052.57	4010.44	3968.31
1.73046	4101.24	4029.81	3987.86	3945.91
1.73246	4078.19	4007.31	3965.33	3923.35
1.73447	4055.35	3984.99	3943.09	3901.19
1.73647	4032.69	3962.74	3921.01	3879.28
1.73848	4010.25	3940.72	3899.18	3857.64
1.74048	3988.09	3919.05	3877.7	3836.35

1.74248	3966.11	3897.47	3856.27	3815.07
1.74449	3944.34	3876.02	3834.94	3793.86
1.74649	3922.86	3855.06	3814.07	3773.08
1.7485	3901.6	3834.34	3793.41	3752.48
1.7505	3880.65	3813.77	3772.99	3732.21
1.7525	3859.93	3793.43	3752.7	3711.97
1.75451	3839.5	3773.42	3732.76	3692.1
1.75651	3819.25	3753.54	3712.97	3672.4
1.75852	3799.17	3733.78	3693.28	3652.78
1.76052	3779.48	3714.46	3674.2	3633.94
1.76252	3759.93	3695.35	3655.28	3615.21
1.76453	3740.48	3676.3	3636.43	3596.56
1.76653	3721.22	3657.44	3617.87	3578.3
1.76854	3701.97	3638.64	3599.34	3560.04
1.77054	3682.68	3619.79	3580.76	3541.73
1.77255	3663.4	3600.92	3562.22	3523.52
1.77455	3644.13	3582.15	3543.81	3505.47
1.77655	3644.13	3582.15	3543.81	3505.47
1.77856	3624.8	3563.33	3525.3	3487.27
1.78056	3605.31	3544.3	3506.53	3468.76
1.78257	3585.69	3525.07	3487.59	3450.11
1.78457	3566.04	3505.82	3468.76	3431.7
1.78657	3546.28	3486.5	3449.85	3413.2
1.78858	3526.29	3466.9	3430.54	3394.18
1.79058	3506.26	3447.27	3411.34	3375.41
1.79058	3486.26	3427.68	3392.17	3356.66
1.79259	3466.2	3407.88	3372.79	3337.7
1.79459	3446.1	3388.12	3353.44	3318.76
1.79659	3426.05	3368.44	3334.02	3299.6
1.7986	3406.08	3348.82	3314.58	3280.34
1.8006	3386.32	3329.49	3295.51	3261.53
1.80261	3366.79	3310.31	3276.62	3242.93
1.80461	3347.45	3291.3	3257.79	3224.28
1.80661	3328.42	3272.62	3239.21	3205.8
1.80862	3309.75	3254.25	3220.99	3187.73
1.81062	3291.5	3236.3	3203.19	3170.08
1.81263	3273.71	3218.79	3185.74	3152.69
1.81463	3256.37	3201.69	3168.62	3135.55
1.81663	3239.59	3185.16	3152.04	3118.92
1.81864	3223.36	3169.2	3135.94	3102.68
1.82064	3207.68	3153.76	3120.38	3087
1.82265	3192.65	3138.93	3105.5	3072.07

1.82465	3178.15	3124.52	3091.05	3057.58
1.82665	3164.16	3110.61	3077.07	3043.53
1.82866	3150.71	3097.27	3063.62	3029.97
1.83066	3137.67	3084.4	3050.47	3016.54
1.83267	3125.07	3072.05	3037.83	3003.61
1.83467	3113	3060.11	3025.86	2991.61
1.83667	3101.32	3048.56	3014.27	2979.98
1.83868	3089.88	3037.28	3002.88	2968.48
1.84068	3078.75	3026.35	2991.94	2957.53
1.84269	3067.8	3015.57	2981.18	2946.79
1.84469	3056.96	3004.98	2970.61	2936.24
1.84669	3046.19	2994.45	2960.11	2925.77
1.8487	3035.4	2983.87	2949.6	2915.33
1.8507	3024.6	2973.28	2939.17	2905.06
1.85271	3013.8	2962.62	2928.73	2894.84
1.85471	3002.93	2952.03	2918.34	2884.65
1.85671	2991.97	2941.36	2907.87	2874.38
1.85872	2980.91	2930.54	2897.29	2864.04
1.86072	2969.71	2919.7	2886.71	2853.72
1.86273	2958.37	2908.64	2875.94	2843.24
1.86473	2946.87	2897.33	2864.9	2832.47
1.86673	2935.28	2886.04	2853.88	2821.72
1.86874	2923.57	2874.63	2842.76	2810.89
1.87074	2911.74	2862.98	2831.44	2799.9
1.87275	2899.85	2851.37	2820.13	2788.89
1.87475	2887.88	2839.68	2808.75	2777.82
1.87675	2875.83	2827.84	2797.25	2766.66
1.87876	2863.74	2816.03	2785.75	2755.47
1.88076	2851.61	2804.22	2774.21	2744.2
1.88277	2839.48	2792.38	2762.61	2732.84
1.88477	2827.36	2780.54	2750.97	2721.4
1.88677	2815.23	2768.71	2739.34	2709.97
1.88878	2803.11	2756.85	2727.68	2698.51
1.89078	2791.09	2745.06	2716.15	2687.24
1.89279	2779.1	2733.32	2704.61	2675.9
1.89479	2767.16	2721.62	2693.08	2664.54
1.89679	2755.3	2709.99	2681.61	2653.23
1.8988	2743.56	2698.48	2670.28	2642.08
1.9008	2731.93	2687.05	2659.06	2631.07
1.90281	2720.34	2675.69	2647.8	2619.91
1.90481	2708.87	2664.44	2636.66	2608.88
1.90681	2697.58	2653.36	2625.77	2598.18

1.90882	2697.58	2653.36	2625.77	2598.18
1.91082	2686.42	2642.47	2615.05	2587.63
1.91283	2675.41	2631.61	2604.4	2577.19
1.91483	2664.52	2620.82	2593.77	2566.72
1.91683	2653.73	2610.19	2583.25	2556.31
1.91884	2643.12	2599.77	2572.97	2546.17
1.92084	2632.65	2589.53	2562.82	2536.11
1.92084	2622.34	2579.46	2552.85	2526.24
1.92285	2612.22	2569.52	2543.05	2516.58
1.92485	2602.18	2559.63	2533.25	2506.87
1.92685	2592.25	2549.84	2523.54	2497.24
1.92886	2582.49	2540.18	2513.98	2487.78
1.93086	2572.9	2530.74	2504.67	2478.6
1.93287	2563.44	2521.45	2495.46	2469.47
1.93487	2554.13	2512.28	2486.42	2460.56
1.93687	2544.94	2503.27	2477.54	2451.81
1.93888	2535.83	2494.34	2468.64	2442.94
1.94088	2526.94	2485.59	2460.01	2434.43
1.94289	2518.18	2476.99	2451.5	2426.01
1.94489	2509.49	2468.42	2443.01	2417.6
1.94689	2500.93	2459.94	2434.66	2409.38
1.9489	2492.52	2451.68	2426.48	2401.28
1.9509	2484.28	2443.56	2418.49	2393.42
1.95291	2476.11	2435.51	2410.54	2385.57
1.95491	2468.03	2427.61	2402.67	2377.73
1.95691	2460.08	2419.77	2394.89	2370.01
1.95892	2452.19	2412.04	2387.15	2362.26
1.96092	2444.45	2404.47	2379.62	2354.77
1.96293	2436.84	2396.98	2372.25	2347.52
1.96493	2429.35	2389.64	2365.02	2340.4
1.96693	2421.91	2382.31	2357.71	2333.11
1.96894	2414.55	2375.06	2350.47	2325.88
1.97094	2407.34	2368.01	2343.5	2318.99
1.97295	2400.23	2361.05	2336.6	2312.15
1.97495	2393.22	2354.11	2329.76	2305.41
1.97695	2386.3	2347.24	2323.01	2298.78
1.97896	2379.44	2340.56	2316.37	2292.18
1.98096	2372.63	2333.88	2309.73	2285.58
1.98297	2365.92	2327.23	2303.14	2279.05
1.98497	2359.33	2320.75	2296.73	2272.71
1.98697	2352.82	2314.34	2290.38	2266.42
1.98898	2346.39	2307.99	2284.12	2260.25

1.99098	2340.02	2301.71	2277.92	2254.13
1.99299	2333.7	2295.58	2271.78	2247.98
1.99499	2327.46	2289.46	2265.71	2241.96
1.99699	2321.24	2283.29	2259.61	2235.93
1.999	2315.1	2277.29	2253.63	2229.97
2.001	2309.11	2271.43	2247.86	2224.29
2.00301	2303.15	2265.55	2242.08	2218.61
2.00501	2297.22	2259.68	2236.29	2212.9
2.00701	2291.34	2253.91	2230.54	2207.17
2.00902	2285.52	2248.18	2224.87	2201.56
2.01102	2279.73	2242.48	2219.19	2195.9
2.01303	2274.02	2236.83	2213.59	2190.35
2.01503	2268.37	2231.24	2208.1	2184.96
2.01703	2262.72	2225.71	2202.62	2179.53
2.01904	2257.12	2220.24	2197.15	2174.06
2.02104	2251.6	2214.76	2191.73	2168.7
2.02305	2246.12	2209.3	2186.36	2163.42
2.02505	2240.69	2203.97	2181.09	2158.21
2.02705	2235.31	2198.67	2175.84	2153.01
2.02906	2229.99	2193.41	2170.63	2147.85
2.03106	2224.72	2188.19	2165.51	2142.83
2.03307	2219.52	2183.03	2160.49	2137.95
2.03507	2214.36	2177.95	2155.49	2133.03
2.03707	2209.19	2172.87	2150.46	2128.05
2.03908	2204.08	2167.81	2145.49	2123.17
2.04108	2199.04	2162.84	2140.59	2118.34
2.04309	2194.01	2157.87	2135.68	2113.49
2.04509	2189.05	2152.93	2130.85	2108.77
2.04709	2184.14	2148.1	2126.1	2104.1
2.0491	2179.24	2143.3	2121.33	2099.36
2.0511	2174.4	2138.55	2116.64	2094.73
2.05311	2169.63	2133.84	2112	2090.16
2.05511	2164.89	2129.14	2107.38	2085.62
2.05511	2160.18	2124.47	2102.79	2081.11
2.05711	2155.5	2119.83	2098.22	2076.61
2.05912	2150.86	2115.19	2093.66	2072.13
2.06112	2146.3	2110.68	2089.23	2067.78
2.06313	2141.76	2106.27	2084.86	2063.45
2.06513	2137.23	2101.82	2080.44	2059.06
2.06713	2132.8	2097.43	2076.05	2054.67
2.06914	2128.52	2093.19	2071.89	2050.59
2.07114	2124.26	2089.03	2067.93	2046.83

2.07315	2119.85	2084.7	2063.72	2042.74
2.07515	2115.32	2080.24	2059.24	2038.24
2.07715	2115.32	2080.24	2059.24	2038.24
2.07916	2110.88	2075.86	2054.89	2033.92
2.08116	2106.52	2071.57	2050.72	2029.87
2.08317	2102.09	2067.17	2046.43	2025.69
2.08517	2097.65	2062.76	2042.01	2021.26
2.08717	2093.33	2058.44	2037.72	2017
2.08918	2089.17	2054.31	2033.65	2012.99
2.09118	2085.12	2050.28	2029.68	2009.08
2.09319	2081.07	2046.2	2025.69	2005.18
2.09519	2077.04	2042.18	2021.73	2001.28
2.09719	2073.09	2038.23	2017.85	1997.47
2.0992	2069.13	2034.29	2013.96	1993.63
2.1012	2065.19	2030.42	2010.09	1989.76
2.10321	2061.32	2026.61	2006.29	1985.97
2.10521	2057.47	2022.81	2002.53	1982.25
2.10721	2053.63	2019.01	1998.75	1978.49
2.10922	2049.89	2015.32	1995.09	1974.86
2.11122	2046.18	2011.66	1991.49	1971.32
2.11323	2042.48	2008	1987.89	1967.78
2.11523	2038.83	2004.39	1984.31	1964.23
2.11723	2035.23	2000.86	1980.8	1960.74
2.11924	2031.65	1997.31	1977.28	1957.25
2.12124	2028.09	1993.77	1973.77	1953.77
2.12325	2024.57	1990.29	1970.32	1950.35
2.12525	2021.13	1986.9	1966.99	1947.08
2.12725	2017.71	1983.49	1963.66	1943.83
2.12926	2014.3	1980.07	1960.3	1940.53
2.13126	2010.93	1976.73	1956.98	1937.23
2.13327	2007.57	1973.41	1953.68	1933.95
2.13527	2004.25	1970.14	1950.46	1930.78
2.13727	2000.98	1966.88	1947.27	1927.66
2.13928	1997.7	1963.64	1944.05	1924.46
2.14128	1994.45	1960.44	1940.88	1921.32
2.14329	1991.26	1957.29	1937.77	1918.25
2.14529	1988.09	1954.13	1934.66	1915.19
2.14729	1984.92	1950.98	1931.54	1912.1
2.1493	1981.79	1947.9	1928.47	1909.04
2.1513	1978.69	1944.85	1925.44	1906.03
2.15331	1975.61	1941.83	1922.44	1903.05
2.15531	1972.57	1938.84	1919.48	1900.12

2.15731	1969.56	1935.85	1916.54	1897.23
2.15932	1966.61	1932.91	1913.67	1894.43
2.16132	1963.66	1929.97	1910.78	1891.59
2.16333	1960.7	1927.05	1907.88	1888.71
2.16533	1957.79	1924.16	1905.04	1885.92
2.16733	1954.93	1921.32	1902.27	1883.22
2.16934	1952.08	1918.44	1899.44	1880.44
2.17134	1949.23	1915.61	1896.62	1877.63
2.17335	1946.42	1912.87	1893.89	1874.91
2.17535	1943.64	1910.15	1891.17	1872.19
2.17735	1940.87	1907.36	1888.41	1869.46
2.17936	1938.15	1904.65	1885.75	1866.85
2.18136	1935.45	1901.97	1883.1	1864.23
2.18337	1932.77	1899.32	1880.48	1861.64
2.18537	1930.13	1896.67	1877.9	1859.13
2.18737	1927.52	1894.08	1875.35	1856.62
2.18938	1924.92	1891.51	1872.81	1854.11
2.19138	1922.35	1888.96	1870.3	1851.64
2.19339	1919.82	1886.45	1867.8	1849.15
2.19539	1917.27	1883.91	1865.25	1846.59
2.19739	1914.75	1881.45	1862.78	1844.11
2.1994	1912.28	1879.02	1860.35	1841.68
2.2014	1909.81	1876.54	1857.88	1839.22
2.20341	1907.37	1874.11	1855.47	1836.83
2.20541	1904.99	1871.76	1853.16	1834.56
2.20741	1902.61	1869.36	1850.78	1832.2
2.20942	1900.26	1867.02	1848.46	1829.9
2.20942	1897.93	1864.7	1846.17	1827.64
2.21142	1895.63	1862.39	1843.9	1825.41
2.21343	1893.37	1860.15	1841.68	1823.21
2.21543	1893.37	1860.15	1841.68	1823.21
2.21743	1891.11	1857.91	1839.45	1820.99
2.21944	1888.84	1855.65	1837.17	1818.69
2.22144	1886.68	1853.5	1835.07	1816.64
2.22345	1884.5	1851.31	1832.94	1814.57
2.22545	1882.32	1849.13	1830.78	1812.43
2.22745	1880.21	1847.05	1828.71	1810.37
2.22946	1878.07	1844.94	1826.62	1808.3
2.23146	1875.93	1842.8	1824.51	1806.22
2.23347	1873.86	1840.75	1822.47	1804.19
2.23547	1871.8	1838.73	1820.45	1802.17
2.23747	1869.73	1836.68	1818.41	1800.14

2.23948	1867.69	1834.63	1816.38	1798.13
2.24148	1865.68	1832.63	1814.42	1796.21
2.24349	1863.68	1830.65	1812.46	1794.27
2.24549	1861.69	1828.68	1810.49	1792.3
2.24749	1859.72	1826.74	1808.55	1790.36
2.2495	1857.8	1824.81	1806.66	1788.51
2.2515	1855.89	1822.91	1804.79	1786.67
2.25351	1853.99	1821.02	1802.92	1784.82
2.25551	1852.13	1819.16	1801.08	1783
2.25751	1850.26	1817.28	1799.23	1781.18
2.25952	1848.4	1815.38	1797.38	1779.38
2.26152	1846.56	1813.55	1795.54	1777.53
2.26353	1844.74	1811.74	1793.74	1775.74
2.26553	1842.93	1809.91	1791.94	1773.97
2.26753	1841.15	1808.13	1790.18	1772.23
2.26954	1839.39	1806.37	1788.44	1770.51
2.27154	1837.65	1804.61	1786.74	1768.87
2.27355	1835.92	1802.88	1785.04	1767.2
2.27555	1834.2	1801.15	1783.32	1765.49
2.27755	1832.5	1799.45	1781.63	1763.81
2.27956	1830.82	1797.8	1780	1762.2
2.28156	1829.17	1796.17	1778.38	1760.59
2.28357	1827.55	1794.57	1776.78	1758.99
2.28557	1825.95	1792.96	1775.22	1757.48
2.28758	1824.34	1791.35	1773.64	1755.93
2.28958	1822.77	1789.8	1772.1	1754.4
2.29158	1821.21	1788.22	1770.55	1752.88
2.29359	1819.65	1786.63	1769.01	1751.39
2.29559	1818.13	1785.13	1767.55	1749.97
2.2976	1816.59	1783.63	1766.04	1748.45
2.2996	1815.05	1782.11	1764.5	1746.89
2.3016	1813.56	1780.57	1763.02	1745.47
2.30361	1812.06	1779.05	1761.52	1743.99
2.30561	1810.56	1777.55	1760.01	1742.47
2.30762	1809.1	1776.07	1758.56	1741.05
2.30962	1807.66	1774.6	1757.13	1739.66
2.31162	1806.22	1773.16	1755.69	1738.22
2.31363	1804.78	1771.72	1754.26	1736.8
2.31563	1803.36	1770.34	1752.88	1735.42
2.31764	1801.98	1768.96	1751.5	1734.04
2.31964	1800.59	1767.55	1750.11	1732.67
2.32164	1799.18	1766.13	1748.71	1731.29

2.32365	1797.84	1764.8	1747.4	1730
2.32565	1796.5	1763.45	1746.08	1728.71
2.32766	1795.14	1762.08	1744.71	1727.34
2.32966	1793.81	1760.75	1743.38	1726.01
2.33166	1792.5	1759.45	1742.1	1724.75
2.33367	1791.19	1758.14	1740.81	1723.48
2.33567	1789.87	1756.81	1739.49	1722.17
2.33768	1788.6	1755.53	1738.24	1720.95
2.33968	1787.35	1754.27	1736.99	1719.71
2.34168	1786.08	1753	1735.73	1718.46
2.34369	1784.82	1751.75	1734.5	1717.25
2.34569	1783.59	1750.52	1733.28	1716.04
2.3477	1782.33	1749.24	1731.99	1714.74
2.3497	1782.33	1749.24	1731.99	1714.74
2.3497	1781.11	1748.03	1730.78	1713.53
2.3517	1779.92	1746.81	1729.6	1712.39
2.35371	1778.71	1745.59	1728.41	1711.23
2.35571	1777.52	1744.39	1727.23	1710.07
2.35772	1776.35	1743.22	1726.05	1708.88
2.35972	1775.17	1742.04	1724.87	1707.7
2.36172	1773.99	1740.86	1723.69	1706.52
2.36373	1772.83	1739.71	1722.51	1705.31
2.36573	1771.7	1738.57	1721.39	1704.21
2.36774	1770.56	1737.45	1720.27	1703.09
2.36974	1769.41	1736.3	1719.11	1701.92
2.37174	1768.3	1735.13	1717.97	1700.81
2.37375	1767.23	1734.06	1716.9	1699.74
2.37575	1766.15	1732.99	1715.84	1698.69
2.37776	1765.06	1731.89	1714.76	1697.63
2.37976	1764.01	1730.87	1713.73	1696.59
2.38176	1762.96	1729.83	1712.69	1695.55
2.38377	1761.89	1728.78	1711.63	1694.48
2.38577	1760.86	1727.73	1710.59	1693.45
2.38778	1759.83	1726.67	1709.54	1692.41
2.38978	1758.8	1725.63	1708.5	1691.37
2.39178	1757.78	1724.62	1707.47	1690.32
2.39379	1756.79	1723.62	1706.51	1689.4
2.39579	1755.8	1722.63	1705.55	1688.47
2.3978	1754.81	1721.64	1704.58	1687.52
2.3998	1753.82	1720.65	1703.6	1686.55
2.4018	1752.82	1719.65	1702.59	1685.53
2.40381	1751.83	1718.68	1701.62	1684.56

2.40581	1750.87	1717.74	1700.69	1683.64
2.40782	1749.93	1716.81	1699.77	1682.73
2.40982	1748.97	1715.85	1698.83	1681.81
2.41182	1748.01	1714.9	1697.88	1680.86
2.41383	1747.08	1713.99	1696.95	1679.91
2.41583	1746.16	1713.05	1696.05	1679.05
2.41784	1745.24	1712.12	1695.15	1678.18
2.41984	1744.32	1711.23	1694.25	1677.27
2.42184	1743.41	1710.32	1693.36	1676.4
2.42385	1742.51	1709.43	1692.47	1675.51
2.42585	1741.63	1708.56	1691.62	1674.68
2.42786	1740.75	1707.67	1690.77	1673.87
2.42986	1739.84	1706.78	1689.86	1672.94
2.43186	1738.93	1705.87	1688.93	1671.99
2.43387	1738.06	1705	1688.07	1671.14
2.43587	1737.19	1704.14	1687.21	1670.28
2.43788	1736.32	1703.26	1686.34	1669.42
2.43988	1735.45	1702.39	1685.47	1668.55
2.44188	1734.59	1701.52	1684.6	1667.68
2.44389	1733.71	1700.66	1683.72	1666.78
2.44589	1732.87	1699.82	1682.89	1665.96
2.4479	1732.05	1699.02	1682.09	1665.16
2.4499	1731.22	1698.21	1681.29	1664.37
2.4519	1730.4	1697.41	1680.51	1663.61
2.45391	1729.58	1696.6	1679.7	1662.8
2.45591	1728.73	1695.76	1678.83	1661.9
2.45792	1727.89	1694.92	1677.98	1661.04
2.45992	1727.06	1694.09	1677.16	1660.23
2.46192	1726.24	1693.27	1676.35	1659.43
2.46393	1725.43	1692.49	1675.55	1658.61
2.46593	1724.61	1691.71	1674.74	1657.77
2.46794	1723.81	1690.92	1673.95	1656.98
2.46994	1723.03	1690.17	1673.19	1656.21
2.47194	1722.24	1689.39	1672.42	1655.45
2.47395	1721.45	1688.6	1671.63	1654.66
2.47595	1720.66	1687.82	1670.83	1653.84
2.47796	1719.86	1687.02	1670.03	1653.04
2.47996	1719.1	1686.28	1669.31	1652.34
2.48196	1718.37	1685.54	1668.6	1651.66
2.48397	1717.6	1684.75	1667.83	1650.91
2.48597	1716.82	1684	1667.07	1650.14
2.48798	1716.06	1683.29	1666.34	1649.39

2.48998	1715.29	1682.55	1665.59	1648.63
2.49198	1714.54	1681.81	1664.87	1647.93
2.49399	1713.79	1681.09	1664.16	1647.23
2.49599	1713.05	1680.38	1663.45	1646.52
2.498	1712.29	1679.64	1662.71	1645.78
2.5	1711.87	1679.22	1662.27	1645.32

Table B4: Surface heat transfer coefficient for pure water at ER=1.67

Axial Position , Z(m)	Re= 50,000	Re= 40,000	Re= 30,000	Re= 20,000
1.502	825.837	791.319	756.801	722.283
1.50401	798.197	765.419	732.641	699.863
1.50601	812.7	781.028	749.356	717.684
1.50802	964.543	927.866	891.189	854.512
1.51002	1201.95	1155.72	1109.49	1063.26
1.51202	1423.83	1369.02	1314.21	1259.4
1.51403	1616.54	1554.43	1492.32	1430.21
1.51603	1791.61	1722.95	1654.29	1585.63
1.51804	1955.12	1880.38	1805.64	1730.9
1.52004	2109.6	2029.16	1948.72	1868.28
1.52204	2256.61	2170.71	2084.81	1998.91
1.52405	2397.13	2306.04	2214.95	2123.86
1.52605	2531.67	2435.63	2339.59	2243.55
1.52806	2660.44	2559.69	2458.94	2358.19
1.53006	2783.66	2678.35	2573.04	2467.73
1.53206	2901.55	2791.84	2682.13	2572.42
1.53407	3014.29	2900.53	2786.77	2673.01
1.53607	3121.89	3004.3	2886.71	2769.12
1.53808	3224.39	3103.03	2981.67	2860.31
1.54008	3322.01	3197.08	3072.15	2947.22
1.54208	3414.9	3286.63	3158.36	3030.09
1.54409	3503.12	3371.7	3240.28	3108.86
1.54609	3586.8	3452.35	3317.9	3183.45
1.5481	3666.14	3528.81	3391.48	3254.15
1.5501	3741.44	3601.39	3461.34	3321.29
1.5521	3812.88	3670.29	3527.7	3385.11
1.55411	3880.87	3735.84	3590.81	3445.78
1.55611	3945.95	3798.54	3651.13	3503.72
1.55812	4008.69	3858.97	3709.25	3559.53
1.56012	4070.22	3918.27	3766.32	3614.37
1.56212	4132.05	3977.71	3823.37	3669.03
1.56413	4193.26	4036.59	3879.92	3723.25
1.56613	4251.72	4093.15	3934.58	3776.01
1.56814	4306.62	4146.2	3985.78	3825.36
1.57014	4357.66	4195.45	4033.24	3871.03
1.57214	4404.86	4240.98	4077.1	3913.22
1.57415	4448.25	4282.77	4117.29	3951.81
1.57615	4487.63	4320.51	4153.39	3986.27

1.57816	4523.45	4354.99	4186.53	4018.07
1.58016	4556.39	4386.81	4217.23	4047.65
1.58216	4586.85	4416.24	4245.63	4075.02
1.58417	4615.09	4443.7	4272.31	4100.92
1.58617	4641.02	4468.58	4296.14	4123.7
1.58818	4664.89	4491.43	4317.97	4144.51
1.59018	4686.6	4512.24	4337.88	4163.52
1.59218	4706.18	4530.93	4355.68	4180.43
1.59419	4723.88	4547.76	4371.64	4195.52
1.59619	4739.7	4562.82	4385.94	4209.06
1.5982	4753.6	4576.06	4398.52	4220.98
1.6002	4765.87	4587.83	4409.79	4231.75
1.6022	4776.73	4598.39	4420.05	4241.71
1.60421	4786.25	4607.6	4428.95	4250.3
1.60621	4794.5	4615.48	4436.46	4257.44
1.60822	4801.37	4621.92	4442.47	4263.02
1.61022	4807.09	4627.32	4447.55	4267.78
1.61222	4811.77	4631.75	4451.73	4271.71
1.61423	4815.33	4634.94	4454.55	4274.16
1.61623	4817.74	4636.83	4455.92	4275.01
1.61824	4819.09	4637.98	4456.87	4275.76
1.62024	4819.6	4638.62	4457.64	4276.66
1.62224	4819.29	4638.38	4457.47	4276.56
1.62425	4818.07	4637.23	4456.39	4275.55
1.62625	4815.99	4635.26	4454.53	4273.8
1.62826	4813.03	4632.48	4451.93	4271.38
1.63026	4809.17	4628.87	4448.57	4268.27
1.63226	4804.47	4624.34	4444.21	4264.08
1.63427	4799.06	4619.08	4439.1	4259.12
1.63627	4792.97	4613.2	4433.43	4253.66
1.63828	4786.12	4606.47	4426.82	4247.17
1.64028	4778.64	4598.93	4419.22	4239.51
1.64228	4778.64	4598.93	4419.22	4239.51
1.64429	4770.73	4591.16	4411.59	4232.02
1.64629	4762.23	4582.98	4403.73	4224.48
1.6483	4753.04	4574.01	4394.98	4215.95
1.6503	4743.41	4564.87	4386.33	4207.79
1.6523	4733.21	4555.17	4377.13	4199.09
1.65431	4722.45	4544.82	4367.19	4189.56
1.65631	4711.27	4534.02	4356.77	4179.52
1.65832	4699.66	4522.85	4346.04	4169.23
1.66032	4687.62	4511.3	4334.98	4158.66

1.66232	4675.33	4499.43	4323.53	4147.63
1.66433	4663.04	4487.68	4312.32	4136.96
1.66633	4650.18	4475.34	4300.5	4125.66
1.66834	4633.5	4459.22	4284.94	4110.66
1.67034	4612.3	4438.91	4265.52	4092.13
1.67234	4594.91	4422.04	4249.17	4076.3
1.67234	4584.3	4411.72	4239.14	4066.56
1.67435	4573.31	4401.19	4229.07	4056.95
1.67635	4558.15	4386.28	4214.41	4042.54
1.67836	4538.55	4367	4195.45	4023.9
1.68036	4515.71	4344.78	4173.85	4002.92
1.68236	4491.74	4321.68	4151.62	3981.56
1.68437	4467.7	4298.52	4129.34	3960.16
1.68637	4443.96	4275.62	4107.28	3938.94
1.68838	4420.65	4253.18	4085.71	3918.24
1.69038	4397.77	4231.13	4064.49	3897.85
1.69238	4375.29	4209.37	4043.45	3877.53
1.69439	4352.88	4187.76	4022.64	3857.52
1.69639	4330.39	4166.13	4001.87	3837.61
1.6984	4307.96	4144.39	3980.82	3817.25
1.7004	4285.55	4122.65	3959.75	3796.85
1.7024	4263.3	4101.25	3939.2	3777.15
1.70441	4241.02	4079.69	3918.36	3757.03
1.70641	4218.72	4058.16	3897.6	3737.04
1.70842	4196.43	4036.78	3877.13	3717.48
1.71042	4174.1	4015.18	3856.26	3697.34
1.71242	4151.72	3993.51	3835.3	3677.09
1.71443	4129.29	3971.87	3814.45	3657.03
1.71643	4106.83	3950.2	3793.57	3636.94
1.71844	4084.45	3928.7	3772.95	3617.2
1.72044	4062.19	3907.42	3752.65	3597.88
1.72244	4039.76	3885.79	3731.82	3577.85
1.72445	4017.27	3863.96	3710.65	3557.34
1.72645	3994.87	3842.29	3689.71	3537.13
1.72846	3972.54	3820.71	3668.88	3517.05
1.73046	3950.39	3799.54	3648.69	3497.84
1.73246	3928.41	3778.63	3628.85	3479.07
1.73447	3906.51	3757.67	3608.83	3459.99
1.73647	3884.72	3736.75	3588.78	3440.81
1.73848	3863.2	3716.15	3569.1	3422.05
1.74048	3841.88	3695.67	3549.46	3403.25
1.74248	3820.77	3675.43	3530.09	3384.75

1.74449	3799.85	3655.36	3510.87	3366.38
1.74649	3779.16	3635.46	3491.76	3348.06
1.7485	3758.78	3615.96	3473.14	3330.32
1.7505	3738.64	3596.63	3454.62	3312.61
1.7525	3718.67	3577.41	3436.15	3294.89
1.75451	3698.99	3558.48	3417.97	3277.46
1.75651	3679.64	3540.03	3400.42	3260.81
1.75852	3660.56	3521.95	3383.34	3244.73
1.76052	3641.55	3503.62	3365.69	3227.76
1.76252	3622.59	3485.25	3347.91	3210.57
1.76453	3603.86	3467.24	3330.62	3194
1.76653	3585.16	3449.1	3313.04	3176.98
1.76854	3566.44	3430.91	3295.38	3159.85
1.77054	3547.72	3412.76	3277.8	3142.84
1.77255	3528.97	3394.54	3260.11	3125.68
1.77455	3510.2	3376.27	3242.34	3108.41
1.77655	3510.2	3376.27	3242.34	3108.41
1.77856	3491.31	3357.82	3224.33	3090.84
1.78056	3472.33	3339.35	3206.37	3073.39
1.78257	3453.23	3320.77	3188.31	3055.85
1.78457	3434.04	3302.04	3170.04	3038.04
1.78657	3414.76	3283.24	3151.72	3020.2
1.78858	3395.31	3264.33	3133.35	3002.37
1.79058	3375.81	3245.36	3114.91	2984.46
1.79058	3356.32	3226.38	3096.44	2966.5
1.79259	3336.78	3207.36	3077.94	2948.52
1.79459	3317.18	3188.26	3059.34	2930.42
1.79659	3297.8	3169.55	3041.3	2913.05
1.7986	3278.58	3151.08	3023.58	2896.08
1.8006	3259.48	3132.64	3005.8	2878.96
1.80261	3240.64	3114.49	2988.34	2862.19
1.80461	3222.07	3096.69	2971.31	2845.93
1.80661	3203.84	3079.26	2954.68	2830.1
1.80862	3185.99	3062.23	2938.47	2814.71
1.81062	3168.55	3045.6	2922.65	2799.7
1.81263	3151.62	3029.53	2907.44	2785.35
1.81463	3135.24	3014.11	2892.98	2771.85
1.81663	3119.35	2999.11	2878.87	2758.63
1.81864	3104.05	2984.74	2865.43	2746.12
1.82064	3089.32	2970.96	2852.6	2734.24
1.82265	3075.17	2957.69	2840.21	2722.73
1.82465	3061.51	2944.87	2828.23	2711.59

1.82665	3048.44	2932.72	2817	2701.28
1.82866	3035.92	2921.13	2806.34	2691.55
1.83066	3023.81	2909.95	2796.09	2682.23
1.83267	3012.13	2899.19	2786.25	2673.31
1.83467	3000.82	2888.64	2776.46	2664.28
1.83667	2989.81	2878.3	2766.79	2655.28
1.83868	2978.99	2868.1	2757.21	2646.32
1.84068	2968.34	2857.93	2747.52	2637.11
1.84269	2957.85	2847.9	2737.95	2628
1.84469	2947.49	2838.02	2728.55	2619.08
1.84669	2937.2	2828.21	2719.22	2610.23
1.8487	2926.92	2818.44	2709.96	2601.48
1.8507	2916.6	2808.6	2700.6	2592.6
1.85271	2906.09	2798.38	2690.67	2582.96
1.85471	2895.48	2788.03	2680.58	2573.13
1.85671	2884.83	2777.69	2670.55	2563.41
1.85872	2874.01	2767.11	2660.21	2553.31
1.86072	2863.02	2756.33	2649.64	2542.95
1.86273	2851.88	2745.39	2638.9	2532.41
1.86473	2840.64	2734.41	2628.18	2521.95
1.86673	2829.28	2723.28	2617.28	2511.28
1.86874	2817.82	2712.07	2606.32	2500.57
1.87074	2806.27	2700.8	2595.33	2489.86
1.87275	2794.58	2689.31	2584.04	2478.77
1.87475	2782.84	2677.8	2572.76	2467.72
1.87675	2771.04	2666.25	2561.46	2456.67
1.87876	2759.15	2654.56	2549.97	2445.38
1.88076	2747.26	2642.91	2538.56	2434.21
1.88277	2735.38	2631.28	2527.18	2423.08
1.88477	2723.52	2619.68	2515.84	2412
1.88677	2711.68	2608.13	2504.58	2401.03
1.88878	2699.89	2596.67	2493.45	2390.23
1.89078	2688.15	2585.21	2482.27	2379.33
1.89279	2676.5	2573.9	2471.3	2368.7
1.89479	2664.91	2562.66	2460.41	2358.16
1.89679	2653.37	2551.44	2449.51	2347.58
1.8988	2641.98	2540.4	2438.82	2337.24
1.9008	2630.69	2529.45	2428.21	2326.97
1.90281	2619.52	2518.7	2417.88	2317.06
1.90481	2608.45	2508.03	2407.61	2307.19
1.90681	2597.43	2497.28	2397.13	2296.98
1.90882	2597.43	2497.28	2397.13	2296.98

1.91082	2586.56	2486.7	2386.84	2286.98
1.91283	2575.88	2476.35	2376.82	2277.29
1.91483	2565.36	2466.2	2367.04	2267.88
1.91683	2554.95	2456.17	2357.39	2258.61
1.91884	2544.68	2446.24	2347.8	2249.36
1.92084	2534.56	2436.47	2338.38	2240.29
1.92084	2524.57	2426.8	2329.03	2231.26
1.92285	2514.75	2417.28	2319.81	2222.34
1.92485	2505.1	2408.02	2310.94	2213.86
1.92685	2495.56	2398.87	2302.18	2205.49
1.92886	2486.18	2389.87	2293.56	2197.25
1.93086	2476.94	2380.98	2285.02	2189.06
1.93287	2467.81	2372.18	2276.55	2180.92
1.93487	2458.81	2363.49	2268.17	2172.85
1.93687	2449.92	2354.9	2259.88	2164.86
1.93888	2441.16	2346.49	2251.82	2157.15
1.94088	2432.57	2338.2	2243.83	2149.46
1.94289	2424.12	2330.06	2236	2141.94
1.94489	2415.75	2322.01	2228.27	2134.53
1.94689	2407.49	2314.05	2220.61	2127.17
1.9489	2399.36	2306.2	2213.04	2119.88
1.9509	2391.35	2298.42	2205.49	2112.56
1.95291	2383.47	2290.83	2198.19	2105.55
1.95491	2375.69	2283.35	2191.01	2098.67
1.95691	2368	2275.92	2183.84	2091.76
1.95892	2360.43	2268.67	2176.91	2085.15
1.96092	2352.99	2261.53	2170.07	2078.61
1.96293	2345.65	2254.46	2163.27	2072.08
1.96493	2338.38	2247.41	2156.44	2065.47
1.96693	2331.24	2240.57	2149.9	2059.23
1.96894	2324.16	2233.77	2143.38	2052.99
1.97094	2317.18	2227.02	2136.86	2046.7
1.97295	2310.32	2220.41	2130.5	2040.59
1.97495	2303.53	2213.84	2124.15	2034.46
1.97695	2296.78	2207.26	2117.74	2028.22
1.97896	2290.15	2200.86	2111.57	2022.28
1.98096	2283.59	2194.55	2105.51	2016.47
1.98297	2277.08	2188.24	2099.4	2010.56
1.98497	2270.74	2182.15	2093.56	2004.97
1.98697	2264.47	2176.12	2087.77	1999.42
1.98898	2258.22	2170.05	2081.88	1993.71
1.99098	2252.05	2164.08	2076.11	1988.14

1.99299	2245.93	2158.16	2070.39	1982.62
1.99499	2239.89	2152.32	2064.75	1977.18
1.99699	2233.91	2146.58	2059.25	1971.92
1.999	2228	2140.9	2053.8	1966.7
2.001	2222.16	2135.21	2048.26	1961.31
2.00301	2216.35	2129.55	2042.75	1955.95
2.00501	2210.63	2124.04	2037.45	1950.86
2.00701	2204.98	2118.62	2032.26	1945.9
2.00902	2199.35	2113.18	2027.01	1940.84
2.01102	2193.74	2107.75	2021.76	1935.77
2.01303	2188.18	2102.34	2016.5	1930.66
2.01503	2182.7	2097.03	2011.36	1925.69
2.01703	2177.29	2091.86	2006.43	1921
2.01904	2171.91	2086.7	2001.49	1916.28
2.02104	2166.58	2081.56	1996.54	1911.52
2.02305	2161.29	2076.46	1991.63	1906.8
2.02505	2156.05	2071.41	1986.77	1902.13
2.02705	2150.91	2066.51	1982.11	1897.71
2.02906	2145.79	2061.59	1977.39	1893.19
2.03106	2140.66	2056.6	1972.54	1888.48
2.03307	2135.58	2051.64	1967.7	1883.76
2.03507	2130.56	2046.76	1962.96	1879.16
2.03707	2125.58	2041.97	1958.36	1874.75
2.03908	2120.64	2037.2	1953.76	1870.32
2.04108	2115.75	2032.46	1949.17	1865.88
2.04309	2110.91	2027.81	1944.71	1861.61
2.04509	2106.12	2023.19	1940.26	1857.33
2.04709	2101.37	2018.6	1935.83	1853.06
2.0491	2096.68	2014.12	1931.56	1849
2.0511	2092.03	2009.66	1927.29	1844.92
2.05311	2087.41	2005.19	1922.97	1840.75
2.05511	2082.83	2000.77	1918.71	1836.65
2.05511	2078.32	1996.46	1914.6	1832.74
2.05711	2073.82	1992.14	1910.46	1828.78
2.05912	2069.38	1987.9	1906.42	1824.94
2.06112	2064.98	1983.66	1902.34	1821.02
2.06313	2060.6	1979.44	1898.28	1817.12
2.06513	2056.28	1975.33	1894.38	1813.43
2.06713	2052.11	1971.42	1890.73	1810.04
2.06914	2047.93	1967.34	1886.75	1806.16
2.07114	2043.56	1962.86	1882.16	1801.46
2.07315	2039.18	1958.51	1877.84	1797.17

2.07515	2034.92	1954.52	1874.12	1793.72
2.07715	2034.92	1954.52	1874.12	1793.72
2.07916	2030.66	1950.44	1870.22	1790
2.08116	2026.33	1946.14	1865.95	1785.76
2.08317	2022.05	1942.01	1861.97	1781.93
2.08517	2017.9	1938.15	1858.4	1778.65
2.08717	2013.86	1934.39	1854.92	1775.45
2.08918	2009.87	1930.57	1851.27	1771.97
2.09118	2005.95	1926.78	1847.61	1768.44
2.09319	2002.1	1923.13	1844.16	1765.19
2.09519	1998.25	1919.46	1840.67	1761.88
2.09719	1994.43	1915.77	1837.11	1758.45
2.0992	1990.64	1912.15	1833.66	1755.17
2.1012	1986.87	1908.55	1830.23	1751.91
2.10321	1983.17	1905.02	1826.87	1748.72
2.10521	1979.48	1901.49	1823.5	1745.51
2.10721	1975.83	1898.03	1820.23	1742.43
2.10922	1972.25	1894.61	1816.97	1739.33
2.11122	1968.7	1891.22	1813.74	1736.26
2.11323	1965.17	1887.86	1810.55	1733.24
2.11523	1961.71	1884.59	1807.47	1730.35
2.11723	1958.27	1881.31	1804.35	1727.39
2.11924	1954.84	1878.03	1801.22	1724.41
2.12124	1951.45	1874.81	1798.17	1721.53
2.12325	1948.11	1871.65	1795.19	1718.73
2.12525	1944.82	1868.51	1792.2	1715.89
2.12725	1941.55	1865.39	1789.23	1713.07
2.12926	1938.31	1862.32	1786.33	1710.34
2.13126	1935.12	1859.31	1783.5	1707.69
2.13327	1931.91	1856.25	1780.59	1704.93
2.13527	1928.71	1853.17	1777.63	1702.09
2.13727	1925.57	1850.16	1774.75	1699.34
2.13928	1922.45	1847.2	1771.95	1696.7
2.14128	1919.35	1844.25	1769.15	1694.05
2.14329	1916.31	1841.36	1766.41	1691.46
2.14529	1913.27	1838.45	1763.63	1688.81
2.14729	1910.24	1835.56	1760.88	1686.2
2.1493	1907.27	1832.75	1758.23	1683.71
2.1513	1904.3	1829.91	1755.52	1681.13
2.15331	1901.37	1827.13	1752.89	1678.65
2.15531	1898.45	1824.33	1750.21	1676.09
2.15731	1895.55	1821.54	1747.53	1673.52

2.15932	1892.72	1818.83	1744.94	1671.05
2.16132	1889.87	1816.08	1742.29	1668.5
2.16333	1887.04	1813.38	1739.72	1666.06
2.16533	1884.29	1810.79	1737.29	1663.79
2.16733	1881.56	1808.19	1734.82	1661.45
2.16934	1878.8	1805.52	1732.24	1658.96
2.17134	1876.1	1802.97	1729.84	1656.71
2.17335	1873.43	1800.44	1727.45	1654.46
2.17535	1870.78	1797.92	1725.06	1652.2
2.17735	1868.17	1795.47	1722.77	1650.07
2.17936	1865.58	1793.01	1720.44	1647.87
2.18136	1862.99	1790.53	1718.07	1645.61
2.18337	1860.42	1788.07	1715.72	1643.37
2.18537	1857.88	1785.63	1713.38	1641.13
2.18737	1855.38	1783.24	1711.1	1638.96
2.18938	1852.91	1780.9	1708.89	1636.88
2.19138	1850.45	1778.55	1706.65	1634.75
2.19339	1848.05	1776.28	1704.51	1632.74
2.19539	1845.65	1774.03	1702.41	1630.79
2.19739	1843.29	1771.83	1700.37	1628.91
2.1994	1840.97	1769.66	1698.35	1627.04
2.2014	1838.64	1767.47	1696.3	1625.13
2.20341	1836.33	1765.29	1694.25	1623.21
2.20541	1834.08	1763.17	1692.26	1621.35
2.20741	1831.84	1761.07	1690.3	1619.53
2.20942	1829.62	1758.98	1688.34	1617.7
2.20942	1827.42	1756.91	1686.4	1615.89
2.21142	1825.22	1754.81	1684.4	1613.99
2.21343	1823.05	1752.73	1682.41	1612.09
2.21543	1823.05	1752.73	1682.41	1612.09
2.21743	1820.9	1750.69	1680.48	1610.27
2.21944	1818.75	1748.66	1678.57	1608.48
2.22144	1816.68	1746.68	1676.68	1606.68
2.22345	1814.59	1744.68	1674.77	1604.86
2.22545	1812.49	1742.66	1672.83	1603
2.22745	1810.47	1740.73	1670.99	1601.25
2.22946	1808.44	1738.81	1669.18	1599.55
2.23146	1806.4	1736.87	1667.34	1597.81
2.23347	1804.43	1735	1665.57	1596.14
2.23547	1802.48	1733.16	1663.84	1594.52
2.23747	1800.51	1731.29	1662.07	1592.85
2.23948	1798.56	1729.43	1660.3	1591.17

2.24148	1796.62	1727.56	1658.5	1589.44
2.24349	1794.73	1725.78	1656.83	1587.88
2.24549	1792.85	1724.01	1655.17	1586.33
2.24749	1790.97	1722.22	1653.47	1584.72
2.2495	1789.14	1720.48	1651.82	1583.16
2.2515	1787.32	1718.75	1650.18	1581.61
2.25351	1785.5	1717.01	1648.52	1580.03
2.25551	1783.7	1715.27	1646.84	1578.41
2.25751	1781.91	1713.56	1645.21	1576.86
2.25952	1780.12	1711.84	1643.56	1575.28
2.26152	1778.35	1710.14	1641.93	1573.72
2.26353	1776.62	1708.5	1640.38	1572.26
2.26553	1774.91	1706.89	1638.87	1570.85
2.26753	1773.22	1705.29	1637.36	1569.43
2.26954	1771.53	1703.67	1635.81	1567.95
2.27154	1769.87	1702.09	1634.31	1566.53
2.27355	1768.23	1700.54	1632.85	1565.16
2.27555	1766.59	1698.98	1631.37	1563.76
2.27755	1764.96	1697.42	1629.88	1562.34
2.27956	1763.33	1695.84	1628.35	1560.86
2.28156	1761.73	1694.29	1626.85	1559.41
2.28357	1760.2	1692.85	1625.5	1558.15
2.28557	1758.68	1691.41	1624.14	1556.87
2.28758	1757.14	1689.94	1622.74	1555.54
2.28958	1755.63	1688.49	1621.35	1554.21
2.29158	1754.13	1687.05	1619.97	1552.89
2.29359	1752.62	1685.59	1618.56	1551.53
2.29559	1751.14	1684.15	1617.16	1550.17
2.2976	1749.69	1682.79	1615.89	1548.99
2.2996	1748.25	1681.45	1614.65	1547.85
2.3016	1746.8	1680.04	1613.28	1546.52
2.30361	1745.37	1678.68	1611.99	1545.3
2.30561	1743.97	1677.38	1610.79	1544.2
2.30762	1742.55	1676	1609.45	1542.9
2.30962	1741.15	1674.64	1608.13	1541.62
2.31162	1739.8	1673.38	1606.96	1540.54
2.31363	1738.42	1672.06	1605.7	1539.34
2.31563	1737.04	1670.72	1604.4	1538.08
2.31764	1735.73	1669.48	1603.23	1536.98
2.31964	1734.39	1668.19	1601.99	1535.79
2.32164	1733.06	1666.94	1600.82	1534.7
2.32365	1731.78	1665.72	1599.66	1533.6

2.32565	1730.48	1664.46	1598.44	1532.42
2.32766	1729.17	1663.2	1597.23	1531.26
2.32966	1727.88	1661.95	1596.02	1530.09
2.33166	1726.62	1660.74	1594.86	1528.98
2.33367	1725.35	1659.51	1593.67	1527.83
2.33567	1724.08	1658.29	1592.5	1526.71
2.33768	1722.85	1657.1	1591.35	1525.6
2.33968	1721.67	1655.99	1590.31	1524.63
2.34168	1720.46	1654.84	1589.22	1523.6
2.34369	1719.24	1653.66	1588.08	1522.5
2.34569	1718.07	1652.55	1587.03	1521.51
2.3477	1716.9	1651.47	1586.04	1520.61
2.3497	1716.9	1651.47	1586.04	1520.61
2.3497	1715.71	1650.31	1584.91	1519.51
2.3517	1714.56	1649.2	1583.84	1518.48
2.35371	1713.4	1648.09	1582.78	1517.47
2.35571	1712.23	1646.94	1581.65	1516.36
2.35772	1711.12	1645.89	1580.66	1515.43
2.35972	1710	1644.83	1579.66	1514.49
2.36172	1708.86	1643.73	1578.6	1513.47
2.36373	1707.75	1642.67	1577.59	1512.51
2.36573	1706.66	1641.62	1576.58	1511.54
2.36774	1705.58	1640.6	1575.62	1510.64
2.36974	1704.5	1639.59	1574.68	1509.77
2.37174	1703.44	1638.58	1573.72	1508.86
2.37375	1702.41	1637.59	1572.77	1507.95
2.37575	1701.36	1636.57	1571.78	1506.99
2.37776	1700.3	1635.54	1570.78	1506.02
2.37976	1699.3	1634.59	1569.88	1505.17
2.38176	1698.29	1633.62	1568.95	1504.28
2.38377	1697.27	1632.65	1568.03	1503.41
2.38577	1696.29	1631.72	1567.15	1502.58
2.38778	1695.3	1630.77	1566.24	1501.71
2.38978	1694.28	1629.76	1565.24	1500.72
2.39178	1693.32	1628.86	1564.4	1499.94
2.39379	1692.37	1627.95	1563.53	1499.11
2.39579	1691.41	1627.02	1562.63	1498.24
2.3978	1690.45	1626.09	1561.73	1497.37
2.3998	1689.5	1625.18	1560.86	1496.54
2.4018	1688.57	1624.32	1560.07	1495.82
2.40381	1687.64	1623.45	1559.26	1495.07
2.40581	1686.71	1622.55	1558.39	1494.23

2.40782	1685.79	1621.65	1557.51	1493.37
2.40982	1684.86	1620.75	1556.64	1492.53
2.41182	1683.93	1619.85	1555.77	1491.69
2.41383	1683.06	1619.04	1555.02	1491
2.41583	1682.17	1618.18	1554.19	1490.2
2.41784	1681.28	1617.32	1553.36	1489.4
2.41984	1680.42	1616.52	1552.62	1488.72
2.42184	1679.55	1615.69	1551.83	1487.97
2.42385	1678.68	1614.85	1551.02	1487.19
2.42585	1677.82	1614.01	1550.2	1486.39
2.42786	1676.96	1613.17	1549.38	1485.59
2.42986	1676.11	1612.38	1548.65	1484.92
2.43186	1675.27	1611.61	1547.95	1484.29
2.43387	1674.44	1610.82	1547.2	1483.58
2.43587	1673.61	1610.03	1546.45	1482.87
2.43788	1672.79	1609.26	1545.73	1482.2
2.43988	1671.96	1608.47	1544.98	1481.49
2.44188	1671.17	1607.75	1544.33	1480.91
2.44389	1670.34	1606.97	1543.6	1480.23
2.44589	1669.53	1606.19	1542.85	1479.51
2.4479	1668.76	1605.47	1542.18	1478.89
2.4499	1667.94	1604.66	1541.38	1478.1
2.4519	1667.13	1603.86	1540.59	1477.32
2.45391	1666.33	1603.08	1539.83	1476.58
2.45591	1665.54	1602.35	1539.16	1475.97
2.45792	1664.77	1601.65	1538.53	1475.41
2.45992	1663.97	1600.88	1537.79	1474.7
2.46192	1663.21	1600.18	1537.15	1474.12
2.46393	1662.46	1599.49	1536.52	1473.55
2.46593	1661.68	1598.75	1535.82	1472.89
2.46794	1660.93	1598.05	1535.17	1472.29
2.46994	1660.18	1597.33	1534.48	1471.63
2.47194	1659.42	1596.6	1533.78	1470.96
2.47395	1658.68	1595.91	1533.14	1470.37
2.47595	1657.95	1595.24	1532.53	1469.82
2.47796	1657.19	1594.52	1531.85	1469.18
2.47996	1656.45	1593.8	1531.15	1468.5
2.48196	1655.76	1593.15	1530.54	1467.93
2.48397	1655.04	1592.48	1529.92	1467.36
2.48597	1654.3	1591.78	1529.26	1466.74
2.48798	1653.58	1591.1	1528.62	1466.14
2.48998	1652.86	1590.43	1528	1465.57

2.49198	1652.15	1589.76	1527.37	1464.98
2.49399	1651.43	1589.07	1526.71	1464.35
2.49599	1650.72	1588.39	1526.06	1463.73
2.498	1650.01	1587.73	1525.45	1463.17
2.5	1649.63	1587.39	1525.15	1462.91